Environmental Control of Seawater Geochemistry in a Mesoarchean Peritidal System, Woman Lake, Superior Province

Brittany Ramsay

Supervised by: Dr Philip Fralick

Thesis submitted to the
Department of Geology
Faculty of Science and Environmental Studies
at Lakehead University
in partial fulfillment of the
requirements for a
Master of Science Degree in Geology
at Lakehead University (2020)

ABSTRACT

The 2.857±5 Ga (this study) carbonate platform at Woman Lake, Ontario, Canada, presents a unique opportunity to fill a 130 million year knowledge gap on early carbonate sedimentology and ocean chemistry between similar platform occurrences at Steep Rock Lake (2.80Ga) and Red Lake (2.93Ga). Woman Lake carbonates are among the few very early and thick carbonate platforms to develop in the Mesoarchean. Field, petrographic, and geochemical investigations were performed on the limestone sequence to better understand the paleoenvironmental context of this understudied, 90-meter-thick succession.

At the base of the carbonate platform, lying atop felsic subaerial Archean tuff, are stratiform stromatolites interbedded with thin beds of massive carbonate grainstone, followed by laterally linked low domal stromatolites, which gradually become larger domes, then bioherms with walled pseudocolumnar stromatolites. They are overlain by cross-stratified and parallel laminated carbonate grainstones and more pseudocolumnar stromatolites. A variety of fenestral microbialites overly this unit, including thrombolites, stromatactis-bearing low domal stromatolites, and narrow isolated columnar stromatolites. This is followed by a cyclic succession of low domal stromatolites alternating with microbial carbonate and carbonate grainstone. Three main stromatolitic morphologies exist and represent a range of low to moderate current energies from upper intertidal to subtidal environments. They are: 1) low relief stratiform to undulating stromatolites 2) laterally linked low domal and pseudocolumnar stromatolites, and 3) isolated to locally isolated domes and narrow columnar stromatolites. Evidence here supports mainly peritidal environments on a carbonate platform with fluctuating sea-level and water energies in an overall deepening succession.

The diverse carbonate facies are comprised of geochemical features reminiscent of both Archean and modern signatures in shale normalized REE patterns. Trace elements indicate that the carbonates precipitated from a mixture of two different fluids: anoxic seawater that carried a positive Eu anomaly, and oxygenated waters that imparted significant negative Ce anomalies. On a microscopic scale, using LA-ICP-MS, there is less compositional contrast between carbonate phases, which indicates that dissolution and precipitation on a small spatial scale homogenized localized areas, but did not affect changes on a metric scale. Geochemical trends paired with stratigraphic depth show decameter cycles of gradual declines in Mg, Fe, Mn, Ba and Sr substitution into the calcite lattice followed by sharp increases throughout the platform's

deposition, possibly reflecting changing accommodation space effecting precipitation rate. Typical Archean values for $\delta^{13}C$ ranging from -3.83‰ to 1.30‰, with an average of 0.53‰ (±0.59, n=31) occur with Y/Ho ratios ranging from 27 to 117 and $^{87}Sr/^{86}Sr$ isotopic values from 0.700346 to 0.711313 (±0.00098 (1σ)). The observed trends suggest that the precipitating carbonates were able to record and retain the effects of an evolving water column had in the local environment. Importantly, the Woman Lake carbonate platform provides context for, and evidence of, free oxygen approximately 500 million years before the Great Oxygenation Event, during a relatively undocumented period in time.

ACKNOWLEDGMENTS

If someone were to tell me as a 2nd year university student in geology that I would write a 25-thousand-word thesis about nearly 3 billion year old stromatolites I would have asked "Why, What are stromatolites?" It goes without saying that I owe great thanks to a number of inspiring professors, researchers, and colleagues. First and foremost, I'd like to extend my thanks to Dr. Philip Fralick for introducing me to a sedimentological approach to exploring Earth's ancient history, for his continued support, countless discussions and learning opportunities. Thank-you for providing me with another opportunity to dive into Earth's deep past.

I'd like to thank Stefan Lalonde and the French National Centre for Scientific Research for supporting this project financially and providing the means to conduct field and lab research. Furthermore, I'd like to thank them for creating the Earthbloom Team: Stefan Lalonde, Philip Fralick, Robert Riding, Martin Homann, Pierre Sans-Jofre, Timothy McIntyre, Sophie Kurucz, Munira Afroz, Dylan Wilmeth, Laureline Patry, and Paul Bielski. To the team itself, I sincerely appreciate all the assistance and discussions we have had in the field, the lab, online, and all the laughs along the way.

Many thanks to Kristi Tavener, Jonas Valiunas, and Anne Hammond from Lakehead University's Lapidary facility for their cheerful and timely effort preparing my polished slabs and thin sections. To Paul for conducting LA-ICP-MS on a number of those sections and only giving me sarcastic grief. To Jeremy Heitela for photographing many of the polished slabs. To Nick Craik and Matt Greco for their assistance powdering what must have seemed like an absurd amount of samples. To Philippe Nonnotte for teaching me how to prepare and calibrate columns necessary for Sr and Nd isotope collection. To the analytical staff at the Pôle Spectométrie Océan in Brest, Bluenne, and Laureline for running my samples through the ICP-MS and to Isabella Ward for digitizing my stratigraphic columns - through each rendition. And of course to my parents, family, Matt, Bailey, Paul and Dana for always lifting my spirits and letting me babble along the way.

If not for this team, this project would not have been possible nor enjoyable. Thanks to all,

Britt

TABLE OF CONTENTS

TABLE OF FIGURES

1.0 INTRODUCTION

Geologists, biologists, and paleontologists alike have become fascinated by Earth's oxygenation and its direct impacts on our planet. Many studies have focused on the Great Oxygenation Event itself at ~2.4Ga (Karhu et al., 1996; Farquhar et al., 2003; Bekker et al., 2004; Holland, 2006; Scott et al., 2008; Konhauser et al., 2011; Pufahl & Hiatt, 2012; Zerkle et al., 2017), while others strive to uncover how oxygen production initially began and its ramifications on paleoenvironmental evolution (Sumner, 1997; Anbar et al., 2007; Kaufman et al., 2007; Planavsky et al., 2014; Riding et al., 2014; Fralick and Riding, 2015; Kendall et al., 2015; Bellefroid et al., 2018; Wilmeth et al., 2019). Furthermore, the rare traces of Archean life and oxygenation are considered our most promising guides in the search for extraterrestrial life and exoplanet "biosignatures" (Gibson et al., 2001; Cady et al., 2003; Barbieri and Cavalazzi, 2004; Seager and Deming, 2010; Bellefroid et al., 2018). Above all, chemical sediments have been the prime target to study early atmosphere evolution due to their exceptional ability to record physical, biological, and geochemical evidence, which can be used to develop interpretations of paleoenvironment (both local and worldwide); depositional processes; seawater composition; surficial redox conditions; and early evolution of life (Grotzinger, 1989; Grotzinger and James, 2000; Sumner and Grotzinger, 2004; Johannesson et al., 2006; Allwood et al., 2009; Satkoski et al., 2017; Homann et al., 2018; Robbins et al., 2019). Geochemically, chert and banded iron formation were a major focus early on (Fryer 1977; Miller & O'Nions 1985; Jacobsen & Pimentel-Klose 1988; Derry and Jacobsen 1990; Bau and Dulski 1995). More recently, carbonates have been recognized as robust proxies for ancient seawater composition (Webb and Kamber, 2000, 2011; Kamber et al., 2004; Nothdurft et al., 2004; Kamber et al., 2014) and the 2857±5 Ma (this study) Woman Lake carbonate platform provides a bridge of evolutionary information during a previously poorly researched time interval.

Remnants of Archean carbonate platforms are scarce in abundance and seldom exhibit ideal preservation. Even so they provide us with one of few gateways into Earth's ancient history and by unravelling the diagenetic, metamorphic and metasomatic overprints and considering all applicable sedimentary and geochemical techniques available, a more comprehensive understanding can be achieved. The number of in-depth Archean carbonate studies is increasing

but there are still major gaps particularily throughout the Mesoarchean (2.8 Ga to 3.2 Ga). The earliest sedimentary carbonate studied is a 1m thick ferroan calcite horizon of the Coonterunah Group (3.52 Ga) at the base of the Pilbara Craton (Green and Buick, 2001; Harnmeijer, 2010) but the oldest putitive evidence of life lies stratigraphically above in the 3.45 Ga Strelley Pool Chert (Van Kranendonk, 2006; Allwood et al., 2007). The 8 to 30m thick unit is comprised of encrusting domical, coniform and wavy laminite stromatolites. Half of a billion years later the oldest known (2.93 Ga) carbonate platform developed, now located in Superior Craton, Canada (Hofmann et al., 1985; Corfu and Wallace, 1986; McIntyre and Fralick, 2017). The 200m thick Red Lake-Wallace Lake carbonate platform contains large crystal fan pseudomorphs, herringbone calcite cement, plus domal and pseudo-columnar stromatolites. At about the same time the ~30m thick Chobeni formation of the Nsuze Group, Pongola Supergroup, was deposited with its stratiform, domal and conical to columnar stromatolites, amongst siliciclastics and dolarenites (Von Brunn and Mason, 1977; Hegner et al., 1994; Siahi et al., 2016). Another c. 130 million years later the 2.8 Ga Steep Rock Carbonate platform developed, now located in Superior Craton (Wilks and Nisbet, 1985; Fralick and Riding, 2015). Its 500m of carbonate displays a diverse range of microbialites including giant domal structures with crystal fans and cuspate fenestral microbialite comparable to the 2.6 Ga Huntsman Limestone of the Bulawayo Belt (Sumner and Grotzinger, 2000). Despite our growing understanding of hydrosphere-biosphere evolution throughout the Archean, many studies could benefit from advanced geochemical techniques, and by revisiting previously underappreciated deposits we may be able to enhance our understanding and fill some gaps in our knowledge on the geochemical evolution of the ocean-atmosphere system.

During the aformentioned c.130 million year gap two carbonate units are known to exist, one being the c.100m thick stromatolitic Mushandike carbonate of the Zimbabwe Craton. Its sedimentology was first described by Orpen and Wilson (1981), though the age relationships are still complicated to decifer. Moorbath et al., (1987) obtained the first direct depositional age of carbonate and the Pb/Pb isochron placed the stromatolites at 2839 ± 33Ma. Collerson and others (2002) tested Pb isotope analysis on the same drill core samples using multi-collector ICP-MS and TIMS reporting a comparable age of 2817 ± 34Ma. Prior to this Abell and others (1985) reported carbon isotopes and most recently Kamber and others (2004) reported trace element geochemistry and Sr-isotope ratios. The second carbonate unit to occur at about this time is the focus of this

study, the 2857±5 Ma old Woman Lake carbonates (WLC) of the Superior Craton. At first the previously recognized stromatolitic carbonate (Hofmann et al., 1985) paled in comparison to its neighbouring Red Lake (2.93 Ga) and Steep Rock Lake (2.8 Ga) successions (Fig. 1) and drew little focus.

The goal here is to provide a comprehensive study on the diverse and newly recognized stromatolitic lithotopes at Woman Lake, their depositional context and its subsequent control on geochemistry in order to gain a better understanding of the paleodepositional environment. Further implications regarding our global ancient hydrosphere are drawn by incorporating detailed stratigraphic columns with systematic geochemistry and comparing the results to formations occuring before, during and after Woman Lake's deposition. Here we present new age constraints; sedimentology and stratigraphic context; interpretation of depositional environments; petrography; Sr, C and O isotopic analyses; and REE and trace element geochemistry obtained by partial carbonate digestion, FE-SEM-EDX analysis and mapping, and LA-ICP-MS analyses.

2.0 PREVIOUS RESEARCH AND REGIONAL GEOLOGY

Thurston and Jackson (1978) first reported stromatolitic features at the south west point of the narrows on Woman Lake (Fig. 1) while mapping for the Ontario Geological Survey. The stromatolites were then briefly mentioned by Thurston, (1980, p.94), Hofmann (1981, Fig. 23.5C), Gupta et al., (1982, p. 238) and Walter (1983, p.199). It was not until 1985 that Hofmann and others presented the first and only study semi-focused on Woman Lake carbonates. In the same paper they recognized carbonates on Red Lake and noted their preservation was comparatively better. Nevertheless, they commented on the geologic setting and described stromatolite-like features at Woman Lake. Their descriptions are discussed relative to this study within the sedimentology chapter (4.0).

The limestone outcrops along the shores of the narrows on Woman Lake Ontario, Canada within the Uchi subprovince of the Superior province (Fig. 1) and are part of the Birch-Uchi-Confederation greenstone belt. The locality is accessible from Ear Falls through a number of logging roads headed northeast then ultimately by boat from Woman River. It is exposed in a relatively thin veneer along the shoreline and is best seen when lake levels are low. The Mesoarchean terrain is dipping subvertically, generally trends north-northeast and youngs to the east. It is comprised predominantly of metavolcanics and lesser metasediments, with rare chemical sediments (Thurston, 1980) all of which were intruded by granitic rocks of Neoarchean age (Ayres et al., 1971; Beakhouse et al., 1999).

Mafic and felsic metavolcanic sequences within the Birch – Uchi greenstone belts were first recognized by Goodwin (1967), then Pryslak (1971) added a third unit. Thurston (1980) interpreted these three major cycles to be approximately 8500 to 11,200 m thick stratigraphically. He also considered the three cycles of volcanism to be sequential with Cycle I at 2959 Ma, Cycle II at 2840 Ma , and Cycle III at 2738 Ma (Nunes and Thurston, 1980; Wallace et al., 1986) and stated that the stromatolitic carbonate lies only at the top of the second cycle (Thurston, 1980). Stott and Corfu (1991) re-examined the regional geology of the Archean greenstone belt with additional geochronology and defined the three cycles as lithotectonic assemblages instead; the Balmer (2.96 Ga), Woman (2.84 Ga) and Confederation (2.735Ga). In this scenario the Balmer and Woman assemblages were considered the western portions of Cycle I and II respectively. They

correlated the stratigraphy to Sanborne-Barrie and other's (2001) interpretations of the older Red Lake belt (2.99-2.85Ga) and drew upon their implications for overall terrain development. Rogers and others (2002) reinterpreted the Uchi-Confederation greenstone belt stratigraphy as; Balmer assemblage (2985 Ma), Narrow Lake assemblage (2880 Ma) and Confederation assemblage (2740 Ma), which loosely corresponded to the original cycles except they split the Woman Lake assemblage and attribute much of the eastern portion, including (but not mentioning) the stromatolitic carbonate to the younger Confederation assemblage. However, they only collected samples for U-Pb geochronology on the eastern side of Woman Lake (Rogers et al., 2000; Fig. 2) which is on the

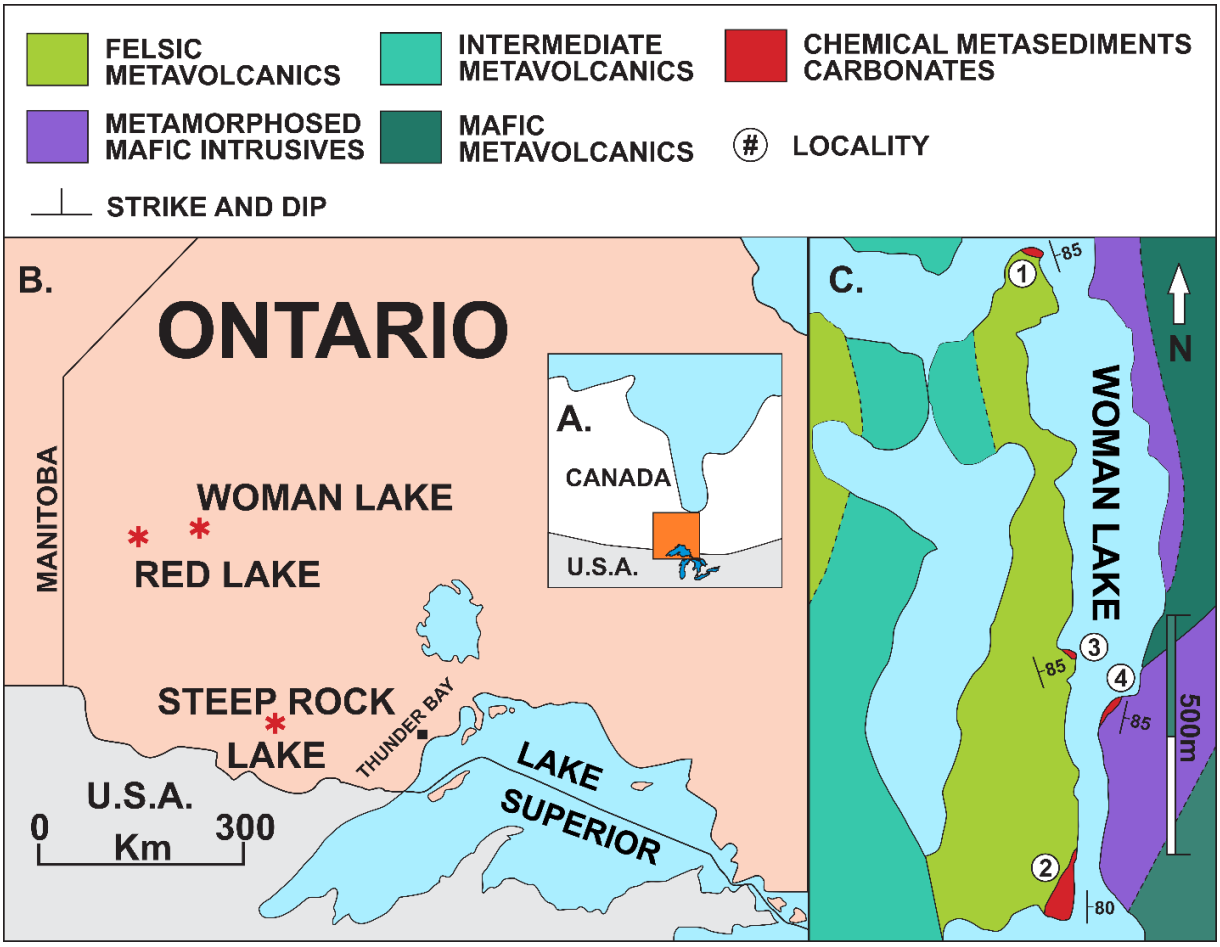

Fig. 1. Regional geology display. A) Location with respect to Canada, orange box represents Figure B. B) Location of Woman Lake with respect to Mesoarchean carbonate platforms at Red Lake and Steep Rock Lake within Ontario, Canada. C) Bedrock geology map of the narrows on Woman Lake modified after Thurston (1980). Circled numbers represent the locality of each carbonate locality referred to throughout text. The base of stratigraphy begins at UTM 15U 517685.00 m E, 5666939.00 m N.

Confederation side of the previously drawn boundary and despite previous geochronologic constraints to the contrary (Nunes and Thurston, 1980; Corfu, unpub. data (1986) reported in Corfu and Wallace (1985); Wallace et al., 1986) they suggested the western portion of the Woman Lake assemblage represented a distinct and potentially significantly older period of volcanism than the eastern portion. Rogers (2002) released an open file report for the Geological Survey of Canada revising the stratigraphy to include 5 distinct volcanic assemblages and regarded Woman Lake as its own assemblage. Most are separated from one another by unconformities. They are now considered; Balmer at 2980 and 2975 Ma (Rogers and McNicoll, 2000), Narrow which is not dated directly but stratigraphically constrained between 2975 and 2870 Ma (Rogers and McNicoll, 2000), Woman at 2870 Ma, (Rogers, 2002), Confederation at 2745 and 2735 Ma (Rogers and McNicoll, 2000), and St. Joseph at 2725 Ma (Rogers, 2002).

Fralick and others (2009) reverted to using the divisions set out by Rogers and McNicoll (2000) and recognized the controversy over the tectonic setting. However, they were focused on the underlying Balmer assemblage where boundary constraints were not as disputed. They investigated the types and ages of igneous rocks that were present in the source areas at 2.9 Ga by conducting a provenance study on the sedimentary unit considered greywacke and siltstone by Rogers et al. (2000), and wacke and argillite by Thurston (1985). Through whole rock geochemistry and U-Pb zircon geochronology they recognized the source terrain for the Balmer assemblage consists of an assortment of igneous rock types that were both lithically and chronologically diverse. However, they were not well mixed before being deposited thus implying that separate sediment input routes existed. Therefore, a submarine ramp with multiple sediment entry points seemed suitable (Fralick et al. 2009). They also noted their zircon geochronology suggests two distinct volcanic suites were interlayered which implies a more complex tectonic interleaving than previously established. This led them to postulate that some sediments may correlate to the base of the Narrow Lake assemblage.

Ultimately, observations by Thurston (1980, 1985) are still largely applicable. Cycle I, which includes the bimodal volcanic rocks of the Balmer and Narrow Lake assemblages terminate with a boundary of marble in the northwest on Narrow Lake and iron formation interbedded with siltstone and shales in the south on Woman Lake (Hofmann et al., 1985; Thurston, 1985; Roger,

2002). The ~90m of highly recrystallized marble at the northwest boundary is not stromatolitic (Hofmann et al., 1985), mostly sheared and heavily recrystallized, yet it does retain some distinct cross-stratified laminations. Basalts at the base of cycle II are part of the Woman Lake assemblage and in direct contact with the underlying sheared marble of cycle I. The contact can be seen on Narrow Lake where it strikes practically east and dips near vertically. The basalt continues, overlying felsic metavolcanics of cycle I toward Quartz Lake and further south to Woman Lake where it trends north and dips subvertically. Woman Lake assemblage begins with pillowed basaltic flows overlain by subaqueous intermediate ash flows, then felsic tuffs, lapilli tuffs, and 300m of eutaxitic textured felsic tuff which indicated local subaerial volcanism (Thurston, 1980). The stromatolitic carbonate conformably overlies the subaerial to very shallow marine welded felsic tuffs. The vast majority of the Woman Lake sequence (~3.5 km in total) forms a monocline that trends north to north east and dips subvertically and slightly east. Aside from the regional fold that created the monocline, no smaller scale folding was observed.

Initial U-Pb dating of the felsic tuff underlying the carbonate provided an age of 2794 Ma (Nunes and Thurston, 1980), however with updated lab techniques abrading the outer zircon rims the age was revised to 2830 Ma (F. Corfu, pers. Communication reported in Hofmann et al., 1985). Rogers (2002) reported a new age of 2870 Ma. In this study we report a comparable age for the Woman Lake tuff; 2857±5 Ma.

Regional metamorphism of the Woman Lake assemblage was considered greenschist facies by Hofmann et al. (1985), and this is thought to be accurate here. Since the carbonates themselves are not associated with siliciclastic or platy minerals, typical metamorphic index minerals are absent along with diagnostic foliation and lineation fabrics. However, petrographic analysis provides some evidence of intracrystalline deformation via microstructural fabrics associated with dislocation creep. The quartz crystals in the silicified features often have subgrains, some highly serrated grain boundaries, and experience undulatory extinction, which all indicate that temperatures reached at least 300ºC (Passchier and Trouw, 2005). Where stromatolitic laminae are semi-preserved within silicified carbonates, the laminae are green in colour.

3.0 METHODOLOGY

A sedimentological study was completed first, followed by geochemical analysis in order to provide a comprehensive understanding of the depositional environments and ultimately their relation to the chemical signatures imparted by the Archean hydrosphere. Detailed stratigraphic sections across each carbonate exposure were logged and photographed while in the field during the summers of 2018 and 2019. Large bulk samples were collected from the Woman Lake tuff, conformably underlying the carbonate for U-Pb geochronology (Fig. 1C). Oriented and representative bulk samples were collected throughout stratigraphy from each carbonate locality using a hammer and or/chisel from the best-preserved areas. Six meters of continuous core was drilled from the top of the second locality using a gas-powered hand drill to acquire small scale, detailed sampling (Fig. 1C). A field map and stratigraphic columns were then generated and lithotopes and sublithotopes were defined. Stratigraphic relationships are discussed within the sedimentology chapter (4.0). Samples were then cut; many were polished and specific areas were selected to be cut and crushed with a tungsten mallet and powdered in an agate mill at Lakehead University's lapidary facility. The powdered samples were purposefully selected with aims to discover systematic geochemical changes throughout individual samples, between sublithotopes, and throughout the broader stratigraphy. The powdered samples were then analyzed for major elements, REE and trace element concentrations, stable C and O isotopes, and radiogenic Sr isotopes. While choosing samples for solution ICP-MS (inductively coupled plasma mass spectrometer), areas for thick and thin sections were also selected for LA-ICP-MS (laser ablation ICP-MS), FE-SEM-EDS (field emission - scanning electron microscope – energy dispersive spectrometry), and petrography. LA-ICP-MS techniques were explored in order to test its validity in comparison to microdrilling and bulk sampling and obtain geochemical differences of the carbonate phases present at smaller scales than micro-drilling enabled. Approximately 230 samples were collected and roughly 200 powders were produced for geochemical sampling. When samples were comprised of diverse fabrics and structures multiple powders were created from a single sample. Thirty-five thick and thin sections were made for petrography, LA-ICP-MS, and SEM analysis.

3.1 U-PB GEOCHRONOLOGY

Bulk samples of the Woman Lake tuff were analyzed in the Geochronology Laboratory at the University of Toronto by Donald Davis (Davis, 2019). There, samples were crushed and pulverized, then heavy mineral separation began using a Wilfley table followed by paramagnetic separations and final separation was done by hand under a microscope to pick the freshest and least cracked zircon grains. Large zircons were mounted in epoxy and polished, small ones were mounted on double sided tape without polishing. Polished surfaces were etched with HF vapour for 1 minute to effectively attack altered and damaged zircon and reveal zonation. Grains were partially ablated using a 193 nm New Wave excimer laser and analyzed by an Agilent 7900 ICP-MS. It was typically operated at 5Hz, 5 J/cm^2, with 20-60 μm beam diameter depending on grainsize. Spots were pre-ablated with a larger beam diameter for 1 sec (5 pulses) to clean the surface prior to analysis. A base line was established for 10 seconds before the laser sampling beam turned on. Data were collected for 25 seconds followed by a washout period for 20 seconds obtaining about 150 measurement cycles per spot, leaving 15 μm deep ablation pits. Two zircon standards were used and sets of 4-5 sample measurements were bracketed by standard analysis. A quartz diorite from the Marmion batholith in northwestern Ontario (DD85-17) and a monzodiorite from the Pontiac province of Quebec (DD91-1) were used as standards. Those at the geochronology laboratory edited and reduced the data using their custom VBA software (UtilLAZ program).

3.2 SOLUTION ICP-MS

Samples were partially dissolved at the Institute for Oceanographic and Marine Sciences (IUEM) in Brest France for analysis on their ICP-MS (Thermo Element2). Powdered samples were weighed (0.25 g) into centrifuge tubes and 5 mL of 5% acetic acid was added, stirred, and left to react at room temperature overnight. Following 5 minutes in a centrifuge the supernatant was separated into Tephlon beakers and 100 μl was extracted while the remainder was dried down and prepared for Sr isotope analysis. Samples were added to 4.9 mL of 2% HNO_3 spiked with 1ppb Indium then put through the high resolution ICP MS in batches of 90. Standards (CAL-S) and blanks were included at the beginning, middle, and end of each run. REE concentrations were normalized to Post Archean Australian Shale (PAAS; Taylor and McLennan, 1985). Anomalies were calculated using methods put forth by Bau and Dulski (1996).

3.3 RADIOGENIC Sr ISOTOPES

The remainder of the partially dissolved solution was dried down at 80º and resuspended in 6N HCL, then dried down again, thus converting the sample into a chloride and likely eliminating any remaining acetic acid. Ion exchange columns were prepared at in a clean lab at IUEM for analysis on their ICP-Q-MS. Once dry the sample was resuspended in 1 mL 2.5 N HCl and ready for loading. The ion exchange columns were prepared by loading 15 mL tubes with 5 mL of resin (AG50W-X8, 200-400 mesh) mixed with 2.5N HCl. The columns were then filled and rinsed with 6N HCl. Ultrapure water (Milli-Q) was passed through the columns twice after being stored in 6N HCl overnight and subsequently prepared for chromatographic separation. The extraction procedure began by conditioning the columns with 2.5N HCl. Once passed, the sample was suspended in 1 mL 2.5N HCl and loaded into the column. It was then rinsed with 5 mL 2.5N HCl to effectively remove Ca + Rb. Finally, the Sr was extracted and collected with 6 mL HCl. In total, 90 Sr samples were collected, including 3 CAL-S standards and 2 blanks.

3.4 LA-ICP-MS

Thick sections (150-200 µm) were prepared at Lakehead University's lapidary facility. They were analyzed and processed at IUEM by a fellow master student. A Copex Pro, 102 coherent laser attached in-line to a high-resolution ICP MS (Thermo2 Element sector field) ablated spots with 12 Hz repetition rate and 7 J/cm^2. Spot size was roughly 120µm in diameter since inclusions were not abundant, carbonate crystals were roughly that size and REE concentration levels were low. Ten thick sections were analyzed with 14 to 20 shots each. The sets of shots were bracketed by a shot in two different reference materials: BIR-1G and NIST612. They were used as calibration points to assess the quality and ascertain accuracy. The MS observed counts for ^{43}Ca and ^{138}La and was tuned using NIST612. The analysis ran for 2 minutes total: the first minute collecting background readings and the following minute collecting sample data. Prior to each spot analysis a burst of 8 shots preablated the surface removing any buildup and steadying the background levels.

The data was processed through MATLAB 2015a using the add on SILLS. Data reduction involved first selecting and setting a background for each sample then selecting multiple windows of the recorded signal thereby avoiding any unwanted inclusions or erratic data. Reference materials (BIR-1G and NIST612) were analyzed to account for the effects of downhole drift. BIR-

1G provided a means to examine the accuracy and precision by comparing to its known values. Through SILLS, NIST-612 was used to convert raw data in counts per second (cps) to parts per million (ppm) in each sequence. Stoichiometric values for Ca were used in the reduction of data using NIST-612.

3.5 STABLE C AND O ISOTOPES

Powdered samples were prepared at Lakehead University's lapidary facility and analyzed at IUEM. To first release CO_2 from ~250 μg of powdered carbonate sample a Kiel IV automated carbonate preparation device was used to liberate CO_2 with phosphoric acid at 70 ºC ± 1 for 400 seconds. After going through the gas transfer and purification system CO_2 is sent to the attached Finnigan MAT 253 mass spectrometer. Vienna Pee Dee Belemnite (V-PDB) was used as a routine internal standard and NBS-18, NBS-19, and CAMIL-21 for normalization. Multiple standards were measured and a calibration curve was made for each session in order to correct the fractionation of O^{18} by comparing known values to the unknown values.

3.6 PETROGRAPHY

In order to better understand the paragenesis of each carbonate phase and the degree of carbon present within the fenestral microbialite, carbon coated thin sections were examined. They were made at Lakehead university's lapidary facility and examined at their Instrument Laboratories (LUIL) using a Hitachi SU-70 Schottky Field Emission scanning electron microscope (SEM). Carbon coated thick sections were also analyzed post LA-ICP-MS for comparison purposes.

4.0 SEDIMENTOLOGY AND DEPOSITIONAL ENVIRONMENTS

Previously, Hofmann and others (1985) recognized three structures in Woman Lake Carbonates (WLC): "1) stratiform, crustose structures with corrugate laminae 2) small hemispheroidal mounds, and 3) columnar structures of problematic affinities" (p. 130). It has been established that our understanding since the first documented stromatolite by Kalkowsky (1908) and more importantly since research truly initiated 5 decades ago, has been convoluted due to inconsistent nomenclature and descriptive terminology. Fortuitously, the first all-encompassing 290-page Handbook for the study and description of microbialites was recently published (Grey & Awramik, 2020). Proceeding here, 35 years after Hofmann and others (1985) first described WLC, with an improved albeit imperfect understanding of Archean microbialites, made possible by continued research, numerous reviews and now the most recent handbook (Grey and Awramik, 2020 and references therein), we can recognize and draw further implications regarding their potential biogenicity, depositional context, and climatic relations.

Herein the limestones are divided into three major lithotopes: 1) carbonate microbialite; 2) carbonate grainstones/micrite; and 3) silicified microbialite. Woman Lake carbonates primarily consist of a blue-gray calcite that is, in places, silicified, and rarely dolomitized. They were divided first based on the presence or absence of microbial features, and then whether silicified or not. They were further subdivided into sublithotopes based on sedimentary, microbial and lithological associations described chronologically in the following sections. However, it is important to understand their context stratigraphically first.

4.1 STRATIGRAPHIC FRAMEWORK

Three stratigraphic sections were measured, with the lowermost northern section (locality 1, Fig. 1 & 2) lying directly above Woman Lake felsic tuff (Thurston, 1980). The basal contact is noticeable a few meters inland from the northwestern-most exposure, though obscured amongst vegetation and mottled or blurred likely due to regional greenschist facies metamorphism. Regardless a sharp contrast between the two units is evident when testing with 5% HCl. Contacts between units in each stratigraphic section are considered gradational. The first section begins with thin millimetric bundles (averaging 2-4 cm thick) of crinkly laminae that are

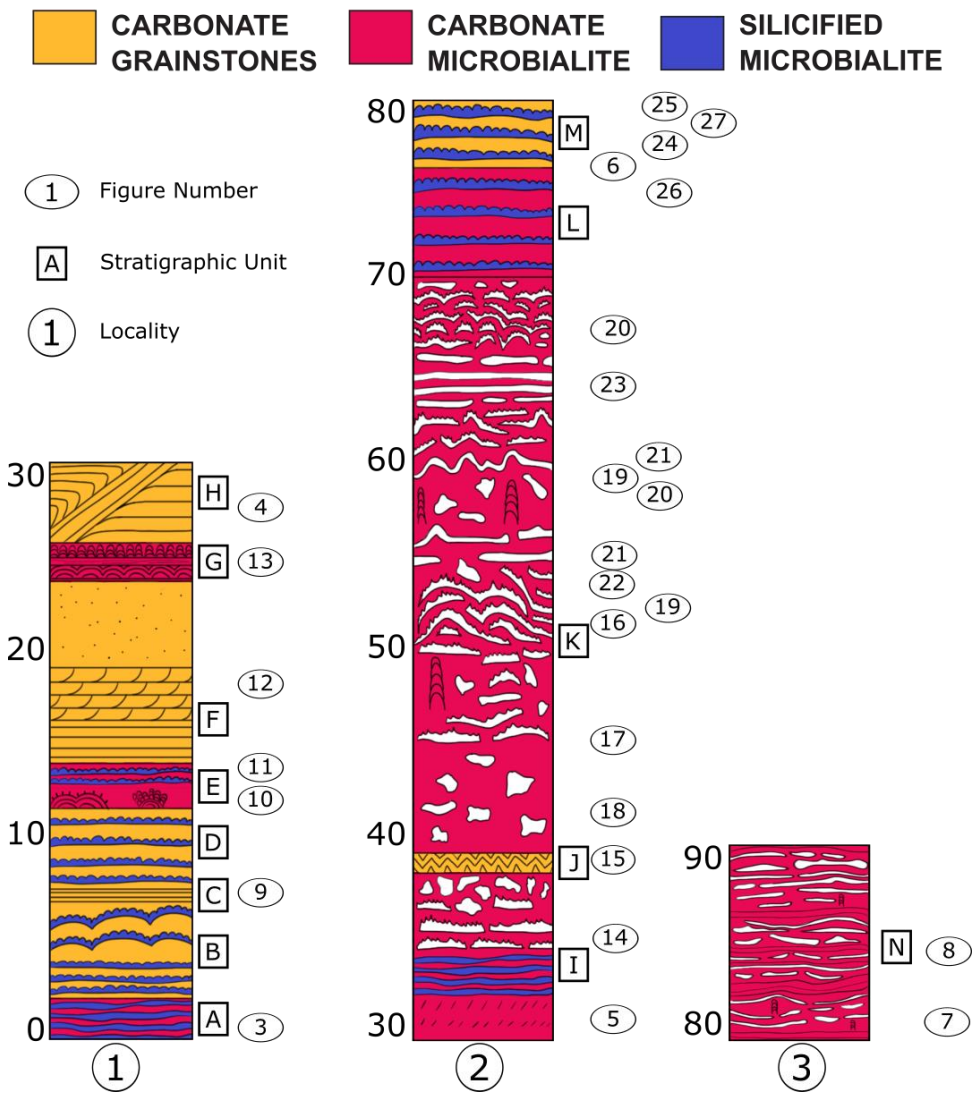

Fig. 2. Woman Lake carbonate stratigraphy from three exposed localities (Figure 1), depth is in meters. Black outlined symbols represent structures and features present. White symbols represent fenestrae and/or associated banded carbonate. They are described in the text and associated photos are denoted by the numbered ovals. Symbols are not to scale.

variably silicified (Fig. 3). The carbonate outcrops in a relatively thin zone around the shoreline for 30m stratigraphically and fortunately, due to low-stand water conditions during field observations, up to 3m was exposed laterally or, depending on the orientation of the shoreline, 2m vertically. The outcrop is very mildly discontinuous up-section though visibility is a little less continuous since the uneven topography dips below water level in some places, thus it is

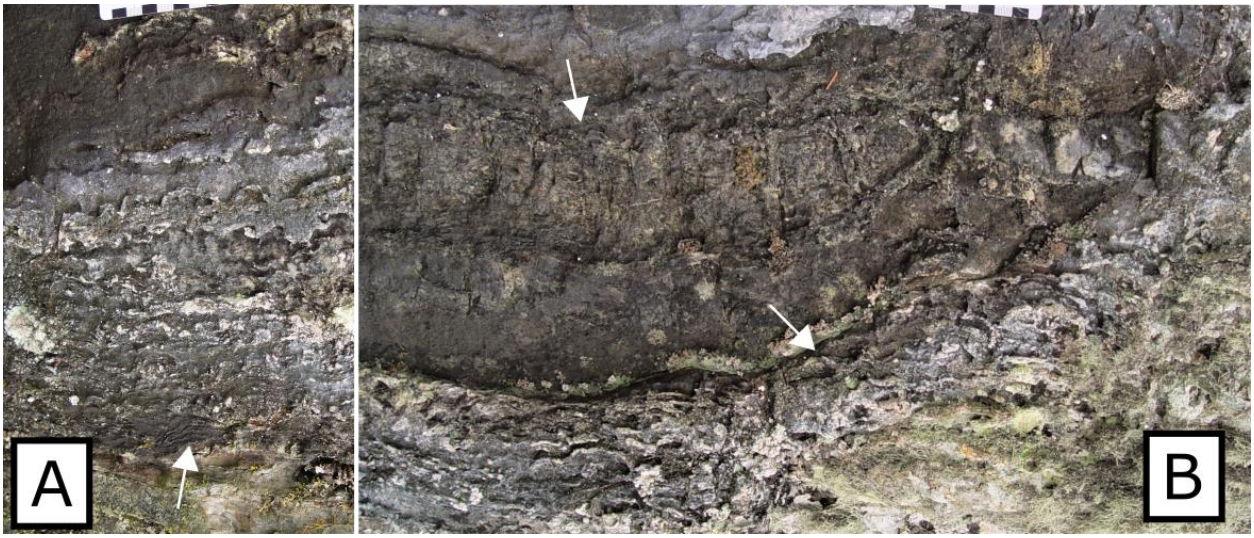

Fig. 3. Unit A. Stratigraphic up is toward the top of the page. Undulating silicified and carbonate microbialite, similar to stratiform stromatolites except the lamination is more wrinkled. Arrow shows fine carbonate lamination. B) Erosive contact within silicified stratiform stromatolites (bottom arrow) and tops of pseudocolumnar stromatolite-like structures (top arrow).

considered a continuous limestone unit despite minor visibility limitations. This first cross-section is the least well preserved of the three stratigraphic segments. The Mesoarchean limestone weathers characteristically orange with concave, irregular, inverted dimples on the surface, highlighting more competent areas; fortunately weathering is not pervasive. A small, 1m wide mafic dyke intrudes the stratigraphy 4m above the base of the sequence and a smaller, ~0.5m wide, mafic sill intrudes toward the top of the sequence at ~19m. Neither one appears to drastically change the surrounding limestone though samples collected in their proximity were treated with caution. This northern section terminates with a ~4m thick convoluted unit comprised of parallel laminated carbonate that in places alternate with centimetric silicified beds, both of which are crosscut, slightly offset, and bent toward the same direction on either side of a 20 cm thick seemingly massive carbonate unit (Fig. 4). Overlying this feature randomly oriented irregular, wavy to crinkly silicified features occur within limestone. No sharp contacts are observed in fact this unit is commonly bent and deformed with large areas of centimeter to decameter fragments and blocks within a finer grained carbonate matrix.

The southern exposure outcrops ~30m stratigraphically above the Woman Lake tuff unit (locality 2, Fig. 1 & 2) between the two units a swampy shoreline persists, devoid of exposed

Fig. 4. Unit H. Scale card is 8 cm long. Stratigraphic up is to the right of the page (east). Parallel laminated carbonate and silicified beds (highlighted by red dots) are slightly offset and curved in the same direction by a 20 cm thick seemingly massive carbonate structure (highlighted by red dashes).

outcrop. Due to the thin zone of shoreline outcrop at this locality, more so than the northern locality, it is often difficult to discern if a macroscopic structure, let alone a megascopic structure, is representative of microbialites. This exposure contains the 3 features Hofmann et al. (1985, locality 8) described and it begins with two 10 cm thick beds of silicified vertically oriented and at times slanted structures that are laterally continuous to the extent of the exposed outcrop (~3m; Fig 5). These silicified beds alternate with millimetric crinkly parallel laminations within blue-grey limestone, weathering less orange than the northern locality and not pervasive. The crinkly laminations are in places highlighted by discontinuous and blebby chert laminations, which Hofmann et al. (1985) termed stratiform structures (1985; Fig. 11). Overall this sequence is 50m thick and terminates with a 10m unit comprised of silicified low domal stromatolites

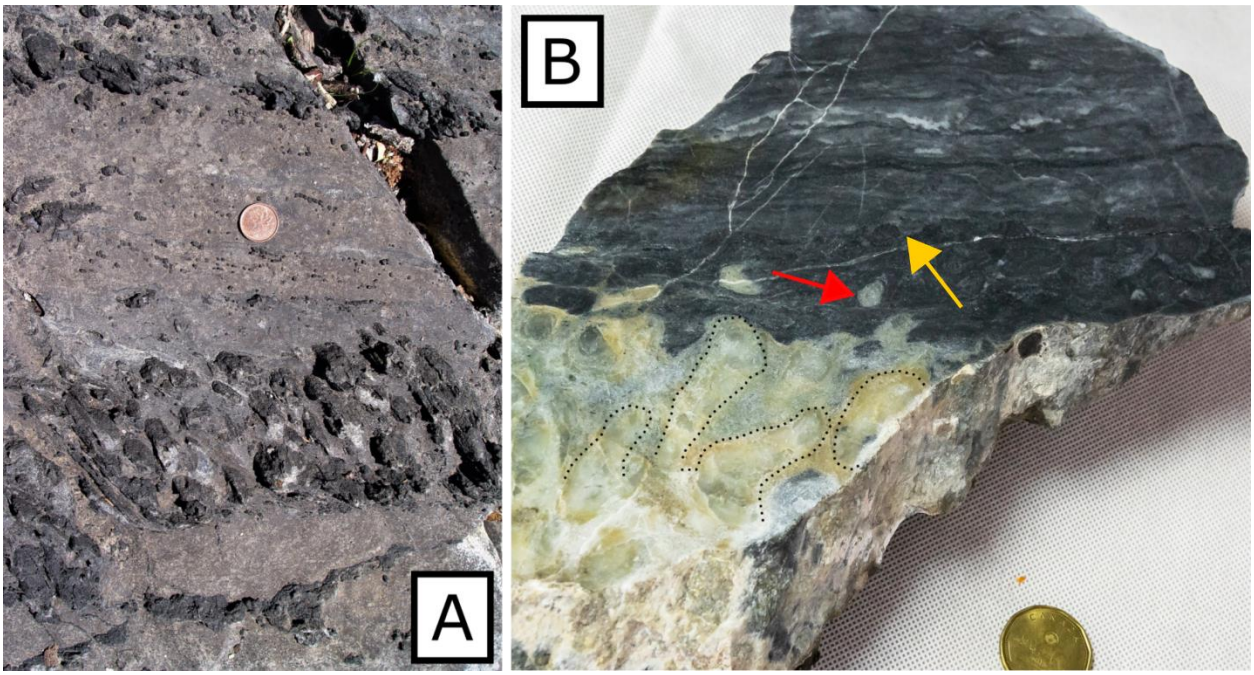

Fig. 5. Unit I. Stratigraphic up is toward the top of the page. Fabrics appear to be fine-grained in the field and micritic in polished slab. A) Silicified vertically oriented features (dark) are overlain and underlain by undulatory microbialite. Coin is 1.9 cm in diameter. B) In polished section the silicified features maintain columnar-like structures (black outline). Few silicified spots (red arrow) are among the overlying dark carbonate, which also has remnant circular or loading features (yellow arrow). The surrounding carbonate is undulating stromatolites with sporadic elongated fenestrae. Coin is 2.6cm in diameter.

averaging 4 cm tall alternating with 5-10 cm thick beds of fenestrated microbialite and nearer the top of section carbonate grainstone, which will be described with more detail in the following sections (Fig. 6). From the top of this unit we drilled 6m down section (Fig. 6D). This southern exposure is considered to lie stratigraphically above the first locality with a negligible amount of depositional time missing since stratigraphic distance between Woman Lake tuff exposure and the overlying Woman Lake carbonate of this section is 30m and that corresponds to the amount of stratigraphy present at the northern locality, which directly overlies the tuff. Despite the lack of a stratigraphic marker this assumption is plausible especially considering these two sections are laterally no more than 1.5km apart and the topmost unit of the first section represents a localized slump event which may not have affected stratigraphy at that distance away. Thus, locality 2 is considered to directly overly stratigraphy at locality 1.

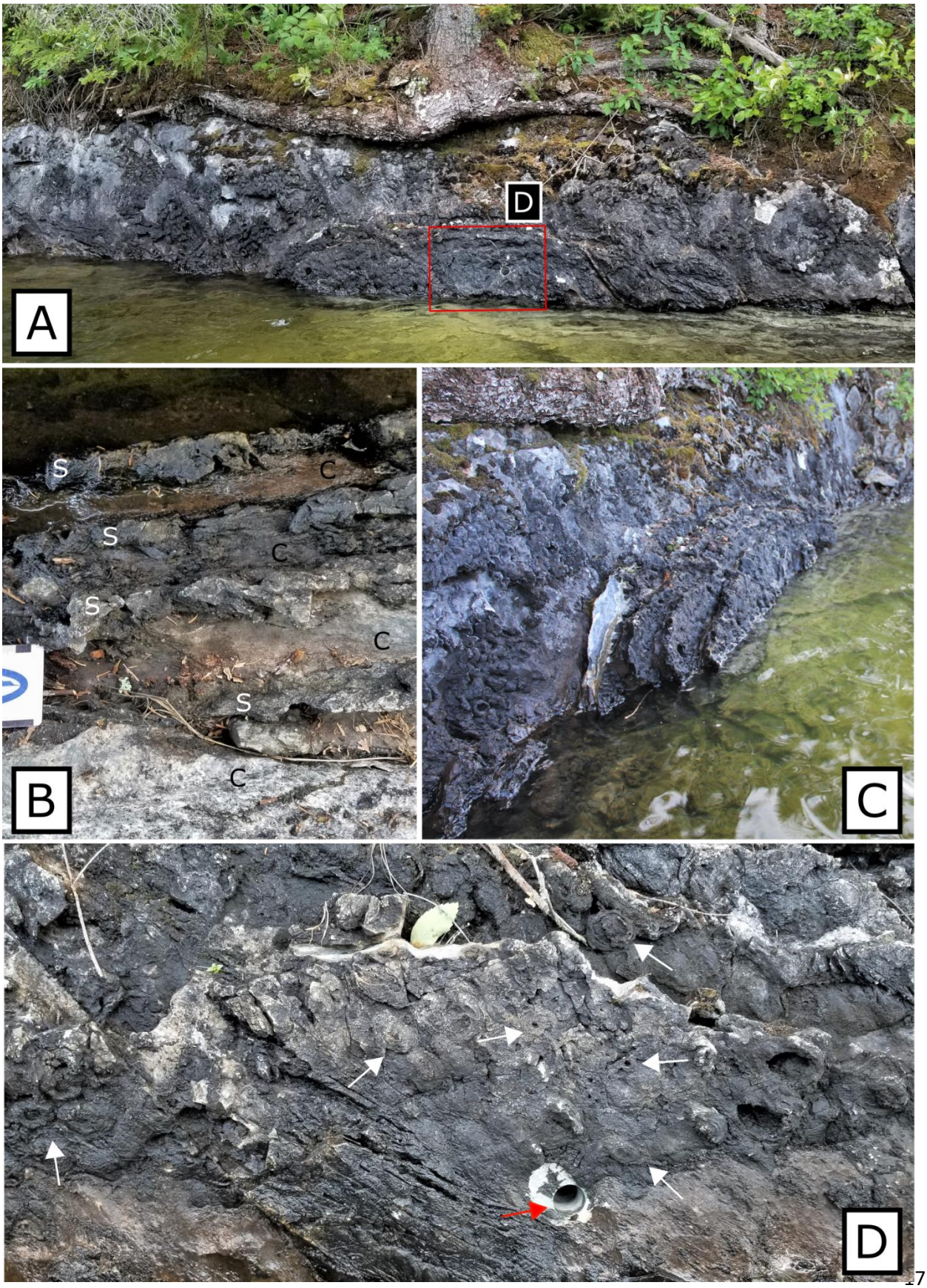
A
D
B
S
C
S
C
S
C
S
C
C
C
D

Fig. 6. (previous page) Unit M. A) Remarkable outcrop locality containing beds of laterally linked small domal stromatolites alternating with possible carbonate grainstone and carbonate microbialite. B) Carbonate (C) and silicified stromatolite (S) beds in cross sectional view, note that the silicified stromatolites are difficult to recognize from this perspective. C) Oblique view of 5 silicified stromatolite beds alternating with possible carbonate grainstone. D) Close-up of circular stromatolite tops (white arrows) in plan view and drill hole locality (red arrow), drill hole diameter is 6 cm.

The eastern most exposure across Woman Lake narrows (Locality 3, Fig. 1) is a 10m thick unit comprised primarily of elongate fenestrated microbialite with banded blue-grey and off-white carbonate (Fig. 7). Silicification is minimal though increases toward the top of the unit. Weathering is not pervasive though there are an abundance of concave circular dimples carved into the surface in a linear fashion following bedding (Fig. 8). A sharp contact with the overlying metamorphosed mafic intrusive terminates this section. Overall, this sequence resembles some of the carbonate microbialite at the top of the southern locality that alternates with silicified microbialite and strongly resembles the middle section of that locality, though with smoother, more elongate fenestrae and less stromatolitic features. The bedding planes tend to strike the same general direction as the northern and southern localities (~340º), beds young to the east, and the lithologies do not differ greatly from those across the narrows at the southern locality, thus locality 2 is considered to stratigraphically overly locality 2. However, it is a possible that Woman Lake narrows itself is a left lateral strike-slip fault that semi obliquely cuts through WLC rendering this eastern locality to represent a repetition of a segment from the southern sequence. However, there is no indication of a fault on the regional map of the area (Thurston, 1984), nor was deformation due to shearing evident along either shoreline.

4.2 NORTHERN LOCALITY DESCRIPTION

4.2.1 Unit A: Carbonate and Silicified Microbialite

The base of the sequence begins with a 4 cm thick seemingly massive carbonate grainstone bed though recrystallization has hidden the original grainsize. It is overlain by a 10 cm thick completely silicified bed with few remnant laminations. Directly above there is 60 cm of undulatory to stratiform stromatolites characterized by flat millimetric layered bundles averaging 2-4 cm thick (Fig. 3). The laminae are variably silicified, which due to differential weathering highlights the lamination by causing silicified ones to protrude in comparison to the

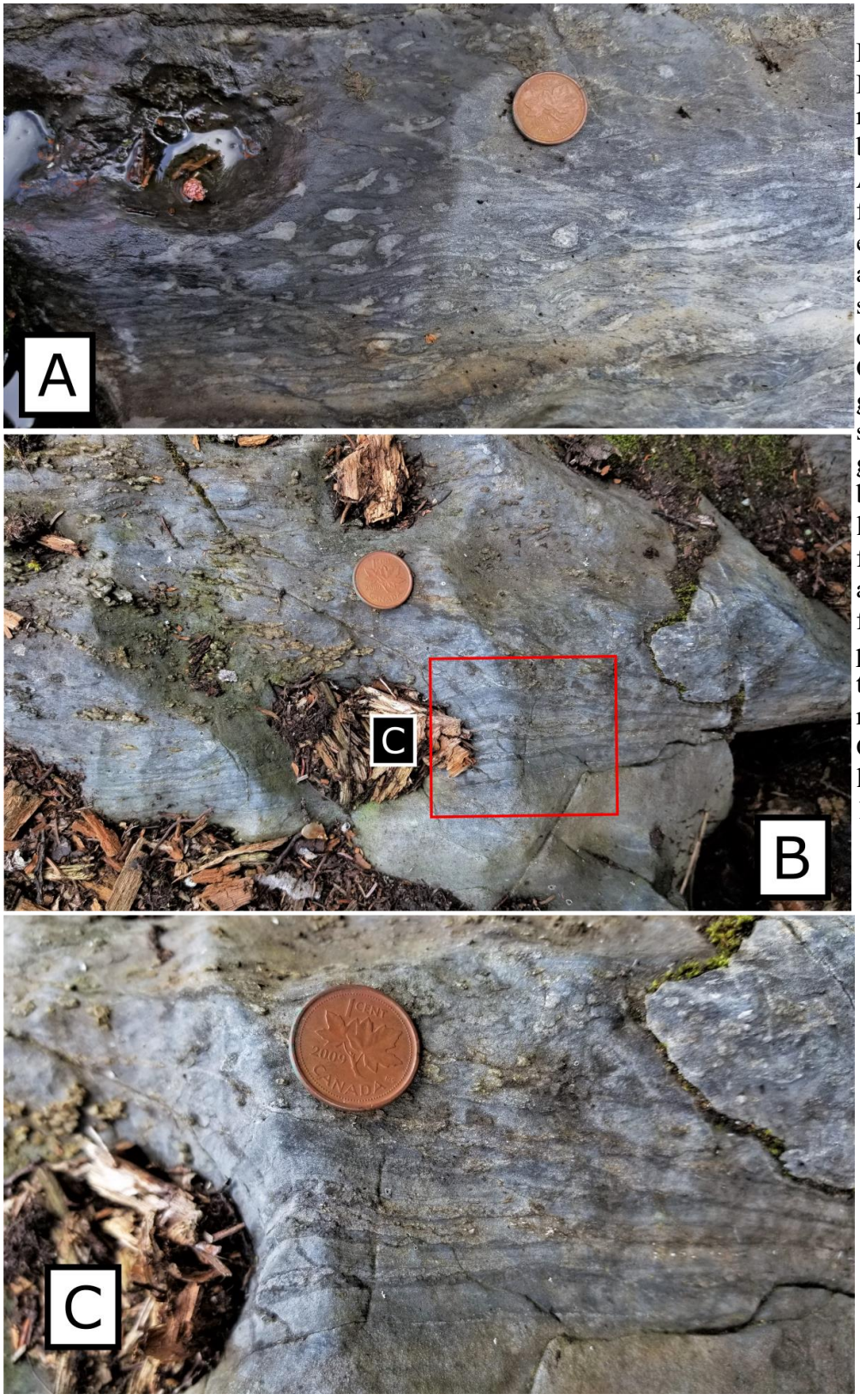

Fig. 7. Unit N. Fenestrated microbialite and banded carbonate. A) Interpreted fenestrae at the eastern locality (4) are frequently smooth and oblong or elongate. B) Carbonate grainstone of seemingly medium grainsize overlain by finer grained layered carbonate followed by clotted and irregular fenestral and potentially thrombolitic microbialite. C) Close-up of fine laminations. Coin is 1.9 cm in diameter.

Fig. 8. Unit N. Eastern outcrop exposure. Note its characteristic dimpled weathering that follows bedding planes.

carbonate between them. Though it is difficult to ascertain with certainty, the laminae seem to be arranged in a couplet laminar pattern where silicification amalgamated the previously dark laminae alternating with lighter carbonate and this is often the case throughout most of the sequence. They seem to exhibit even or film bounded alternations that are wrinkly to wavy with low to moderate degrees of inheritance that are laterally continuous and microcross-laminated in places. This package is erosively cut by a 10 cm bed of massive cherty-carbonate, overlain by a bed of equal thickness that is similar to underlying undulatory stromatolites although remnants of continuous low relief convex laminae are connected at their depressions with vertically oriented silicified features that are more obviously capped by silicified gently convex laminae. Overall they are similar to walled columnar stromatolites but preservation is too poor to be certain (Fig. 3B). Stratiform to undulating stromatolites with flat wavy laminae continue with ~3 cm silicified packages and gradationally become as thick as 5 cm with thicker fully silicified laminations.

4.2.2 Unit B: Grainy Carbonate and Silicified Microbialite

The silicified undulating laminae in the underlying unit gradationally become thicker, completely silicified horizontal beds averaging 5 cm. They alternate sharply with 10-15 cm thick beds of massive carbonate that occasionally contain smooth parallel laminations. The silicified black chert beds are commonly smoother on the bottom than the top (Fig. 9B). Two meters up section the carbonate laminations become more prominent and less silicified beds are present. The carbonate laminations resemble larger scale, linked and semi-closely spaced, stubby hemispheric domal stromatolites (Fig. 9A). They are semi-steeply complex at first though they are encompassed by a larger crustose (low relief) dome. Although preservation is not ideal the laminar patterns seem to be isopachous on a larger scale and synoptic relief ranges from 20 cm to 45 cm in places. The topmost layer is 5 cm thick and silicified with a relatively smooth base and irregular top.

4.2.3 Unit C: Grainy Carbonate

Overlying Unit B is .5m of apparently massive carbonate, with few subtle smooth laminations at the base for 10 cm, some of which are parallel while some resemble cross stratification. More competent carbonate ridges highlight parallel bedding that increase in thickness up section from 5 cm thick to 15 cm thick (Fig. 9C).

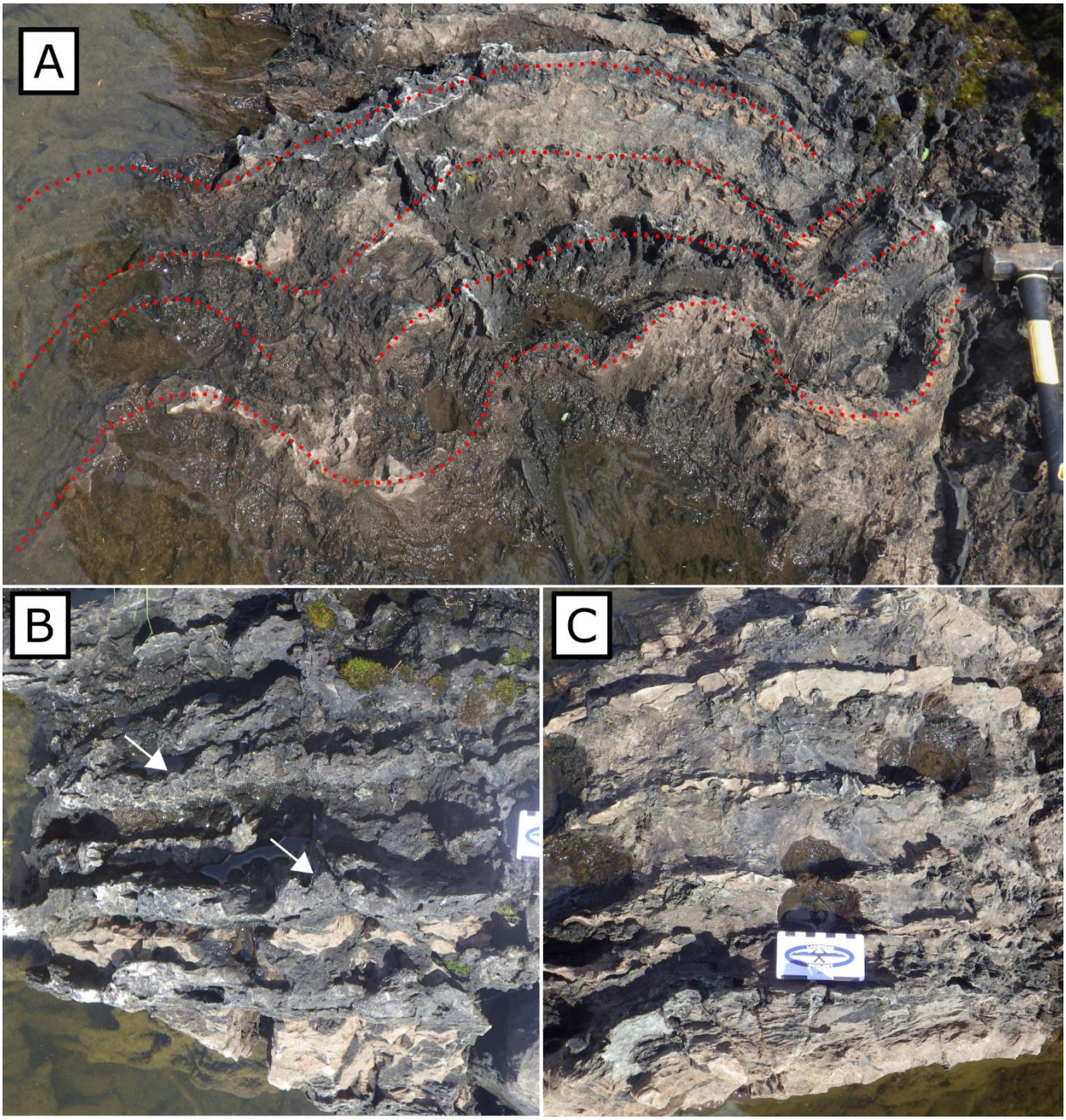

Fig. 9. A) Unit B. Large scale domal features with prominent carbonate ridges and silicified beds highlighting bedding planes (red dots). Smaller domes are encompassed by larger domal structures. These domes overly the undulating silicified beds (black) in B). Arrows in B) denote curved irregular tops of stromatolites compared to the smooth base. Silicified stromatolites alternate with massive carbonate grainstone (orange). C) Unit C. Massive carbonate grainstone, bedding planes highlighted by more prominent carbonate ridges. Basal bed exhibits some lamination, overlying beds are massive and thicken upwards.

4.2.4 Unit D: Grainy Carbonate and Silicified Microbialite

This unit strongly resembles the base of Unit B with seemingly massive carbonate alternating with silicified beds.

4.2.5 Unit E: Carbonate Microbialite and Silicified Microbialite

A 20 cm tall domal bioherm initiates from a flat, smooth, stratiform stromatolite overlying Unit D. The bioherm is comprised of a hemispheric stubby and domal stromatolite that is gently convex, has wrinkly laminations and moderate inheritance (Fig. 10). The laminae are laterally continuous, though in places associated with microcross-laminations, and overall has relatively low synoptic relief. Seven columnar stromatolites initiate atop the low dome. They are laterally linked, contiguous and simply walled. Most are stubby and a few are slender though they are all uniform, erect and range from gently to steeply convex with fairly smooth and unimodal laminae, some topset laminae resemble conical profiles. Synoptic relief is moderate with good inheritance and laminae are seemingly continuous with deep cuspate depressions between the columns. A massive carbonate grainstone layer coats the columnar stromatolites and is thicker at the crest of the bioherm (5 cm) compared to the sides (3 cm). It has a sharp contact with circular and "wormy" silicified features while carbonate (grainstone/micrite?) infill the spaces.

The bioherm is overlain by a 5-15 cm, recessively weathered layer, then flat undulating to gently domal stromatolites with a few more probable walled and columnar stromatolites (Fig. 11). They are overlain by a set of three low domal hemispheric stromatolites that are linked contiguously, gently convex with wavy to wrinkly laminae, which are parallel stacked with moderate degrees of inheritance (Fig. 11B). Vertically oriented, stubby silicified features that are at times radiating initiate directly atop the low domal stromatolites. The overlying layer is recessively weathered providing an aerial view of the vertically oriented structures. They are semicircular (~1 cm in diameter, ~3 cm tall) and cluster in places but are also stand alone with seemingly massive carbonate infilling the spaces between (Fig. 11C).

Above them is a 3-4 cm thick silicified unit with short locally linked slender to stubby columnar stromatolites that are steeply to gently convex respectively. They have smooth laminations with low synoptic relief and good inheritance. The narrow stromatolites are commonly turbinate and otherwise cylindrical in shape and associated with vertically oriented features between columns (Fig. 11D, E, & F).

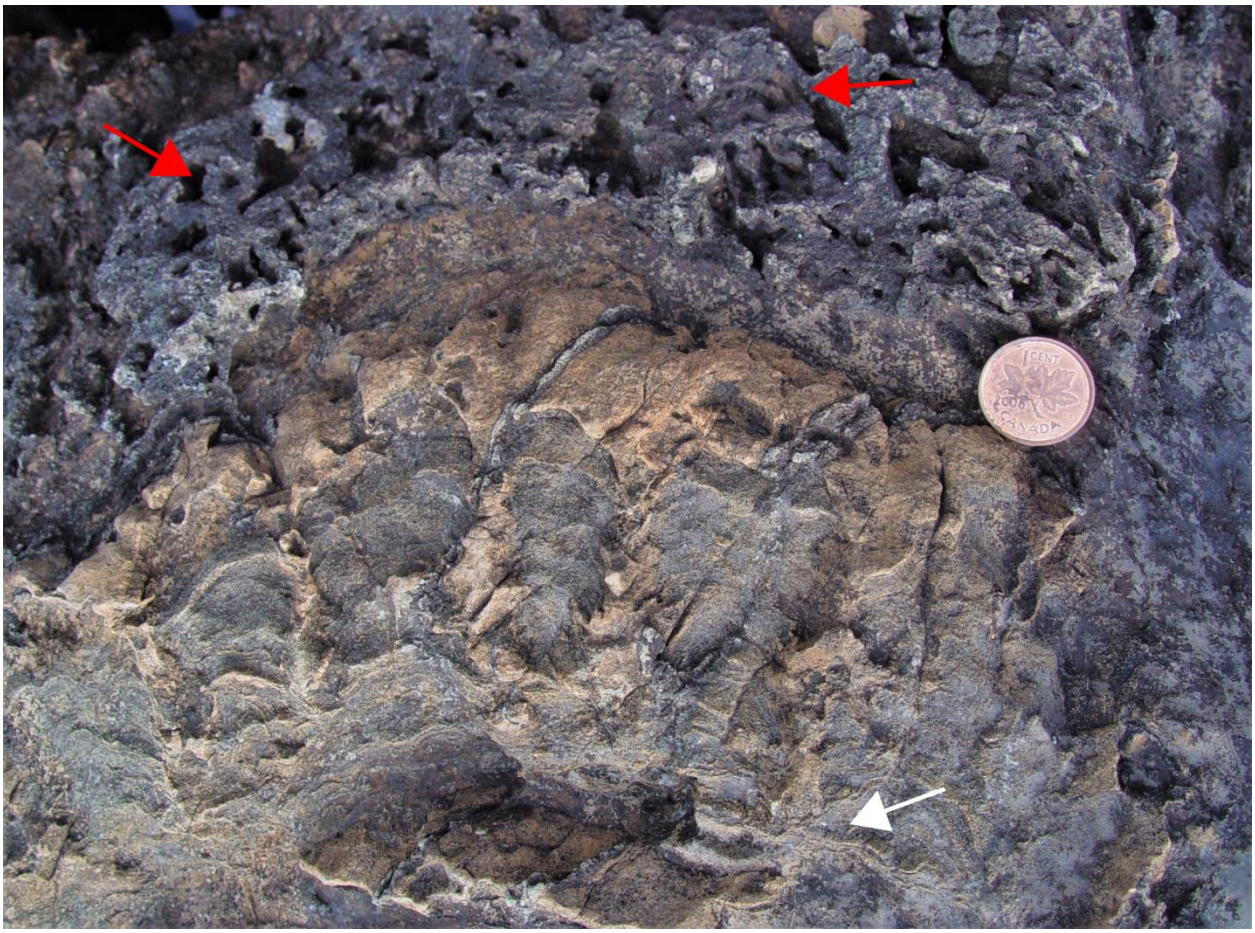

Fig. 10. Unit E. Domical bioherm comprised of stratiform to domal then columnar stromatolites overlain by a massive carbonate grainstone layer then silicified microbialite reminiscent of roll up structures or stromatolites that toppled over (red arrow). Note white arrow where the columnar stromatolite lamination initiates from the underlying domal stromatolite. Stromatolites are laterally linked with low synoptic relief and walled simply. Coin is 1.9 cm in diameter.

4.2.6 Unit F: Clastic Carbonate

Unit E gradationally becomes Unit F with thin beds (~3 cm thick) of parallel laminated, coarse textured carbonate. Thin slightly wrinkled bedding plains are partially silicified and thus more resistive to weathering (Fig. 12). Original grainsizes have been hidden by recrystallization though the silicified bedding planes lie at low angles that are truncated by horizontal beds (Fig. 12B & C). They are followed by half a meter of parallel laminated carbonate then largely recrystallized carbonate.

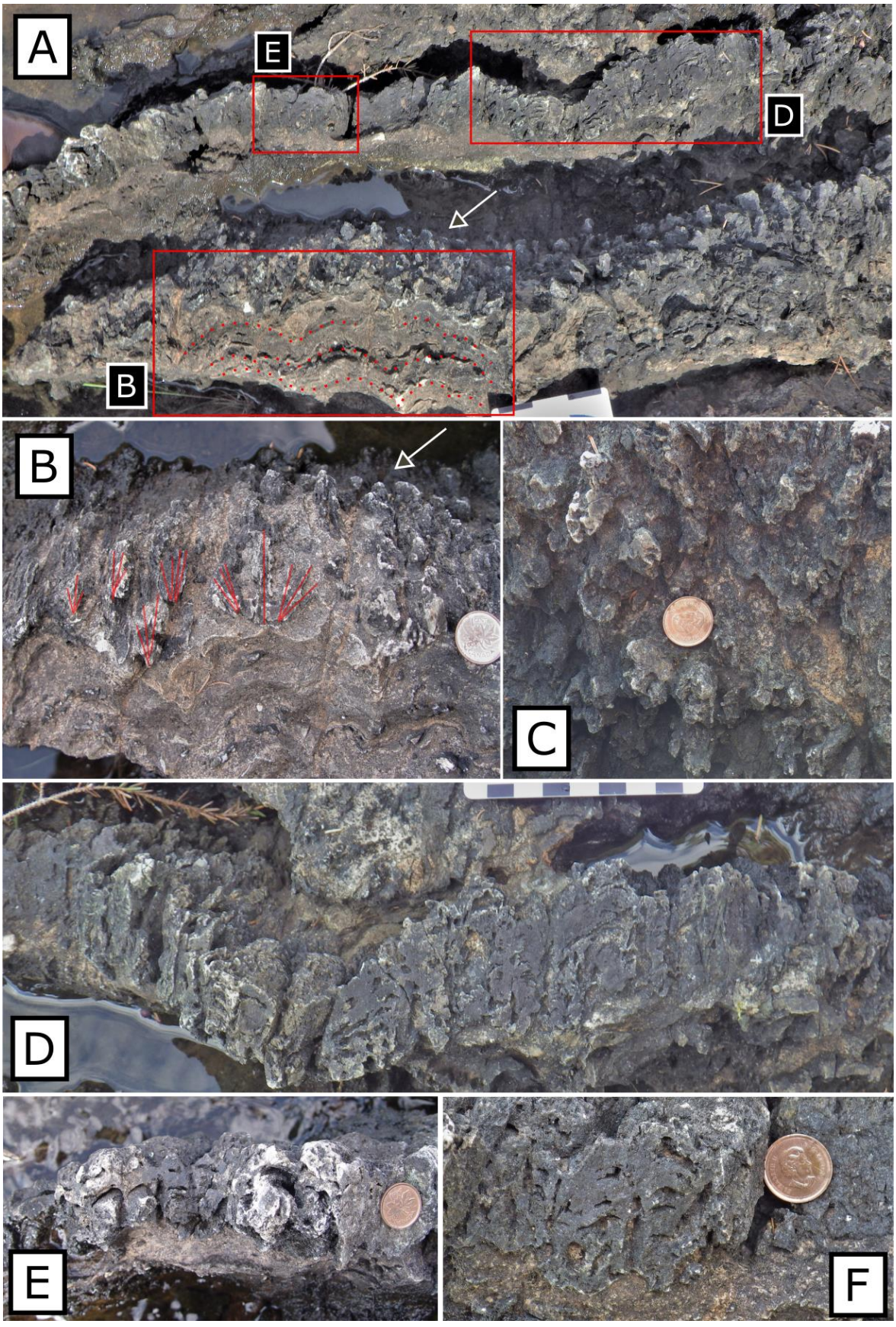
A
E
D
B
B
C
D
E
F

Fig. 11. (previous page) Unit E continued. A) A set of 3 laterally linked, low domal stromatolites, highlighted by red dots in box 'B'. The domes are directly overlain by silicified vertically oriented and often radiating structures, followed by a recessively weathered bed, then silicified small domal to columnar stromatolites seen in box 'D' and 'E'. B) Close-up of laterally linked domal stromatolite lamination and radiating silicified features highlighted in red. The arrow in the top right shows where photo in C) was taken. C) A bedding plane view of the pointed tops of the vertically oriented silicified features with carbonate infilling the spaces between (orange). D) Close-up of laterally linked silicified stubby columnar stromatolites with low synoptic relief amongst vertically oriented structures. E) Close-up of silicified stromatolites, initiating atop massive carbonate grainstone. Note that most stromatolites in this bed are cylindrical but a few are terete (triangular) shown in F). Coin is 1.9cm in diameter.

4.2.7 Unit G: Carbonate Microbialite

Overlying the cross-stratified, parallel laminated and massive probable grainstones are poorly defined remnants of larger domal stromatolites approaching 75 cm tall. They appear to be linked contiguously, cylindrical, gently convex and smooth with low synoptic relief, and their lateral continuity seems partially discontinuous (Fig. 13). They appear to initiate atop flat stratiform stromatolites and are overlain by convolute, silicified carbonate for 30 cm followed by more stratiform stromatolites that are in places silicified for 15 cm. They are overlain by a seemingly massive layer of carbonate that extends for 50 cm. A sharp contact with a 2cm layer of partially silicified carbonate is overlain by stratiform stromatolites, which become columnar stromatolites that are comparatively medium-sized, reaching 20 cm tall with moderate synoptic relief. They are similar to the underlying columnar stromatolites in that they are: linked contiguously, simply walled and cylindrical, with smooth gently convex lamination and good inheritance. However, they initiate directly atop flat, smooth, stratiform stromatolites instead of domal stromatolites, reach 20 cm in cumulative height, have partially silicified walls, and one stromatolite is epinastic where the top half of the column bends to the right while the columns on either side are erect. However, this column may be normal or slightly divergent and branching. The top of another stromatolite begins to branch as well (Fig. 13C). The pseudocolumns are overlain by partially silicified carbonate.

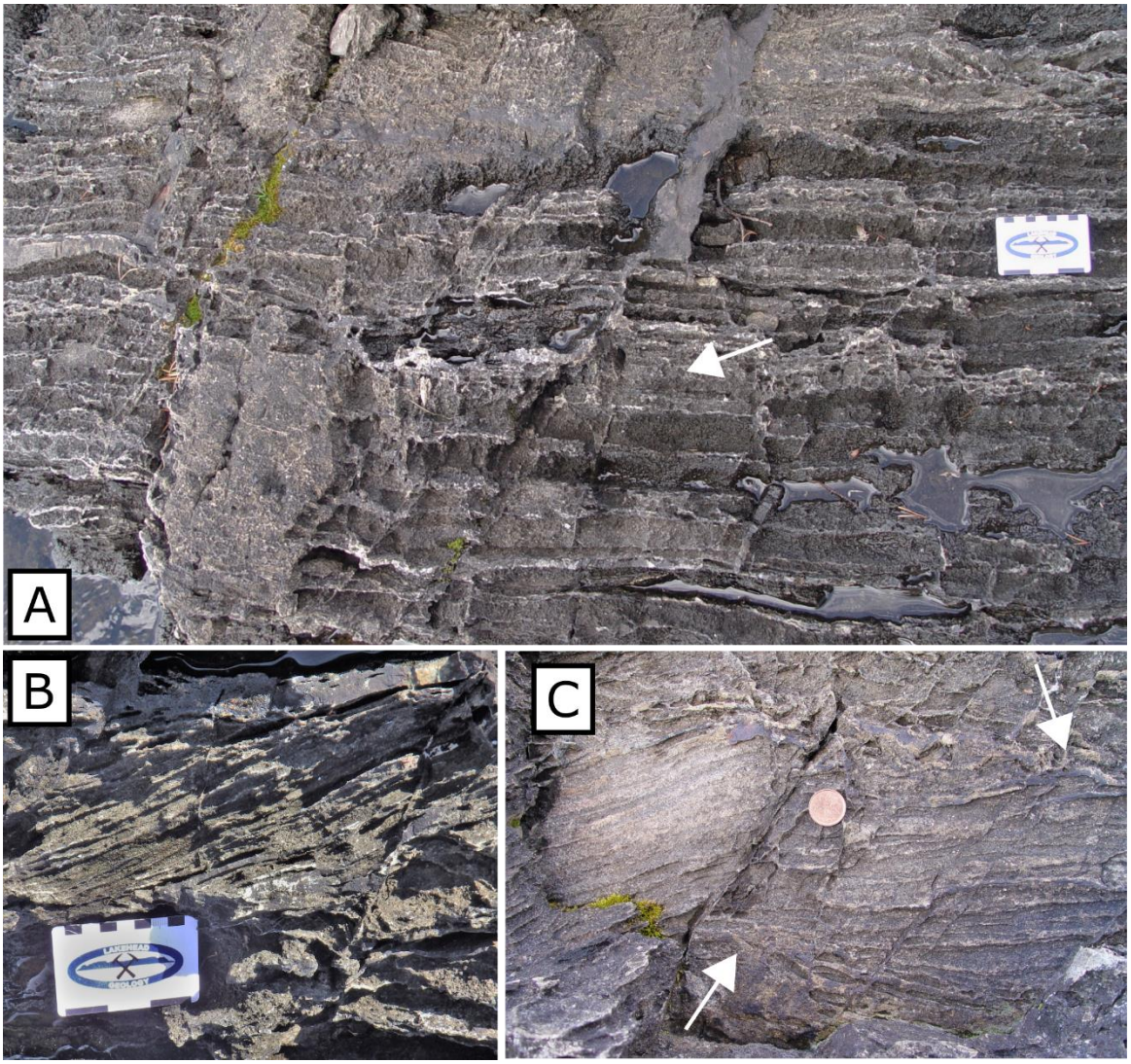

Fig. 12. Unit F. Coarse fabrics tentatively considered grainstone or packstone. A) Parallel laminated carbonate grainstones. B) bed of low angle cross-stratification overlain by a non-dipping silicified bed. C) cross-stratification in carbonate grainstones with dipping sets (white arrows) erosively truncated by overlying laminae. Coin is 1.9 cm in diameter.

4.2.8 Unit H: Carbonate Grainstones and Silicified Microbialite

This northern sequence ends with a ~4m thick poorly sorted and chaotic assemblage of sub-angular fragments and oblong rectangular blocks within a finer grained recrystallized matrix. In places the matrix has faint horizontal laminations. The fragments are roughly 5 by 10 cm and

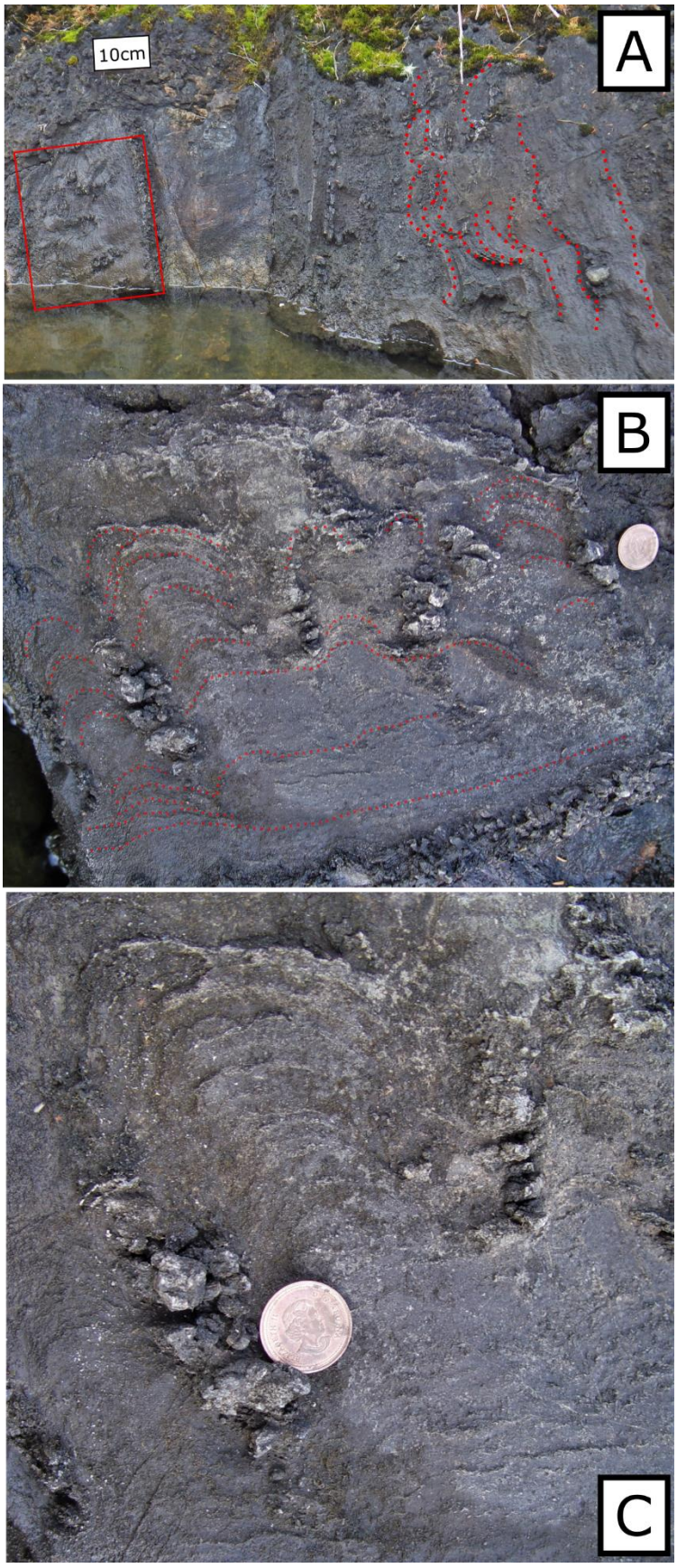

Fig. 13. Unit G. A) Poorly defined low domal to columnar stromatolites (highlighted by red dots) initiate atop stratiform stromatolites. Above them medium sized walled, laterally continuous columnar stromatolites develop atop stratiform stromatolites. Top to left. B) Close-up of the erect stromatolites with one epinastic (top half bent to the right) or slightly divergent and branching columnar stromatolite between them with red dots accenting some lamination. C) Close-up of the stromatolitic lamination, showing a smaller stromatolite was developing on the top left. Lamination is laterally continuous with good inheritance and moderate synoptic relief. Coin is 1.9 cm in diameter.

the rectangular blocks range in size from 0.10 by 0.45 m to 0.30 by 0.15 m. Some fragments are largely recrystallized and seemingly massive while others retain partially silicified laminations. Few large (1 by 0.5 m tall) remnant domal features and large areas of contorted partially silicified laminations are also present. The silicified beds are ~1 cm thick and alternate with recrystallized carbonate averaging a few centimeters thick. In a localized area the parallel laminations are crosscut by a 20 cm thick seemingly massive carbonate unit that slightly offsets and bends the parallel laminations toward the same direction (Fig. 4). This feature is overlain gradationally by more of the chaotic assemblage with randomly oriented fragments and irregular, wavy to crinkly silicified features.

4.3 SOUTHERN LOCALITY DESCRIPTION

4.3.1 Unit I: Carbonate Microbialite

The base of the sequence at the second locality is comprised of two 10 cm thick beds of silicified vertically oriented and slanted structures (Fig. 5). Although they are entirely recrystallized the silicified features are arranged with a spherical fabric (Fig. 5B). Hofmann et al. (1985, Fig. 15) noted these structures at the base of the section to be problematic columnar structures due to their lack of primary convex lamination and presence of roughly concentric silicified shells in some columns. These silicified beds alternate with grey-blue limestone comprising dark organic rich, millimetric, horizontal and wrinkly lamination, which are highlighted by discontinuous and blebby chert laminations (Fig. 5B & 14). Hofmann et al. (1985) termed these features stratiform structures (1985; Fig. 11). They are recrystallized and exhibit non-couplet, mostly gradational laminations between smooth to wrinkly, light and dark grey-blue laminae (Fig. 5B). The laminae have low to moderate degrees of inheritance and are semi-continuous. Elongated fenestrae appear more abundant toward the top of the unit in close association with the dark, semi-continuous and partially, to completely, silicified laminae (Fig. 14). Two vertically oriented and cross cutting laminated features 5 cm thick are present in the last meter of section, one contact is straight and light coloured carbonate while the other is irregular and dark (Fig. 14B, C, & D).

4.3.2 Unit J: Grainy Carbonate

The underlying stratiform structures quickly become very finely bedded, millimetric, smooth, isopachous and continuous laminations for 50 cm then become softly bent or

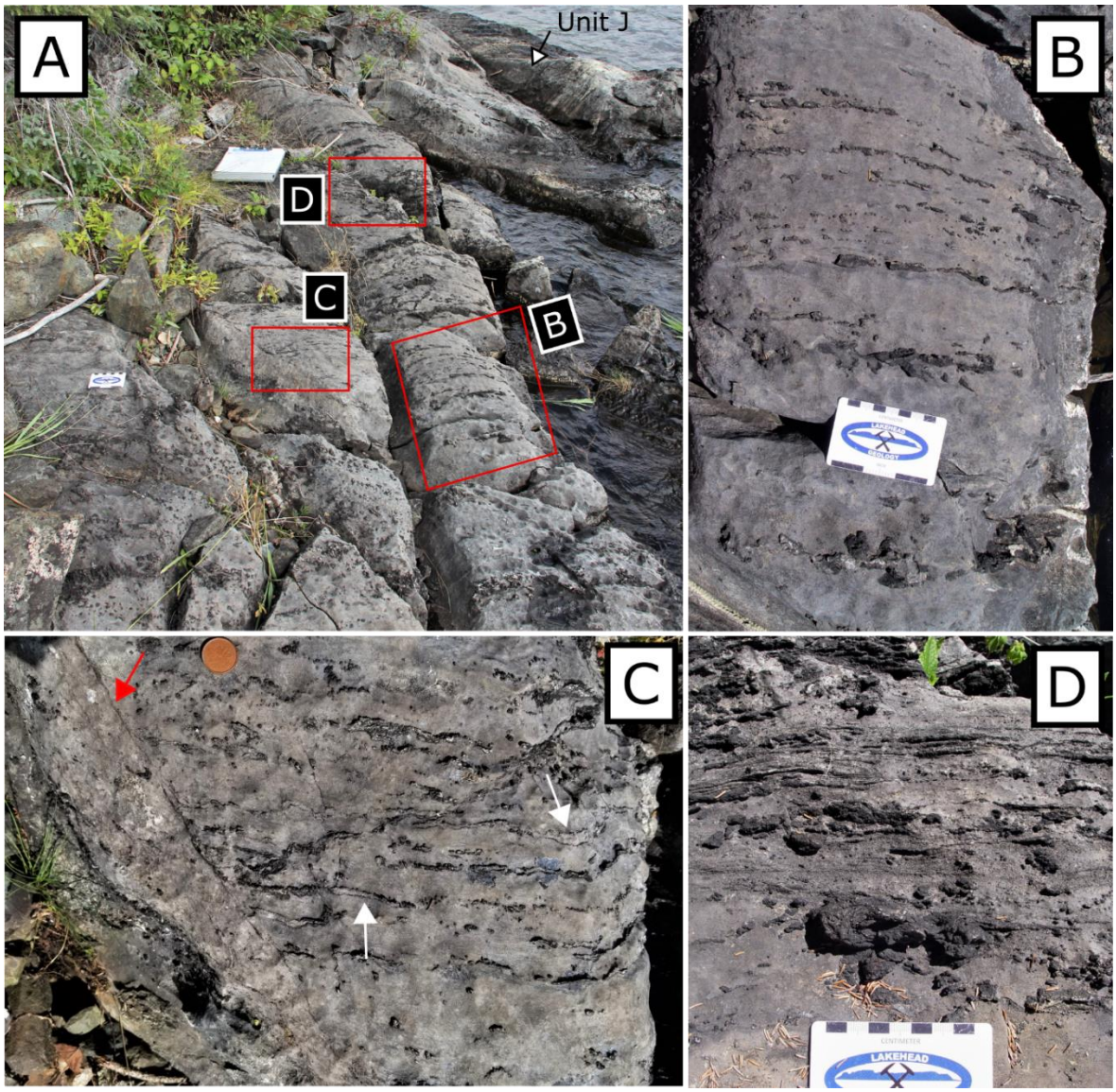

Fig. 14. Unit I. A) Some of the outcrop exposure at the base of the southern locality, displaying the spatial relationship with Unit J. Close-up photos in B, C, and D. B) Close up of blebby and discontinuous silicified laminae. C) Note the light cross cutting feature (red arrow), and the stromatactis filled with white cement and outlined with dark organic rich micrite (white arrows). D) Parallel and isopachous millimetric cherty lamination gradationally becoming Unit J. Coin is 1.9 cm in diameter.

deformed but remain isopachous and continuous (Fig. 14D & 15). The slightly bent laminations contain very subtle peaks and depressions that accent their isopachous nature (Fig. 15D). A localized area (Fig. 15E) is abruptly divided into a dozen or so thin columns, 2-3 cm wide over 40 cm stratigraphically and have visibly sharp contacts with one another, the parallel laminations are offset, yet they maintain millimetric, straight isopachous laminations that are often slanted in one

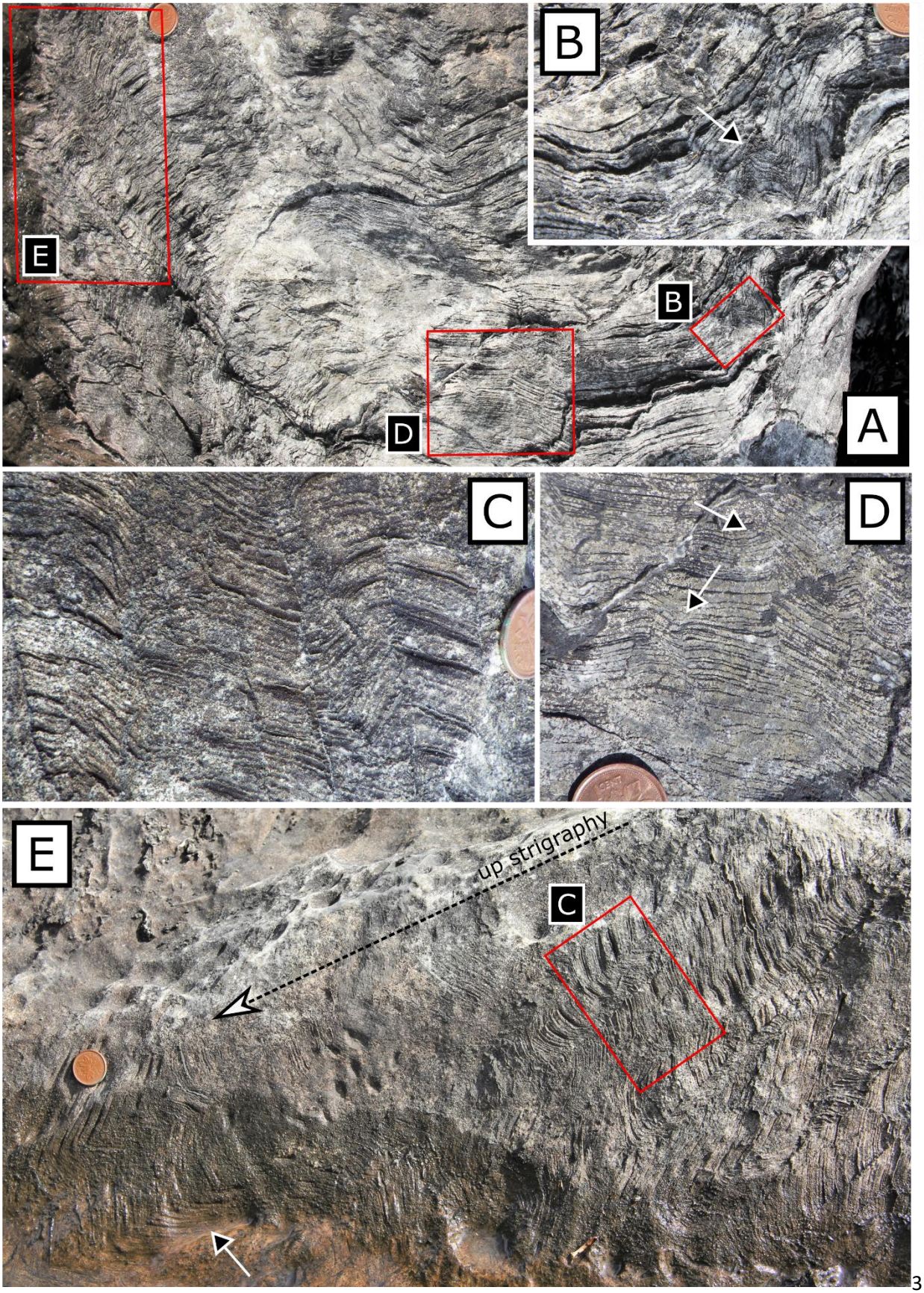
B
E
B
D
A
C
D
E
up strigraphy
C

Fig. 15. (previous page) Unit J. Stratigraphic up is toward top of page for A, B, C and D. A) Cross sectional view displaying the spatial relationship of the close-up photos in B-E. Black millimetric and isopachous lamination is very smooth and continuous. B) Lamination exhibits rare zig-zagged features (arrow) and otherwise is loftily bent, with subtle tufted peaks and depressions (arrows) (D). The lamination becomes locally offset with a number of sharp contacts making columns of slanted lamination in a complex chevron pattern (C). The offset lamination quickly become continuous conical or zig zagged patterns (E). Coin is 1.9 cm in diameter.

direction or the other (Fig. 15C). They are offset for 40 cm then quickly become laterally continuous again, producing a zig-zag pattern where the depressions and peaks of the pattern align with the sharp contacts that previously offset lamination (Fig. 15E). The zig zag laminations are commonly bent at acute or slightly obtuse angles.

4.3.3 Unit K: Carbonate Microbialite

This 30-meter-thick carbonate microbialite unit is comprised of 5 main features considered here as sublithotopes; undulatory stromatolites, fenestrated thrombolites, fenestrated domal stromatolites, banded carbonate and narrow columnar stromatolites, in relative order of abundance. They are frequently closely intermingled with one another. In many scenarios they may be considered a composite microbialite where it exhibits attributes from all 5 sublithotopes. Here they are termed fenestrated microbialite. Fenestrae commonly range in shape depending on which sublithotope they are associated with though they are consistently filled with white cement that is usually blocky or its recrystallized equivalent. Additionally, the fenestrae are either outlined entirely or partially with a dark organic-rich micrite which shows up black on SEM imagery (Fig. 16). The mega and macrostructure of some features are often unidentifiable due to outcrop exposure and visibility.

Clean exposed patches of the outcrop exhibit stratiform to undulatory stromatolites, much like Unit I, though they also consistently contain thin elongated fenestrae and stromatactis intercalated with other sublithotopes, particularly low domal fenestrated stromatolites and fenestrated thrombolites (Fig. 17).

Polymorphic mesoclots with variable and inconsistent shapes of various light shades of gray within a typically dark matrix characterize sporadic thrombolitic fabrics. The mesoclots are typically diffuse with indistinct borders and their major axes are often aligned horizontally, lying

parallel to thrombolite growth axis or normal to inferred bedding. Otherwise, they are oriented randomly, often oblong in shape or lobate and less frequently saccate. They are internally massive and commonly associated with fenestrae of similar shapes to the mesoclots except the fenestrae are most frequently saccate and lobate. (Fig. 18).

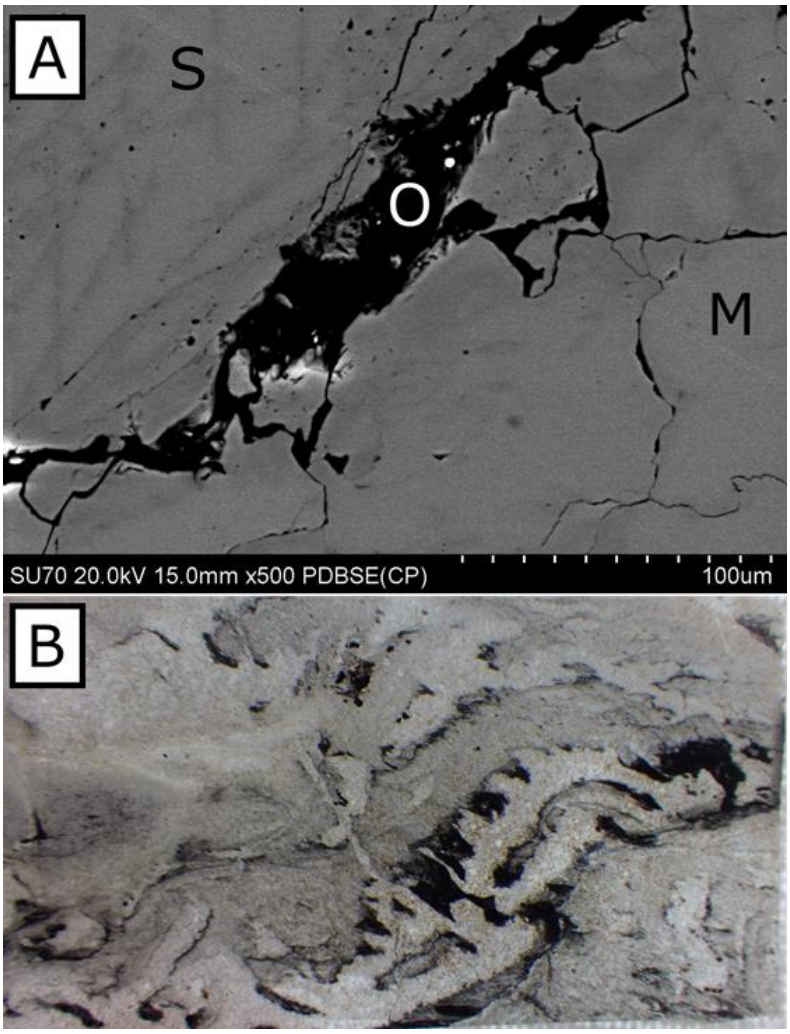

Fig. 16. Unit K. A) SEM back-scatter electron image of the boundary between a white fenestral cement, labelled S, the black organic-rich micritic coating labelled O, and the surrounding carbonate matrix, labelled M. B) Close-up of the petrographic thin section analyzed in A.

Low domal fenestrated stromatolites typically initiate on layered undulatory microbialite or banded carbonate. Smaller domes (1-2 cm wide by 1.5 cm tall) are usually isolated while the larger domes (3-5 cm wide by 4-5 cm tall) are usually locally linked and contiguously or closely

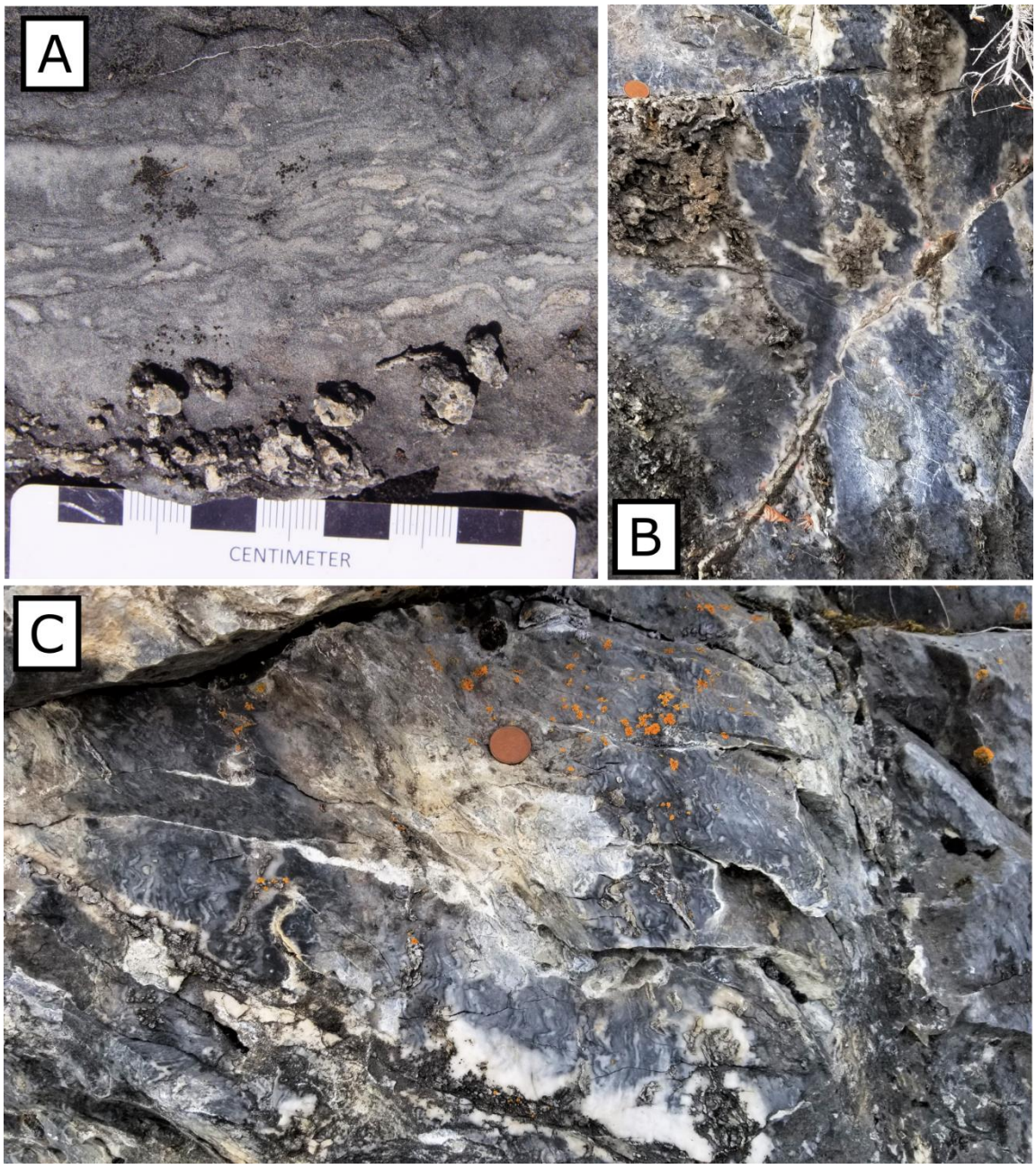

Fig. 17. Unit K, outcrop exposures, up for B and C is to the right. A) Displays an example of the interpreted elongate fenestral microbialite with silicified blebs. B) Example of the typical nature of the bedded gray-blue microbial carbonate alternating with poorly preserved thin beds of silicified microbialite. Silicification often produced a white halo of carbonate surrounding it. C) Segment with more prominent fenestral carbonate comprised of undulatory stromatolites and abundant fenestrae amongst lesser silicified microbialite. Coin is 1.9 cm in diameter.

spaced. They are domical and hemispherical in shape, crustose to stubby in size. In outcrop and polished slabs, the lamination exhibits parallel, non-couplet patterns and are commonly intercalated with crescentic stromatactis or fenestrae (Fig. 19). Laminations are typically smooth to wavy and unimodal with low relief and moderate inheritance. They are discontinuous and at times irregular especially with respect to the fenestrae.

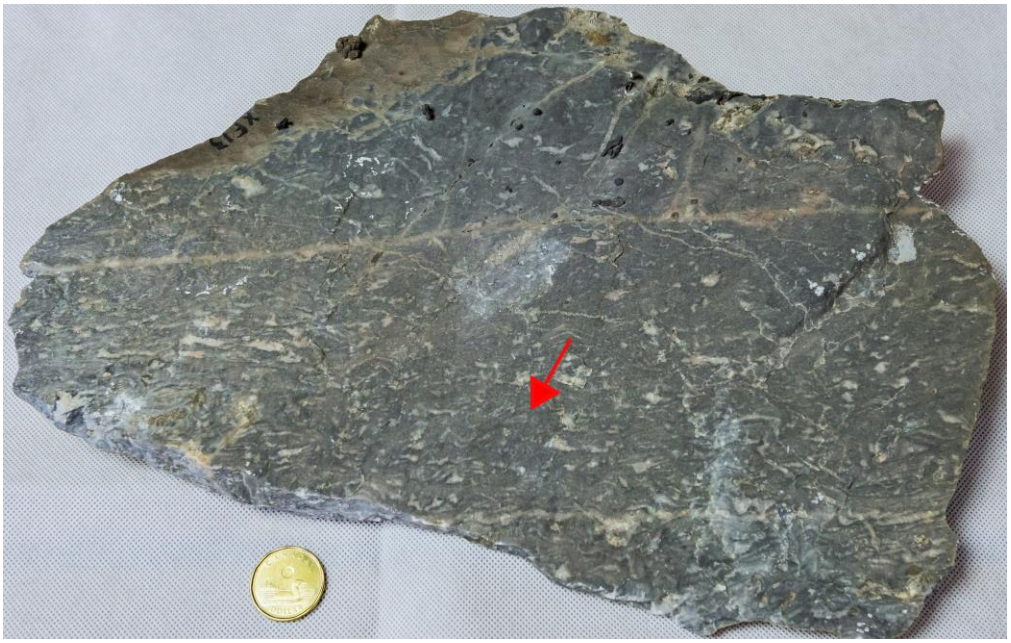

Fig. 18. Unit K. Fenestral thrombolites with various shades of light gray polymorphic mesoclots of varying elongate shapes within a dark micritic carbonate matrix. They are associated with white fenestrae and tend to follow general bedding planes. Coin is 2.6cm in diameter.

Narrow columnar stromatolites are evident in a range of sizes from 2 to 10 cm tall and frequently initiate atop stratiform or undulatory microbialite that are bifurcate or beta branching in appearance (Fig. 20). They are slender, unlinked and isolated, cylindrical and columnar and most commonly uniform though constringed in places with simple walls. They are mostly erect and potentially inclined though preservation and deformation makes it difficult to discern. In polished slabs couplet laminar patterns were observed with parallel, even alternations that are intercalated with crescentic fenestrae in places (Fig. 20). The laminae are gently to steeply convex and some

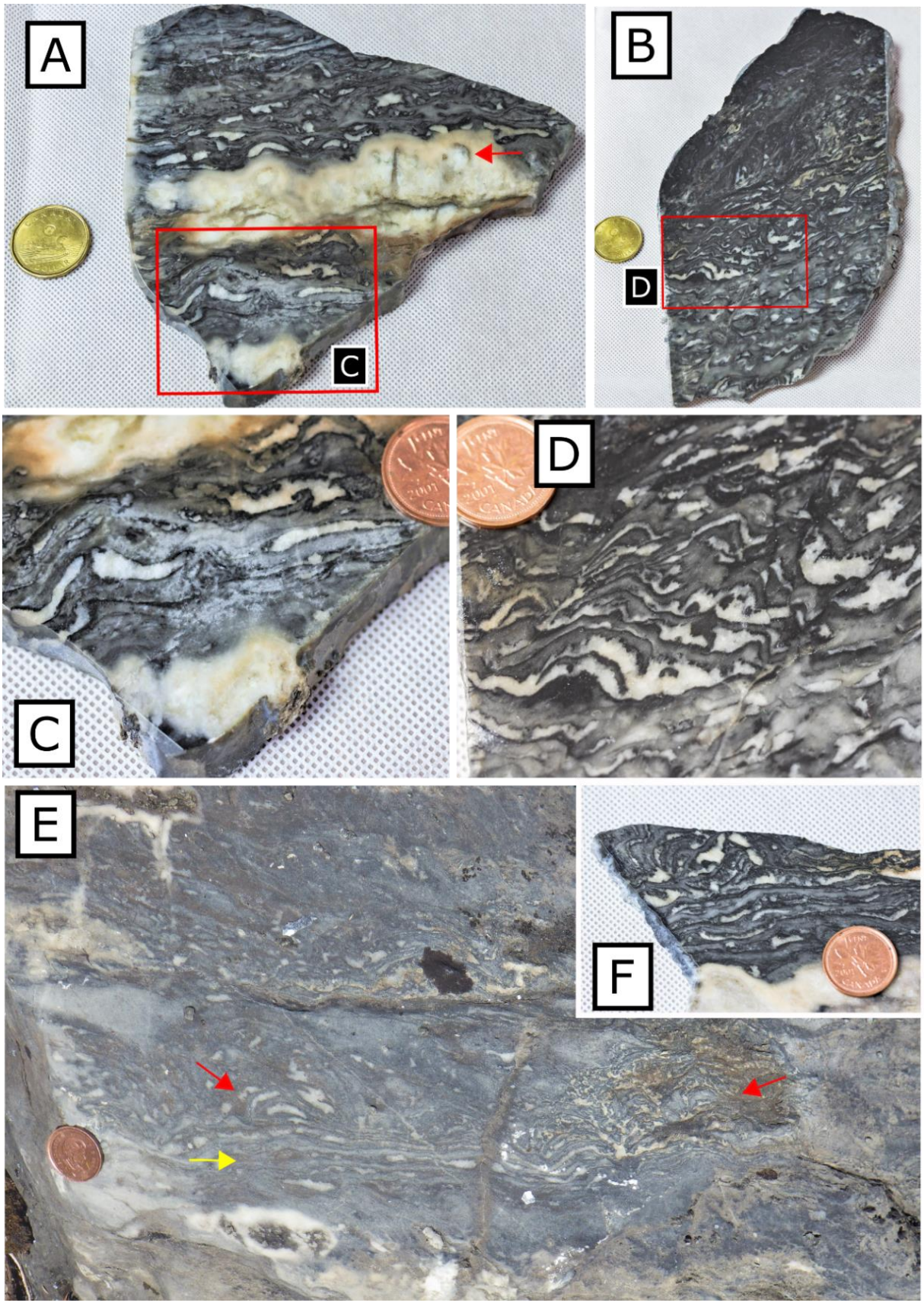
A
B
C
D
C
D
E
F

Fig. 19. (previous page) Unit K, low domal fenestral stromatolites. A and B) two samples containing domal stromatolitic laminae that are various shades of gray, often gradational, discontinuous and intercalated with fenestrae and stromatactis. They exhibit low degrees of synoptic relief and inheritance. Sample in A) contains silicified microbial features with remnant domal shapes (arrow). C and D) provide close-ups of the fenestrated domal features. E) Illustrates domal stromatolites (red arrows) present in outcrop atop undulating stromatolitic and laminated carbonate (yellow arrow). Note red arrow on right showing a cluster of semi-continuous low domes. F) A polished slab of the left most dome and underlying laminated carbonate in (E). Coin in (A) is 2.6 cm in diameter and in (E) is 1.9cm in diameter.

are unimodal, while others are asymmetric and exhibit moderate synoptic relief with good inheritance. Though the columns are discontinuous the laminae themselves are continuous and macrolaminae are predominantly light in colour. Thrombolitic, i.e. mottled and clotted dark and light gray carbonate matrix infills the spaces between with an abundance of fenestrae and mesoclots. Fenestrae are typically elongate with a smooth base and irregular top, which is characteristic of stromatactis. Otherwise associated fenestrae are crescentic, lobate and saccate.

Banded or laminated carbonate is comprised of sharp alternating beds of thicker light (1-3 cm) and thinner dark (~3mm) carbonate. The dark micritic bands are often associated with smooth elongated fenestrae. Lighter bands commonly contain mottled dark blotches. In places the light bands contain an abundance of micritic carbonate making them appear darker overall (Fig. 21). They are frequently associated with the other lithotopes, for example: in one location they are underlain by thrombolitic and clotted fenestrae microbialite with few domal features and overlain by stromatactis, elongate fenestrae microbialite, and undulating stromatolites (Fig. 22). In places, the dark lamination has a sharp bottom contact and wavy top (Fig. 23). Additionally, they are often associated with highly silicified structures that retain faint remnants of slender vertically oriented or domal features (Fig. 21). Microfabrics appear to indicate fine to medium grainsizes although recrystallization inhibits proper judgement.

4.3.4 Unit L: Carbonate and Silicified Microbialite

Unit K quickly becomes irregular, yet horizontal, silicified beds averaging 4 cm thick that alternate with 10 cm thick seemingly massive carbonate grainstone or micrite. This unit is very similar to Units B and D from the northern locality, however; fenestrae and ghostly or faint remnants of columnar stromatolites are visible between the silicified beds in drill core and the

silicified structures are defined into more distinct domal shapes, though altered green and largely lacking laminations.

Fig. 20. (preceding page) Unit K, narrow columnar stromatolites. Red boxes denote close-up photos. A) Tall, slightly sinuous and very slender stand-alone columnar stromatolites amongst irregular, thrombolitic microbialite with abundant irregular fenestrae and few stromatactis. B) A few narrow columnar stromatolites with ghostly lamination that exhibit non-couplet and gradational contacts between laminae, some initiate atop a wider column, producing a branching appearance (box 'F'). The ghostly appearance may be due to the quality of preservation. D) Smaller slender columns with more distinct laminae (box 'C'). They are overlain by an abundance of clotted and irregular lobate fenestrae (yellow arrow), then smooth, flat lying laminae reminiscent of low domal stromatolites (red arrow) followed by some laminated carbonate with elongate fenestrae (blue arrow). Note that the laminae within these narrow columns are not intercalated with fenestrae as much as the low domal stromatolites in Fig. 19. Nor are they closely associated with elongate fenestrae, but lobate and irregular fenestrae instead.

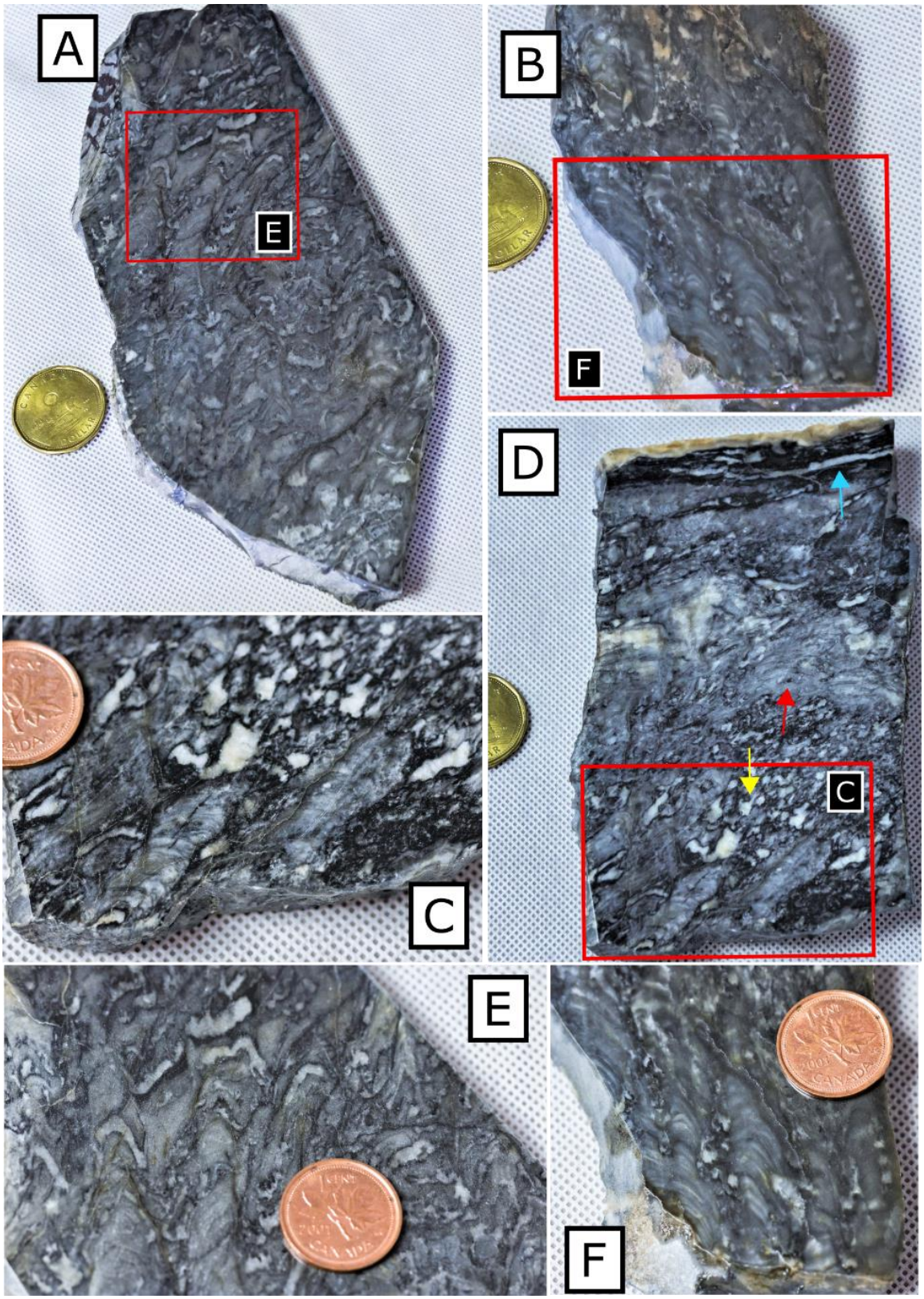
A
E
B
F
D
C
C
E
F

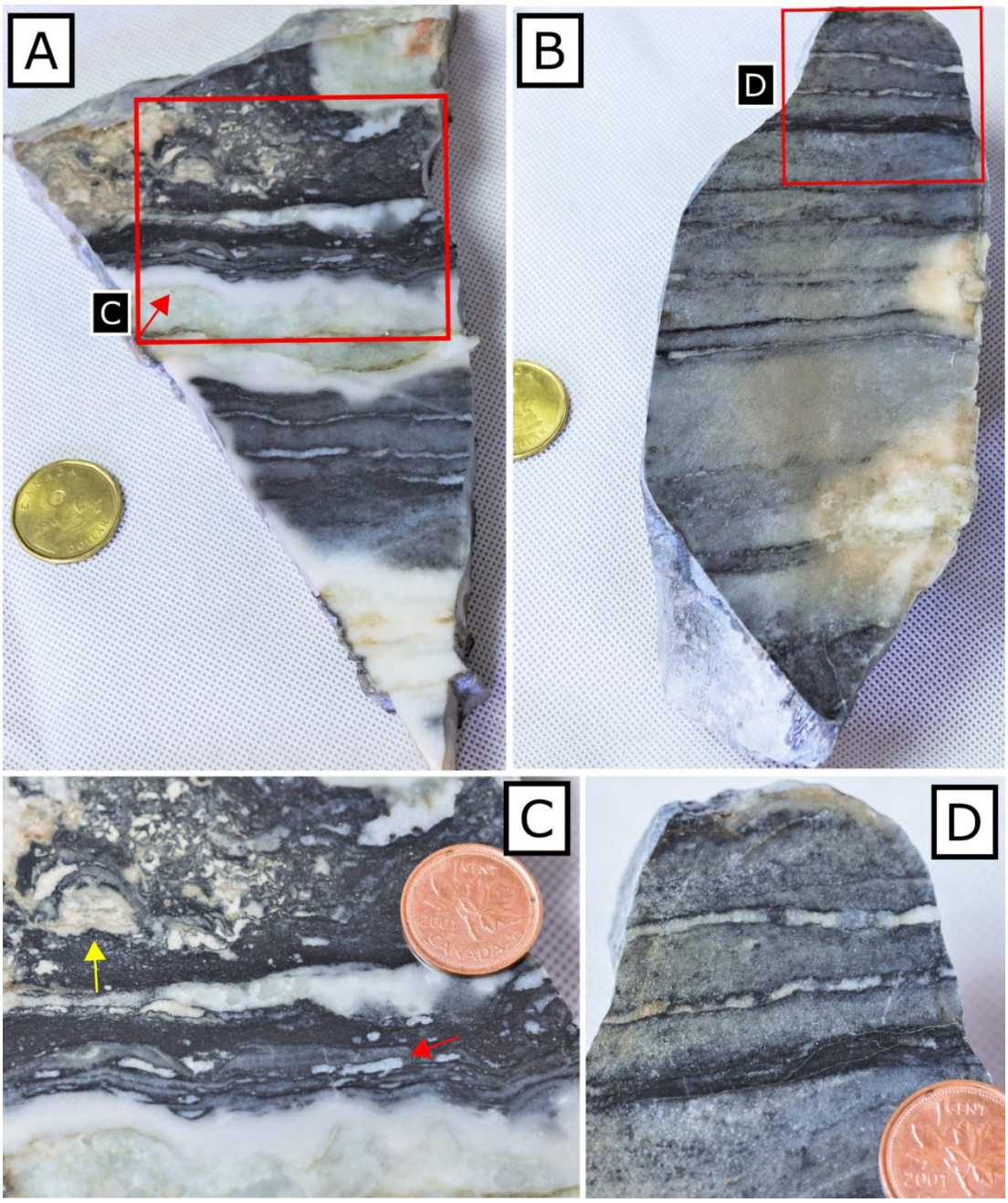

Fig. 21. Unit K, banded carbonate. A) Centimetric beds of light gray carbonate contain an abundance of dark mottled blotches of organic-rich, micritic textured carbonate at the base of the sample, compared to the few blotches in the layered sample shown in 'D'. Beds are separated by smooth elongate fenestrae and some stromatactis that are all rimmed by dark, carbon-rich material. The center of the sample in 'A' contains silicified microbialite that has a remnant domal top contact (arrow) and an undulating basal contact with a white silicified hallow surrounding the feature. C) Close-up photo displays undulating relatively continuous lamination with few elongate fenestrae (red arrow) underlying a silicified bed and a partially silicified domal feature (yellow arrow) next to clotted and irregular fenestrae. B and D) Display a similar centimetric example of banded carbonate that is lighter with lesser organic matter.

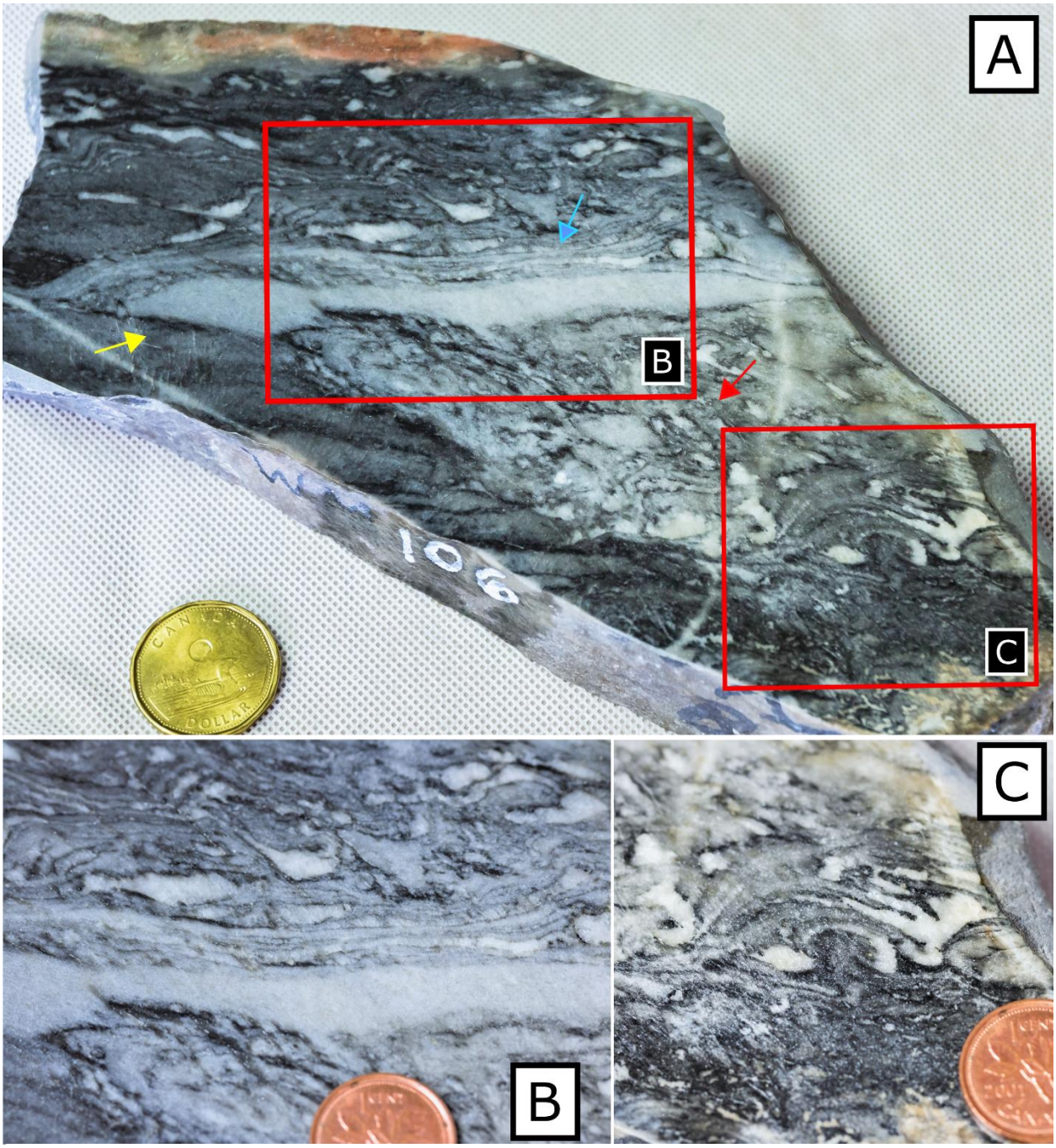

Fig. 22. Unit K. A) Banded carbonate underlain by domal (box 'C') and clotted/irregular fenestrated microbialite (thrombolite?) (red arrow) and overlain by undulating microbial or laminated carbonate (blue arrow). Note the eroded edge or onlapping growth of banded carbonate along the left side, juxtaposed to the fenestrated microbialite (yellow arrow). B) The single centimeter thick, light coloured carbonate band overlies the layered banded carbonate on the left. Note the clotted nature underlying the band and the laminated nature above. C) Domal shaped fenestral microbialites.

Fig. 23. Unit K. Banded carbonate exhibiting dark beds with sharp smooth basal contacts and wavy tops that become mottled, wispy and irregular to the right with sporadic fenestrae.

4.3.5: Unit M Grainy and Microbial Carbonate

This segment is visible in both cross sectional and plan view from within Woman Lake narrows at the northeastern most extent of the exposure at the top of locality 2. The way weathering preferentially erodes carbonate and the orientation of the sequence provides a spectacular three-dimensional view of distinct silicified framework retaining the original structure and in places lamination of low domal stromatolites. These stromatolites continue to alternate with massive or parallel laminated carbonate toward the topmost meter of the sequence. Beds are laterally extensive for the extent of the exposure, where the outcrop remains. Stromatolites develop on the grainstone/micrite substrate and in plan view they are circular to ovate ranging from golf ball to baseball in size (Fig. 6, 24, & 25). They are often contiguously linked and domal, otherwise sporadically linked and closely spaced. They are either hemispheric or nodular, stubby, and in polished slab and thick sections remnant laminations are present. Laminae are couplet-like, parallel, seemingly even, range from gently to steeply convex in shape and are smooth, typically unimodal with moderate synoptic relief and high inheritance (Fig. 26). The walls between each dome are typically simple and their architecture is banded. In places, micro-columnar stromatolites develop atop the low domal stromatolites (Fig. 26A).

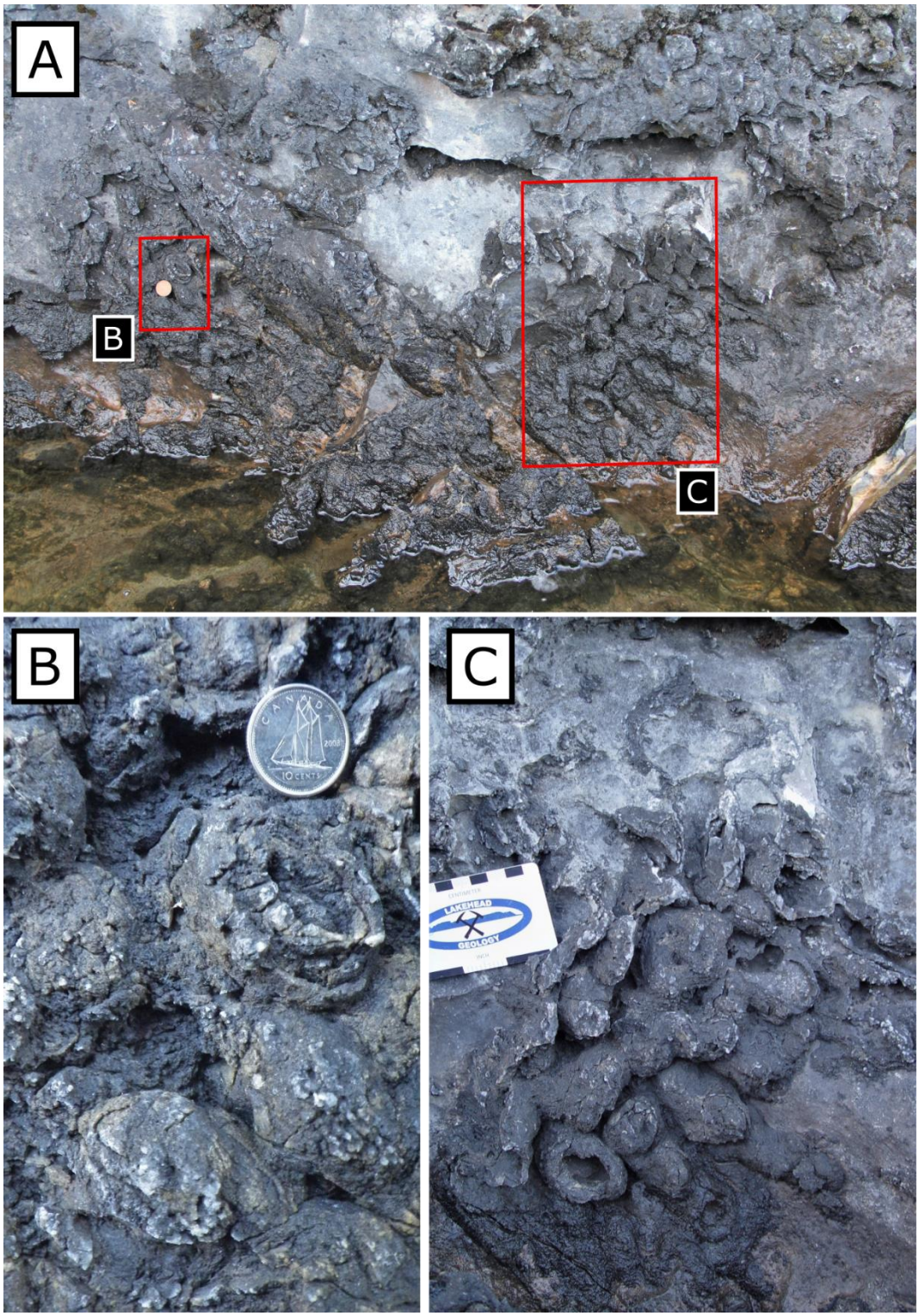

Fig. 24. Unit M. Partially silicified low domal stromatolites. A) Close-up of Fig. 5 at locality 2. In 'B' and 'C' note the clusters of silicified stromatolites are hollow, where the carbonate center has weathered out, and partially preserved on the basal bed. Some remain laterally linked, others have space surrounding the dome. Coin in A is 1.9 cm, coin in B is 1.8 cm in diameter.

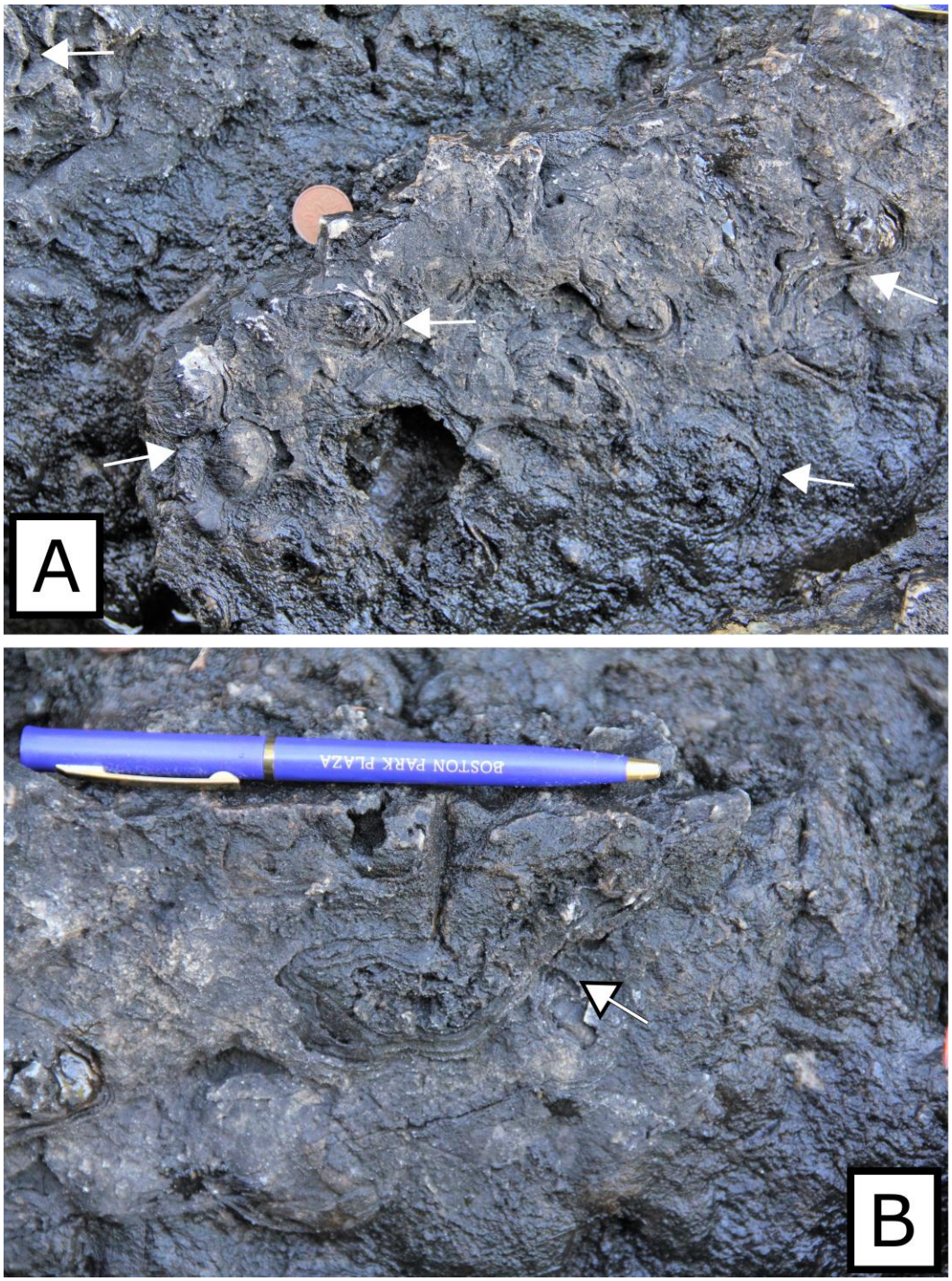

Fig. 25. Unit M. Beds of laterally linked silicified low domal stromatolites. Close-up of Fig. 5 (locality 2), to the left of drill hole. Note the rounded knobs of the stromatolite tops that frequently have recessively weathered and silicified lamination that encompass multiple stromatolites (arrows) indicating that they were or became laterally linked.

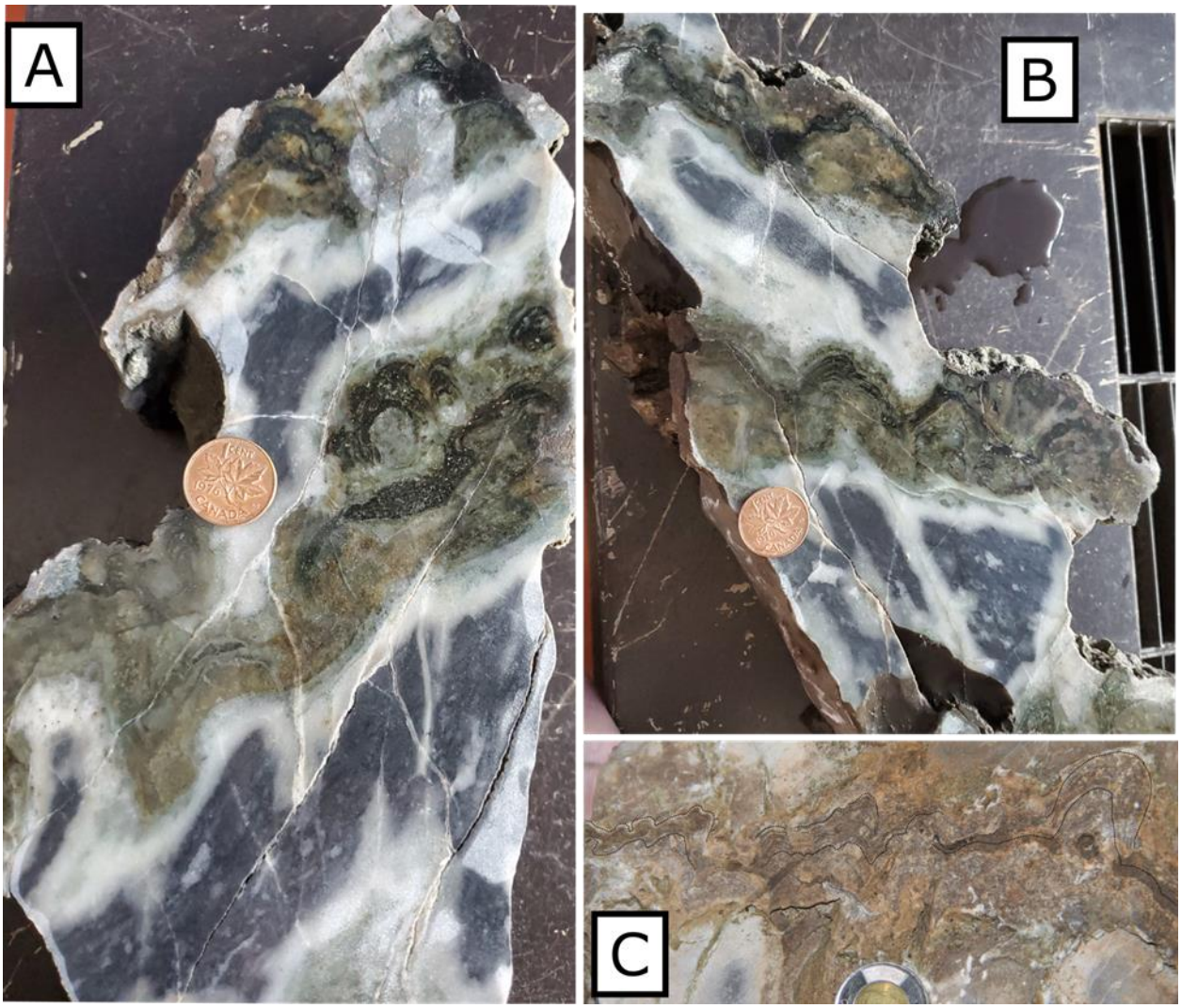

Fig. 26. Unit L. A and B) Polished slab of the laterally linked, domal, silicified stromatolites (green and black) alternating with fenestrated microbial carbonate. Note that the black lamination is very fine though mostly replaced by fibrous tremolite, actinolite and/or chlorite. The silicified stromatolites are commonly surrounded by a white siliceous carbonate halo. They initiate directly atop the microbial carbonate mounds or undulating surface and commonly occur in clusters with microcolumnar stromatolites developing on top of them. C) Weathered surface of laterally continuous stromatolitic lamination, top and bottom laminae are highlighted by black dots. Coin in A is 1.9 cm coin in B is 2.8 cm in diameter.

The silicified stromatolites alternate in a cyclic manner with approximately 10 cm thick beds of carbonate that is either parallel laminated or massive which are similar to the banded carbonate except that the lighter bands seem to show dark millimetric lamination within them (Fig. 27). Unfortunately, the crystals are neomorphic and the original grainsizes are greatly destroyed. The topset of the bed has a symmetrically wavy surface (Fig. 27).

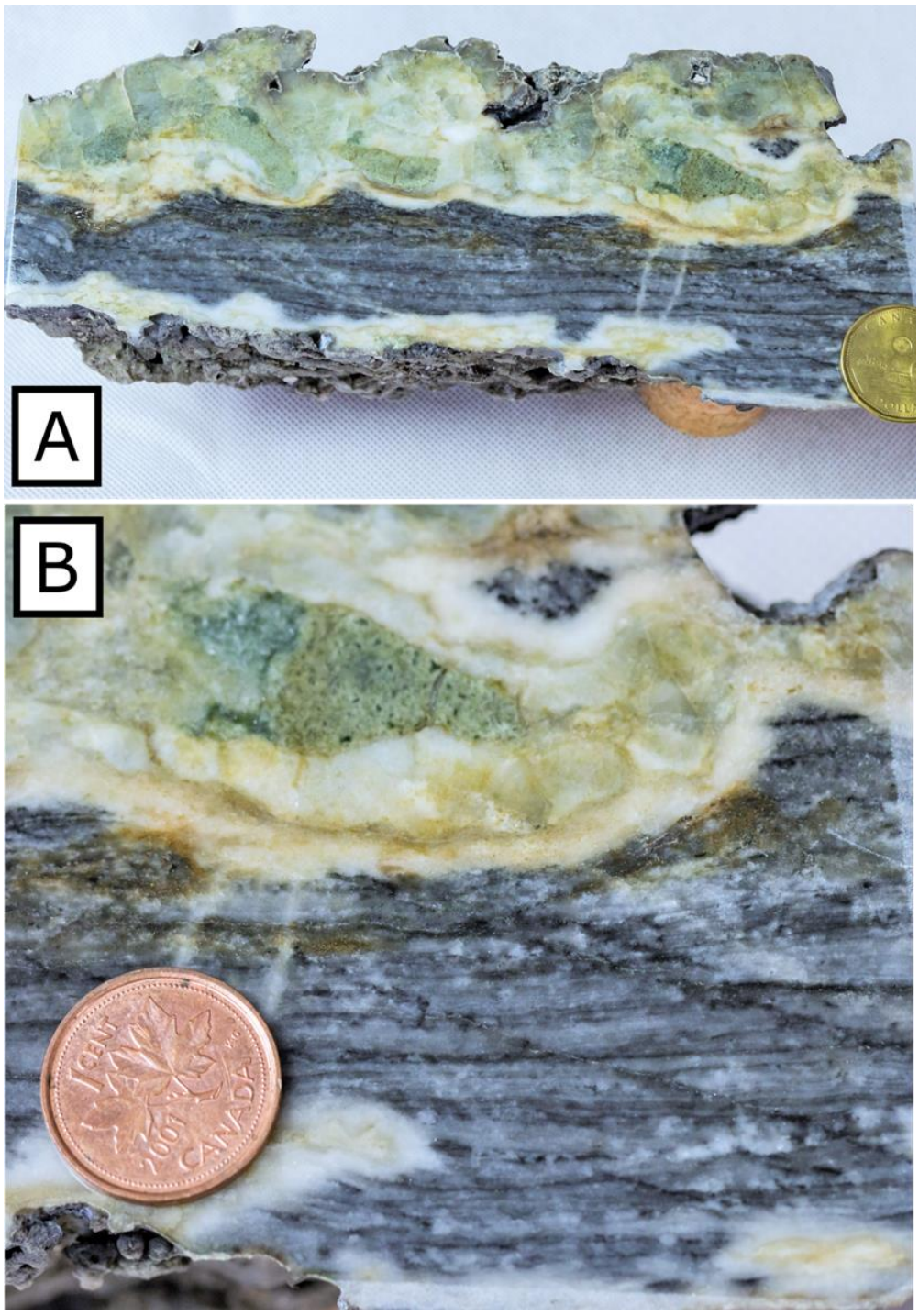

Fig. 27. Unit M. Polished slab of silicified stromatolites that only retain partial domal shapes and no stromatolitic lamination, overlying millimetric parallel laminated grainstone or laminated, recrystallized micrite.

4.4 EASTERN LOCALITY DESCRIPTION

4.4.1 Unit N: Carbonate Microbialite

This eastern locality strongly resembles Unit K in that it contains an abundance of fenestrated microbialite, though it mostly consists of undulatory stromatolites and banded carbonate with elongated fenestrae and stromatactis (Fig. 7 & 8).

4.5 DEPOSITIONAL ENVIRONMENT INTERPRETATIONS AND DISCUSSION

4.5.1 Stromatolite Morphology Implications: Background

Stromatolitic variants are the dominant diagnostic sedimentary structure present in WLC, which is both exciting and intriguing, however it complicates precise depositional environmental assessment. Perspective and depositional context is crucial to improving our understanding of paleoatmospheric-ocean conditions, particularly those that facilitated life and ultimately Earth's oxygenation. Not only paleoatmospheric-ocean conditions but our understanding of paleotectonic settings and carbonate platform evolution benefit from accurate and precise depositional environment assessments. It has been discussed that the appearance of thick carbonate platforms in the mid-Archean could reflect a significant environmental threshold (Fralick and Riding, 2015). Due to stromatolite's perseverance throughout geologic time and their various morphologies they provide good, respectful analogues to a variety of depositional environments. Their morphologies provide clues about their formation because both physical characteristics, intrinsic (microbial mat influence) and extrinsic (environmental influence) have an effect on stromatolitic development. Which means that energy, water depth, mat cohesiveness/strength, mat affinity to nutrients, sediment supply, and nutrient availability all contribute to a stromatolite's development and final morphology (Hofmann, 1976; Grotzinger, 1989; Dupraz, et al., 2006; Tice et al., 2011). However, the abundance of contributing factors typically blur distinct ways that certain forms can be made, meaning one morphology can form through a range of factors (Dupraz et al., 2006). Additionally, stromatolites that developed in the Paleozoic were exposed to different atmospheric conditions than those growing today, which are both vastly different than their Archean predecessors. Thus, exact depositional environmental assessments are complicated when based on stromatolite morphology alone, but accurate implications can be made.

Dupraz and others (2006) use DLA-CA (Diffusion Limited Aggregation-Cellular Automata) models to simulate stromatolite growth through interaction of a set of holistic variables

and provide a means to interpret small-scale features where diffusive transport dominates. Tice and others (2011) note that previous models generally fail to provide a natural explanation for hydrodynamic controls on mat and stromatolite morphology and review modern theory of spatial ecology, sedimentology, and biofilm mechanics. Together they show that the various parameters can produce four main morphologies within a range of tidal environments, some of which are represented within Woman Lake carbonates.

Thin discontinuous mat lenses in a detrital matrix (recrystallized and similar to host carbonate) and low lying stromatolitic morphologies for example, form when current induced shear stress is greater than mat cohesion on topographic highs, thus limiting mat development to hydraulically protected areas like topographic lows (Dupraz et al., 2006; Tice et al., 2011). This is very similar to the undulating to stratiform stromatolites in Units A, I and K (Fig. 3, 5, 17, & 22) and low lying discontinuous or only locally continuous fenestral domes in Unit K (Fig. 19). Isolated domes, columns and branching columns tend to arise when current induced shear stress is less than mat cohesion (Dupraz et al., 2006; Tice et al., 2011). If mat cohesion between the domes is less than the current induced shear stress, then continued erosion of those low-lying laminae and or deposition of particulates between the domes will subsequently isolate columns and allow branching. This means that detrital supply is also important in the development of columnar and branching stromatolites (Dupraz et al., 2006). This is very similar to the isolated domes and narrow columnar stromatolites in Unit K. However, the narrow and potentially branching columns here typically have thrombolitic or clotted fenestral microbialite between them (Fig. 19). This means there was likely less contrast between mat cohesion and current induced shear stress, if there was, little microbial varieties would remain between the domes, like those of the Chobeni Formation (Siahi et al., 2016; Fig. 12 & 13). Structurally massive and linked stromatolitic forms tend to arise when current induced shear stress and sediment supply are less than mat cohesion entirely, then nutrient diffusion and water depth tend to dominate stromatolitic production (Dupraz et al., 2006; Tice et al., 2011). Diffusion limited processes like; boundary Reynolds number, nutrient concentration and nutrient-mat affinity, may limit growth between the domes, creating massive and linked morphologies. This morphology type strongly resembles the laterally linked low domal to columnar varieties that are abundant throughout the sequence (Fig. 25, for example). Lastly, large columnar stromatolites may develop with low sediment supply if the nutrient-mat affinity is

large (Dupraz et al., 2006; Tice et al., 2011). Woman Lake stromatolites are only ~25 cm tall at most, perhaps sediment supply (carbonate) was too much or nutrient supply too low to allow larger varieties to form.

Thus, mat cohesiveness and current induced shear stress seem to have great effect on stromatolitic morphology. Current induced shear stress or energy and thus water depth in particular have been recognized as main factors affecting stromatolitic morphology. Grotzinger (1989) characterized stromatolitic varieties in two end members; low energy, deep subtidal environments and comparatively high energy, shallow peritidal coastal environments. Low energy coasts typically have non-elongate domal or linked domal stromatolites which may occur either in back reef lagoonal settings behind a barrier reef or in lower intertidal to subtidal facies of low energy ramp systems (Logan et al., 1974; Beakes, 1987; Ricketts and Donaldson, 1988). In contrast, higher energy coastlines are characterized by discontinuous to partially linked columnar stromatolites that may be elongate, though elongated and linked domes tend to be rare in higher energy settings. Stromatolitic mounds may intertwine with lenses of grainstone to form mound and channel belts along platform margins of rimmed shelved, along barrier reefs on rimmed shelves or in deeper subtidal to intertidal settings in higher-energy ramps. Current energy is proportionally related to water depth or rather interaction with wave base and the accommodation space available largely reflects the size and morphology of stromatolites (Grotzinger, 1989; Siahi, et al., 2016). Shallow waters typically endure stronger current energy and generally have lower synoptic relief stromatolites (Grotzinger, 1986a; Beaukes, 1987; Hofmann, 1988a, Ricketts and Donaldson, 1988). In contrast, larger columns and domes can develop in somewhat lower energies and deeper waters like those in Exuma, Bahamas tidal channels today.

4.5.2 Stromatolite Morphology Implications: Woman Lake

Despite some preservation limitations and generally unclear depositional environment constraints for Archean stromatolite morphology, we can infer that the WLC were deposited on what was likely a carbonate ramp due to the absence of larger domal structures or features forming a barrier reef or rim. Additionally, due to the abundance of low relief and laterally continuous morphotypes present, it was likely a low to moderate energy ramp comprised of peritidal and lesser subtidal environments. The overall diversity of stromatolitic morphologies and sizes range from upper intertidal with relatively higher energies to subtidal or lagoonal environments with lower

energies. Three main morphologies are noted; 1) low relief stratiform to undulating stromatolites, 2) laterally linked low domal and pseudocolumnar stromatolites, and 3) isolated to locally isolated domes and narrow columnar stromatolites listed in order of abundance. Each will be related to similar examples from modern tidal environments discussed in published literature.

Intertidal environments withstand normal high and low tidal ranges and are thus exposed either once or twice a day, every day, depending on the tidal regime and weather conditions (Shinn, 1983). Within the intertidal environment are many sub-environments such as tidal creeks, channels and levees and between them slight depressions allow ponds to accumulate which fill with water and only partially empty during each tidal cycle (James, 1984). This area is often called the pond and channel belt and ultimately means there are numerous environments exposed to different current energies that may exist in very close proximity both perpendicular and parallel to the shore. Thus, in the geologic record we are more likely to see rapid lithological changes both vertically and laterally instead of smooth gradational changes of progressively shallower or deeper environments (James, 1984) and Woman Lake carbonates are no exception.

The low relief, flat lying, undulating to stratiform stromatolites are for the most part laterally continuous and similar to those within the Mesoarchean Chobeni Formation described by Siahi and others (2016; Fig. 8). They suggested their stratiform stromatolites formed by lateral growth as a result of limited accommodation space in the supratidal environments, which has been suggested for comparable stratiform stromatolites from the Proterozoic as well (Seong-Joo and Golubic, 1999; Seong-Joo et al., 2000; Préat et al., 2011). The thicker packages of undulating to stratiform stromatolites within WLC (Fig. 3), overlying the basal tuff for example, likely developed from similar processes as a result of limited accommodation space. However, they are not associated with desiccation cracks which are characteristic in modern supratidal environments. The upper intertidal flat typically has good mat growth and fenestral porosity throughout that are less frequently broken into desiccation cracks in comparison to the supratidal setting. They are flat lying, irregular, and crinkled with low relief. Fenestrae in the upper intertidal flat follow similar patterns: pustular, crinkled, and irregular. In central areas mats have puffed surfaces with more convolute and crenulated forms. Overall, irregular yet flat lying bedding typically alternates with somewhat thick storm layers and thinner spring tidal layers, which occur as graded carbonate beds of varying thickness (Shinn, 1983; James, 1984). In general, storm beds tend to be thicker in more

landward positions of the system and thinner seaward (Shinn, 1983). Although grading is not evident, the flat lying, undulating to stratiform stromatolites at Woman Lake are commonly associated with beds of recrystallized carbonate (Fig. 9), which are thicker than those associated with the overlying low domal and pseudocolumnar stromatolites (Fig. 10 & 11). Consequently, they likely developed in an upper intertidal environment much like those described within the modern upper intertidal environments like: Shark Bay, the Persian Gulf, and Bahama Banks (Shinn, 1983; James, 1984). Although, they are commonly associated with other stromatolitic varieties, which means they were not limited to the upper intertidal environment.

Stratifera as a stromatolite group in general has likely the widest spatial and temporal distribution of all stromatolite types (Fralick and Riding, 2015). At Woman Lake they are almost always overlain or underlain by laterally linked low domal and short pseudocolumnar stromatolites (Fig. 10, 12, 13, & 19). They are similar to those in the Chobeni Formation (Pongola Supergroup, Siahi et al., 2016; Fig. 12) and the Hogarth Member (Steep Rock Lake, Fralick and Riding 2015); Fig. 8, and 15A) which have also been compared to those within the Cheshire Formation (Belingwe greenstone belt, Martin et al., 1980; Fig. 19). Fralick and Riding (2015) suggest that the succession of stratiform to domal stromatolites within the Hogarth Member could reflect a deepening trend during the initial platform flooding stages plus, the linked domal varieties there tend to form within quiet and more restricted settings. They elaborate upon Hofmann, (1976b) and Grotzinger (1989) to say that low relief pseudocolumns and sheets of microstromatolites can occur in very shallow environments and commonly occur in cyclic arrangements of small laterally linked domes and pseudocolumns, together with stratiform stromatolites, then transition to bioherms composed of those varieties. Although bioherms are relatively rare at Woman Lake, this cyclic arrangement is comparable to the overall succession and suggests WLC were predominantly deposited within intertidal settings. Stromatolite size tends to increase with increasing water depths or vice versa, in the same way fringing reefs on ramps will adjust to accommodation space (Logan and others, 1974; Ricketts and Donaldson, 1988); Beukes, 1987). Accordingly, the thicker packages of undulating to stratiform stromatolites are considered here to form in the upper intertidal environments while the laterally continuous low domal to short pseudocolumnar stromatolites likely formed on the lower intertidal flat. However, where the flat lying stromatolites directly

overlie and underlie stromatolites of greater relief, it is more likely that they developed in the lower intertidal flat together.

In modern environments, the lower intertidal flat is often compared to subtidal environments since both undergo calmer current energies relative to the upper intertidal flat, levees, and reefs. It is inherently difficult to characterize and compare modern lower intertidal and subtidal environments to Archean equivalents simply due to the presence of gastropods and formanifera, which often graze the mats and leave the sediments bioturbated and unrecognizable (Shinn, 1983; James, 1984). However, in areas of hypersalinity, mats will grow well into the subtidal zone (James 1984). In the lower intertidal flat, mats are typically thicker and exhibit more regular or smooth and horizontal or planar fenestral lamination (James, 1984), while the opposite is true for the upper intertidal to supratidal flat. Fenestrae are more abundant or potentially better preserved in the stratigraphy at location 2 and 3. There, planar, elongate and smooth laminae are associated with the undulating to stratiform stromatolites (Fig. 5 & 14), which means they likely formed in the lower intertidal flat as opposed to those at the base of the section that likely formed in the upper intertidal flat (Fig. 3). Overall, since the undulating to stratiform stromatolites and the laterally linked low domal and short pseudocolumnar stromatolites occur in close proximity to one another without desiccation features it is likely that they developed within a lower intertidal environment.

The laterally linked domal stromatolites and short pseudocolumnar stromatolites are comparable to small scale digitate or micro-pseudocolumnar stromatolites of the Chobeni Formation. Siahi and others (2016) suggests that they developed in restricted settings subjected to periodic wetting by strong currents. But, at Woman Lake they are overlain by parallel laminated and cross-stratified grainstones which are followed by larger pseudocolumnar varieties rendering them more likely to be fully submerged in the transition from lower intertidal to subtidal environment. Further discussion regarding the grainy carbonates follow in section 4.5.4. The larger pseudocolumns (Fig. 13) are curious, particularly because all but one column is erect. If the epinastic column were bending toward a light source each column should be bending in the same direction and in the same manner current activity should bend each column not just one. This may be an example of poor microbial mat strength and cohesion, where the stromatolite broke and bent, although it is more likely that the column began to slightly diverge and branch (Fig. 13). Branching

varieties could form in higher energy areas where mat strength is poor between columns (Dupraz et al., 2006; Tice et al., 2011). As previously discussed, morphotype typically scales with accommodation space, thus these comparatively larger pseudocolumns (Fig. 13) and the bioherm (Fig. 10) likely developed in the subtidal environments or potentially tidal channels cutting through the intertidal environment.

The last major stromatolitic morphology present at Woman Lake are locally linked to isolated domal and completely isolated narrow columnar stromatolites. Comparable narrow columnar stromatolites from Steep Rock are overlain by an abrupt contact with atikokania. They are ankerite with accordingly high Fe and Mn concentrations, lower Sr and Ba content, and a 2.5% fall in $\delta^{13}C$ isotopes, which all suggest an open depositional environment with increased offshore seawater exchange (Fralick and Riding, 2015; Fig. 9). Isolated columnar stromatolites from the Chobeni Formation were interpreted to form within high energy tidal channels along with conical stromatolites that were also single, erect, slender and unbranched (Siahi et al., 2016; Fig. 13 and 14). In a lacustrine environment, isolated domal and columnar stromatolites of the Neoarchean Tumbiana Formation are overlain by flat-pebble conglomerate facies in the highest energy, near-shore, shallow water environment (Awramik and Buchheim, 2009). They interpret the conglomerate to reflect a bar migrating offshore or a micro-delta infilling. Additionally, they note sedimentary structures such as climbing ripples and wavy to planar laminations associated with stromatolites, which provide better constraints and show that with decreasing energy, stromatolitic abundance and variety increased. Sumner and Grotzinger (2004) associated columnar stromatolites from the Neoarchean Campbellrand-Malmani carbonate platform with their intertidal to shallow subtidal facies. The shallow somewhat higher energy environment was dominated by columnar stromatolites but also contained isolated bioherms, oolitic and non-oolitic grainstones and aragonite fan pseudomorphs. Ultimately, isolated columnar and domal varieties tend to form within higher energy environments, suggesting that current energy was greater than mat strength and eroded the sides of stromatolites or sedimentation rates were greater and enabled vertical growth rather than lateral growth. Most spaces between stromatolites at Woman Lake however, are comprised of clotted and potentially thrombolitic microbialite with abundant irregular fenestrae and micritic sized carbonate (Fig. 20). Sometimes the spaces between columns have semi-continuous lamination with stromatactis. The narrow columns are often bent in one direction or

the other (Fig. 20), which may be due to deformation, although some are associated with parallel laminated grainstones with little evidence of strain (Fig. 20D), suggesting their nature is primary. If so, they may be bent in predominant current direction like the current molded Mesoproterozoic sinuous columnar stromatolites of the Tieling Formation (Tosti and Riding, 2017). However, the isolated stromatolitic varieties present at Woman Lake most likely formed in a more tranquil environment since they are small compared to the previous examples from other localities and are associated with micritic-sized carbonate and clotted fenestral microbialite (Fig. 20). Fine grain sizes tend to be reworked and removed with regular tidal activity; thus it is more likely that they formed within a protected lagoon or tidal pond like those in Shark Bay for example (James, 1984; James and Jones, 2015). From the rock record, they are fairly similar to tidal flat tufa (microstromatolites) from the Pethei Group of the Slave Province. They appear to record a diverse depositional history influenced by benthic microbial communities, seafloor cement precipitation and passive settling of carbonate mud from the water column within quiet peritidal environments (James and Jones, 2015; Fig. 18.6). Although better preserved, the fabric is similar to textures seen here (Fig. 17 & 19). Small stromatolites from the Pethei Group, interbedded with their slope carbonate mudstones are also strikingly similar to the low domal stromatolites here, especially when associated with banded carbonate (Fig. 21 & 22).

In general, compared to the common morphotypes and characteristics of tidal flats in modern environments like Shark Bay, the Persian Gulf, and Bahama Banks (Shinn, 1983; James, 1984; James and Jones, 2015) it is likely that the laterally continuous, low relief, undulating to stratiform stromatolites developed within the upper intertidal settings, in shallow waters with, moderate energies. Similarly, the low domal to pseudocolumnar stromatolites probably developed in lower intertidal environments with comparatively lower but still moderate current energies. Lastly, the isolated domal and narrow columnar stromatolites associated with clotted fenestral microbialite likely formed in a more tranquil environment such as a tidal pond or lagoon.

4.5.3 Grainy Carbonate Deposits: Implications

Today carbonate sands are made from the degradation and decomposition of various brightly coloured corals and shells or precipitated as ooids. However, without coral and shells in the Archean, carbonate sands are rare and their existence is disputed. The presence of low angled lamination truncated by another set of low angle laminae and planar laminate is indicative of cross-

stratified and parallel laminated beds, which suggests that sand-sized grains were being deposited. They were likely sourced from microbial carbonate deposits in the WLC ramp itself. However, in the field massive carbonate or parallel laminated grainstones were often difficult to distinguish from recrystallized stratiform or undulating microbialite and precipitated carbonate, thus inferences were made with caution.

The massive carbonate beds that are recrystallized, lack primary internal structures and grainsize, the erosive bed in Unit A, and the cross stratification in Unit F, are generally similar to features at Steep Rock Lake (Fralick and Riding, 2015; Fig. 11). Following their interpretation, the massive grainstone beds here may also represent tempestite deposits similar to the Paleoproterozoic Gunflint Formation, where the carbonate grains were originally deposited as carbonate mud and subsequently reworked by wave activity into tempestites layers (Simonson and Goode, 1989; Fralick, 1989; Pufahl and Fralick, 2004; Fralick et al., 2017), likewise tidal activity has been suggested for producing carbonate grains (Ojakangas, 1983). Increased wave activity brought on by a storm event could be responsible for erosively scouring and redepositing the seemingly massive carbonate grainstone. The wrinkly nature of some bedding planes are similar to stratiform and undulating stromatolites, however their association with cross-stratification is more indicative of laminated grainstones. The cross-stratification may have resulted after a storm deposited the potentially parallel laminated tempestite layers, perhaps in an intertidal channel, or in the subtidal environment as a sand bar. This correlates well with stromatolite morphotypes since the larger pseudocolumns overlying the cross stratification have greater synoptic relief and begin to branch which both tend to indicate that water depths were increasing.

The chaotic assemblage (Unit H) at the top of the northern section overlying the stromatolites could result from a slumping event on an unsteady slope with partially lithified carbonate. However, since the assemblage partly overlies stromatolites it is unlikely that the chaotic debris fell deeper than the photic zone, consequently there must have been a slope in relatively shallow water (less than 10-15m) rather than deep water off the edge of the platform. A slight slope at the edge of a tidal channel or lagoon may have been enough to trigger a slumping event, however some blocks are quite large. This could be the result of large tsunami waves crashing into the ramp, ripping up chunks of partially lithified stromatolites and depositing them as the wave recedes and dissipates. A large event like this may also explain the feature crosscutting

the parallel laminated sediments (Fig. 4). The overwhelming waves may have induced extreme pressures causing an injection feature to exploit a week point in the partially lithified lamination causing sediment laden fluid to intrude, drag and displace the surrounding laminae. Thus, the chaotic grainy assemblage may represent a localized slump event within the shallow subtidal environment or a catastrophic tsunami event.

Overlying the chaotic Unit H, though at a lateral distance away, banded carbonate is associated with elongate and clotted fenestral microbialite, small isolated domal and columnar stromatolites and soft sediment deformation features. It is relatively rare in abundance but strongly resembles the banded limestone facies within the Hogarth Member at Steep Rock Lake (Fralick and Riding 2015; Fig. 13 & 14). However, some of the banded carbonate there form broad, smooth, locally steep-sided domes, up to 0.75m tall and 1.5 to 2m wide. They are then termed banded limestone domes which contain sheet-like fenestrae (Fralick and Riding, 2015; Fig. 14C). The macrostructure at Woman Lake is difficult to observe, thus it is unknown whether the bands here are part of a larger structure. Fralick and Riding (2015) note that the banded limestone (those not necessarily associated with large domes) somewhat resemble ribbon limestone (Taylor and Cook, 1976), ribbon carbonate (Pfeil and Read, 1980) and ribbon rock (Demicco, 1983) from the late Cambrian of Laurentia. There the bands are associated with sand-silt ripple laminations with mud drapes, scour and fill structures, cracks and soft sediment deformation features which made them suggest that the bands were a part of a low to moderate current energy environment in the shallow subtidal to intertidal facies. At Woman Lake they are associated with multiple sublithotopes in Unit K and N, which contains: low isolated to locally linked domes, isolated narrow columnar stromatolites, abundant elongated and clotted fenestrae, and some soft sediment deformation features (loading and injection features; Fig. 14 & 21). As previously described, since these isolated stromatolitic morphotypes are associated with fine grained carbonate, they likely formed within a tranquil environment like a lagoon or tidal pond intertidal facies much like the ribbon rock described from the late Cambrian (Taylor and Cook, 1976; Pfeil and Read, 1980; Demicco, 1983).

Stratigraphically above Unit K, there is fairly well preserved, millimetric parallel laminations that alternate with low domal stromatolites (Fig. 27). They have apparent dark laminations with various lighter coloured laminae in between that are all fairly smooth and

isopachous. The darker lamination appears to be finer grained. However, this cannot be confirmed due to thorough recrystallization: they too may be tempestites layers. Otherwise they could be situated in a quiet lagoonal environment as precipitates or as sediment settled out of suspension depositing them as laminites.

4.5.4 Zig-Zagged Features

The structures within Unit J pose interesting questions because they possess some biogenic and abiogenic qualities that are associated with micro-faulting, and peaked tufts with depressions. Over a small distance the millimetric and isopachous lamination that is loftily bent with peaked tuffs and depressions and rare tee-pee-like structures, quickly become offset then continuous again showing conical or chevron patterned lamination (Fig. 15). Features like microbially induced sedimentary structures (MISS) are often characterized by isopachous lamination. However, literature descriptions of MISS commonly feature those associated with siliciclastics (Noffke et al., 2006) and these are carbonates. In 2008, Riding discussed the views of Perry and others (2007) who stated that "microbially constructed stromatolites should not … be confused with abiotic, chemically precipitated carbonate crusts" along with Pope and other's (2000) views that isopachous stromatolites have been dominated by chemical precipitation where microbial mats are absent and peloidal stromatolite growth have been controlled by sedimentation where microbial mats are present. Pope and others (2000) surmised that "thinly laminated isopachous stromatolites are considered to have largely abiotic origin". Riding (2008) introduced an intermediate between the essentially abiogenic Sparry Crust and the biogenic Fine-Grained Crust (lithified microbial mat), termed Hybrid Crust. The dark millimetric laminae here are undeniably isopachous with generally good inheritance at the base, which seems to continue throughout the zig-zagged patterns at the top. Key features distinguishing between biogenic Fine-Grained Crust and abiogenic Sparry Crusts involves the microfabric of their lamination. If the layering is comprised of micritic spar that is irregular with poor inheritance it is likely biogenic, in contrast to even lamination with good inheritance comprised of spar (Fig. 28 after Riding, 2008). By these terms the zig-zagged patterns present here do not seem biogenic. They do have strikingly similar mesofabrics to Upper Permian stromatolites of the Zechstein Group (England, Perri et al, 2013; Fig. 2) and the Paleoproterozoic Pethei Group (Athapuscow Basin, Canada, Pope et al., 2000; Fig. 4). Those of the Pethei Group are thought to form in restricted settings through evaporative precipitations and are considered to

have largely abiogenic origins. Pope and others (2000), recognize that microbes were almost certainly present on the precipitating crystals but the role they played remains ambiguous. Similarily, the stromatolites of the Zechstein Group were thought to form in a back-reef lagoon following a major phase of subaerial exposure. Perri and others (2013) consider the isopachous stromatolites to form through microbially mediated precipitation, synsedimentary and postsedimentary processes together. The microfabrics of the zig-zagged lamination herein have been largely recrystallized, however the mesostructures suggest they may have been stratiform stromatolites or parallel laminated carbonate, that went through soft sediment deformation and micro-faulting which produced the soft tufted peaks, depressions, and the offset laminae (Fig. 15). Continued sedimentation or microbial growth atop the pseudo-micro-faults gradationally seemed to have produced the isopachous zig-zagged conical-like laminae. At this time the laterally continuous conical-like zig-zagged structures are considered dubiomicrobialites or pseudomicrobialites which, according to the microbialite handbook (Grey and Awramik, 2020) are structures of uncertain origin that resemble a stromatolite or other microbialite and may be of either biogenic or abiogenic origin.

4.5.5 Silicified Potential Roll-Up Structures and Crystal Fan Pseudomorphs

Extensive silicification is both beneficial and not because it can preserve some of the original features, but not with ideal quality especially after enduring metamorphism. The "wormy" features directly overlying the bioherm at the northern locality have some thin wispy lamination,

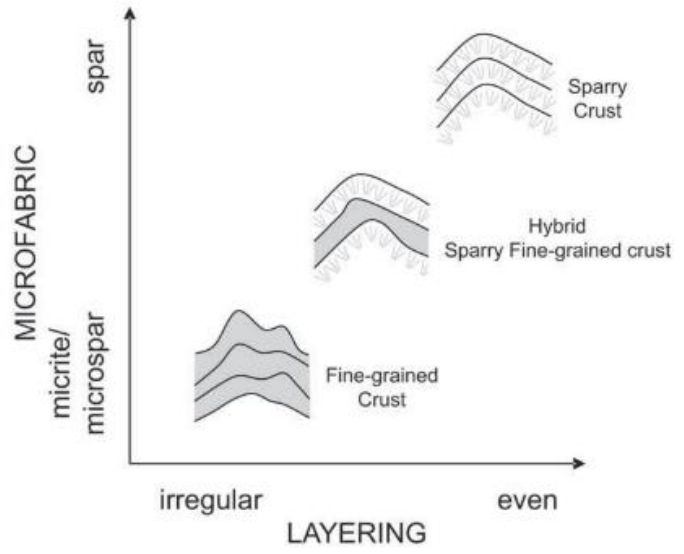

Fig. 28. Key features of crust discrimination by Riding (2008). Illustrates the difference between microfabric (fine-grained or sparry) and layer arrangement (irregular, poor inheritance or even and good inheritance).

many of which are amalgamated and some retain crescent-like convex columns. At the end of numerous wisps and irregular lamination, they form circular features some with hollow centers (Fig. 10). In places, some silicified features are composed of more circular features than any kind of lamination (Fig. 5). They resemble the mesostructure of roll-up features within the Wittenoom Formation of the Hamersley Group (Simonson, and Carney, 1999; Sumner and Grotzinger, 2004) and of the Sturtian cap carbonate of the Rasthof Formation ((Pruss et al., 2010). However, the microstructure is not preserved here. If the delicately bent and folded microbial laminations within the Wittenoom and Rasthof Formations were amalgamated by thorough silica replacement and then metamorphosed and recrystallized the final result may resemble these "wormy" features at Woman Lake. Some circular features that are not silicified are present just above silicified ones (Fig. 5B). However, only broad shapes are noticed with faintly lighter laminations among the overall dark circles. Preservation is too poor to be certain. Sumner and Grotzinger (2004) attribute the Hammersley roll up structures to form in deep subtidal environments exclusively, they say they are widespread in basinal carbonates and absent from platformal carbonates that display an abundance of standard stromatolitic structures. The potential roll up structures at Woman Lake are associated with a bioherm that would occur in a subtidal environment, although in another location they are associated with stratiform to undulating mats. Thus, it is difficult to say with certainty. They could be a useful indicator of deposition below storm wave base and potentially serve as evidence of, or guides to, paleo-seismic activity (Allen, 1986; and Simonson and Carney, 1999). Earthquakes with Richter magnitude exceeding 5 can produce horizons of soft sediment deformation structures that are preserved in the stratigraphic record (Allen, 1986). However, the roll-ups would need to be transported there and WLC does not have any other evidence suggesting deposition below wave base. Otherwise, the "wormy" features here may be a product of silicification preferentially preserving certain stromatolites or certain parts of stromatolites. The hollow centers and recessively weathered areas are assumed to be preferentially weathered carbonate. The "wormy" features could potentially be stromatolites that toppled over since they partially resemble stromatolites seen in plan view near the top of the sequence (Fig. 6 & 24).

The silicified and vertically oriented features above the locally linked carbonate domes (Fig. 11B & C) resemble amalgamations of crystal fan pseudomorphs in a similar manner to the potential roll-up structures. If the crystal fans at Steep Rock (Fralick and Riding, 2015) were

extensively silicified and metamorphosed and recrystallized, they may resemble the vertically oriented and radiated features seen in Fig. 11. However, they too are not preserved well enough to be confidentially identified.

5.0 GEOCHEMICAL ANALYSIS

5.1 BRIEF REVIEW OF REE SYSTEMATICS AND GEOCHEMICAL STUDIES ON CHEMICAL SEDIMENTS

Chemical sediments act as proxies for ancient waters by incorporating, without significantly fractionating, rare earth elements (REE) and isotopic signatures into their crystal lattice as they precipitate, thereby documenting the chemical composition of the waters from which they form (Kamber et al., 2004; Nothdurft et al., 2004; Webb et al., 2009). Geochemical analyses of these chemical precipitates have become a reliable tool used to uncover signatures that provide valuable insight to our intricate paleo-spheres (Bohlar et al., 2004). The unique chemical and physical properties of rare earth elements enable them to deviate from a flat pattern thus highlighting anomalous signatures when normalized to a known shale; for example, Post Archean Australian Shale (PAAS, used in this study; Taylor and McLennan, 1985), or Mud of Queensland (MUQ; Kamber et al., 2005). Identical trivalent charges and their systematic decrease in ionic radius with consecutive atomic numbers allow REEs to be used as proxies for both modern and ancient geochemical processes in oceans, rivers, estuaries, lakes and groundwater (Johannesson and Zhuo, 1998; Shields and Stille, 2001; Kamber at al., 2004; Klinkhammer et al., 2004; Bohlar et al., 2005; Bohlar and Kranendonk, 2007; Allwood et al., 2010; Planavsky et al., 2010; Fralick and Riding, 2015; Fralick et al., 2017).

Two elements are of particular interest when interpreting ancient seawater chemistry; Eu and Ce. They each have two valance states which allows them to behave differently than their neighbouring REEs that have only one valence state. However, because Eu has a redox equilibrium at very low oxygen fugacity, only high temperatures can reduce Eu^{3+} to Eu^{2+}, which then renders it more soluble than its trivalent neighbours (Bau, 1991). Unlike today, the Archean ocean had a significant component of hot hydrothermal fluids, which enriched the ocean with Eu and thus imparted a positive Eu anomaly on precipitating chemical sediments (Bau, 1991; Derry and Jacobsen, 1990; Bau and Dulski, 1995). Conversely, Ce is a very sensitive redox proxy. In the presence of free oxygen Ce^{3+} is oxidized to Ce^{4+} and subsequently the less soluble Ce^{4+} is removed from solution. Once oxidized, Ce^{4+} readily adsorbs onto particulate matter and manganese oxide, leaving the fluid with a negative Ce anomaly (Elderfield and Greaves, 1981; Klinkhammer et al.,

1983; Bau and Koschinski, 2009; Bekker et al., 2012). Thus, positive Eu and negative Ce anomalies are generally accepted as robust indicators for hydrothermal fluid influence and the presence of free oxygen, respectively (Bau, 1991; Derry and Jacobson, 1990; Bau and Dulksi, 1995). Modern seawater, meteoric water and ground water are typically characterized by light REE (LREE) depletion, a strongly superchondritic Y/Ho ratio (above 28), a strong positive La anomaly, a positive Gd anomaly, a negative Ce anomaly, and sometimes a Lu anomaly (Bohlar et al., 2004).

Yttrium and Ho have nearly the same chemical behavior due to their trivalent oxidation state and almost identical effective ionic radii (Shannon, 1976), thus allowing Ho to be used as a proxy for the activity of Y in crustal rocks (Nozaki et al., 1997; Bau and Dulski, 1999). Typically crustal rocks have Y/Ho ratios that range from 26-28 (Kamber & Webb, 2001). However, this changes if Y and Ho interact with aqueous solutions. Higher ratios, 44-120, are expected due to Ho being preferentially scavenged and complexing with varying particulate matter (Nozaki et al., 1997; Kamber and Webb, 2001) and solution-surface complexation behavior (Bau and Dulski, 1999; Luo and Byrne, 2004; Quinn et al., 2006) resulting in an enrichment of Y compared to Ho in seawater precipitates. Consequently, the ratio is used when studying carbonate minerals to understand the amount of fractionation that occurred within the water column.

5.2 MINERALOGY AND PROXY VALIDATION

Considering the age of this carbonate unit and the aim of this study it is vital to understand its post-depositional and diagenetic state and ensure the REEs and isotopic signatures are indeed representing the carbonate fraction. Woman Lake carbonates are primarily calcite, which are, silicified in places, and only a few samples have been appreciably dolomitized (Fig. 29A). Samples that contained more than 5% dolomite were excluded from analysis. The carbonate is likely calcite rather than aragonite because Sr concentrations are lower than those expected for aragonite. The trace element typically fits into the aragonite crystal lattice far better than it fits into the calcite lattice. Thus, with only one main lithology three lithotopes were defined: 1) carbonate microbialite 2) grainy carbonate, and 3) silicified microbialite. They were divided into sublithotopes listed in Figure 30 with their associated symbol used throughout the geochemistry chapter. Samples approaching 50% Mg and above were collected near intrusions and may be affected by contact metamorphism, for this reason they were typically excluded from further analysis. During silicification remnants of the carbonate were left behind and weak acid dissolution was used to

isolate that portion. Using the pure carbonate fraction is critical as it is commonly employed as a proxy for the seawater from which it precipitated (Kamber and Webb, 2001; Kato and Nakamura, 2003; Van Kranendonk et al., 2003; Bolhar et al., 2004). In theory, using partial dissolution methods to extract elements within the carbonate fraction as opposed to any siliciclastic contamination is reasonable and well supported in the literature, regardless; a simple bivariant scatter plot can illustrate this well. Siliciclastic contamination can affect the concentration of elements and suppress anomalies in REE patterns (Kamber & Webb, 2001; Peter, 2003). Figure 29D compares Al, an immobile element that is abundant in siliciclastic material but absent from carbonates, to total REEs. If the REEs were coming from siliciclastic

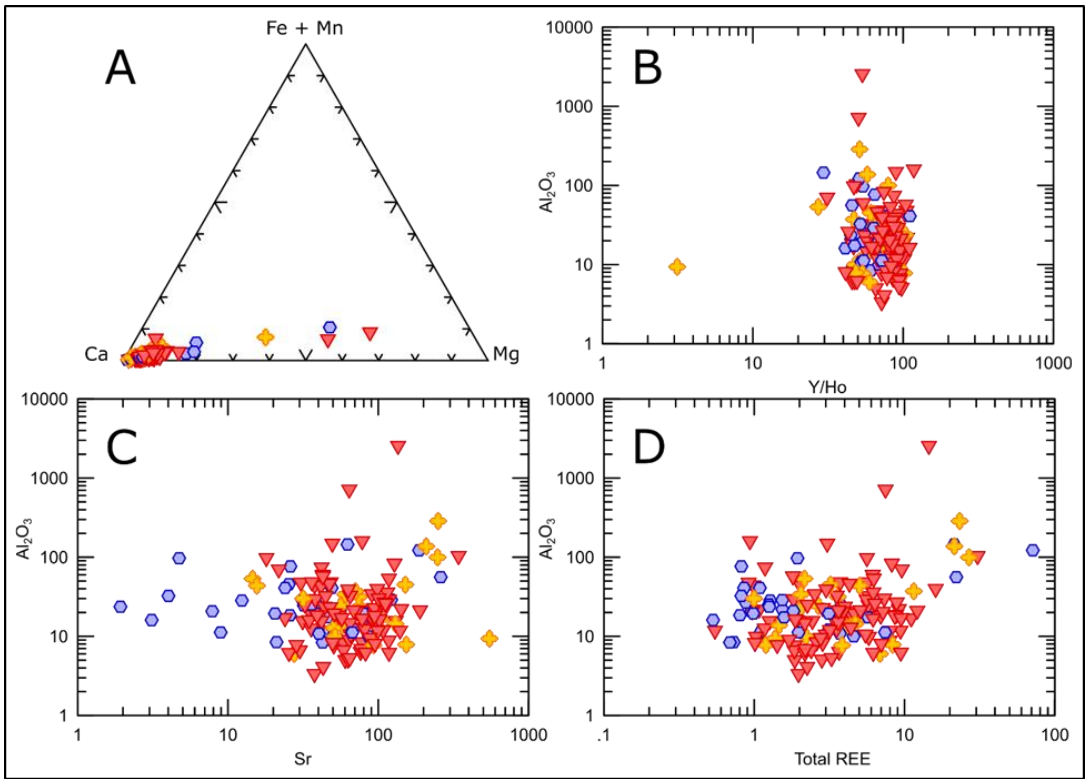

Fig. 29. Ternary diagram with all samples plotted against atomic weights of Ca, Fe+Mn, and Mg showing that the primary mineralogy of carbonates at Woman Lake are pure calcites. Majority of samples plot within >90% atomic weight Ca, a few are enriched in Mg thus approaching the dolomite field and 3 outliers contain anomalous amounts of Mg (potentially due to contact metamorphism with small intrusions). Those samples were noted and analyzed with caution. B) Bivariant plots of Y/Ho, C) Sr, and D) Total REE against Al_2O_3. Aluminum is an immobile element abundant in siliclastic material. A correlation between it and the REE would suggest they are present in the same mineral phases. The scattered array denotes REE are not contaminated by their presence in siliciclastics and represent the water column of the precipitating carbonates. Al_2O_3 vales in wt%, Sr and Total REE in ppm. Blue hexagons are silicified microbialite, red triangles are carbonate microbialite, and yellow crosses are clastic carbonate.

Fig. 30. Legend listing lithotopes and sublithotopes of WLC and their associated symbols used consistently throughout the geochemistry section.

contamination, they would show a positive linear correlation where an increase in Al causes an increase in REEs. This is not the case at Woman Lake, instead the scatter illustrates the lack of a relationship between the REEs and siliciclastics. Therefore, the partial dissolution obtained data from the carbonates successfully making them a suitable seawater proxy. In addition to this Y/Ho ratios may be used to validate true seawater proxies. Crustal rocks, which typically source siliciclastics, are known to have chondritic ratios near 28 but higher values result with continued interaction with freshwater and seawater. Carbonate precipitates typically exhibit ratios greater than 44 and modern seawater exhibits ratios between 44 and 120 (Nozaki et al., 1997; Kamber & Webb, 2001; Bolhar et al., 2004). Contamination with siliciclastic material would be suspected for lower Y/Ho ratios and although Woman Lake carbonates range from 27 to 117, the samples are predominantly greater than 44 (Fig. 29B).

Concentration of Sr in the samples does not correlate with Al_2O_3 (Fig. 29C), indicating it is representative of the Sr contained in the carbonate phase. Strontium isotopic values range from 0.700346 to 0.711313 with an average precision error of 0.00098 (to 1σ) in all sampled lithologies, which are reasonable results compared to the value for seawater at this time, 0.7018 (Veizer and Jansen, 1979; Taylor & McLennan, 1985; Veizer et al., 1989a; Veizer et al., 1989b; Godderis & Veizer, 2000; Satkoski et al., 2017). Strontium isotopes are sensitive to resetting; a small water/rock ratio can reset them (Veizer et al., 1989b) the fact that some of these isotopes were unaltered speaks highly in regard to the preservation at Woman Lake. Carbon isotopic ratios need higher water/rock interaction ratios to alter their signature compared to $^{87}Sr/^{86}Sr$ and since a number of the $^{87}Sr/^{86}Sr$ did not suffer post-depositional alteration, the $\delta^{13}C$ are likely valid as well (Jacobsen and Kaufman, 1999;Veizer, 2003), and with a range from -3.83‰ to 1.17‰ they possess values typical of Archean carbonates. Oxygen isotopes on the other hand can be affected by the lowest water/rock ratios and range from -17.96‰ to -8.82‰, which are likely reset. Figure 31 illustrates only a slight relationship between $\delta^{13}C$ and $\delta^{18}O$ for some samples, most samples plot in a scatter meaning those samples likely retained original carbon isotopes but not oxygen. Depleted oxygen isotopes like those seen here are classic alteration values for burial diagenesis (Veizer, 2003)

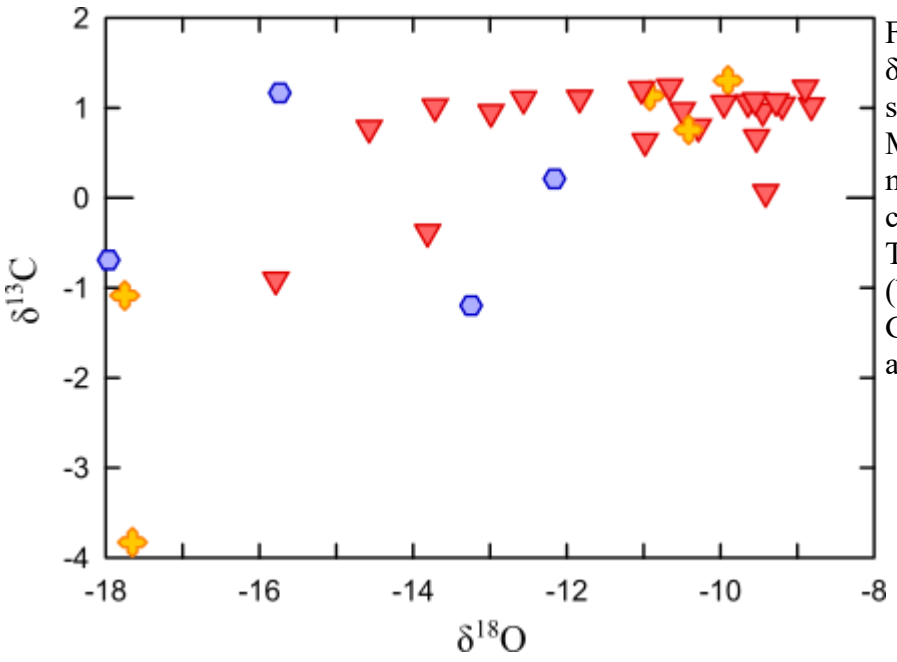

Fig. 31. Bivariant plot of $\delta^{13}C$ against $\delta^{18}O$ for 32 samples. The Carbonate Microbialite (red) are the most enriched in heavy carbon and heavy oxygen. The Silicified Microbialite (blue) and the Carbonate Grainstones (yellow) values are more varied.

5.3 U-Pb GEOCHRONOLOGY: RESULTS

About 55 small rounded and euhedral grains of zircon were recovered from the Woman Lake Tuff and analyzed for U-Pb geochronology. Zircon ages ranged from 2715 to 3269 Ma (Fig. 32A) but the vast majority of determinations provided an age of 2857±5 Ma (Fig. 32B). The anomalous zircons can be attributed to inherited older cores and younger overgrowths.

5.4 PAAS NORMALIZED REE TRENDS: ICP MS RESULTS

Pass normalized spectra for WLC typically exhibit one of four trends for all lithotopes; a significant negative Ce anomaly (Ce anomaly < 0.95) with a positive Eu anomaly (Eu anomaly > 2), either one of the two anomalies, or neither (Fig. 33 to 36). Trends analyzed via ICP MS data most commonly display both a negative Ce anomaly and positive Eu anomaly (45 out of 152 samples) or just a negative Ce anomaly (44/152 samples). They show a Eu anomaly alone just as often as they show neither (31/152 and 32/152 samples respectively). Altogether, 89 samples contain a negative Ce anomaly while 76 contain a positive Eu anomaly, 45 of those samples contain both anomalies and 32 samples have neither. In general, each trend is depleted in light REE (LREE) compared to the heavies, with lower concentrations exhibiting increased LREE

depletion. Each sample exhibits a small negative Yb anomaly and a positive to strong positive La anomaly regardless of which other anomaly is or is not present across each lithotope.

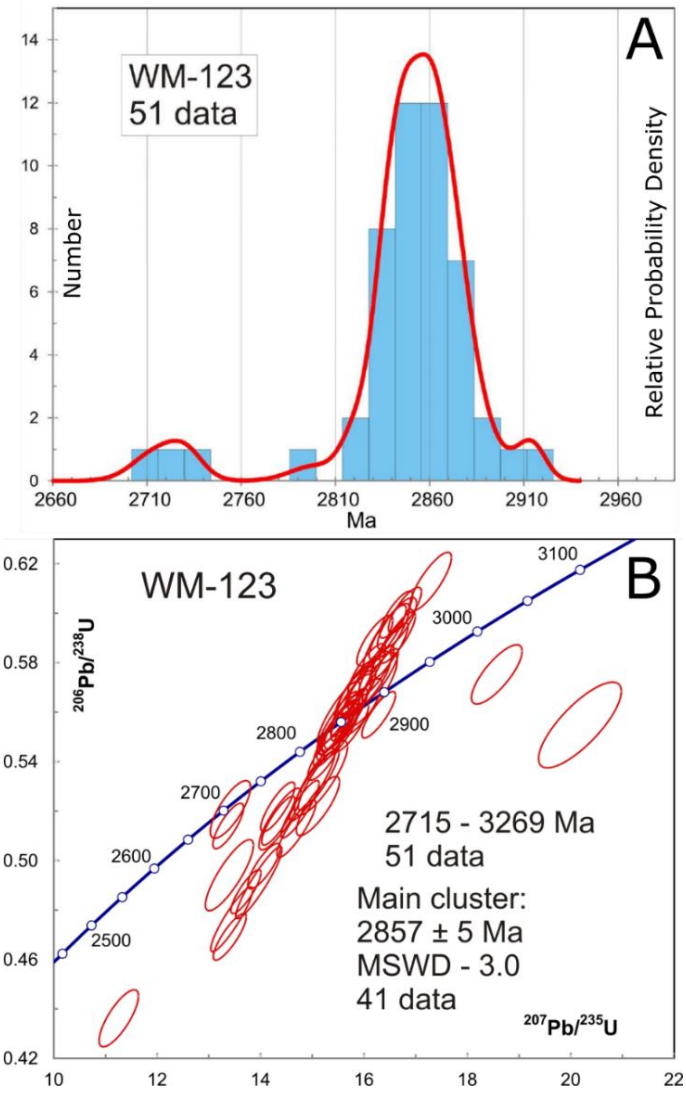

Fig. 32. U-Pb geochronology from Woman Lake tuff conformably underlying the carbonate succession. A) Relative probability density B) Concordia plot. The vast majority of zircons provided an age of 2857±5 Ma.

There is little distinction between the trends according to lithotopes and sublithotopes. The Silicified Microbialite samples rarely contain a positive Eu anomaly and generally have similar albeit suppressed anomalies (Fig. 35) compared to Carbonate Microbialite (Figure 33 and 34) and Carbonate Grainstones/Micrite (Fig. 36). The Silicified Stratiform Microbialite did not retain

anomalies very well, otherwise trends are nearly identical to other lithotopes (Fig. 35). The Carbonate Stratiform Microbialites almost always show a Eu anomaly and rarely contain a negative Ce anomaly (Fig. 33). Banded Carbonates typically have a negative Ce anomaly and commonly have a Eu anomaly (Fig. 33). Fenestrated Stromatolites show a negative Ce anomaly in bulk analyzed samples, and microdrilled sampling 6 times out of 10, while the organic-rich micrites do not exhibit Eu anomalies (Fig. 34). The Zig Zags all contain a positive Eu anomaly (Fig. 36).

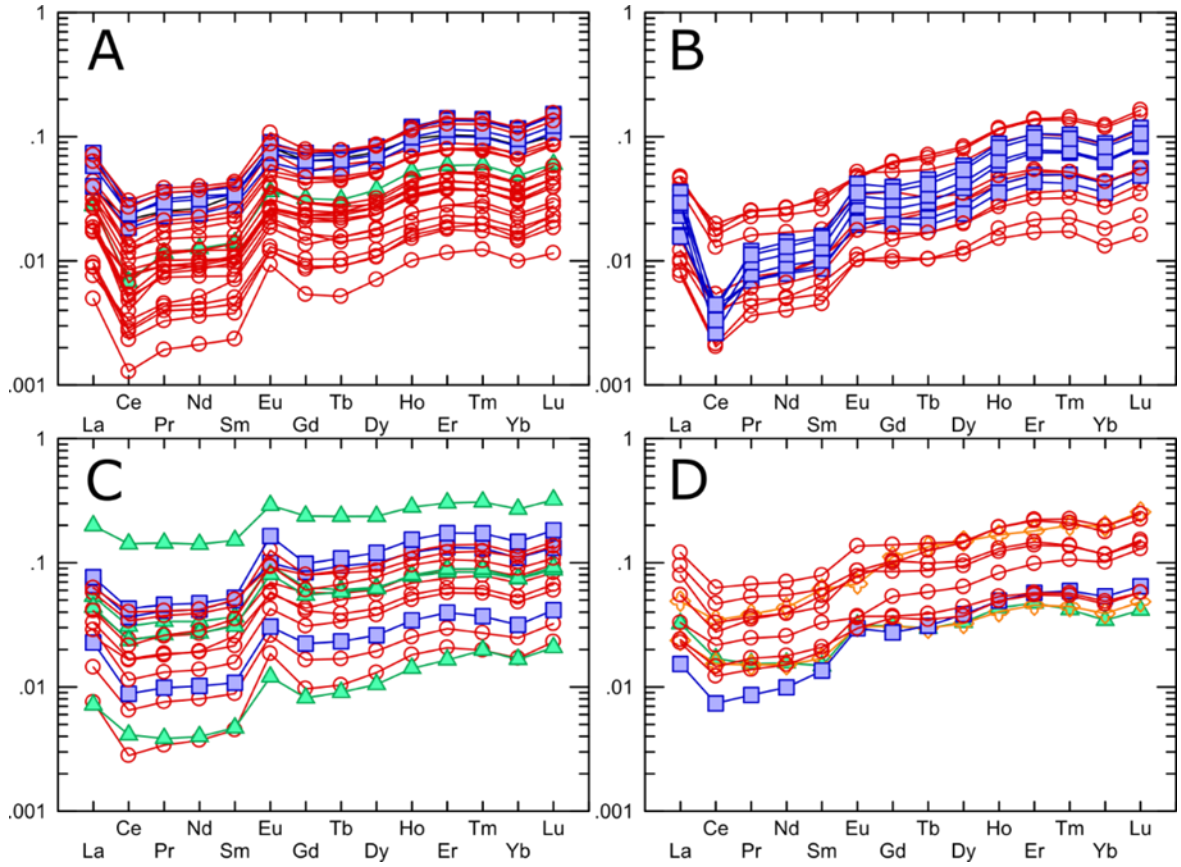

Fig. 33. PAAS normalized REE patterns for Microbial Carbonate. Symbols represent sublithotopes, for legend see Fig. 30. A) Samples with both a negative Ce and positive Eu anomaly. B) Samples that only have a negative Ce anomaly. C) Samples with only a positive Eu anomaly, and D) samples with neither anomaly. The Microbial Carbonates exhibit a consistent LREE depletion regardless of which trends are present although stronger LREE depletions are associated with lower concentrations. The majority of the banded carbonate (blue squares) contain a negative Ce anomaly.

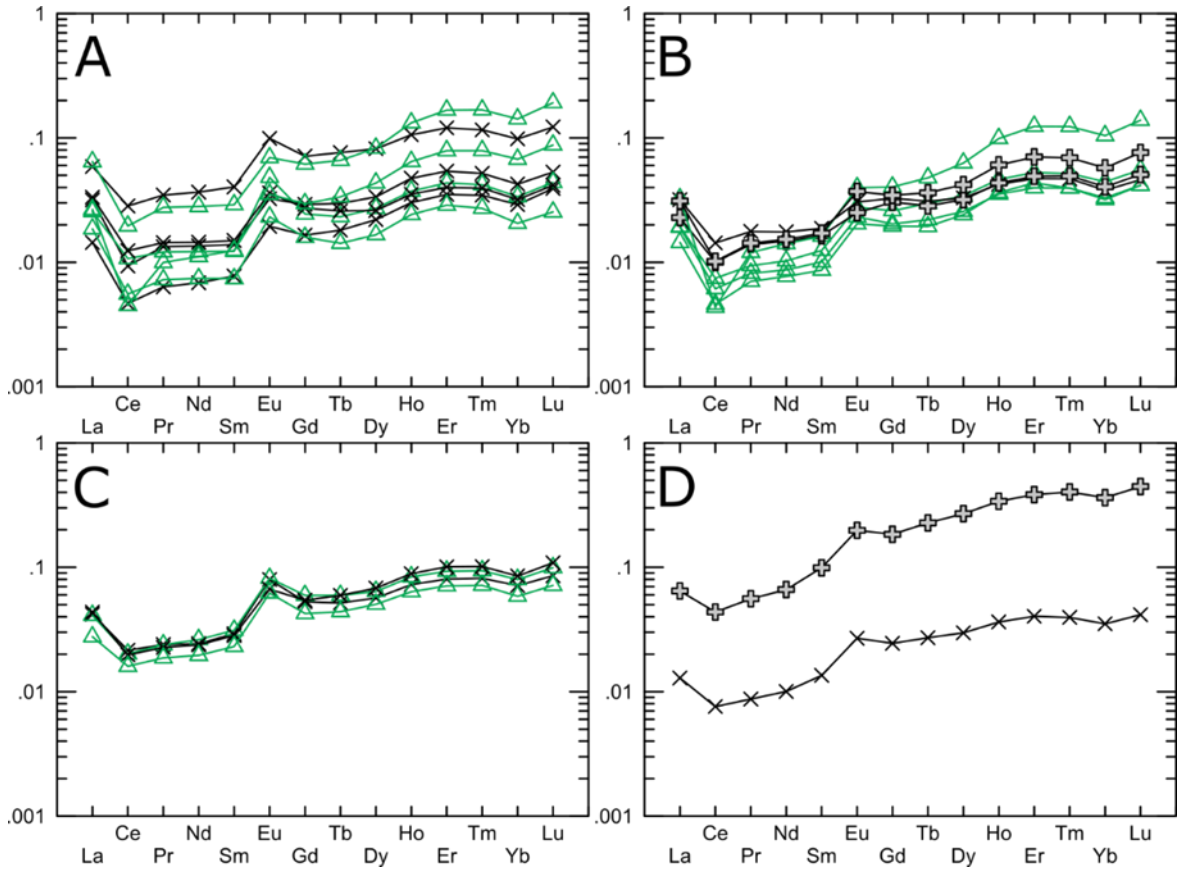

Fig. 34. PAAS normalized REE spectra for specifically sampled Microbial Carbonate lithotopes using microdrill techniques. Symbols represent sublithotopes, for legend see Fig. 30. A) Samples with both a negative Ce and positive Eu anomaly. B) Samples that only have a negative Ce anomaly. C) Samples with only a positive Eu anomaly, and D) samples with neither.

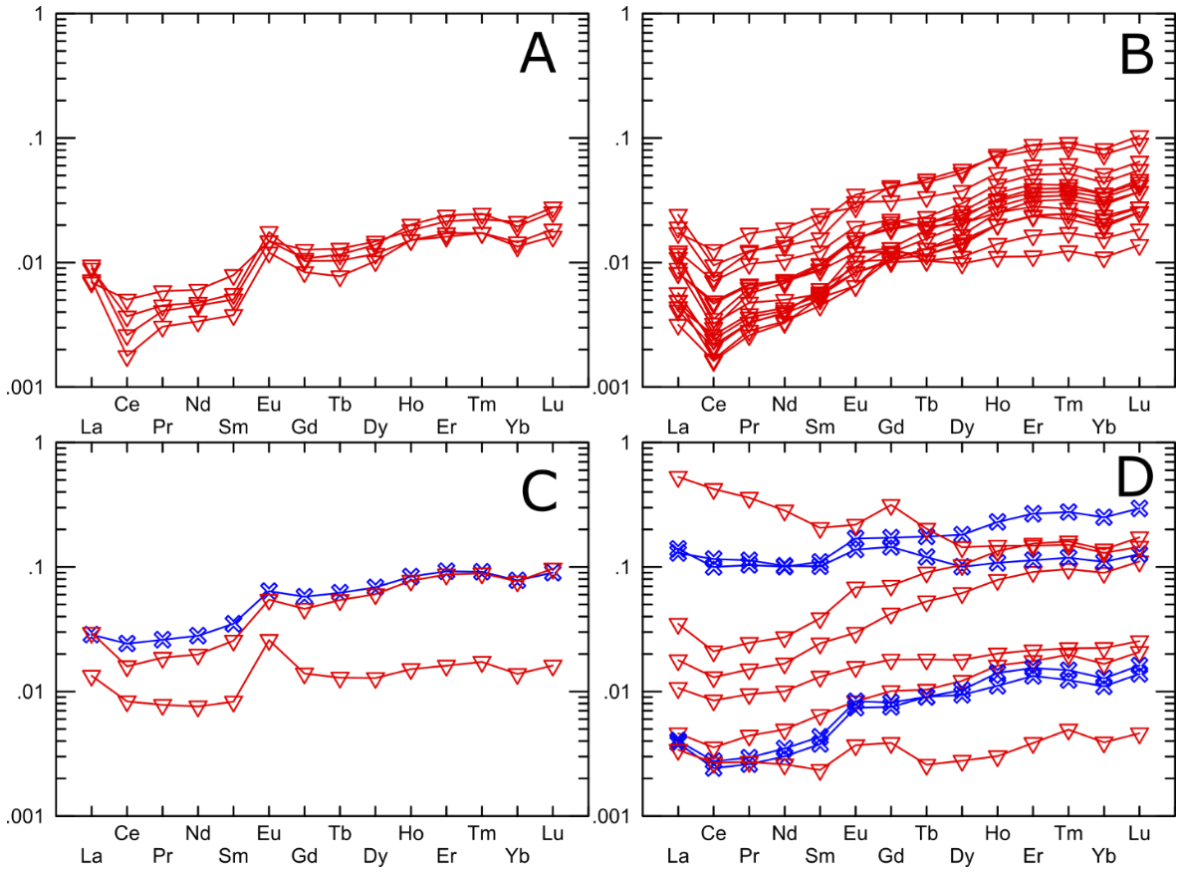

Fig. 35. PAAS normalized REE spectra for Silicified Microbialite. Symbols represent sublithotopes, for legend see Fig. 30. A) Samples with both a negative Ce and positive Eu anomaly. B) Samples that only have a negative Ce anomaly. C) Samples with only a positive Eu anomaly, and D) samples with neither anomaly. The silicified stratiform stromatolites (blue X's) generally do not exhibit anomalous trends.

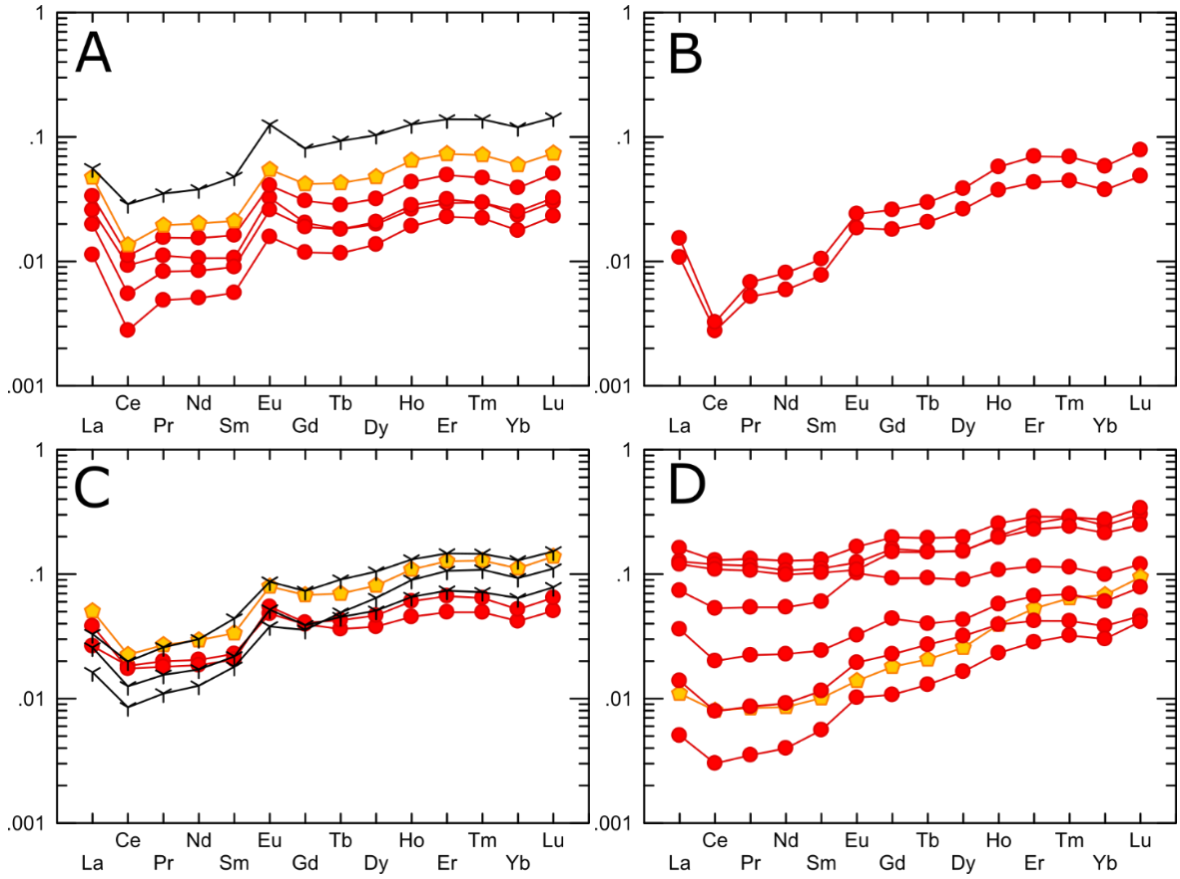

Fig. 36. PAAS normalized REE spectra for Carbonate Grainstones. Symbols represent sublithotopes, for legend see Fig. 30. A) Samples with both a negative Ce and positive Eu anomaly. B) Samples that only have a negative Ce anomaly. C) Samples with only a positive Eu anomaly, and D) samples with neither anomaly. Zig Zags always exhibit a positive Eu anomaly and no Ce anomaly.

5.5 PAAS NORMALIZED REE TRENDS: LA-ICP-MS RESULTS

Trends produced using LA-ICP-MS techniques closely resemble those analyzed through ICP MS techniques where bulk or representative pieces of the samples were powdered or specific areas were powdered using a microdrill, and the carbonate isolated by partial digestion (Figs. 7, 8). They too exhibit negative Ce anomalies, positive Eu anomalies and sometimes neither, however; they rarely exhibit both (Fig. 37 & 38). Fenestrae and matrix cement within Fenestrated Microbialite often exhibit one anomaly or the other depending on the sample, and some samples, such as X20 and X21 for example, exhibit some different attributes even though they are only 4m apart stratigraphically (Figs. 37 & 38). Organic-rich recrystallized micrites infrequently display Eu anomalies, if they do they are typically masked by Gd anomalies and at very low values. Very suprachondtridic Y/Ho values are evident for each sample much like bulk ICP MS data. The concentration of primary ions that commonly substitute into a calcite crystal lattice (Sr, Mg, Mn, and Fe) are quite similar to one another; although, some samples show more variance than others (Figs. 39-42).

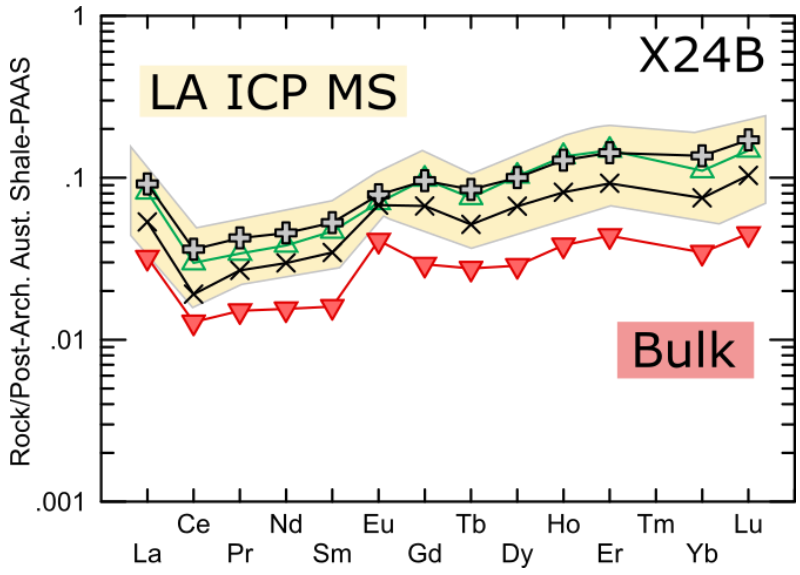

Fig. 37. PAAS normalized REE spectra of microbial carbonate sample X24B. Comparison between the two different techniques: (1) LA highlighted in yellow and (2) regular whole rock partial dissolution ICP MS in red. It simply shows striking similarities which suggests both analytical procedures were acceptable. Symbols represent sublithotopes, for legend see Fig. 30.

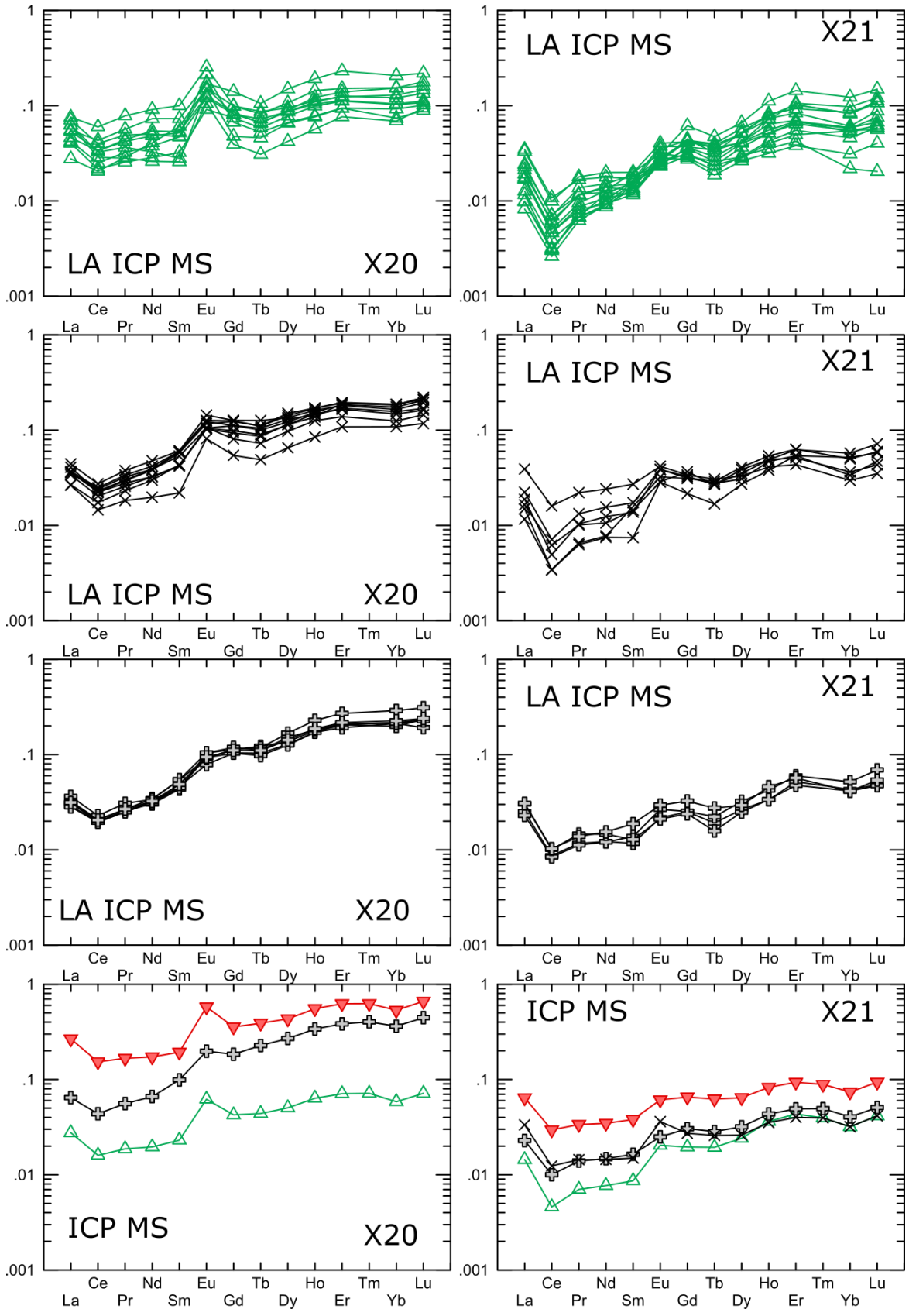
LA ICP MS
X20
LA ICP MS
X21
LA ICP MS
X20
LA ICP MS
X21
LA ICP MS
X20
LA ICP MS
X21
ICP MS
X20
ICP MS
X21
1
.1
.01
.001
La Ce Pr Nd Sm Eu Gd Tb Dy Ho Er Tm Yb Lu

Fig. 38. (previous page) Comparison between PAAS normalized REE results for two analytical techniques, ICP MS and LA-ICP-MS (labelled accordingly) on two microbial carbonate samples (X20 and X21). Bulk powder sampling and microdrilling techniques were tested via ICP MS, thus symbols for specific microdrilled samples match the LA spot analysis and the representative bulk sample is shown for comparison (red closed triangles). Microdrilling ICP MS results are comparable to LA-ICP-MS, both further define the representative bulk sample which often mutes anomalies with larger (~4X) REE concentrations compared to LA and microdrilled results. This may in part be due to slight siliciclastic contamination or areas within the bulk sample were more enriched in REE than the spot analysis. The fenestrae (green open triangles) are markedly different between the two samples and are internally quite consistent. The fenestrae resemble the matrix precipitates (black exes) and the organic-rich component (black crosses) with more prominent anomalies. Sample X20 displays a positive Eu anomaly in the fenestrae while X21 shows a negative Ce anomaly. Considering the observations above and their stratigraphic relationship with X21 overlying X20 by ~4m we suggest dissolution of the surrounding ground mass and precipitation was occurring quite locally.

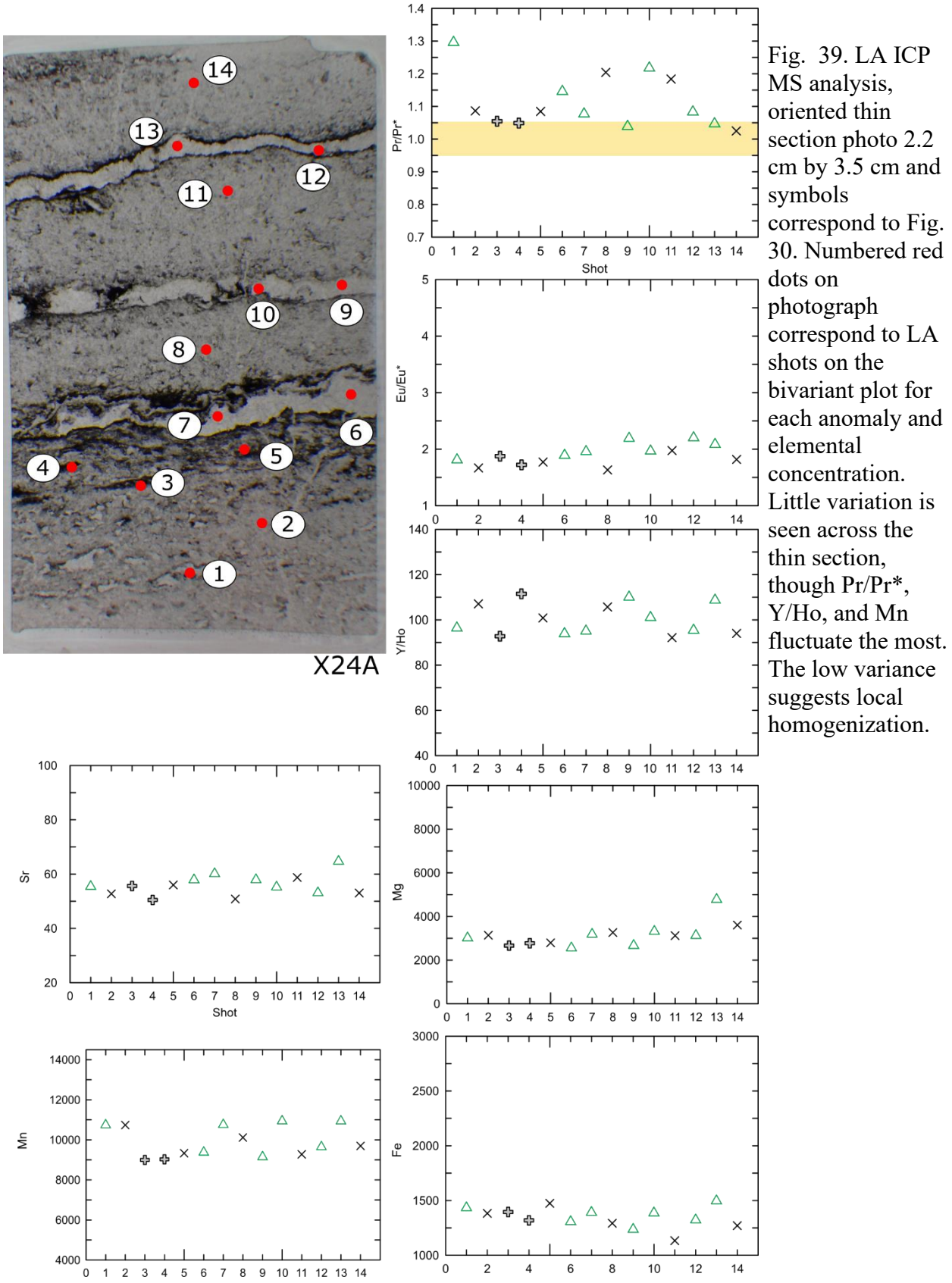

Fig. 39. LA ICP MS analysis, oriented thin section photo 2.2 cm by 3.5 cm and symbols correspond to Fig. 30. Numbered red dots on photograph correspond to LA shots on the bivariant plot for each anomaly and elemental concentration. Little variation is seen across the thin section, though Pr/Pr*, Y/Ho, and Mn fluctuate the most. The low variance suggests local homogenization.

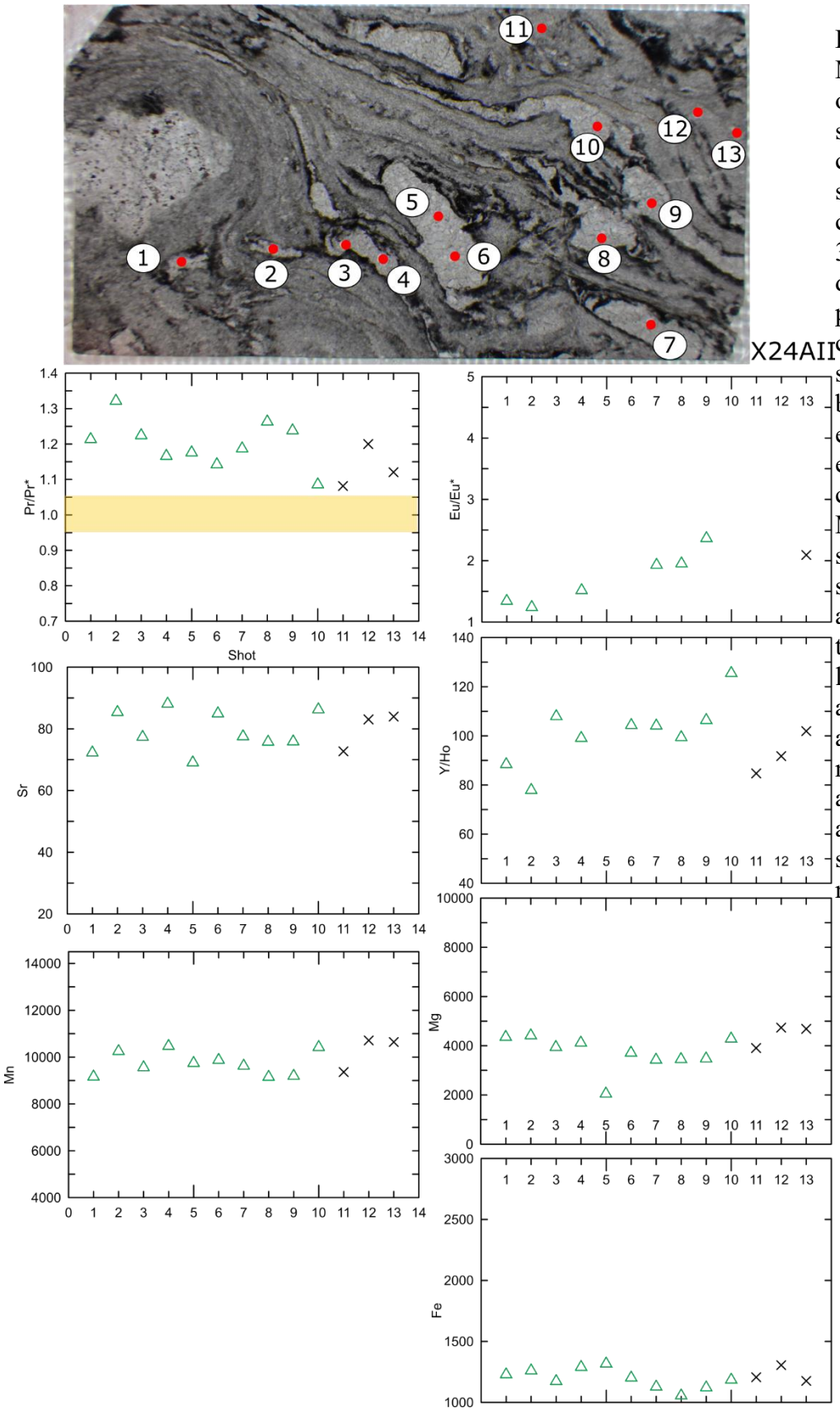

Fig. 40. LA-ICP-MS analysis, oriented thin section photo 2.2 cm by 3.5 cm and symbols correspond to Fig. 30. Numbered red dots on photograph correspond to LA shots on the bivariant plot for each anomaly and elemental concentration. More variation is seen in this photo, stratigraphically above Fig. 39, though some areas lack Eu anomalies. Note all shots contain a negative Ce anomaly (Pr/Pr*) and a greater spread in Y/Ho ratios.

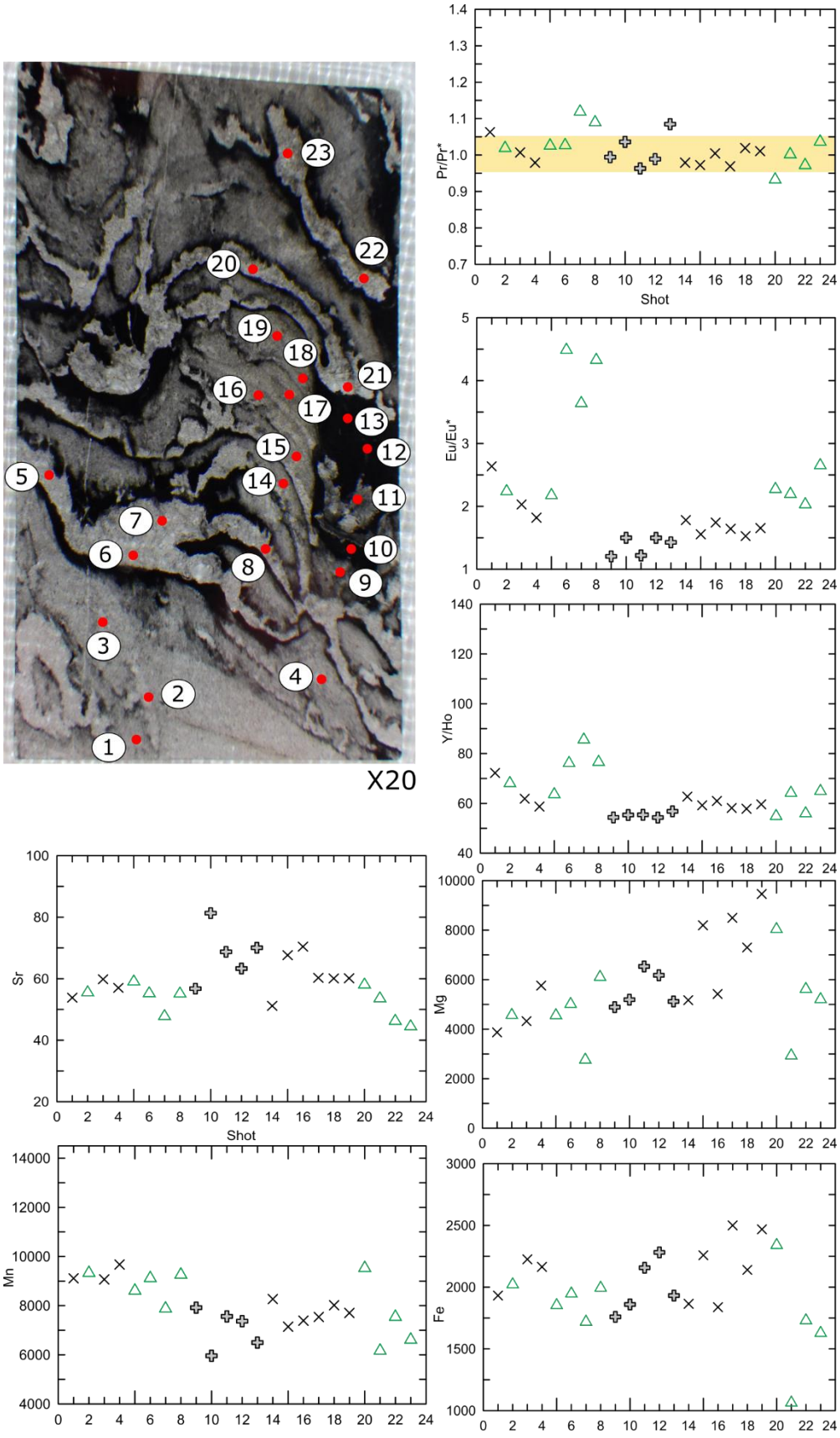

Fig. 41. LA-ICP-MS analysis, oriented thin section photo 2.2 cm by 3.5 cm and symbols correspond to Fig. 30. Numbered red dots on photograph correspond to LA shots on the bivariant plot for each anomaly and elemental concentration. This sample is nearly 7m above the sample shown in Fig. 40 and shows very few (Pr/Pr*) but some markedly positive Eu anomalies in the fenestrae, see text for interpretation. Note the lower Y/Ho ratios and elevated Fe and Mg values compared to samples shown in Fig. 39 through 42.

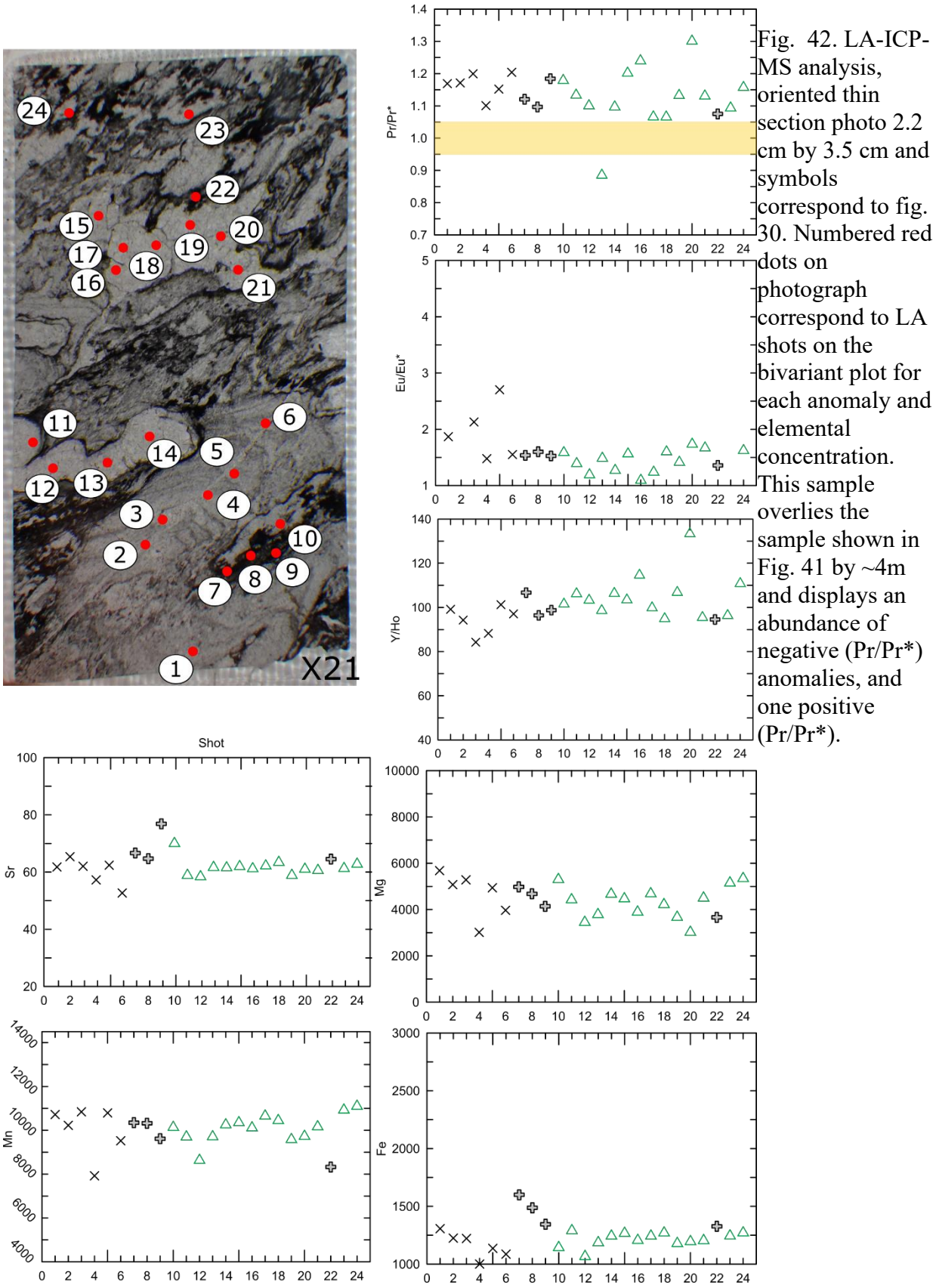

Fig. 42. LA-ICP-MS analysis, oriented thin section photo 2.2 cm by 3.5 cm and symbols correspond to fig. 30. Numbered red dots on photograph correspond to LA shots on the bivariant plot for each anomaly and elemental concentration. This sample overlies the sample shown in Fig. 41 by ~4m and displays an abundance of negative (Pr/Pr*) anomalies, and one positive (Pr/Pr*).

5.6 GEOCHEMISTRY VS DEPTH PROFILE: RESULTS

Plotting various anomalies and compositional ratios against stratigraphic depth highlights how the geochemistry evolved through deposition of the succession. Five meter moving averages of molar ratios, REE anomalies, $^{87}Sr/^{86}Sr$ and $\delta^{13}C$ are plotted against stratigraphic depth (Fig. 43, 44, 45, & 46). Molar ratios of calcium to other elements that commonly substitute into different carbonate minerals (Mg, Fe, Mn, Sr, and Ba) display a striking and consistent trend (Fig. 43). Three significant cycles of gradually decreasing and rapidly increasing abundances of ions that substitute for Ca in the carbonate lattice occur in the 90m succession. The substitution of elements for Ca is increased for the first 3 to 5m of section, followed by a decrease over the next approximately 30 m. Then there is a rapid increase in substitution followed by a gradual decrease up to the 58 m mark where, once again, a rapid increase in the substitution of ions for Ca occurs. The final cycle extends from 58m to 79m with the gradual decrease in substitution ended by an abrupt increase, though Ba and Sr begin their increased substitution rates at 76 m above the base of section.

The three cycles are not prominent when looking at ratios of elements that commonly substitute for Ca in carbonate without normalizing to Ca (Fig. 43). Aside from a couple of points at the beginning of the section Mn and Fe maintain the same ratio up to 20m above the base of section. Through the first half of this interval Sr is gaining in importance compared to these elements. Above 20 m Mn increases in importance compared to both Fe and Sr up to 76 m where Sr concentrations increase and 78 m where Fe in the carbonate drastically increases. Despite the poor sample distribution throughout the $\delta^{13}C$ display, the curve resembles Mn/Sr in the lower $2/3^{ds}$ of the section.

The REE anomalies and $^{87}Sr/^{86}Sr$ trends are not as drastic comparatively (Fig. 45). Higher in the section strontium isotope ratios become closer to the projected value for this time interval, denoted by the black line at 0.7018 (Veizer & Jansen, 1979; Taylor & McLennan, 1985; Veizer et al., 1989a,b; Godderis & Veizer, 2000; Veizer, 2003; Satkoski et al., 2017). Non-reset $^{87}Sr/^{86}Sr$ correspond to more significant negative Ce anomalies (Pr/Pr*), which increase strongly just before 60 and 80 meters. Overall, the La anomalies (Ce/Ce*) act oppositely to Pr/Pr* and decrease up section. The Y/Ho molar ratios are moderately above chondritic values in the first 30m, followed by an increase from 30 to 45 m, and fairly consistent high ratios for the remainder of the section.

The Eu anomaly (Eu/Eu*) is moderately scattered but exhibits some variation with a general increase up section.

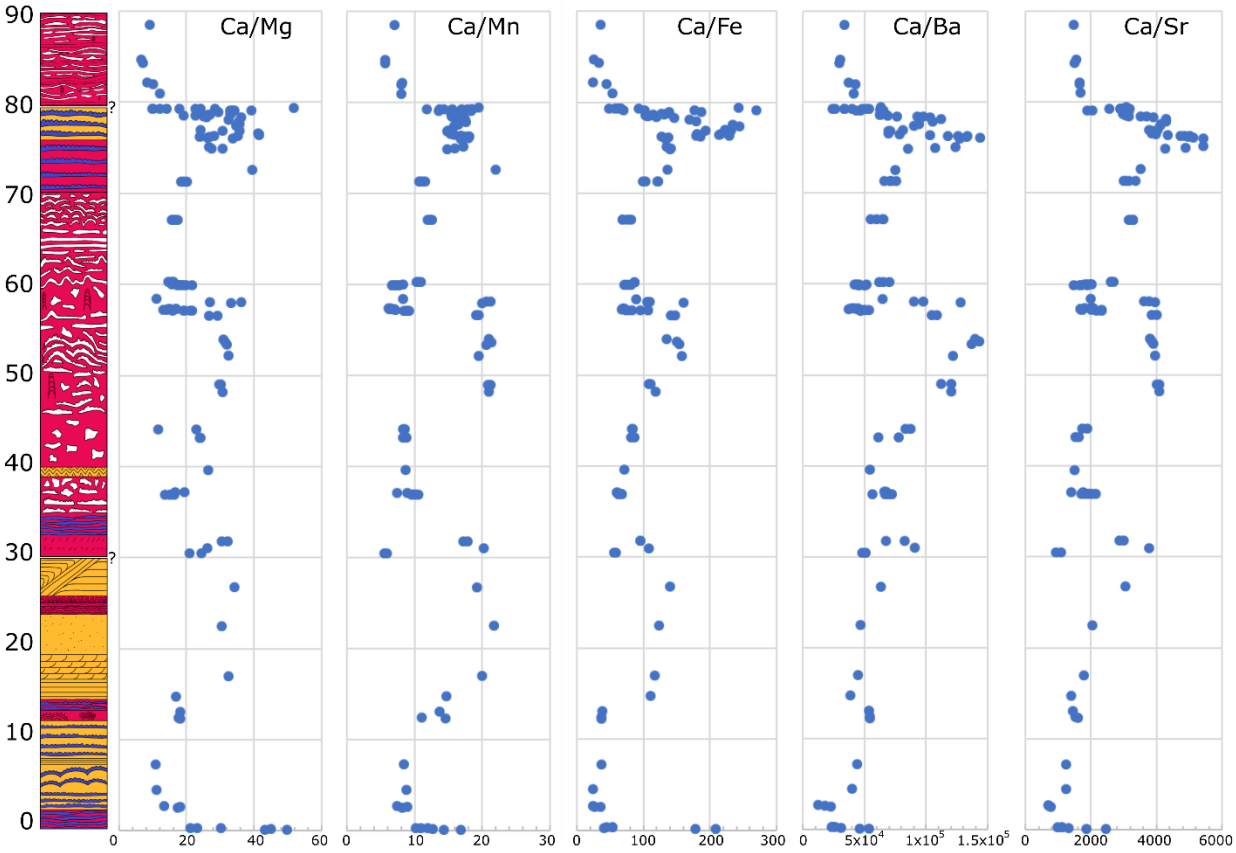

Fig. 43. Five meter moving averages of molar weight ratios normalized to Ca are plotted against stratigraphic depth. Ratios are of common carbonate group elements that substitute into various carbonate minerals. Three cycles of increasing and decreasing concentrations are evident. Decreasing trends represent times of higher substitution rates and an increase represents lower substitution rates relative to Ca (numerator).

Finer details and facies distinction can be observed on a smaller scale throughout a 6 m drill core from 74 to 80 m depth (Fig. 46). It highlights both the vertical evolution chemically and the facies relationships. What previously looked like a cluster of points is now more defined. The negative Ce anomaly (Pr/Pr*) is evident throughout most of this section but shows greater and sharp depletions of Ce (increasing Pr/Pr*) at approximately 76.25, 76.9, 78.5, and 79.5 m, which matches the Y/Ho trends over the same interval. The most interesting segment lies between 76 and 77 m where both trends begin increasing, followed by a sharp decrease then they quickly increase

again. During this interval, Ca/Mn and Mn/Sr display a similar, though more gradual, decrease to increase cycle.

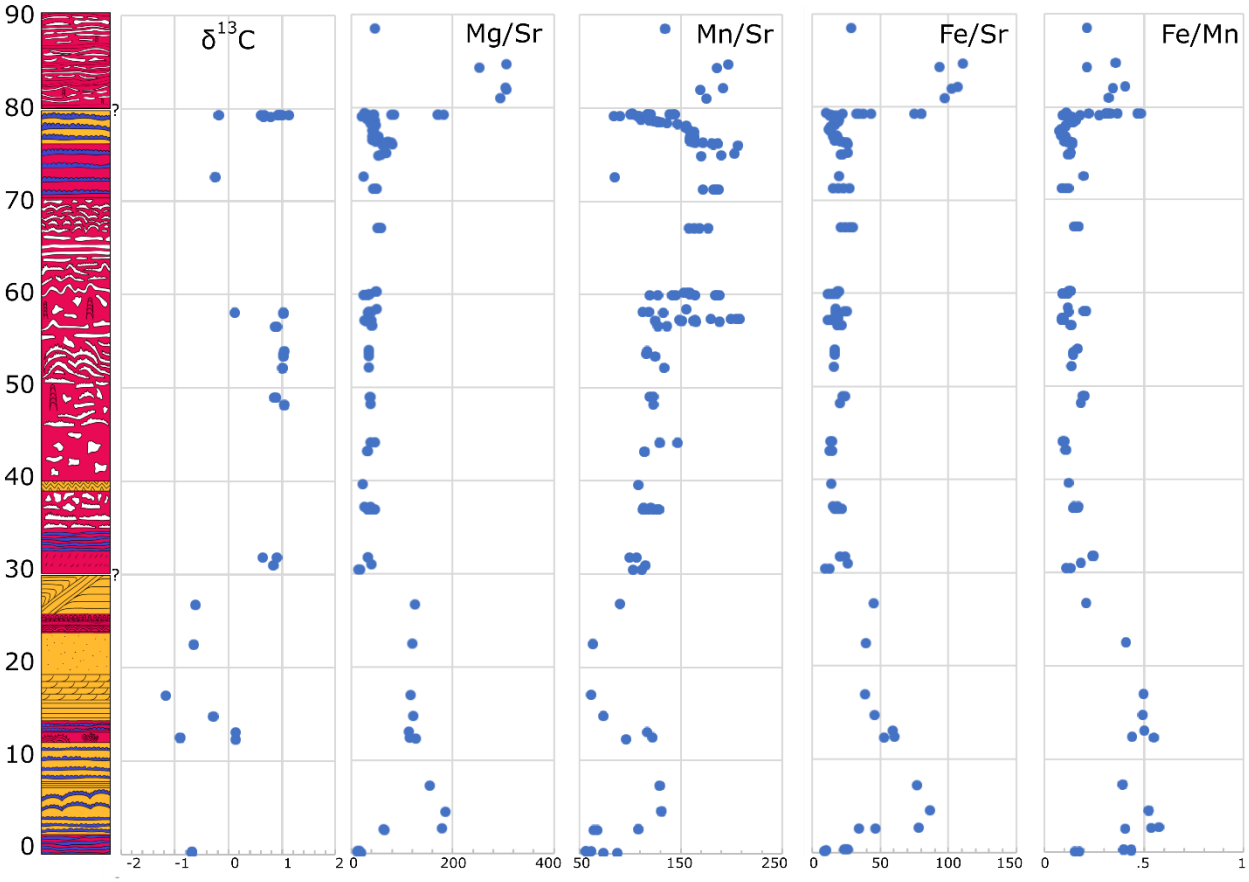

Fig. 44. Five meter moving averages of $\delta^{13}C$ and molar weight ratios normalized to Sr are plotted against stratigraphic depth. Ratios are of common carbonate group elements that substitute into various carbonate minerals, now normalized to Sr to differentiate how the elements are behaving without respect to Ca. Decreasing trends represent times of lower substitution rates and an increase represents higher substitution rates relative to Sr (denominator). The carbon isotopic ratios define a trend similar to that for Mn/Sr and the opposite of Ca/Mn.

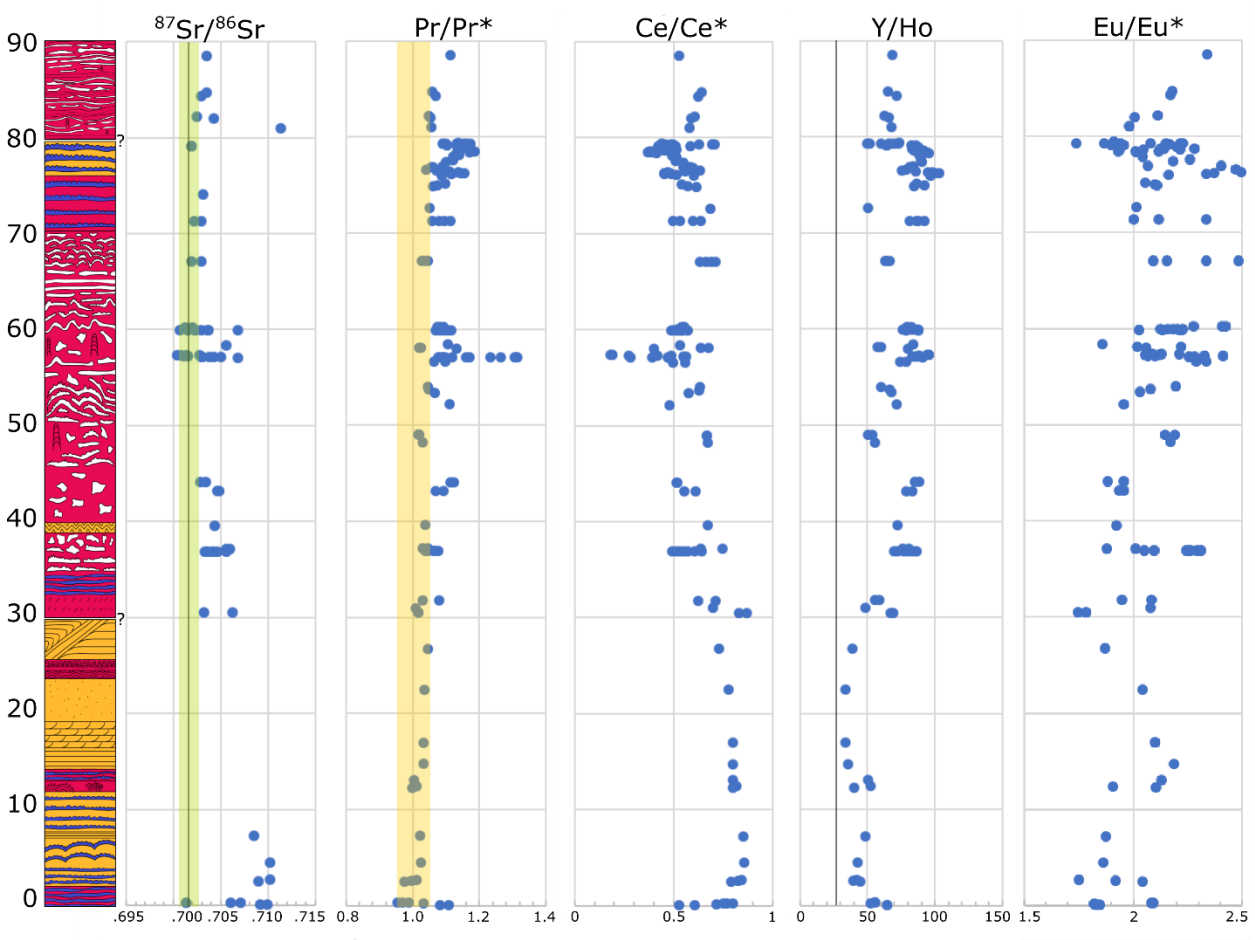

Fig. 45. Five meter moving averages of $^{87}Sr/^{86}Sr$ and REE anomalies plotted against stratigraphic depth. Strontium isotopes become less altered up section denoted by the black line at 0.7018 (Goddèris and Veizer 2000). Negative Ce anomaly (Pr/Pr*) becomes more significant (>1.05) where $^{87}Sr/^{86}Sr$ are less altered. The La anomaly (Ce/Ce*) slightly decreases up section while Y/Ho are only moderately super-chondritic from 3 to 30m, then increase to very super-chondritic, the black line is at 28 representing chondritic average. The Eu anomaly (Eu/Eu*) shows considerable scatter, though it does tend to increase up section.

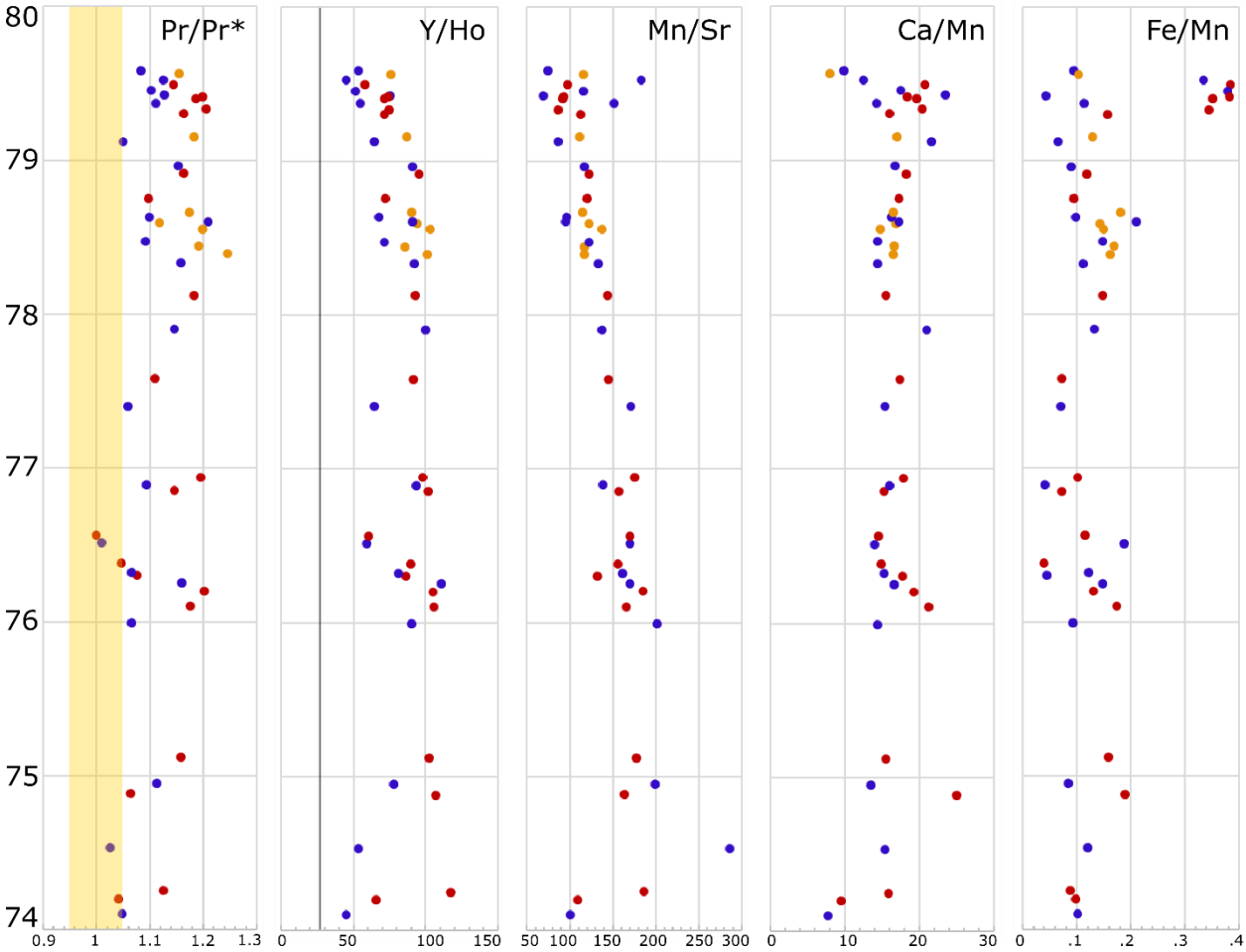

Fig. 46. Rare earth element anomalies and carbonate group mineral ratios from drill core samples taken between 74 and 80m of stratigraphic depth. Coloured circles correspond to lithotopes in stratigraphic column. Blue circles are silicified microbialite, red circles are carbonate microbialite, and yellow circles are carbonate grainstone.

5.7 GEOCHEMISTRY INTERPRETATIONS

Woman Lake carbonates are predominantly calcite and very few are dolomitized (Fig. 29A); those few are associated with mafic dikes. Carbonate production in today's ocean is primarily high magnesium calcite and aragonite, which surely incorporate calcium, carbon and oxygen as their major elements but within the mineral structure Ca^{2+} and CO_3^{2-} are commonly substituted for by secondary ions (Mg^{2+}, Sr^{2+}, Mn^{2+}, Fe^{2+}, SO_4^{2-}, UO_2^{2+}; Fantle, 2020). Their elemental compositions and isotopic signatures are dependent on a variety of seawater characteristics including: pH, temperature, salinity, elemental abundance or concentrations, and

redox conditions (Zhang & Nozaki, 1996), thus archiving a record of seawater conditions and compositions much like other chemical sediments (Kamber and Webb, 2001; Kato and Nakamura, 2003; Van Kranendonk et al., 2003; Bolhar et al., 2004). Analysis of common secondary ions that substitute into carbonate precipitates permit comparisons of their substitution rates, while analysis of trace element anomalies provide further depositional context. In addition to this, trace elements in the calcite lattice record effects of diagenesis; an alteration influenced by mass balance between primary and secondary fluid phases and their geochemical differences (Fantle et al., 2020). Diagenesis has the potential to homogenize carbonate geochemistry, and due to the number of trends that vary systematically throughout WLC's stratigraphic succession it is unlikely that it was greatly affected by such a process on a macro-scale. However, on a smaller scale, using LA-ICP-MS to differentiate between primary precipitated carbonate groundmass, organic-rich neomorphic cements after micrite, and the secondary precipitated fenestral cements within one thin section, the effects of local homogenization occur (Figs. 39-42). Frequently, within an individual thin section (2.2 cm by 3.5 cm) anomalies and concentrations only vary slightly, nonetheless significant differences are present between thin sections sampled 4 to 8 meters apart. For example, Fig. 38 compares two samples that were taken ~4m apart, and the fenestrae in the stratigraphically lower sample (X20) displays a positive Eu anomaly with no Ce anomaly while the fenestrae in the overlying sample (X21) exhibits no Eu anomaly and a negative Ce anomaly. The REE patterns for the fenestrae cements of both samples are similar to the individual sample's stromatolitic cements, organic-rich recrystallized micrite and bulk rock analysis (Fig. 38). Note that the organic-rich recrystallized micrite has subdued patterns compared to the fenestrae. Overall, this indicates that dissolution and precipitation on a small spatial scale homogenized localized areas but did not affect changes on the meter-scale.

The break in stratigraphic section at 30 m and again at 80 m is noteworthy, however geochemical trends tend to gradually change over both intervals suggesting minimal depositional time is missing. This is particularly evident in the core samples, drilled from 74 to 80 m (Fig. 46). At a smaller scale what otherwise looks like a cluster of points (Figs. 43, 44, & 45), resolves into gradual changes. This is evident in the drop in Ca/Mn between 79.3 and 79.6 m and the well-defined trends below this on Fig. 46 compared to the mass of points in this small interval on Fig. 43. Similarly, Y/Ho decreases from 78 to 80 m (Fig. 46) and, similar to most trends, the changes

in ratios below 80 m matches the values above 80m demonstrating that insignificant depositional time is missing between sections 2 and 3.

A positive Eu anomaly has become a well-known signature in Archean marine chemical sediments (Bau & Dulski, 1999; Derry & Jacobsen, 1990; Kamber & Webb, 2001; Webb & Kamber, 2011). It has become *prima facie* evidence which infers a large proportion of REE came from hot (<250 ºC) hydrothermal fluids which vented into, and thus enriched, Archean seawater (Derry and Jacobsen, 1988, 1990; Bau and Dulski, 1996). The existence of a positive Eu anomaly eludes to not only the presence of Archean seawater but also provides water depth estimates such as; semi-restricted lagoon, shallow onshore, to deep offshore (Kamber and Webb, 2001). Both Eu and La anomalies tend to increase with increasing water depth, which Kamber and Webb (2001) attribute to deeper offshore water masses that are saturated with REE, particularly near hydrothermal vent sources. Thus, shallow onshore waters are the least mixed with offshore waters and have lesser Eu and La anomalies. In a similar manner, Y/Ho ratios tend to increase with continued seawater interaction, particularly with particulate matter, and are affected by the degree of mixing. Terrigenous weathering products typically boast subchondritic values (<28) leaving the fluid suprachondritic, and further fractionation with seawater, especially in carbonate-rich environments produces very suprachondritic values from 44-110 (see Quinn et al., 2006 and references therein for discussion). Woman Lake carbonates often display positive Eu anomalies that only broadly increase up section while Y/Ho trends noticeably increase up through stratigraphy (Fig. 45) which have a prominent, positive, linear correlation with Pr/Pr* (Fig. 47). This suggests with increased Y/Ho fractionation, Ce was also depleted, both scenarios likely occur in shallow water carbonate environments. The gradual increase in Eu suggests increasing effects of open/deep seawater sources and the Y/Ho values suggest ample fractionation typical of shallow marine environments. The Eu/Eu* anomalies only reaches 2.5 unlike deeper water deposits of iron formation which can reach up to 8 (Chert from Steep Rock for example; Fralick and Riding 2015). Consequently, with suprachondritic Y/Ho ratios and comparatively low Eu/Eu* anomalies it is more likely that the fluids were predominantly marine with variable albeit small influxes of hydrothermal fluids and terrigenous input, much like shallow marine environments recognized in the: Strelley Pool Chert (Allwood et al., 2010), Red Lake Carbonates (McIntyre and Fralick, 2017), Steep Rock- Mosher Carbonates (Fralick and Riding, 2015), Chobeni Formation (Viezer and

McKenzie, 2014; Kamber et al., 2014), and Kalache, Marikanve, and Bhimasamudra Carbonates of the Dharwar Craton (Khelen et al., 2019). Then again, larger positive Eu anomalies could result from interaction with highly reducing fluids reducing Eu^{3+} to Eu^{2+} (MacRae et al., 1992). The dark, organic-rich carbon coating numerous fenestrae (Fig. 19, 21, & 39-42) suggests that organic fluid moved through those pores prior to filling with white cement. These organic-rich reducing fluids would be able to reduce Eu^{3+} from surrounding carbonate making it more soluble than other REE and returning Eu^{2+} to solution. Eventually that fluid will reprecipitate elsewhere with additional Eu, producing a more significant positive anomaly. In Figure 38 for instance, sample X20 has significantly positive Eu anomalies in the fenestrae while those in the ground mass and organic-rich matter are subdued. Laser ablation shots 6, 7, and 8 in particular have an elevated Eu anomaly compared to the other shots (Fig. 39), likely a product of highly reducing fluids extracting Eu from surrounding carbonate during dissolution resulting in later carbonate cements having larger Eu anomalies.

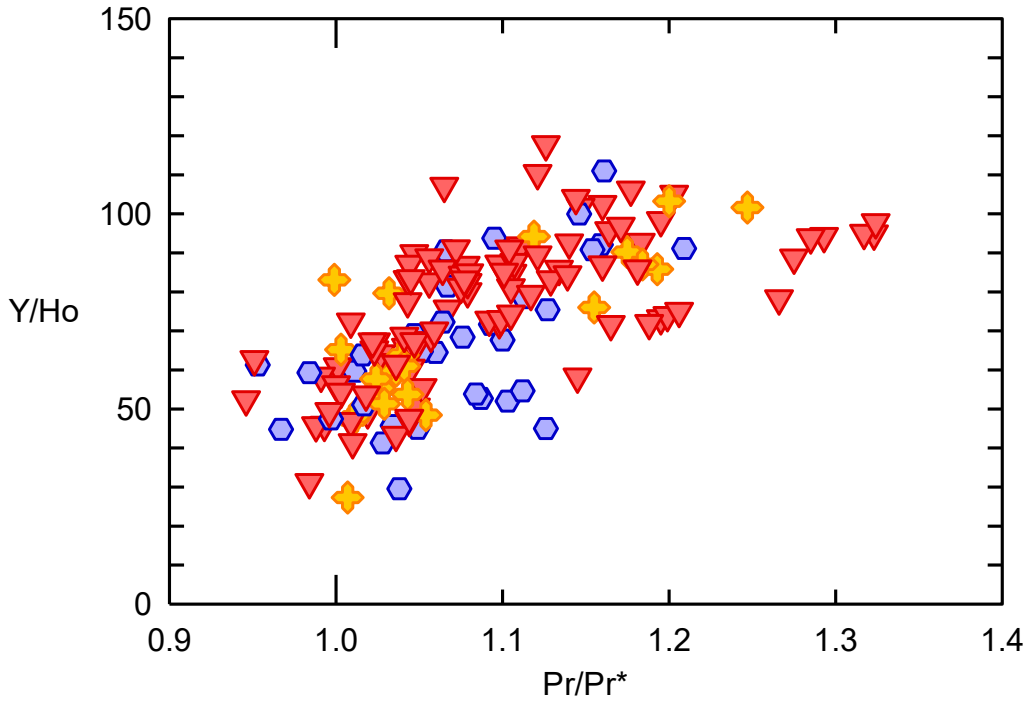

Fig. 47. Bivariant plot of Ce anomaly (Pr/Pr*) vs. Y/Ho displaying a positive correlation suggesting that with increased Y/Ho fractionation the negative Ce anomaly is, on average, increased. Superchondritic Y/Ho values >44 are indicative of shallow marine waters (Nozaki et al., 1997; Kamber and Webb, 2001) and negative Ce anomalies greater than 1.05 suggest the waters from which these carbonates precipitated encountered free oxygen Bau and Dulski (1996).

Significant, or true negative, Ce anomalies were first defined by Bau and Dulski (1996) and later refined by Bekker and others (2010) to limit the possibility of an anomaly appearing due to analytical error. Samples with La anomalies ($Ce/Ce^*_{SN} = (Ce_{SN}/(0.5(Pr_{SN} + La_{SN}))$) and Ce anomalies ($Pr/Pr^*_{SN}$ $(Pr_{SN}/(0.5Ce_{SN} + 0.5Nd_{SN})) < 0.95$ and >1.05 are considered significant for their respective anomalies (Fig. 48A). Over half of the carbonate collected from outcrop and drill-core contain true negative Ce anomalies (89/152), indicating the waters that precipitated WLCs encountered free oxygen, which preferentially removed Ce from solution rendering the remaining fluids with reduced Ce, and capable of producing Ce depleted carbonates. This signature is characteristic of modern seawater and searched for in the Archean to indicate signs of free oxygen. Although there is a shortage of REE geochemical studies on Archean carbonates, there are a fair amount and thus far very few places have significant negative Ce anomalies Fig. 48B. The Woman Lake carbonates are therefore one of the few oldest carbonate platforms to contain *prima facie* evidence for free oxygen in the water column, 60my before similar negative Ce anomalies at Steep Rock Lake (Fralick and Riding, 2015). Prior to the deposition of WLC, there is U-isotopic evidence supporting oxidative weathering of continental derived detritus within 3.07 to 2.90 Ga marine and lacustrine shales from the Kaapvaal Craton, SA (Wang et al., 2020).

Veizer and others (1989b) estimated that $\delta^{13}C$ for the Archean seawater spans from -3 to +3‰ although further evidence is suggesting that deeper water carbonates have considerably lesser values (Hammersley - Bekker and Clayton, 1972; Kaufman, 1990, Transvaal Supergroup - Beukes et al., 1990; Schneiderhan et al., 2006; Fischer et al., 2009, and Steep Rock - Fralick and Riding, 2015 for example). More recently in Red Lake, McIyntire and Fralick (2017) noted a difference between shallow water carbonates and deeper water carbonate deposits, associated with distal chert and oxide facies iron formation where isotopic values become more negative with greater depths. Woman Lake carbonates tend to behave accordingly with isotopic values ranging from -3.83‰ to 1.30‰, with an average of 0.53‰ (±0.59, n=31). The most negative value came from the cross-stratified and parallel laminated grainstones (near the top of the 1st stratigraphic section), which are interpreted here as potential sand bars in the subtidal environment or tidal channels in the intertidal. Light carbon isotopes are also found in silicified stratiform mats (-0.69‰) found in the upper intertidal flat. By contrast the highest value is from the chaotic assemblage (Unit H, 1.3‰), which, as indicated by the amount of stromatolitic debris it contains, likely slumped from a very

shallow environment. Other positive values are typically present in the Microbial Carbonates (1.20, 1.08, 1.22‰), which were deposited in a comparatively very shallow water environment, the lower intertidal flat. With some discrepancies, WLC are characteristically heavier at shallow depths compared to deeper. Overall, $\delta^{13}C$ do not vary drastically throughout stratigraphy. There is a subtle increase up section (Fig. 44); granted, there is an uneven sampling distribution. For the scope of this thesis the distribution is enough to draw basic inferences, though further analysis is warranted.

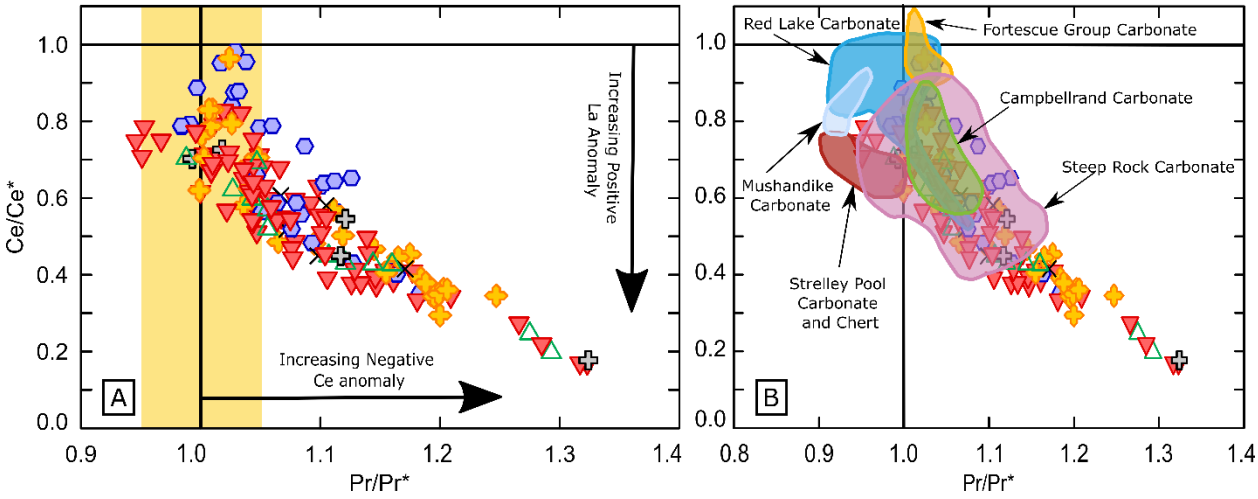

Fig. 48. A) Bivariant plot of Ce anomalies (Pr/Pr*) represented by Pr/(0.5*Ce+0.5*Nd) against La anomalies (Ce/Ce*) represented by Ce/(0.5*Pr+0.5*La) normalized (*) to PAAS (Taylor and Mclennen, 1994) and highlighting significant negative Ce anomalies defined by Bau and Dulski (1996) and Bekker et al., (2010) present within WLC. B) Samples from Woman Lake plotted with other Meso and Neoarchean Archean carbonate deposits for comparison. Samples from Woman Lake extend farther with more significant (Pr/Pr*) than other deposits. This may reflect a larger sample size and/or indicate a more prominent degree of free oxygen circulation within WLC. Data from: Bau and Dulski (1996), Kamber and Webb (2001), Bolhar et al. (2004), Kamber et al. (2004), Fralick and Riding (2015) and McIntyre and Fralick (2017).

In general, it is important to note that the $\delta^{13}C$ are shifting throughout WLC deposition and since $\delta^{13}C$ are affected by more attributes than precipitation and substitution rates are, they reflect the water chemistry, and by proxy the depositional environment, differently. Stable carbon isotopes are sensitive to evaporation and the small rise in $\delta^{13}C$ ratio throughout the sequence (also corresponds to the Mn/Sr ratio and inversely to the Ca/Mn ratio) may suggest that WLC precipitated on a semi-restricted environment prone to evaporation. Evaporation promotes heavier

isotopes over time while continuously evaporating the light carbon and concentrating the heavy in the water column (Stiller et al., 1985; Schidlowski et al., 1985; Casanova and Marcell, 1993; Valero-Garcés et al., 1999; Fralick and Riding 2015). Thus, shallow environments that are more susceptible to evaporation are expected to have heavy carbon isotope enrichment compared to deeper offshore environments. However, freshwater interaction in a shallow water environment may provide lighter carbon isotopes. Modern freshwaters draining into the Jade Bay of the southern North Sea exhibit markedly light $\delta^{13}C$ (Winde et al., 2014, Table 1). Therefore, the light $\delta^{13}C$ at the base of the stratigraphic section where silicified stratiform mats are prevalent in an upper intertidal environment may have been exposed to fresh water coming from the landmass (Fig. 44). This is followed by a quick increase that remains until ~7m where samples are enriched in heavy $\delta^{13}C$ throughout its transition to the lower intertidal flat before they gradually return to lighter enrichments in the low domal and digitate stromatolites within the subtidal environment. We have light isotopes in a relatively shallow environment and the isotopes quickly become heavy and are gradually getting lighter as we transition into deeper environments which is unlikely a product of a restricted evaporitic environment. If the environment was restricted it would have to become so very quickly in order to explain the quick transition from negative to positive values, then gradually become less restricted to explain the slow transition from positive back to negative values, which is typically against the most common natural formation and degradation of restricted environments. Otherwise the progressively lighter values with increasing depth may result from a regression, moving the shoreline closer to the previously subtidal environment and thus its inherit proximity to a freshwater source can then cause the isotopically lower values. After this, semi-restricted to restricted conditions may commence, as the gradual and sustained isotopically heavy values resume within the suspected intertidal environment from ~30 to ~75m (Fig. 45).

Strontium isotopic ratios exhibit similar overarching trends with an overall increase and although they too have an uneven sampling distribution, 16 of the samples were not likely reset and reflect the hypothetical seawater compositions at this time (black line and green error bar in Fig. 45; Veizer & Jansen, 1979; Taylor & McLennan, 1985; Veizer et al., 1989a,b; Godderis & Veizer, 2000; Veizer, 2003; Satkoski et al., 2017). Those that are not reset correspond to greater negative Ce anomalies (Pr/Pr*) in the latter half of the sequence suggesting preservation there is quite good. However, these are mixed with some reset values.

Analysis of trace elements, specifically secondary ions that commonly substitute into carbonate precipitates permit comparison of their substitution rates. By normalizing each element to calcium in Fig. 43, we can see how elemental concentrations vary throughout the stratigraphy and thus throughout the platform's deposition with respect to calcium. Additionally, substitution rates of common secondary ions can be compared to one another by normalizing to a common but less abundant ion such as Sr (Fig. 44). A gradual increase in Figure 43 indicates the slow continuously diminishing substitution rates of secondary ions into the calcite crystal lattice. The gradually diminishing substitution rates are commonly followed by a sharp decrease on the graph (Fig. 43), which infers substitution rates are quickly rising.

A fair amount of work has been focused on how trace elements are incorporated into the crystal lattice, or how elements are partitioned from an aqueous solution into a solid. In terms of $CaCO_3$ crystal structure this can be done in one of four ways: 1) substitution for Ca^{2+}, 2) interstitial substitution between planes, 3) substitution into vacant lattice positions due to defects in the structure, and 4) adsorption due to remnant ionic charges (Veizer, 1983). Studies generally tend to focus on the thermodynamics and kinetics of each element, they quantify the distribution coefficient (K_d) of trace elements which determines each elements ability to be partitioned between a carbonate mineral and an aqueous solution. It is calculated from the solubility products of major element carbonate (MCO_3) and trace element carbonate (TrCO3; McIntire, 1963). The K_d assumes the system is at equilibrium, however substitution depends on not only pressure and temperature but more importantly the compositions of the solid and liquid phases. When $K_d > 1$ the precipitated solid will contain (relative to Ca or Ca+Mg) more trace elements than the water from which it was in equilibrium with. For $K_d < 1$ the precipitated solid will contain less trace elements than the water column it precipitated from (Veizer, 1983). Most work however, is experimental and focuses on a very small-scale, like zoning in a specific crystal (Reeder, and John, 1987; Paquette and Reeder, 1995; and references therein) plus, they focus on systems with only two elements precipitating out of solution at a time. This becomes a problem because in nature the system is inherently more complex.

A study focused on the growth rate of a calcite crystal noticed that divalent metals are differentially incorporated into the lattice due to the inherent differences between site and ion sizes. These steric or spacial differences result in ions larger than Ca^{2+} (Sr^{2+} + Ba^{2+}) having an

incorporation trend opposite to those that are smaller (Mn^{2+}, Fe^{2+}, Zn^{2+}, etc.) (Temmam and Paquette (2000). Despite these trends, the presence of one trace element has been recognized to enhance the K_d of another through coupled substitution. Sr for example, has a high K_d in the presence of Mn and Mg meaning these elements enhance Sr's ability to be incorporated into the lattice (Ichikuni, 1973; Carpenter and Lohmann, 1992; Takano, 1985). Similarly, sulfate will be incorporated when carbonate contains more than 4 wt% MnO (Takano, 1985). In addition to this, an elements' ability to be incorporated into the lattice is quite sensitive to the precipitation rate of calcite. These rates are often unknown, plus they can be transport limited, which means calcite precipitating in a quiet tidal pond may be different than a wave-washed shoal (Rimstidt, 1998). Thus, understanding substitution rates in complex solutions becomes incredibly difficult and as some have stated previously, the distribution coefficients should be applied in natural systems with considerable caution in mind (Morse and Bender 1990).

Regardless, some comparative generalizations can be made. Rimstidt and others (1998), state that under diagenetic conditions and particularly when cement is precipitating slowly in pore spaces, the experimental K_d (approximates equilibrium) probably provides more realistic estimates of trace elements being incorporated into the lattice. Especially Fe and Mn, which have nearly the same theoretical K_d (which assumes equilibrium) and are influenced by precipitation rates equally. Accordingly, the molar fraction ratio of Fe and Mn in calcite would be unaffected by the rate of precipitation and should directly reflect the concentration ratio of the water column (Rimstidt, 1998). In respect to WLC, by normalizing the trace elements (secondary ions) to Sr rather than Ca (Fig. 44) we can see their substitution rates and how they are responding regardless of Ca concentrations. Most importantly, Mn and Fe begin with the same trend for the first 30 m, after that point Mn concentrations increase gradually with respect to Fe; indicating that Fe became less available (Fig. 44). Redox conditions must be considered since over half of the sampled WLC exhibit a negative Ce anomaly (Pr/Pr*: Fig. 45 & 48), suggesting that free oxygen was present. The negative Ce anomaly gradually increases in abundance and becomes more significant up section, which corresponds to an increase in Y/Ho ratio, and the substitution rates of Fe/Sr and Fe/Mn (Fig. 45 & 47). Under oxidizing conditions Fe will be preferentially scavenged at the redox boundary relative to Mn. Therefore, with greater isolation of the shelf or more likely, increased organic productivity, Fe would have been removed from solution offshore preferentially to Mn

and as a result influxing seawater would have a lower Fe/Mn ratio for the precipitates to originate from. As platforms develop, they provide a larger areal space that is readily available for organic productivity to prosper which provides a likely reason for the increased amount of significant negative Ce anomalies as the sequence progresses. It follows that this would have led to more prolific precipitation of iron hydroxide or oxyhydroxide in an offshore redox zone thereby decreasing the Fe/Mn ratio in the carbonate shelf. Plus, more iron hydroxides or oxyhydroxides precipitating would have also preferentially removed Ho through adsorption thus increasing the Y/Ho ratio in a shoreward direction.

At approximately 75m Fe/Mn ratios along with all elements relative to Sr quickly plummet and rise, a decrease here suggests Sr was incorporated into the lattice more than Mn (Fig. 44). There are two primary sources of Sr in seawater: (1) oceanic hydrothermal fluids and (2) continental weathering (Satkoski et al., 2016) and today, continental weathering dominantly provides trace elements to seawater. Thus, it is possible that increased weathering and continental runoff may have provided additional Sr to the water column thereby decreasing the Mn/Sr ratio. However, to do so abruptly becomes complicated and the Sr content in the world ocean could not have changed significantly during the time scale represented by the WLC, therefore this is not considered a viable explanation. Instead, the increase in Sr in the carbonate lattice was likely caused by a shift in the carbonate phase precipitating. Strontium substitutes into aragonite in far greater quantities than into calcite. Thus, commencement of sporadic aragonite precipitation could drive the surge in Sr concentration. Such a change has been documented from the 2.8 Ga Steep Rock carbonate platform where it has been ascribed to an increase in dissolved Fe, which pushes carbonate stability into the aragonite field (Riding et al., 2014). Continued increase in Fe^{2+} in the water moves the precipitating carbonate phase into the dolomite/ankerite field (Riding et al., 2014). This could explain the rapid increase directly above the spike in Sr concentration of Mg, Fe and Mn relative to Ca and Sr in the carbonate lattice (Figs. 43 & 44). Since calcite is the predominant carbonate phase precipitating at Woman Lake, a complete phase change to dolomite may not be necessary. The Ca/Mg and Ca/Fe activity ratios of some samples do indicate that they have considerably more Fe and Mg in them than most other samples and perhaps the Ca/Mg ratio was great enough to drive replacement reactions (rather than substitution) causing a decrease in Ca/Mg, Ca/Fe, and Ca/Mn concentrations and an increase in Fe/Sr for the last 10m (Fig. 44). Since

additional degrees of dissolved Fe^{2+} due to the redox boundary moving toward shoreline explains both the drop in Ca/Sr and increase in Sr/Mn between 75 and 80 m as well as the subsequent rapid increase in Mg, Fe, and Mn in the carbonate lattice, it is the preferred mechanism for these trends. However, for elements other than Fe and Mn the rate of precipitation complicates our ability to infer whether or not it will be added to the precipitating phase.

One of the primary factors controlling the rate of reaction of carbonate minerals in aqueous solutions is the degree of disequilibrium that is: its degree of over or undersaturation (Morse and Mackenzie, 1990). The general rule is that the rate of reaction increases with increasing disequilibrium (Morse and Mackenzie, 1990). Thus, with greater levels of super saturation, the rate of precipitation will increase and with greater levels of undersaturation the rate of dissolution will increase compared to the rates at equilibrium. In systems where the precipitated solid phase is minor compared to the amount of water (lower saturation) the equilibrium situation applies. In contrast, in systems where the precipitated solid phase is major compared to the amount of water (supersaturated), the water changes its composition in the course of precipitation and this is reflected in the trace element concentration gradients within the solid phase (Veizer, 1983). The oscillating cycles present in WLC (Fig. 43) developed over 90m of stratigraphic section and could result if the water column had limited access to the open ocean, by the same manner a back-reef lagoon may develop for example. Once semi-restricted, minerals would continue to precipitate from the water column and without a constant influx of sea water to replenish those elements the mineral precipitates must use the remaining elements, thus evolving the chemistry of precipitating minerals. Veizer (1983) states that K_d appears to shift toward unity and thus towards less pronounced partitioning of trace elements with increased precipitation rates (rate of reaction when supersaturated). In other words, with increased precipitation rates, less trace elements appear to be incorporated to the crystal lattice.

Through experimentally measured K_d analysis for trace elements in carbonate, Rimstidt and others (1998) showed that experimental K_d increases or decreases systematically with decreasing or increasing precipitation rates respectively. The experimental K_d value only approximates equilibrium unlike the theoretical K_d value. For theoretical K_d values >1, the experimental K_d values are systematically decreased with increased precipitation rates. Thus, less elements were substituting in with more precipitation when the theoretical value expected more

trace elements would be incorporated, relative to Ca. In contrast, for theoretical K_d values <1, the experimental K_d values are systematically increased with decreasing precipitation rates. Thus, when the calculated value was low (<1) and few trace elements were expected to be incorporated, its ability determined experimentally showed more trace elements were being incorporated with lower precipitation rates. This is due to processes occurring in the solution boundary layer of the growing crystals (Rimstidt et al., 1998) which would inherently occur in nature as well. Through their experimental data, they also noticed that trace elements are less likely to be incorporated with increasing precipitation rates and vice-versa.

In spite of the inherent complications behind not knowing exact precipitation rates, the affects some elements have on one another, and transport limitations between ions and the crystal lattice itself, some general relationships can be made with respect to the depositional environment. Consider the dynamics as a series between two end members, open and restricted oceanic conditions. Open water circulation promotes disequilibrium where the solution is less saturated, which is more in favour of dissolution than precipitation. As the system becomes semi-restricted to restricted the water column is still at disequilibrium, however elemental concentrations are able to build up due to evaporation and without being entirely diluted by constant water circulation, thus raising saturation levels and promoting precipitation. The trace elemental ratios in Fig. 43 display 3 cycles where substitution rates are slowly diminishing, then quickly rising. This could potentially mean that the system gradually became restricted with increased saturation levels and subsequently increased precipitation rates. Through Veizer's observations and Rimstidt and others (1998) experimental data, lesser trace elemental substitution appears to be related to increased precipitation rates. Thus, with gradual restriction, increased saturation and subsequent precipitation, substitution rates would probably slowly decrease as seen in Fig. 43. The trend reaches its lowest point in substitution rates, then increased amounts of trace elements are abruptly incorporated into WLC. This drastic change implies that rates of precipitation were declining. This could potentially be due to the platform reconnecting to the open ocean if the barrier structure was rapidly deteriorated in a large-scale storm event thus promoting seawater circulation on the shelf. However, this is difficult to invoke without physical evidence of a barrier structure at Woman Lake plus desiccation cracks and crystal fans characteristic of restricted environments are not present here. Also, cycles tend to correlate with increasing depth which is unlikely to occur with increased

restriction. Instead, it is more important to recognize the relationship between environmental depth and substitution rates in the WLC.

Interestingly, as the sequence proceeds into deeper environments, substitution rates slowly diminish. Then, with an abrupt change back to shallow depositional environments, substitution rates quickly rise (Fig. 43). This may showcase how precipitation rates are affected by transport-limited processes or more importantly accommodation space. With respects to sequence stratigraphy, carbonate systems commonly operate in the opposite manner compared to siliciclastic systems. When sea-level rises, carbonate production increases with increasing accommodation space as opposed to siliciclastic systems where the highest rate of sediment progradation occurs when sea-level falls (Coe et al., 2003). Thus, carbonate can only precipitate up to sea-level and subsequently precipitation rates scale with the amount of accommodation space available. In a similar manner and as discussed previously, stromatolite morphologies scale in size or at least synoptic relief with accommodation space as well. Within Archean carbonate environments it's generally accepted that stromatolites form through precipitation, where the microbial mats change their immediate microenvironment to induce precipitation thus lithifying the microbial mat (James and Jones, 2016; Shapiro and Wilmeth, 2020). Repeated microbial growth and precipitation produces the characteristic layering we see now, thus it is reasonable and anticipated that precipitation rates and thus stromatolite sizes should scale with accommodation space. As discussed above, Rimstidt and others (1998) noted that an increase in precipitation is associated with substitution rates that systematically decrease and by using approximate water depths (given by depositional features and stromatolitic morphologies) as a proxy for the degree of precipitation rate we can infer that water depth may ultimately be responsible for the 3 cycles of trace element substitution rates at Woman Lake (Fig. 43).

For example, in the first stratigraphic column (Fig. 43), samples may begin partially altered near the contact with the underlying felsic tuff, but as stromatolites and sedimentary features indicate the deposition environment is getting deeper and the substitution rates are slowly diminishing. At the base of the section stratiform to undulating mats are indicative of an upper intertidal environment, they are followed by, low domal and laterally continuous mats characteristic of central or lower intertidal environments, then domal bioherms, pseudocolumnar stromatolites, and cross stratified grainstones arise as the system transitions to tidal channels and/or

the subtidal environment. The environment gained more accommodation space which subsequently increased the rate of precipitation and decreased the rate of substitution (Fig. 43). The second stratigraphic column was likely deposited mostly within a tranquil lagoon environment due to the abundance of micritic sized carbonate, thrombolitic textures and abundant fenestrae. Again, as the environment transitions from an upper intertidal environment at the base with undulating microbialite it gains more elongated and smooth fenestral microbialite up section. This suggest the system is getting somewhat deeper, potentially reaching the edges of a lagoon since modern lower intertidal flats (which are also comparatively deeper than the upper intertidal) typically exhibit more smooth and horizontal fenestral lamination (James, 1984). Low domal fenestrated stromatolites increase in size around 50m stratigraphic height suggesting the environment gained accommodation space, likely within the central portions of the lagoon. With more accommodation space in the central lagoon precipitation rates are likely higher and this infers that substitution rates should decrease, which they do until ~58m. Then substitution rates increase which correspond once more with elongated and smooth fenestrae as well as banded carbonate suggesting that water depths and thus precipitation rates are decreasing again, perhaps reaching the opposite edge of the lagoon. From there, substitution rates decrease again (70-78m; Fig. 43), which are associated with low domal and laterally continuous stromatolites characteristic of central to lower intertidal environments much like those at the base of the section which is relatively deeper than the edge of the lagoon. Overall, there is a correlation between water depth, inferred precipitation rates, and substitution of trace element rates within WLC but with our current understanding of the interplay between complex aqueous solutions, precipitation and the incorporation of trace elements into those precipitates, it is unwise to boast further interpretations.

6.0 FINAL SYNTHESIS

The Mesoarchean carbonate platform at Woman Lake contains a record of carbonate platform development that fills what was previously a 130 million year void between Red Lake (2.93Ga; Corfu and Wallace, 1986) and Steep Rock Lake (2.8 Ga; Riding et al., 2014). Since the carbonates lie conformably above subaerial tuff (Thurston, 1980), it is assumed that WLC are on the shelf of a landmass. The 90-meter accumulation of limestone, its sedimentary features and microbial varieties suggest that the WLC precipitated in warm shallow waters under basic conditions thus permitting carbonate precipitation. Sedimentological evidence infers that each lithotope (carbonate microbialite, grainy carbonate, and silicified microbialite) was deposited in low to mid energy shallow waters on what was likely a carbonate ramp due to the apparent absence of larger features forming a barrier reef or rim. Three main stromatolitic morphologies exist and represent a range from low to moderate energy in shallow intertidal to sub-tidal environments. They are: 1) low relief stratiform to undulating stromatolites 2) laterally linked low domal and pseudocolumnar stromatolites, and 3) isolated to locally isolated domes and narrow columnar stromatolites. The presence of cross-stratification and parallel lamination within the WLC indicates that sand-sized grains were being deposited and its stratigraphic relationships place them in a lower intertidal to subtidal environment. Since their geochemical trends are exceptionally similar to microbial carbonate, they were likely sourced from microbial carbonate deposits like WLC itself.

Geochemical trends paired with stratigraphic depth show gradual to sharp changes throughout the platform's deposition. The observed trends suggest that the precipitating carbonates were able to record and retain the effects an evolving water column and environment had on stromatolitic morphology and mineralogy on a metric scale 2.86 Gya. On a microscopic scale, using LA-ICP-MS there is less contrast between carbonate phases which indicates that dissolution and precipitation on a small spatial scale homogenized localized areas, but did not affect changes on a metric scale. The main geochemical implications made herein follow:

1) Comparison of bulk sampling, microdrilling, and spot analysis indicate that microdrilling and spot analysis produce exceptionally similar results despite lower concentrations in the

spot analysis. Elemental ratio analysis obtained through LA-ICP-MS proved useful (Fig. 38).

2) The Woman Lake carbonates are one of the few oldest carbonate platforms to contain *prima facie* evidence for free oxygen in the water column, 60my before similar negative Ce anomalies at Steep Rock Lake (Fralick and Riding, 2015). Over half of the limestone collected from outcrop and drill-core contain true negative Ce anomalies (89/152), indicating that the waters which precipitated WLCs encountered free oxygen (Fig. 48). The anomaly varies but overall, increase gradually up section, which corresponds to increasing Y/Ho and decreasing Fe/Mn (Fig. 47 & 48). The fluctuations and general increasing trends suggest that organic productivity may have increased causing greater oxygen production. This would have led to more prolific precipitation of iron hydroxide or oxyhydroxide in an offshore redox zone, decreasing the Fe/Mn ratio on the carbonate shelf. The increasing precipitation of iron hydroxides or oxyhydroxides would have also preferentially removed Ho through adsorption, increasing the Y/Ho ratio in the shoreward carbonates.

3) Woman Lake carbonates often display positive Eu anomalies that only broadly increase up section while Y/Ho trends noticeably increase up through stratigraphy (Fig. 45). The gradual increase in Eu suggests increasing effects of open/deep seawater sources and the Y/Ho values suggest ample fractionation typical of shallow marine environments. With suprachondritic Y/Ho ratios (mostly 40 to 110) and comparatively low Eu anomalies it is more likely that the fluids were predominantly coastal marine with variable influxes of open seawater form deeper zones and possibly small additions of water from the adjacent landmass much like shallow marine environments recognized in the: Strelley Pool Chert (Allwood et al., 2010), Red Lake Carbonates (McIntyre and Fralick, 2017), Steep Rock-Mosher Carbonates (Fralick and Riding, 2015), Chobeni Formation (Viezer and McKenzie, 2014; Kamber et al., 2014), and Kalache, Marikanve, and Bhimasamudra Carbonates of the Dharwar Craton (Khelen et al., 2019).

4) $\delta^{13}C$ ranges from -3.83‰ to 1.30‰, with an average of 0.53‰ (±0.59, n=31), which is typical for Archean carbonates. With some discrepancies, WLC are characteristically heavier at shallow depths compared to deep, which is a trend also noticed within the peritidal environments at Red Lake (McIntyre and Fralick, 2017). Overall, there is a subtle

increase up section and they do not vary drastically throughout stratigraphy. More analyses are necessary to confirm any inferences made.

5) Strontium isotopic ratios exhibit similar overarching trends compared to $\delta^{13}C$ and although they too have an uneven sampling distribution, 16 of the samples were not likely reset and reflect the hypothetical seawater compositions at this time (black line and green error bar in Fig. 45; Veizer & Jansen, 1979; Taylor & McLennan, 1985; Veizer et al., 1989a,b; Godderis & Veizer, 2000; Veizer, 2003; Satkoski et al., 2017). Those that are not reset correspond to greater negative Ce anomalies in the latter half of the sequence suggesting preservation there is quite good.

6) Analysis of secondary ions that commonly substitute into carbonate precipitates permit comparison of their substitution rates. Oscillating cycles (Fig. 43-46) developed over 90m of stratigraphic sequence and represent increasing or decreasing substitution rates. The fluctuations correspond to changes in depth in the intertidal to subtidal system and could result from increasing precipitation rate as depth gradually increases ending with rapid regression causing less accommodation space and decreased precipitation rates.

This study demonstrates the strength of combining sedimentological and geochemical data to obtain a complete and as comprehensive an understanding of Archean environments as possible. The geochemical trends up stratigraphy highlight that water column evolution was being recorded. It is difficult to suggest with confidence why the water column chemistry evolved long term, though it could be due to one of four reasons or a combination of them to varying degrees: 1) changes in biologic productivity, 2) periods of restricted circulation, 3) transgressions and regressions, and/or 4) diagenesis. Simply put, fluctuating geochemical trends and diverse stromatolitic morphology suggests some process must be modifying geochemical development, otherwise consistently homogenous trends would be observed, which is not the case for WLC.

Importantly, this succession is a transitional period in Earth's atmosphere when oxygen was able to accumulate in localized areas. Evidence herein prods an enduring curiosity and prompts a compelling question: What initiated oxygenation on Earth and how? Fralick and Riding (2015) discussed that theoretically, i.e if oxygen was being produced by the microbes themselves an

oxidation front should be observed. Due to the limited exposure and preservation at Woman Lake it is likely that the redox boundary itself occurred farther offshore and was not preserved.

REFERENCES

Abell, P. I., McClory, J., Martin, A., Nisbet, E.G., & Kyser, T. K. (1985). Petrography and stable isotope ratios from Archaean stromatolites, Mushandike Formation, Zimbabwe. Precambrian Research, 27(4), 385-398.

Allen, J.R.L. (1986) Earthquake magnitude-frequency, epicentral distance, and soft-sediment deformation in sedimentary basins. Sedimentary Geology. 46. 67-75.

Allwood, A. C., Walter, M. R., Burch, I. W., & Kamber, B. S. (2007). 3.43 billion-year-old stromatolite reef from the Pilbara Craton of Western Australia: ecosystem-scale insights to early life on Earth. Precambrian Research, 158(3-4), 198-227.

Allwood, A. C., Grotzinger, J. P., Knoll, A. H., Burch, I. W., Anderson, M. S., Coleman, M. L., & Kanik, I. (2009). Controls on development and diversity of Early Archean stromatolites. Proceedings of the National Academy of Sciences, 106(24), 9548-9555.

Allwood, A.C., Kamber, B.S., Walter, M.R., Burch, I.W. and Kanik, I. (2010). Trace elements record depositional history of an Early Archean stromatolitic carbonate platform. Chem. Geol., 270, 148-163

Anbar, A.D., Duan, Y., Lyons, T.W., Arnold, G.L., Kendall, B., Creaser, R.A., Kaufman, A.J., Gordon, G.W., Scott, C., Garvin, J. and Buick, R. (2007). A whiff of oxygen before the Great Oxidation Event? Science, 317(5846), 1903–1906. https://doi.org/10.1126/science.1140325

Awramik, S.M. & Buchheim, H.P. (2009). A giant, Late Archean lake system: The Meentheena Member (Tumbiana Formation; Fortescue Group), Western Australia. Precambrian Research, 174, 215–240.

Ayres, L. D., Lumbers, S. B., Milne, V. G., & Robeson, D. W. (1971). Ontario geological map 2197.

Barbieri R, & Cavalazzi, B. (2004). Astrobiological implications of microbial morphologies in cold fluid-generated carbonates. Adv Space Res 33:1262–1267.

Bau, M., & Dulski, P. (1995). Comparative study of yttrium and rare-earth element behaviours in fluorine-rich hydrothermal fluids. Contributions to Mineralogy and Petrology, 119(2-3), 213-223.

Bau, M., & Dulski, P. (1996). Distribution of yttrium and rare-earth elements in the Penge and Kuruman iron-formations, Transvaal Supergroup, South Africa. Precambrian Research, 79(1-2), 37-55.

Bau, M. (1991). Rare-earth element mobility during hydrothermal and metamorphic fluid-rock interaction and the significance of the oxidation state of europium. Chemical Geology, 93(3-4), 219-230. https://doi.org/10.1016/0009-2541(91)90115-8

Bau, M., & Dulski, P. (1999). Comparing yttrium and rare earths in hydrothermal fluids from the Mid-Atlantic Ridge: Implications for Y and REE behaviour during near-vent mixing and for the Y/Ho ratio of proterozoic seawater. Chemical Geology, 155(1–2), 77–90. https://doi.org/10.1016/S0009-2541(98)00142-9

Bau, M., & Koschinsky, A. (2009). Oxidative scavenging of cerium on hydrous Fe oxide: evidence from the distribution of rare earth elements and yttrium between Fe oxides and Mn oxides in hydrogenetic ferromanganese crusts. Geochemical Journal, 43, 37–47.

Beakhouse, G. P., Heaman, L. M., & Creaser, R. A. (1999). Geochemical and U–Pb zircon geochronological constraints on the development of a Late Archean greenstone belt at Birch Lake, Superior Province, Canada. Precambrian Research, 97(1-2), 77-97.

Becker, R.H., & Clayton, R.N. (1972). Carbon isotopic evidence for the origin of a banded iron-formation in Western Australia. Geochimica et Cosmochimica Acta 36, 577–595.

Bekker A., Holland H. D., Wang P. L., Rumble D., Stein H. J., Hannah J. L., Coetzee L. L. and Beukes N. J. (2004). Dating the rise of atmospheric oxygen. Nature 427, 117–120.

Bekker, A., Krapež, B., Slack, J. F., Planavsky, N., Hofmann, A., Konhauser, K. O., & Rouxel, O. J. (2012). Iron formation: The sedimentary product of a complex interplay among mantle, tectonic, oceanic, and biospheric processes-a reply. Economic Geology, 107(2), 379–380. https://doi.org/10.2113/econgeo.107.2.379

Bellefroid, E. J., V.S. Hood, A., Hoffman, P. F., Thomas, M. D., Reinhard, C. T., & Planavsky, N. (2018). Constraints on paleoproterozoic atmospheric oxygen levels. Proceedings of the National Academy of Sciences of the United States of America, 115(32), 8104–8109. https://doi.org/10.1073/pnas.1806216115

Beukes, N. J. (1987). Facies relations, depositional environments and diagenesis in a major early Proterozoic stromatolitic carbonate platform to basinal sequence, Campbellrand Subgroup, Transvaal Supergroup, Southern Africa. Sedimentary Geology, 54(1-2), 1-46.

Beukes, N. J., Cornelis, K., Kaufman, A. J., & Hayes, J. M. (1990). Carbonate petrography, kerogen distribution, and carbon and oxygen isotope variations in an early Proterozoic transition from limestone to iron-formation deposition, Transvaal Supergroup, South Africa. Economic Geology, 85(4), 663–690.

Bolhar, R., Kamber, B. S., Moorbath, S., Fedo, C. M., & Whitehouse, M. J. (2004). Characterisation of early Archaean chemical sediments by trace element signatures. Earth and Planetary Science Letters, 222(1), 43–60. https://doi.org/10.1016/j.epsl.2004.02.016

Bolhar, R., Van Kranendonk, M.J., & Kamber, B.S. (2005). A trace element study of siderite-jasper banded iron formation in the 3.45 Ga Warrawoona Group, Pilbara Craton – formation from hydrothermal fluids and shallow seawater. Precambrian Research, 137, 93–114.

Bolhar, R., & Van Kranendonk, M.J. (2007). A non-marine depositional setting for the northern Fortescue Group, Pilbara Craton, inferred from trace element geochemistry of stromatolitic carbonates. Precambrian Research, 155, 229–250.

Bond, G., Wilson, J. F., & Winnall, N. J. (1973). Age of the Huntsman limestone (Bulawayan) stromatolites. Nature, 244(5414), 275-276.

Cady S.L, Farmer J.D, Grotzinger J.P, & Schopf J.W, Steele A. (2003). Morphological biosignatures and the search for life on Mars. Astrobiology 3:351–368.

Casanova, J., & Marcell, C.H., (1993). Carbon and oxygen isotopes in African lacustrine stromatolites: palaeohydrological interpretations. In: Swart, P.K., Lohmann, K.C., mckenzie, J., Savin, S. (Eds.), Climate Change in the Continental Isotopic Record. American Geophysical Union Geophysical Monograph, 94, pp. 123–133.

Chafetz, H. S., & Buczynski, C. (1992). Bacterially induced lithification of microbial mats. Palaios, 7(3), 277–293. https://doi.org/10.2307/3514973

Collerson, K. D., Kamber, B. S., & Schoenberg, R. (2002). Applications of accurate, high-precision Pb isotope ratio measurement by multi-collector ICP-MS. Chemical Geology, 188(1–2), 65–83. https://doi.org/10.1016/S0009-2541(02)00059-1

Corfu, F., & Wallace, H. (1986). U-Pb zircon ages for magmatism in the Red Lake greenstone belt, northwestern Ontario. Canadian Journal of Earth Sciences, 23(1), 27–42. https://doi.org/10.1139/e86-004

Davis, D.W. (2019) U-Pb Geochronology of Detrital Zircon by LA-ICPMS in samples from northern Ontario. Department of earth Sciences, University of Toronto

Demicco, R.V. (1983). Wavy and lenticular-bedded carbonate ribbon rocks of the Upper Cambrian Conococheague Limestone, central Appalachians. Journal of Sedimentary Petrology. 53, 1121–1132.

Derry L. A. & Jacobsen S. B. (1988). The Nd and Sr isotopic evolution of Proterozoic seawater. Geophysical Research Letters, 15(4), 397-400.

Derry, L. A., & Jacobsen, S. B. (1990). The chemical evolution of Precambrian seawater: Evidence from REEs in banded iron formations. Geochimica et Cosmochimica Acta, 54(11), 2965–2977. https://doi.org/10.1016/0016-7037(90)90114-Z

Dupraz, C., Pattisina, R., & Verrecchia, E. P. (2006). Translation of energy into morphology: Simulation of stromatolite morphospace using a stochastic model. Sedimentary Geology, 185(3-4 SPEC. ISS.), 185–203. https://doi.org/10.1016/j.sedgeo.2005.12.012

Elderfield, H., & Greaves, M. J. (1981). Negative cerium anomalies in the rare earth element patterns of oceanic ferromanganese nodules. Earth and Planetary Science Letters, 55(1), 163–170. https://doi.org/10.1016/0012-821X(81)90095-9

Fantle, M. S., Barnes, B. D., & Lau, K. V. (2020). The Role of Diagenesis in Shaping the Geochemistry of the Marine Carbonate Record. Annual Review of Earth and Planetary Sciences, 48(1), 549–583. https://doi.org/10.1146/annurev-earth-073019-060021

Farquhar, J., & Wing, B. A. (2003). Multiple sulfur isotopes and the evolution of the atmosphere. Earth and Planetary Science Letters, 213(1-2), 1-13.

Fischer, W.W., Schröder, S., Lacassie, J.P., Beukes, N.J., Goldberg, T., Strauss, H., Horstmann, U.E., Schrag, D.P., & Knoll, A.H. (2009). Isotopic constraints on the late Archean carbon cycle from the Transvaal Supergroup along the western margin of the Kaapvaal Craton, South Africa. Precambrian Research 169, 15–27. https://doi.org/10.1016/j.precamres.2008.10.010

Follmi, K. B., Weissert, H., & Funk, H. (1994). Phosphogenesis, carbon-isotope stratigraphy, and carbonate-platform evolution along the Lower Cretaceous northern Tethyan margin. Geological Society of America Bulletin, 729–746.

Fralick, P., (1989). Microbial bioherms, Lower Proterozoic Gunflint Formation, Thunder Bay, Ontario. In: Geldsetzer, H.H.J., James, N.P., Tebbutt, G.E. (Eds.), Reefs Canada and Adjacent Areas. Canadian Society Of Petroleum Geology Memoir. 13, pp. 24–29.

Fralick, P. ., Hollings, P., Metsaranta, R., & Heaman, L. M. (2009). Using sediment geochemistry and detrital zircon geochronology to categorize eroded igneous units: An example from the Mesoarchean Birch-Uchi Greenstone Belt, Superior Province. Precambrian Research, 168(1–2), 106–122. https://doi.org/10.1016/j.precamres.2008.05.009

Fralick, P., Planavsky, N., Burton, J., Jarvis, I., Addison, W. D., Barrett, T. J., & Brumpton, G. R. (2017). Geochemistry of Paleoproterozoic Gunflint Formation carbonate: Implications for hydrosphere-atmosphere evolution, 290, 126–146. https://doi.org/10.1016/j.precamres.2016.12.014

Fralick, P., & Riding, R. (2015). Steep Rock Lake: Sedimentology and geochemistry of an Archean carbonate platform. Earth-Science Reviews, 151, 132–175. https://doi.org/10.1016/j.earscirev.2015.10.006

Fryer, B.J. (1977). Rare-earth evidence in iron-formations for changing Precambrian oxidation-states. Geochimica et Cosmochimica Acta, 41, 361–367.

Gibson, E. K., McKay, D. S., Thomas-Keprta, K. L., Wentworth, S. J., Westall, F., Steele, A., … Toporski, J. (2001). Life on Mars: Evaluation of the evidence within Martian meteorites

ALH84001, Nakhla, and Shergotty. Precambrian Research, 106(1–2), 15–34. https://doi.org/10.1016/S0301-9268(00)00122-4

Godderis, Y. And Veizer, J. (2000). Tectonic control of chemical and isotopic composition of ancient oceans: the impact of continental growth. Am. J. Sci., 300, 434–461.

Goodwin, A.M. (1967). Volcanic studies in the Birch-Uchi Lakes Area of Ontario; Ontario Department of Mines, Miscellaneous Paper 6, 96p.

Green, M. G., & Buick, R. P. (2001). Early Archaean crustal evolution: evidence from ~3.5 billion year old greenstone successions in the Pilgangoora Belt, Pilbara Craton, Australia. School of Geosciences. Doctoral Dissertation. University of Sydney, Australia.1-288

Grey, K., & Thorne, A.M. (1985). Stratigraphic significance of stromatolites in shallowing sequences of the early Proterozoic Duck Creek dolomite, Western Australia. Precambrian Research. 29, 183–206.

Grey, K., & Awramik, S. M. (2020). Handbook for the study and description of microbialites. Geological Survery of Western Australia Bulletin, 147, 279.

Grotzinger, J.P. (1986a) Cyclicity and paleoenvironmental dynamics Rock Nest

Platform northwest Canada. Geological society of america bulletin. 97. 1208-1231

Grotzinger, j. P. (1989). Facies and evolution of precambrian carbonate depositional systems: emergence of the modern platform archetype. Society of economic paleontologists and mineralogists, 44, 1.

Grotzinger, J. P., & James, N. P. (2000). Precambrian Carbonates: Evolution of Understanding. Society for Sedimentary Geology, 67.

Gupta, V.K., Thurston, P.C., and Dusanowskj, T.H. (1982). Constraints upon Models of Greenstone Belt Evolution by Gravity Modelling, Birch- Uchi Greenstone Belt, Northern Ontario; Precambrian Research, Volume 16, p.233-255.

Haley, B. A., Klinkhammer, G. P., & mcmanus, J. (2004). Rare earth elements in pore waters of marine sediments. Geochimica et Cosmochimica Acta, 68(6), 1265-1279.

Harnmeijer, J. P. (2010). Squeezing Blood from a Stone: Inference into the Life and Depositional Environments. Doctoral dissertation. University of Washington, Seattle. 1-617.

Hegner, E., Kröner, A., & Hunt, P. (1994). A precise UPb zircon age for the Archaean Pongola Supergroup volcanics in Swaziland. Journal of African Earth Sciences, 18(4), 339–341. https://doi.org/10.1016/0899-5362(94)90072-8

Hofmann, H.J., (1976). Environmental diversity of Precambrian stromatolites. In: Walter, M.R. (Ed.), Stromatolites. Elsevier, New York, 599–612.

Hofmann, H. J. (1981). Precambrian fossils in Canada—the 1970s in retrospect. In Proterozoic Basins of Canada, Geological Survey of Canada, 81, 419-443.

Hofmann, H. J., Thurston, P. C., & Wallace, H. (1985). Archean stromatolites from Uchi greenstone belt, northwestern Ontario. In Evolution of Archean Supracrustal Sequences 28, 125-132.

Hoffman, P.F, (1976a). Stromatolite morphogenesis in Shark Bay, Western Australia. In: Walter, M.R. (Ed.), Stromatolites, Developments in Sedimentology. Elsevier, Amsterdam. 20. 261–271.

Hoffman, P.F, (1976b). Environmental diversity of Middle Precambrian stromatolites. In: Walter, M.R. (Ed.) Stromatolites, Developments in Sedimentology. Elsevier, Amsterdam. 20. 599–611.

Hoffman, P. F. (1988). Pethei reef complex (1.9 Ga), Great Slave Lake, N.W.T.:in Geldsetzer, H., James, N. P., and Tebbutt, G., eds., "Reefs-Canada and Adjacent Areas": Canadian Society of Petroleum Geologists Memoir. 13. 38-48.

Holland, H. D. (2006). The oxygenation of the atmosphere and oceans. Philosophical Transactions of the Royal Society B: Biological Sciences, 361(1470), 903–915. https://doi.org/10.1098/rstb.2006.1838

Homann, M., Sansjofre, P., Van Zuilen, M., Heubeck, C., Gong, J., Killingsworth, B., … Lalonde, S. V. (2018). Microbial life and biogeochemical cycling on land 3,220 million years ago. Nature Geoscience, 11(9), 665–671. https://doi.org/10.1038/s41561-018-0190-9

Howe, W.B. (1966). Digitate algal stromatolite structures from the Cambrian and Ordovician of Missouri. Journal of Paleontology 40, 64–77.

Jacobsen, S.B. & Pimentel-Klose, M.R. (1988). A Nd isotopic study of the Hamersley and Michipicoten banded iron formations: the source of REE and Fe in Archean oceans. Earth and Planetary Science Letters, 87, 29–44.

James, N.P. (1983) Reef environment. In Scholle P.A Beboue D.G. and Moore C.H (eds) Carbonate Depositional Environments. Tulsa OK: American Association of Petroleum Geologists. 33. 345-440.

James, N.P. (1984) Introduction to Carbonate Facies Models and Shallowing -Upward Sequences in Carbonates. In Walker, R.G., (eds) Facies Models. Geological Association of Canada. 209-213

James, N. P., & Jones, B. (2015). Origin of carbonate sedimentary rocks. John Wiley & Sons. 1-446.

Johannesson, K. H., & Zhou, X. (1999). Origin of middle rare earth element enrichments in acid waters of a Canadian High Arctic lake. Geochimica et Cosmochimica Acta, 63(1), 153-165.

Johannesson, K. H., Hawkins Jr, D. L., & Cortés, A. (2006). Do Archean chemical sediments record ancient seawater rare earth element patterns?. Geochimica et Cosmochimica Acta, 70(4), 871-890.

Kalkowsky, E. (1908). Oolith und Stromatolith im norddeutschen Buntsandstein. Zeitschrift der deutschen geologischen Gesellschaft, 68-125.

Kamber, B. S., Bolhar, R., & Webb, G. E. (2004a). Geochemistry of late Archaean stromatolites from Zimbabwe: Evidence for microbial life in restricted epicontinental seas. Precambrian Research, 132(4), 379–399. https://doi.org/10.1016/j.precamres.2004.03.006

Kamber, B. S., Greig, A., & Collerson, K. D. (2005). A new estimate for the composition of weathered young upper continental crust from alluvial sediments, Queensland, Australia. Geochimica et Cosmochimica Acta, 69(4), 1041-1058.

Kamber, B. S., & Webb, G. E. (2001). The geochemistry of late Archaean microbial carbonate: Implications for ocean chemistry and continental erosion history. Geochimica et Cosmochimica Acta, 65(15), 2509–2525. https://doi.org/10.1016/S0016-7037(01)00613-5

Kamber, B. S., Webb, G. E., & Gallagher, M. (2014). The rare earth element signal in Archaean microbial carbonate: Information on ocean redox and biogenicity. Journal of the Geological Society, 171(6), 745–763. https://doi.org/10.1144/jgs2013-110

Karhu, J. A., Holland, H. D., Survey, G., Espoo, F., Holland, H. D., Survey, G., & Espoo, F.-. (1996). Carbon isotopes and the rise of atmospheric oxygen. Geology, 24(10), 867–870. https://doi.org/10.1130/0091-7613(1996)024<0867:CIATRO>2.3.CO;2

Kato, Y., & Nakamura, K. (2003). Origin and global tectonic significance of Early Archean cherts from the Marble Bar greenstone belt, Pilbara Craton, Western Australia. Precambrian Research, 125(3–4), 191–243. https://doi.org/10.1016/S0301-9268(03)00043-3

Kaufman, A. J., Hayes, J. M., & Klein, C. (1990). Primary and diagenetic controls of isotopic compositions of iron-formation carbonates. Geochimica et Cosmochimica Acta, 54(12), 3461–3473. https://doi.org/10.1016/0016-7037(90)90298-Y

Kaufman, A. J., Johnston, D. T., Farquhar, J., Masterson, A. L., Lyons, T. W., Bates, S., … Buick, R. (2007). Late Archean biospheric oxygenation and atmospheric evolution. Science, 317(5846), 1900–1903. https://doi.org/10.1126/science.1138700

Kendall, B., Creaser, R. A., Reinhard, C. T., Lyons, T. W., & Anbar, A. D. (2015). Transient episodes of mild environmental oxygenation and oxidative continental weathering during the late Archean. Science Advances, 1(10), 1–7. https://doi.org/10.1126/sciadv.1500777

Khelen, A. C., Manikyamba, C., Subramanyam, K. S. V., Santosh, M., Ganguly, S., Kalpana, M. S., & Subba Rao, D. V. (2019). Archean seawater composition and depositional environment – Geochemical and isotopic signatures from the stromatolitic carbonates of Dharwar Craton, India. Precambrian Research, 330(April), 35–57. https://doi.org/10.1016/j.precamres.2019.04.020

Klinkhammer, G., Elderfield, H. & Hudson, A. (1983). Rare earth elements in seawater near hydrothermal vents. Nature, 305, 185–188.

Konhauser, K. O., Lalonde, S. V, Planavsky, N. J., Pecoits, E., Lyons, T. W., Mojzsis, S. J., … Bekker, A. (2011). Aerobic bacterial pyrite oxidation and acid rock drainage during the Great Oxidation Event. Nature, 478(7369), 369–373. https://doi.org/10.1038/nature10511

Logan, B. W., Read, J. F., Hagan, G. M., Hoffman, P. F., Brown, R. G., Woods, P. J., And Gebelein, C. D., (1974). Evolution and Diagenesis of Quaternary Carbonate Sequences, Shark Bay, Western Australia: American Association of Petroleum Geologists Memoir 22, 358.

Luo, Y. & Byrne, R.H. (2004) Carbonate complexation of yttrium and the rare earth elements in natural waters. Geochim. Cosmochim. Acta, 69, 691–699

MacRae, N.D., Nesbitt, H.W., Kronberg, B.I., (1992) Development of a positive Eu anomaly during diagenesis. Earth Planetary Science Letters. 109, 585–591.

Martin, A., Nisbet, E.G., & Bickle, M.J. (1980). Archaean stromatolites of the Belingwe Greenstone Belt, Zimbabwe (Rhodesia). Precambrian Research, 13, 337–362.

McIntyre, T., & Fralick, P. (2017). Sedimentology and Geochemistry of the 2930 Ma Red Lake-Wallace Lake Carbonate Platform, Western Superior Province, Canada. The Depositional Record, 3(2), 258–287. https://doi.org/10.1002/dep2.36

Miller, R.G. & O'Nions, R.K. (1985). Source of Precambrian chemical and clastic sediments. Nature, 314(6009), 325–329.

Moorbath, S., Taylor, P. N., Orpen, J. L., Treloar, P., & Wilson, J. F. (1987). First direct radiometric dating of Archaean stromatolitic limestone. Nature, 326(6116), 865-867.

Morse, J. W., & Mackenzie, F. T. (1990). Geochemistry of sedimentary carbonates. Elesevier.

Noffke, N., Gerdes, G., Klenke, T., & Krumbein, W. E. (1996). Microbially induced sedimentary structures—examples from modern sediments of siliciclastic tidal flats. Zentralblatt für Geologie und Paläontologie Teil I, 1996, 307-316.

Noffke, N., Eriksson, K.A., Hazen, R.M. and Simpson, E.L. (2006) A new window into Early Archean life: microbial mats in Earth's oldest siliciclastic tidal deposits (3.2 Ga Moodiess Group, South Africa). Geology 34: 253–256.

Nothdurft, L. D., Webb, G. E., & Kamber, B. S. (2004). Rare earth element geochemistry of Late Devonian reefal carbonates, Canning Basin, Western Australia: Confirmation of a seawater REE proxy in ancient limestones. Geochimica et Cosmochimica Acta, 68(2), 263–283. https://doi.org/10.1016/S0016-7037(03)00422-8

Nozaki, Y., Zhang, J., & Amakawa, H. (1997). The fractionation between Y and Ho in the marine environment, 148, 329–340.

Nunes, P.D. & Thurston, P.C., (1980). Two hundred and twenty million years of Archean evolution: a zircon U-Pb age stratigraphic study of the Uchi-Confederation Lakes Greenstone Belt; Canadian Journal of Earth Sciences, 17, 710-721.

Ojakangas, R.W. (1983). Tidal deposits in the early Proterozoic basin of the Lake Superior region – the Palms and Pokegama Formations: evidence for subtidal- shelf deposition of Superior type banded iron formations. In: Medaris, L.G. (Ed.), Early Proterozoic Geology of the Great Lakes Region, Memoir, 160. Geological Society of America, 49–66.

Orpen, J. L., & Wilson, J. F. (1981). Stromatolites at ~3,500 Myr and a greenstone-granite unconformity in the Zimbabwean Archaean. Nature, 291(5812), 218–220. https://doi.org/10.1038/291218a0

Passchier, C. & Trouw, R. A. . (2005). Microtectonics. Springer, Berlin. https://doi.org/10.1017/CBO9781107415324.004

Perry, R.S., Mcloughlin, N., Lynne, B.Y., Sephton, M.A., Oliver, J.D., Perry, C.C., Campbell, K., Engel, M.H., Farm Er, J.D., Brasier, M.D. & Staley, J.T. (2007). Defining Biominerals and Organominerals: Direct And Indirect Indicators of Life. – Sedimentary Geology, 201, 157–179.

Peter, J. (2003). Ancient iron formations: their genesis and use in the exploration for strataform base metal sulfide deposits, with examples from the Bathurst Mining Camo. In, ed. D.R. Lentz, Geochemistry of Sediments and Sedimentary Rocks. Geological Association of Canada, Geotext, 4, 192–207.

Perri, E., Tucker, M. E., & Mawson, M. (2013). Biotic and Abiotic Processes In the Formation and Diagenesis of Permian Dolomitic Stromatolites (Zechstein Group, NE England)

Biotic and Abiotic Processes in Dolomitic Stromatolites Formation and Diagenesis. *Journal of Sedimentary Research*, *83*(10), 896-914.

Pfeil, R.W., Read, J.F. (1980). Cambrian carbonate platform margin facies, Shady Dolomite, southwestern Virginia, U.S.A. Journal of Sedimentary Petrology. 50, 91–116.

Planavsky, N. J., Asael, D., Hofmann, A., Reinhard, C. T., Lalonde, S. V., Knudsen, A., … Rouxel, O. J. (2014). Evidence for oxygenic photosynthesis half a billion years before the Great Oxidation Event. Nature Geoscience, 7(4), 283–286. https://doi.org/10.1038/ngeo2122

Planavsky, N., Bekker, A., Rouxel, O. J., Kamber, B., Hofmann, A., Knudsen, A., & Lyons, T. W. (2010). Rare earth element and yttrium compositions of Archean and Paleoproterozoic Fe formations revisited: new perspectives on the significance and mechanisms of deposition. Geochimica et Cosmochimica Acta, 74(22), 6387-6405.

Pope, M. C., Grotzinger, J. P., & Schreiber, B. C. (2000). Evaporitic subtidal stromatolites produced by in situ precipitation: Textures, facies associations, and temporal significance. Journal of Sedimentary Research, 70(5), 1139–1151. https://doi.org/10.1306/062099701139

Préat, A.L., Delpomdor, F., Kolo, K., Gillan, D.C., & Prian, J.P. (2011). Stromatolites and cyanobacterial mats in peritidal evaporative environments in the Neoproterozoic of Bas-Congo (Democratic Republic of Congo) and South Gabon. In: Tewari, V.C., Seckbach, J. (Eds.), Stromatolites: Interaction of Microbes with Sediments, Cellular Origin, Life in Extreme Habitats and Astrobiology, Springer, 18, 43–63.

Pruss, S. B., Bosak, T., Macdonald, F. A., McLane, M., & Hoffman, P. F. (2010). Microbial facies in a Sturtian cap carbonate, the Rasthof Formation, Otavi Group, northern Namibia. Precambrian Research, 181(1–4), 187–198. https://doi.org/10.1016/j.precamres.2010.06.006

Pryslak, A.P. (1971b). Knott Township, District of Kenora (Patricia Portion); Ontario Department of Mines and Northern Affairs, Preliminary Map P. 635.

Pufahl, P.K., & Fralick, P.W. (2004). Depositional controls on Paleoproterozoic shallow water iron formation accumulation, Gogebic Range, Wisconsin, U.S.A. Sedimentology 54, 791–808

Pufahl, P. K., & Hiatt, E. E. (2012). Oxygenation of the Earth' s atmosphere e ocean system: A review of physical and chemical sedimentologic responses, 32. https://doi.org/10.1016/j.marpetgeo.2011.12.002

Quinn, K., Byrne, R.H. & Schijf, J. (2006) Sorption of yttrium and rare earth elements by amorphous ferric hydroxide: influence of solution complexation with carbonate. Geochimica et Cosmochima Acta, 70, 4151–4165.

Reeder, R. J., & Grams, J. C. (1987). Sector zoning in calcite cement crystals: Implications for trace element distributions in carbonates. Geochimica et Cosmochimica Acta, 51(2), 187-194.

Ricketts, B.D. & Donaldson, J.A. (1989) Stromatolite reef development on a mud-dominated platform in the Middle Precambrian Belcher Group of Hudson bay. In: Reefs - Canada and Adjacent Areas (Ed. by H. Geldsetzer, N. P. James & G. Tebbutt). Mern. Can. SOC. Petrol. Geol., Calgary, 13, 113-119.

Riding, R.E. (2008) Abiogenic, microbial and hybrid authigenic carbonate crusts: components of Precambrian stromatolites. Geologia Croatica 61:73–103.

Riding, R., Fralick, P., & Liang, L. (2014). Identification of an Archean marine oxygen oasis. Precambrian Research, 251, 232–237. https://doi.org/10.1016/j.precamres.2014.06.017

Rimstidt, J. D., Balog, A., & Webb, J. (1998). Distribution of trace elements between carbonate minerals and aqueous solutions. Geochimica et Cosmochimica Acta, 62(11), 1851-1863.

Rivers, J., Varghese, L., Yousif, R., Whitaker, F., Skeat, S., & Al-Shaikh, I. (2019). The Geochemistry of Qatar Coastal Waters and Its Impact on Carbonate Sediment Chemistry and Early Marine Diagenesis. Journal of Sedimentary Petrology, 89, 293–309.

Robbins, L. J., Konhauser, K. O., Warchola, T. J., Homann, M., Thoby, M., Foster, I., … Lalonde, S. V. (2019). A comparison of bulk versus laser ablation trace element analyses in banded iron formations: Insights into the mechanisms leading to compositional variability. Chemical Geology, 506(September 2018), 197–224. https://doi.org/10.1016/j.chemgeo.2018.12.036

Rogers, N., McNicoll, V., Van Stall, C.R., & Tomlinson, K.Y. (2000). Lithogeochemical studies in the Uchi-Confederation Greenstone Belt, northwestern Ontario: implications for Archean tectonics. Geological Survey of Canada, Current Research, 1-11.

Rogers, N. (2002). Whole-rock chemical analyses from the Birch–Uchi greenstone belt, Superior Province. Geological Survey of Canada, Open File Report, 4271.

Sanborne-Barrie, M., Skulski, T., & Parker, J., (2001). Three hundred million years of tectonic history recorded by the Red Lake Greenstone Belt, Ontario. Geological Survey of Canada, Current Research. 2002-C19, 19.

Satkoski, A. M., Fralick, P., Beard, B. L., & Johnson, C. M. (2017). Initiation of modern-style plate tectonics recorded in Mesoarchean marine chemical sediments. Geochimica et Cosmochimica Acta, 209, 216–232. https://doi.org/10.1016/j.gca.2017.04.024

Satkoski, A. M., Lowe, D. R., Beard, B. L., Coleman, M. L., & Johnson, C. M. (2016). A high continental weathering flux into Paleoarchean seawater revealed by strontium isotope analysis of 3.26 Ga barite. Earth and Planetary Science Letters, 454, 28–35. https://doi.org/10.1016/j.epsl.2016.08.032

Schidlowski, M., Matzigkeit, U., Mook, W.G., & Krumbein, W.E. (1985). Carbon isotope geochemistry and 14C ages of microbial mats from the Gavish Sabkha and the Solar Lake. In: Friedman, G.M., Krumbein, W.E. (Eds.), Hypersaline ecosystemsecological Studies 5. Berlin, Springer-Verlag, 381–401.

Scott, C., Lyons, T. W., Bekker, A., Shen, Y., Poulton, S. W., Chu, X., & Anbar, A. D. (2008). Tracing the stepwise oxygenation of the Proterozoic ocean. Nature, 452(7186), 456–459. https://doi.org/10.1038/nature06811

Schneiderhan, E.A., Gutzmer, J., Strauss, H., Mezger, K. & Beukes, N.J. (2006). The chemostratigraphy of a Paleoproterozoic mnf-BIF succession – the Voelwater Subgroup of the Transvaal Supergroup in Griqualand West, South Africa. South African Journal of Geology, 109, 63–80.

Seager S, & Deming D. (2010). Exoplanet atmospheres. Annual Review Astronomy Astrophysics 48, 631–672.

Seong-Joo, L., Browne, K.M., & Golubic, S., (2000). On stromatolite lamination. In: Riding, R.E., Awramik, S.M. (Eds.), Microbial Sediments. Springer-Verlag, Heidelberg, 16–24.

Seong-Joo, L., & Golubic, S., (1999). Microfossil populations in the context of synsedimentary micrite deposition and acicular carbonate precipitation: Mesoproterozoic Gaoyuzhuang Formation, China. Precambrian Research, 96, 183– 208.

Shields, G., & Stille, P. (2001). Diagenetic constraints on the use of cerium anomalies as palaeoseawater redox proxies: an isotopic and REE study of Cambrian phosphorites. Chemical Geology, 175(1-2), 29-48.

Shinn, E. A. (1983). Tidal flat environment. In: Carbonate depositional environments: AAPG Memoir, 33, 172-210.

Siahi, M., Hofmann, A., Hegner, E., & Master, S. (2016). Sedimentology and facies analysis of Mesoarchaean stromatolitic carbonate rocks of the Pongola Supergroup, South Africa. Precambrian Research, 278, 244–264. https://doi.org/10.1016/j.precamres.2016.03.004

Simonson, B. M., Carney, K. E., Simonson, B. M., & Carney, K. E. (2014). Mats in Roll-Up Structures: Evidence of in situ Microbial Late Archean Deep Shelf Environments, 14(1), 13–24.

Simonson, B.M., & Goode, A.D.T. (1989). First discovery of ferruginous chert arenites in the early Precambrian Hamersley Group of Western Australia. Geology 17, 269– 272.

Simonson BM, Carney KE (1999) Roll-up structures: evidence of situ microbial mats in Late Archean deep shelf environments. Palaios 14, 13–24.

Sumner, D. Y. (1997). Carbonate precipitation and oxygen stratification in late Archean seawater as deduced from facies and stratigraphy of the Gamohaan and Frisco Formations, Transvaal Supergroup, South Africa. American Journal of Science, 297(5), 455–487. https://doi.org/10.2475/ajs.297.5.455

Sumner, D. Y., & Grotzinger, J. P. (2000). Late archean aragonite precipitation: petrography, facies associations, and environmental significance. Society of Economic Paleontologists and Mineralogists Carbonate Sedimentation and Diagenesis in the Evolving Precambrian

World: SEPM, 67, 123–144.

Stott, G.M. and Corfu, F. 1991. Uchi Subprovince; in Geology of Ontario, Ontario Geological Survey, Special Volume 4, Part 1, p.145-236.

Sumner, D. Y., & Grotzinger, J. P. (2004). Implications for Neoarchaean ocean chemistry from primary carbonate mineralogy of the Campbellrand-Malmani Platform, South Africa. Sedimentology, 51(6), 1273–1299. https://doi.org/10.1111/j.1365-3091.2004.00670.x

Takano, B. (1985). Geochemical implications of sulfate in sedimentary carbonates. Chemical Geology, 49(4), 393-403.

Taylor, M.E., & Cook, H.E., (1976). Continental shelf and slope facies in the Upper Cambrian and lowest Ordovician of Nevada. Brigham Young University Geology Studies, 23 (2), 181–214.

Taylor, S. R., & McLennan, S. M. (1985). The Continental Crust: Its Composition and Evolution. Blackwell Scientific Publication, Palo Alto, CA.

Temmam, M., Paquette, J., & Vali, H. (2000). Mn and Zn incorporation into calcite as a function of chloride aqueous concentration. Geochimica et Cosmochimica Acta, 64(14), 2417-2430.

Thurston, P. C. (1980). Subaerial Volcanism in the Archean Uchi-Confederation Volcanic Belt. Precambrian Research, 12, 79–98.

Thurston, P.C. (1985). Physical volcanology and stratigraphy of the Confederation Lake area, District of Kenora (Patricia Portion). Ontario Geological Survey. Report 236, 117.

Thurston, P. C., & Jackson, M. C. (1978). Confederation Lake area, District of Kenora (Patricia portion). Ontario Geological Survey. Preliminary Map P. 1975.

Thurston, P.C., Stott, G.M. & Corfu, F. (1991). Uchi Subprovince; in Geology of Ontario, Ontario Geological Survey, 4, 1, 145-238.

Tice, M. M., Thornton, D. C. O., Pope, M. C., Olszewski, T. D., & Gong, J. (2011). Archean Microbial Mat Communities. Annual Review of Earth and Planetary Sciences, 39(1), 297–

319. https://doi.org/10.1146/annurev-earth-040809-152356

Tosti, F., & Riding, R. (2017). Current molded, storm damaged, sinuous columnar stromatolites: Mesoproterozoic of northern China. Palaeogeography, Palaeoclimatology, Palaeoecology, 465, 93–102. https://doi.org/10.1016/j.palaeo.2016.10.019

Vahrenkamp, V. C. (1996). Carbon isotope stratigraphy of the upper Kharaib and Shuaiba formations: Implications for the early cretaceous evolution of the Arabian Gulf region. AAPG Bulletin, 80(5), 647–661.

Valero-Garcés, B.L., Delgado-Huertas, A., Ratto, N., & Navas, A. (1999). Large 13C enrichment in primary carbonates from Andean Altiplano lakes, northwest Argentina. Earth Planetary. Science Letter. 171, 253–266.

Van Kranendonk, M. J. (2006). Volcanic degassing, hydrothermal circulation and the flourishing of early life on Earth: A review of the evidence from c. 3490-3240 Ma rocks of the Pilbara Supergroup, Pilbara Craton, Western Australia. Earth-Science Reviews, 74(3–4), 197–240. https://doi.org/10.1016/j.earscirev.2005.09.005

Van Kranendonk, M. J., Webb, G. E., & Kamber, B. S. (2003). Geological and trace element evidence for a marine sedimentary environment of deposition and biogenicity of 3.45 Ga stromatolitic carbonates in the Pilbara Craton, and support for a reducing Archaean ocean. Geobiology, 1(2), 91–108. https://doi.org/10.1046/j.1472-4669.2003.00014.x

Veizer, J. (1983). Trace elements and isotopes in sedimentary carbonates. Reviews in mineralogy, 11, 265-300.

Veizer, J., 2003. Isotopic evolution of seawater on geological time scales: sedimentological perspective, in Lentz, D.R., ed., Geochemistry of Sediments and Sedimentary Rocks: Evolutionary Considerations to Mineral Deposit-Forming Environments: Geological Association of Canada, GeoText 4, 53-68.

Veizer, J., & Jansen, S. L. (1979). Basement and sedimentary recycling and continental evolution. Journal of Geology, 87(4), 341–370. https://doi.org/10.1086/628425

Veizer, J, Hoefs, J., Lowe, D. R., & Thurston, P. C. (1989a). Geochemistry of Precambrian

carbonates: II. Archean greenstone belts and Archean sea water. Geochimica et Cosmochimica Acta, 53(4), 859–871. https://doi.org/10.1016/0016-7037(89)90031-8

Veizer, J, Hoefs, J., Ridler, R. H., Jensen, L. S., & Lowe, D. R. (1989b). Geochemistry of Precambrian carbonates: I. Archean hydrothermal systems. Geochimica et Cosmochimica Acta, 53(4), 845–857. https://doi.org/10.1016/0016-7037(89)90030-6

Veizer, J. & Mackenzie, F. T. (2014). Evolution of sedimentary rocks. In: Treatise on Geochemistry, 2nd ed. (Holland, H. D. And Turekian, K. K., Eds.), V.9 Sediments, diagenesis, and sedimentary rocks (Mackenzie, F.T., Ed.), Elsevier- Pergamon, Oxford, 399-435.

Von Brunn, V., & Mason, T. R. (1977). Siliciclastic-carbonate tidal deposits from the 3000 M.Y. Pongola Supergroup, South Africa. Sedimentary Geology, 18(1–3), 245–255. https://doi.org/10.1016/0037-0738(77)90014-8

Wallace, H., Thurston, P.C., & Corfu, F. (1986) Developments in stratigraphic correlation: western Uchi Subprovince; in Volcanology and Mineral Deposits; Ontario Geological Survey, Miscellaneous Paper 129, p. 88–102.

Walter, M. R. (1983). Archean stromatolites: evidence of the Earth's earliest benthos: In Schopf, J.W., ed., Earths Earliest Biosphere: Princetown university Press, Chapter 8, 187-213. Earth's Earliest Biosphere., 187-213.

Wang, X., Ossa, F. O., Hofmann, A., Agangi, A., Paprika, D., & Planavsky, N. J. (2020). Uranium isotope evidence for Mesoarchean biological oxygen production in shallow marine and continental settings. Earth and Planetary Science Letters, 551, 116583.

Webb, G. E., & Kamber, B. S. (2000). Rare earth elements in Holocene reefal microbialites: A new shallow seawater proxy. Geochimica et Cosmochimica Acta, 64(9), 1557–1565. https://doi.org/10.1016/S0016-7037(99)00400-7

Webb, G. E., & Kamber, B. S. (2011). Trace element geochemistry as a tool for interpreting microbialites. In Earliest Life on Earth: Habitats, Environments and Methods of Detection (127-170). Springer, Dordrecht. https://doi.org/10.1007/978-90-481-8794-2

Webb, G. E., Nothdurft, L. D., Kamber, B. S., & Gge, J. T. K. (2009). Rare earth element geochemistry of scleractinian coral skeleton during meteoric diagenesis: a sequence through neomorphism of aragonite to calcite, 1433–1463. https://doi.org/10.1111/j.1365-3091.2008.01041.x

Wilks, M. E., & Nisbet, E. G. (1985). Archaean stromatolites from the Steep Rock Group, northwestern Ontario, Canada. Canadian Journal of Earth Sciences, 22(9), 792–799. https://doi.org/10.1017/CBO9781107415324.004

Wilmeth, D. T., Corsetti, F. A., Beukes, N. J., Awramik, S. M., Petryshyn, V., Spear, J. R., & Celestian, A. J. (2019). Neoarchean (2.7 Ga) lacustrine stromatolite deposits in the Hartbeesfontein Basin, Ventersdorp Supergroup, South Africa: Implications for oxygen oases. Precambrian Research, 320(July 2018), 291–302. https://doi.org/10.1016/j.precamres.2018.11.009

Winde, V., Böttcher, M. E., Escher, P., Böning, P., Beck, M., Liebezeit, G., & Schneider, B. (2014). Tidal and spatial variations of DI13C and aquatic chemistry in a temperate tidal basin during winter time. Journal of Marine Systems, 129, 396–404. https://doi.org/10.1016/j.jmarsys.2013.08.005

Xie, H., Hofmann, A., Hegner, E., Wilson, A., Wan, Y., & Liu, D. (2012). Zircon SHRIMP dating confirms a Palaeoarchaean supracrustal terrain in the southeastern Kaapvaal Craton, southern Africa. Gondwana Research, 21(4), 818–828. https://doi.org/10.1016/j.gr.2011.08.014

Zerkle, A. L., Poulton, S. W., Newton, R. J., Mettam, C., Claire, M. W., Bekker, A., & Junium, C. K. (2017). Onset of the aerobic nitrogen cycle during the Great Oxidation Event. Nature, 542(7642), 465–467. https://doi.org/10.1038/nature20826

Zhang, J., & Nozaki, Y. (1996). Rare earth elements and yttrium in seawater: ICP-MS determinations in the East Caroline, Coral Sea, and South Fiji basins of the western South Pacific Ocean. Geochimica et Cosmochimica Acta, 60(23), 4631–4644. https://doi.org/10.1016/S0016-7037(96)00276-1

Appendix A: Partial Dissolution ICP MS, REE, Majors, and Trace

Silicified Microbialite (Partial Dissolution - ICP MS: REE)																
Sublitho-tope	**Sample #**	**Depth (m)**	**La (ppm)**	**Ce (ppm)**	**Pr (ppm)**	**Nd (ppm)**	**Sm (ppm)**	**Eu (ppm)**	**Gd (ppm)**	**Tb (ppm)**	**Dy (ppm)**	**Ho (ppm)**	**Er (ppm)**	**Tm (ppm)**	**Yb (ppm)**	**Lu (ppm)**
Stratiform Stromatolite	WM55y	0.1	5.345	7.956	0.915	3.409	0.610	0.183	0.801	0.136	0.849	0.228	0.763	0.112	0.707	0.128
	WM 57	0.2	0.154	0.219	0.026	0.118	0.024	0.009	0.038	0.007	0.044	0.011	0.038	0.005	0.031	0.006
	WM60	2.53	4.943	9.220	0.999	3.462	0.561	0.149	0.675	0.093	0.470	0.107	0.323	0.048	0.310	0.055
	X3-R		1.093	1.929	0.230	0.951	0.194	0.069	0.269	0.048	0.321	0.083	0.263	0.037	0.220	0.039
Low Domal Stromatolites	A-1	74.1	0.176	0.283	0.039	0.168	0.036	0.009	0.047	0.008	0.057	0.016	0.050	0.008	0.047	0.009
	A-5	74.53	0.407	0.675	0.084	0.340	0.073	0.017	0.084	0.014	0.084	0.020	0.061	0.009	0.063	0.011
	A-10	74.95	0.189	0.192	0.032	0.139	0.032	0.009	0.049	0.010	0.071	0.020	0.067	0.010	0.063	0.012
	A-14	75.99	0.559	0.607	0.069	0.239	0.039	0.026	0.062	0.010	0.066	0.019	0.065	0.009	0.056	0.011
	A-18A	76.25	0.362	0.208	0.036	0.153	0.028	0.016	0.050	0.009	0.065	0.020	0.068	0.010	0.055	0.011
	A-18C	76.32	0.341	0.294	0.040	0.161	0.031	0.019	0.048	0.008	0.055	0.015	0.046	0.007	0.038	0.007
	A-20A	76.51	0.681	1.036	0.133	0.569	0.135	0.032	0.197	0.041	0.289	0.078	0.260	0.039	0.253	0.048
	A-23A	76.89	0.217	0.173	0.029	0.133	0.028	0.011	0.049	0.009	0.065	0.020	0.068	0.010	0.057	0.011
	A-27	77.4	0.264	0.401	0.052	0.205	0.044	0.016	0.059	0.010	0.069	0.018	0.061	0.009	0.060	0.012
	A-31	77.9	0.447	0.257	0.042	0.170	0.031	0.013	0.057	0.009	0.067	0.020	0.067	0.009	0.054	0.011
	A-35A	78.33	0.341	0.238	0.050	0.231	0.053	0.016	0.098	0.018	0.140	0.042	0.145	0.021	0.124	0.024
	A-37	78.47	0.732	0.601	0.107	0.494	0.118	0.038	0.185	0.036	0.261	0.070	0.227	0.034	0.208	0.039
	A-41A	78.63	0.316	0.372	0.058	0.245	0.054	0.017	0.086	0.016	0.112	0.031	0.104	0.015	0.094	0.018
	A-38B	78.6	0.275	0.141	0.027	0.114	0.021	0.013	0.039	0.006	0.048	0.015	0.049	0.007	0.041	0.008
	A-48B	78.96	0.417	0.281	0.055	0.245	0.049	0.017	0.089	0.016	0.120	0.036	0.121	0.017	0.101	0.020
	A-52A	79.12	0.121	0.129	0.023	0.111	0.029	0.007	0.056	0.012	0.094	0.028	0.096	0.014	0.086	0.016
	A-56	79.42	0.187	0.133	0.025	0.114	0.025	0.007	0.050	0.010	0.078	0.025	0.089	0.013	0.082	0.016
	WM 61	2.6	0.130	0.213	0.024	0.088	0.013	0.004	0.018	0.002	0.013	0.003	0.011	0.002	0.011	0.002
	WM 66	13.1	0.511	0.663	0.069	0.257	0.046	0.028	0.065	0.010	0.060	0.015	0.046	0.007	0.039	0.007
	WM 116x	31.8	0.659	1.004	0.151	0.638	0.136	0.030	0.192	0.034	0.245	0.073	0.252	0.037	0.230	0.045
	WM117x	79.58	0.157	0.163	0.029	0.134	0.034	0.010	0.061	0.014	0.107	0.032	0.111	0.016	0.100	0.019
	WM 129Q	79.52	0.314	0.388	0.059	0.239	0.048	0.013	0.061	0.008	0.046	0.011	0.032	0.005	0.031	0.006
	WM 129-S	79.45	0.167	0.208	0.034	0.146	0.030	0.009	0.047	0.008	0.052	0.014	0.047	0.007	0.044	0.008
	WM 129-Z	79.37	0.469	0.564	0.086	0.354	0.068	0.021	0.103	0.015	0.096	0.025	0.080	0.011	0.067	0.012
	X3-Q		20.228	33.678	3.177	9.636	1.144	0.236	1.467	0.157	0.675	0.147	0.422	0.061	0.366	0.063

Silicified Microbialite Continued (Partial Dissolution - ICP MS: REE)																
Sublitho-tope	**Sample #**	**Depth (m)**	**La (ppm)**	**Ce (ppm)**	**Pr (ppm)**	**Nd (ppm)**	**Sm (ppm)**	**Eu (ppm)**	**Gd (ppm)**	**Tb (ppm)**	**Dy (ppm)**	**Ho (ppm)**	**Er (ppm)**	**Tm (ppm)**	**Yb (ppm)**	**Lu (ppm)**
Low Domal Stromatolites Continued	X10B-u	36.9	1.131	1.268	0.165	0.672	0.142	0.059	0.215	0.042	0.283	0.077	0.248	0.036	0.216	0.042
	X10B-w	36.9	1.334	1.672	0.217	0.925	0.215	0.074	0.330	0.070	0.486	0.133	0.439	0.065	0.390	0.075
	X23A-R	57.12	0.923	0.756	0.110	0.460	0.087	0.033	0.145	0.026	0.176	0.052	0.172	0.025	0.145	0.028
	X24-v	59.95	2.106	1.999	0.268	1.087	0.205	0.078	0.322	0.057	0.392	0.110	0.366	0.053	0.318	0.063

Carbonate Grainstones (Partial Dissolution - ICP MS: REE)																
Sublitho-tope	**Sample #**	**Depth (m)**	**La (ppm)**	**Ce (ppm)**	**Pr (ppm)**	**Nd (ppm)**	**Sm (ppm)**	**Eu (ppm)**	**Gd (ppm)**	**Tb (ppm)**	**Dy (ppm)**	**Ho (ppm)**	**Er (ppm)**	**Tm (ppm)**	**Yb (ppm)**	**Lu (ppm)**
Massive	A-35B	78.39	0.431	0.222	0.043	0.172	0.031	0.017	0.055	0.009	0.064	0.019	0.065	0.009	0.050	0.010
	A-36	78.44	0.412	0.220	0.046	0.200	0.043	0.020	0.084	0.016	0.123	0.037	0.123	0.018	0.106	0.021
	A-38A	78.55	0.585	0.258	0.060	0.274	0.058	0.026	0.121	0.023	0.180	0.057	0.199	0.028	0.164	0.034
	A-39	78.59	0.985	0.738	0.098	0.359	0.059	0.035	0.095	0.014	0.093	0.026	0.084	0.012	0.066	0.013
	A-41B	78.66	1.276	0.883	0.137	0.521	0.090	0.044	0.143	0.022	0.149	0.043	0.141	0.019	0.110	0.022
	A-52B	79.15	0.756	0.437	0.073	0.285	0.050	0.028	0.088	0.014	0.097	0.028	0.090	0.012	0.071	0.014
	WM 63	4.5	1.009	1.464	0.176	0.693	0.127	0.052	0.184	0.028	0.177	0.045	0.141	0.020	0.118	0.022
	WM64	7.25	2.818	4.228	0.478	1.837	0.334	0.110	0.432	0.072	0.423	0.107	0.330	0.046	0.280	0.052
	WM 73	22.5	0.530	0.630	0.076	0.310	0.064	0.021	0.106	0.021	0.149	0.039	0.120	0.017	0.108	0.020
	WM125		1.378	1.595	0.197	0.772	0.135	0.035	0.205	0.031	0.201	0.057	0.190	0.028	0.170	0.034
	X6-Q		6.175	10.285	1.172	4.336	0.725	0.179	0.921	0.151	0.927	0.253	0.825	0.117	0.695	0.131
	X6-R		4.838	9.506	1.029	3.633	0.616	0.134	0.744	0.118	0.712	0.201	0.729	0.116	0.774	0.147
	X6-S		4.588	8.704	0.943	3.359	0.570	0.117	0.702	0.116	0.724	0.195	0.652	0.098	0.603	0.108
	X8-x	30.5	1.459	1.385	0.159	0.629	0.114	0.059	0.190	0.033	0.218	0.060	0.190	0.026	0.147	0.028
	X8-y	30.5	0.193	0.240	0.031	0.135	0.031	0.011	0.050	0.010	0.077	0.023	0.081	0.013	0.085	0.018
Laminated	WM 69	14.75	<0.01	0.090	0.041	0.225	0.282	0.113	0.172	0.035	0.164	0.007	0.121	0.083	0.021	0.022
	WM 71A	17	0.419	0.638	0.074	0.290	0.056	0.015	0.084	0.016	0.120	0.039	0.151	0.026	0.192	0.041
	WM 74	26.75	1.930	1.789	0.238	1.000	0.186	0.086	0.317	0.054	0.379	0.108	0.362	0.052	0.314	0.060
	WM117y	79.56	1.807	1.077	0.172	0.685	0.117	0.059	0.195	0.033	0.223	0.064	0.208	0.029	0.168	0.032
Zig Zags	X12	39.6	0.622	0.678	0.097	0.430	0.100	0.041	0.166	0.038	0.301	0.089	0.303	0.044	0.262	0.048
	B-1	~39	0.983	0.998	0.137	0.581	0.121	0.056	0.181	0.035	0.238	0.065	0.210	0.029	0.181	0.034
	B-5	~39	2.141	2.290	0.310	1.285	0.265	0.136	0.376	0.072	0.484	0.125	0.395	0.056	0.337	0.062
	B-7	~39	1.259	1.580	0.228	1.017	0.244	0.094	0.341	0.070	0.491	0.130	0.418	0.059	0.364	0.066

Carbonate Microbialite (Partial Dissolution - ICP MS: REE)																
Sublitho-tope	**Sample #**	**Depth (m)**	**La (ppm)**	**Ce (ppm)**	**Pr (ppm)**	**Nd (ppm)**	**Sm (ppm)**	**Eu (ppm)**	**Gd (ppm)**	**Tb (ppm)**	**Dy (ppm)**	**Ho (ppm)**	**Er (ppm)**	**Tm (ppm)**	**Yb (ppm)**	**Lu (ppm)**
Low Domal Strom-atolite	WM 65	12.45	0.903	1.222	0.133	0.513	0.094	0.033	0.143	0.023	0.152	0.040	0.130	0.018	0.110	0.021
	WM 67	12.3	1.874	2.741	0.339	1.477	0.340	0.073	0.520	0.104	0.699	0.166	0.515	0.081	0.557	0.111
Stratiform Stromatolite	WM55x	0.1	7.590	11.295	1.272	4.776	0.840	0.313	1.108	0.183	1.107	0.278	0.864	0.125	0.762	0.139
	WM58x	0.3	0.273	0.327	0.034	0.135	0.026	0.013	0.038	0.007	0.049	0.014	0.047	0.008	0.047	0.009
	WM58y	0.3	1.234	1.345	0.136	0.529	0.082	0.034	0.145	0.023	0.155	0.043	0.135	0.017	0.097	0.018
	WM 115	31	2.049	2.454	0.298	1.141	0.204	0.103	0.295	0.047	0.296	0.077	0.240	0.034	0.209	0.038
	WM 116y	31.8	1.060	0.537	0.102	0.427	0.078	0.039	0.148	0.024	0.174	0.052	0.167	0.024	0.137	0.026
	X31	82.2	1.672	1.884	0.233	0.926	0.171	0.087	0.255	0.045	0.290	0.079	0.254	0.036	0.211	0.040
Banded Carbonate	WM 104	72.6	0.584	0.587	0.076	0.336	0.075	0.032	0.128	0.024	0.180	0.049	0.163	0.024	0.151	0.028
	WM 107x	56.6	0.616	0.308	0.062	0.275	0.051	0.021	0.102	0.017	0.128	0.041	0.140	0.020	0.119	0.024
	WM 107y	56.6	0.599	0.340	0.061	0.267	0.048	0.022	0.093	0.015	0.112	0.035	0.123	0.017	0.100	0.021
	X10B-R	36.9	0.870	0.701	0.087	0.345	0.060	0.033	0.104	0.018	0.122	0.034	0.113	0.015	0.089	0.018
	X10B-v	36.9	2.503	2.902	0.361	1.419	0.276	0.108	0.391	0.073	0.466	0.120	0.379	0.053	0.309	0.057
	X20-y	67.1	2.917	3.394	0.406	1.599	0.290	0.177	0.458	0.084	0.563	0.152	0.494	0.070	0.416	0.079
	X23D-y	57.27	1.361	0.321	0.106	0.481	0.088	0.045	0.183	0.035	0.272	0.087	0.302	0.042	0.249	0.051
	X23E-w	57.33	0.882	0.209	0.069	0.312	0.056	0.030	0.121	0.023	0.180	0.059	0.212	0.030	0.176	0.036
	X23E-x	57.34	1.069	0.265	0.086	0.383	0.070	0.036	0.144	0.026	0.202	0.064	0.222	0.031	0.183	0.037
	X23E-z	57.36	1.119	0.354	0.099	0.440	0.085	0.038	0.169	0.032	0.253	0.081	0.281	0.039	0.233	0.046
	X24-Q	59.9	1.524	1.468	0.203	0.814	0.156	0.067	0.247	0.043	0.297	0.086	0.286	0.040	0.236	0.047
	X24-R	59.91	2.740	1.862	0.277	1.132	0.191	0.089	0.326	0.055	0.388	0.119	0.400	0.056	0.328	0.066
	X24-t	59.93	2.822	2.219	0.313	1.240	0.218	0.097	0.345	0.057	0.388	0.114	0.386	0.054	0.319	0.064
	X24-u	59.94	2.223	1.905	0.262	1.060	0.189	0.080	0.298	0.050	0.333	0.098	0.325	0.045	0.270	0.053
Fenestrated Stromatolite	WM 105x	58.1	1.599	1.711	0.211	0.825	0.162	0.086	0.246	0.040	0.265	0.072	0.229	0.033	0.201	0.037
	WM 114y	49	0.492	0.604	0.077	0.340	0.075	0.029	0.114	0.021	0.139	0.036	0.115	0.016	0.099	0.018
	WM 124		1.448	1.710	0.222	0.895	0.188	0.089	0.298	0.052	0.351	0.095	0.294	0.041	0.239	0.044
	WM 130	~55	0.346	0.197	0.031	0.134	0.024	0.011	0.049	0.008	0.059	0.018	0.062	0.009	0.053	0.011
	X10A-x	37.15	0.551	0.371	0.056	0.232	0.043	0.021	0.077	0.014	0.103	0.030	0.100	0.014	0.082	0.017
	X10B-t	36.9	1.662	1.573	0.200	0.806	0.157	0.072	0.253	0.046	0.318	0.088	0.287	0.041	0.240	0.047
	X14-x	43.15	1.210	0.744	0.118	0.459	0.077	0.035	0.136	0.023	0.157	0.047	0.154	0.021	0.120	0.023
	X16-Q	44.1	1.215	1.140	0.156	0.595	0.104	0.033	0.152	0.024	0.154	0.042	0.134	0.019	0.107	0.020
	X19-x	60.25	2.249	2.256	0.306	1.242	0.224	0.107	0.332	0.059	0.383	0.105	0.343	0.047	0.277	0.053

Carbonate Microbialite Continued (Partial Dissolution - ICP MS: REE)																
Sublitho-tope	**Sample #**	**Depth (m)**	**La (ppm)**	**Ce (ppm)**	**Pr (ppm)**	**Nd (ppm)**	**Sm (ppm)**	**Eu (ppm)**	**Gd (ppm)**	**Tb (ppm)**	**Dy (ppm)**	**Ho (ppm)**	**Er (ppm)**	**Tm (ppm)**	**Yb (ppm)**	**Lu (ppm)**
Fenestrated Stromatolite Continued	X21-y	71.3	1.274	0.985	0.127	0.491	0.083	0.039	0.127	0.020	0.122	0.035	0.114	0.016	0.090	0.018
	B-10B	~39	1.257	1.624	0.231	1.068	0.263	0.106	0.376	0.083	0.590	0.160	0.541	0.080	0.518	0.102
Fenestrae	WM 105y	58.1	1.566	1.601	0.210	0.889	0.173	0.088	0.277	0.046	0.299	0.083	0.265	0.038	0.225	0.043
	X10A-y	37.15	0.729	0.488	0.072	0.294	0.056	0.025	0.095	0.017	0.120	0.035	0.113	0.016	0.093	0.018
	X10B-Q	36.9	0.739	0.593	0.083	0.348	0.069	0.030	0.121	0.023	0.160	0.046	0.150	0.021	0.125	0.024
	X19-M	60.25	0.975	0.852	0.107	0.413	0.068	0.052	0.114	0.018	0.127	0.037	0.124	0.017	0.095	0.019
	X-20-N	67.1	1.054	1.273	0.165	0.664	0.128	0.067	0.198	0.034	0.236	0.063	0.202	0.029	0.165	0.031
	X-21-M	71.3	0.551	0.366	0.062	0.261	0.048	0.022	0.091	0.015	0.113	0.036	0.124	0.016	0.090	0.018
	X23D-x	57.26	1.013	0.358	0.088	0.377	0.069	0.038	0.138	0.026	0.203	0.064	0.225	0.032	0.190	0.038
	X23E-y	57.35	1.236	0.347	0.106	0.479	0.090	0.043	0.188	0.037	0.294	0.098	0.353	0.050	0.294	0.060
	X-23A-M	57.1	0.708	0.442	0.064	0.251	0.041	0.025	0.074	0.011	0.078	0.024	0.082	0.011	0.058	0.011
	X24-S	59.92	2.458	1.558	0.244	0.952	0.161	0.075	0.287	0.051	0.387	0.131	0.477	0.068	0.401	0.083
Organic Rich Mud	X-20-M	67.1	2.460	3.475	0.493	2.242	0.550	0.214	0.857	0.176	1.261	0.336	1.093	0.163	1.023	0.193
	X-21-N	71.3	0.874	0.797	0.123	0.500	0.091	0.027	0.142	0.022	0.149	0.043	0.140	0.020	0.114	0.022
	X23A-t	57.15	1.189	0.811	0.126	0.519	0.095	0.040	0.161	0.028	0.197	0.060	0.200	0.028	0.162	0.033
Fenestrated Microbialite	A-2	74.2	0.550	0.516	0.067	0.271	0.049	0.028	0.077	0.013	0.091	0.025	0.084	0.011	0.070	0.014
	A-3	74.25	0.343	0.185	0.029	0.121	0.021	0.013	0.040	0.007	0.050	0.016	0.053	0.008	0.043	0.009
	A-9	74.88	0.463	0.327	0.043	0.168	0.030	0.011	0.050	0.008	0.053	0.015	0.048	0.007	0.037	0.007
	A-12	75.12	0.338	0.216	0.035	0.139	0.025	0.013	0.042	0.007	0.051	0.015	0.051	0.007	0.041	0.008
	A-16	76.1	0.366	0.227	0.038	0.152	0.028	0.014	0.048	0.008	0.057	0.017	0.058	0.008	0.048	0.010
	A-17	76.2	0.291	0.162	0.032	0.135	0.025	0.011	0.046	0.008	0.059	0.018	0.061	0.009	0.051	0.010
	A-18B	76.3	0.289	0.264	0.040	0.174	0.039	0.020	0.063	0.012	0.085	0.024	0.080	0.012	0.067	0.013
	A-18D	76.38	0.288	0.223	0.030	0.126	0.025	0.020	0.045	0.008	0.061	0.018	0.059	0.008	0.048	0.010
	A-20B	76.56	0.963	1.311	0.159	0.658	0.143	0.061	0.201	0.039	0.261	0.068	0.214	0.032	0.194	0.036
	A-22	76.85	0.189	0.102	0.017	0.072	0.013	0.010	0.025	0.004	0.033	0.010	0.033	0.005	0.028	0.005
	A-23B	76.94	0.315	0.171	0.038	0.173	0.037	0.012	0.069	0.013	0.095	0.029	0.101	0.015	0.086	0.018
	A-28	77.58	0.654	0.597	0.081	0.305	0.050	0.024	0.077	0.011	0.074	0.020	0.066	0.009	0.052	0.010
	A-32	78.12	0.575	0.309	0.062	0.274	0.057	0.023	0.106	0.020	0.146	0.044	0.148	0.021	0.122	0.024
	A-43	78.75	0.369	0.430	0.066	0.277	0.060	0.019	0.099	0.019	0.142	0.041	0.139	0.020	0.123	0.023
	A-48A	78.91	0.708	0.414	0.065	0.254	0.042	0.022	0.077	0.012	0.083	0.024	0.080	0.011	0.063	0.012
	WM 108	58	1.405	1.025	0.142	0.576	0.099	0.037	0.168	0.025	0.163	0.048	0.155	0.021	0.122	0.024
	WM 109	52.15	0.917	1.162	0.150	0.604	0.116	0.032	0.168	0.027	0.174	0.049	0.157	0.022	0.131	0.025

Carbonate Microbialite Continued (Partial Dissolution - ICP MS: REE)																
Sublitho-tope	**Sample #**	**Depth (m)**	**La (ppm)**	**Ce (ppm)**	**Pr (ppm)**	**Nd (ppm)**	**Sm (ppm)**	**Eu (ppm)**	**Gd (ppm)**	**Tb (ppm)**	**Dy (ppm)**	**Ho (ppm)**	**Er (ppm)**	**Tm (ppm)**	**Yb (ppm)**	**Lu (ppm)**
Fenestrated Microbialite Continued	WM 110	53.4	1.609	1.925	0.226	0.909	0.176	0.075	0.267	0.044	0.283	0.078	0.252	0.036	0.220	0.042
	WM 111	53.7	0.649	0.625	0.081	0.325	0.061	0.029	0.104	0.016	0.112	0.032	0.106	0.015	0.088	0.018
	WM 112	54	1.261	1.337	0.164	0.645	0.119	0.063	0.191	0.030	0.200	0.055	0.178	0.025	0.149	0.029
	WM 113	48.2	0.869	0.973	0.122	0.512	0.107	0.040	0.173	0.030	0.207	0.053	0.163	0.023	0.138	0.025
	WM 114x	49	1.611	1.947	0.243	1.050	0.236	0.077	0.362	0.067	0.454	0.117	0.367	0.052	0.312	0.057
	WM 129-R	79.49	1.445	1.068	0.173	0.705	0.126	0.057	0.215	0.035	0.238	0.068	0.223	0.033	0.211	0.041
	WM 129-T2	79.41	1.031	0.532	0.100	0.413	0.076	0.042	0.137	0.022	0.149	0.045	0.146	0.020	0.118	0.023
	WM 129-T	79.4	0.669	0.384	0.070	0.289	0.054	0.027	0.097	0.016	0.110	0.033	0.108	0.015	0.086	0.017
	WM 129 X	79.3	0.391	0.287	0.053	0.225	0.044	0.019	0.077	0.013	0.093	0.027	0.090	0.013	0.076	0.015
	WM 129-Y	79.33	0.782	0.424	0.080	0.329	0.059	0.029	0.109	0.018	0.125	0.037	0.124	0.017	0.102	0.020
	X2		1.662	1.589	0.216	0.845	0.165	0.082	0.246	0.046	0.301	0.080	0.253	0.035	0.201	0.038
	X10B-S	36.9	1.099	0.905	0.116	0.466	0.087	0.046	0.144	0.026	0.178	0.050	0.163	0.023	0.136	0.026
	X14-y	43.15	1.821	1.278	0.199	0.796	0.144	0.056	0.242	0.042	0.296	0.089	0.299	0.041	0.244	0.049
	X16-R	44.1	1.582	1.578	0.221	0.897	0.184	0.052	0.293	0.055	0.389	0.116	0.396	0.058	0.349	0.071
	X18	58.4	1.503	0.928	0.150	0.627	0.115	0.053	0.198	0.034	0.238	0.070	0.229	0.032	0.186	0.037
	X19-y	60.25	2.096	2.204	0.309	1.338	0.302	0.084	0.466	0.097	0.681	0.191	0.635	0.091	0.556	0.107
	X20-x	67.1	2.180	2.710	0.331	1.329	0.247	0.136	0.372	0.067	0.450	0.122	0.396	0.057	0.335	0.064
	X21-z	71.3	3.629	3.720	0.469	1.859	0.339	0.093	0.483	0.077	0.480	0.129	0.419	0.056	0.327	0.063
	X23B	57.16	1.231	1.023	0.133	0.525	0.089	0.044	0.136	0.021	0.134	0.038	0.125	0.017	0.098	0.020
	X23C	57.19	1.760	1.415	0.224	0.910	0.174	0.050	0.287	0.052	0.371	0.113	0.386	0.055	0.334	0.066
	X23A-S	57.14	1.196	0.810	0.106	0.412	0.068	0.034	0.118	0.019	0.126	0.037	0.126	0.017	0.098	0.020
	X23A-Q	59.9	4.603	5.013	0.593	2.378	0.440	0.147	0.650	0.111	0.695	0.191	0.620	0.085	0.500	0.097
	X24-x	59.97	3.021	2.618	0.324	1.320	0.244	0.093	0.396	0.067	0.442	0.122	0.395	0.055	0.330	0.066
	X24-W	59.96	1.076	0.676	0.089	0.347	0.058	0.028	0.104	0.017	0.111	0.034	0.111	0.015	0.084	0.017
	X29	81	1.256	1.725	0.218	0.868	0.183	0.039	0.249	0.045	0.299	0.082	0.280	0.043	0.285	0.056
	X30	82	1.504	1.388	0.186	0.758	0.139	0.064	0.218	0.037	0.247	0.068	0.226	0.031	0.185	0.037
	X32	84.7	2.721	2.423	0.340	1.345	0.239	0.116	0.367	0.060	0.392	0.111	0.360	0.051	0.296	0.058
	X33	84.3	2.409	2.151	0.312	1.255	0.229	0.094	0.347	0.060	0.403	0.116	0.400	0.056	0.334	0.067
	X34	88.5	0.784	0.314	0.073	0.310	0.058	0.028	0.109	0.019	0.140	0.043	0.148	0.021	0.120	0.025
	B-8	~39	1.563	1.711	0.230	0.963	0.196	0.102	0.281	0.052	0.358	0.095	0.302	0.042	0.254	0.047
	B-10A	~39	2.398	3.188	0.361	1.421	0.280	0.100	0.373	0.064	0.403	0.105	0.345	0.050	0.314	0.059

Standards (Partial Dissolution - ICP MS: REE)														
Standard	**La (ppm)**	**Ce (ppm)**	**Pr (ppm)**	**Nd (ppm)**	**Sm (ppm)**	**Eu (ppm)**	**Gd (ppm)**	**Tb (ppm)**	**Dy (ppm)**	**Ho (ppm)**	**Er (ppm)**	**Tm (ppm)**	**Yb (ppm)**	**Lu (ppm)**
CAL-S	1.026	0.370	0.109	0.442	0.077	0.020	0.116	0.019	0.129	0.034	0.106	0.015	0.082	0.014
CAL-S	0.721	0.263	0.077	0.321	0.057	0.014	0.083	0.014	0.093	0.025	0.077	0.011	0.060	0.010
CAL-S	0.961	0.350	0.102	0.426	0.076	0.019	0.115	0.019	0.126	0.033	0.104	0.014	0.081	0.014
CAL-S	0.681	0.243	0.073	0.302	0.053	0.014	0.084	0.013	0.090	0.024	0.076	0.010	0.058	0.010
CAL-S	0.867	0.313	0.094	0.386	0.069	0.018	0.105	0.017	0.118	0.031	0.097	0.014	0.078	0.013
CAL-S	1.258	0.445	0.126	0.501	0.086	0.022	0.127	0.022	0.144	0.038	0.119	0.016	0.090	0.015
CAL-S	1.230	0.441	0.129	0.514	0.093	0.023	0.136	0.024	0.155	0.041	0.130	0.018	0.102	0.018
CAL-S	1.655	0.596	0.174	0.706	0.126	0.032	0.182	0.033	0.214	0.057	0.183	0.025	0.143	0.025

Silicified Microbialite (Partial Dissolution - ICP MS: MAJORS)												
Sublitho-tope	**Sample #**	**Depth (m)**	**Al (ppm)**	**Ba (ppm)**	**Ca (ppm)**	**Fe (ppm)**	**K (ppm)**	**Mg (ppm)**	**Mn (ppm)**	**Na (ppm)**	**P (ppm)**	**Ti (ppm)**
Low Domal Stromatolites	**A-1**	74.1	5.477	1.182	4531.866	82.863	82.863	54.491	792.137	BD	2.286	<0.17
	A-5	74.53	25.666	0.793	15325.591	166.421	166.421	188.917	1355.702	BD	3.917	0.080
	A-10	74.95	12.021	1.560	50606.009	434.197	434.197	898.494	5082.099	BD	3.418	0.056
	A-14	75.99	4.866	1.643	54955.662	498.759	498.759	608.167	5223.908	BD	4.124	0.054
	A-18A	76.25	10.783	3.044	101894.797	1267.145	1267.145	3355.834	8360.408	BD	2.461	0.080
	A-18C	76.32	3.032	3.748	77704.096	867.055	867.055	2465.155	6941.314	BD	3.754	0.026
	A-20A	76.51	6.485	3.537	56092.027	1044.905	1044.905	1830.421	5448.749	BD	3.874	0.080
	A-23A	76.89	7.052	3.367	62790.939	229.526	229.526	879.423	5356.326	BD	1.535	0.045
	A-27	77.4	7.507	0.822	23878.766	153.452	153.452	204.163	2120.288	BD	3.351	0.024
	A-31	77.9	6.681	1.953	76567.671	668.055	668.055	2403.375	4965.828	BD	3.799	0.041
	A-35A	78.33	5.773	2.743	78681.702	848.168	848.168	1192.399	7452.544	BD	2.940	0.049
	A-37	78.47	3.244	5.843	87692.867	1266.152	1266.152	2699.763	8340.137	BD	2.829	0.028
	A-41A	78.63	7.604	1.820	36175.292	304.464	304.464	393.312	3023.183	BD	2.769	0.041
	A-38B	78.6	4.881	3.614	55837.536	945.188	945.188	1910.372	4410.456	BD	3.357	<0.02
	A-48B	78.96	4.590	3.829	66544.639	495.484	495.484	1081.415	5395.878	BD	3.675	0.029
	A-52A	79.12	20.236	1.666	35663.410	150.107	150.107	314.838	2254.933	BD	3.081	0.054

Silicified Microbialite Continued (Partial Dissolution - ICP MS: MAJORS)												
Sublitho-tope	**Sample #**	**Depth (m)**	**Al (ppm)**	**Ba (ppm)**	**Ca (ppm)**	**Fe (ppm)**	**K (ppm)**	**Mg (ppm)**	**Mn (ppm)**	**Na (ppm)**	**P (ppm)**	**Ti (ppm)**
Low Domal Stromatolites	**A-56**	79.42	10.789	1.680	28573.493	73.437	73.437	154.671	1662.528	BD	3.720	0.040
	WM 61	2.6	4.245	0.509	1604.505	48.073	48.073	49.946	134.854	BD	2.355	0.020
	WM 66	13.1	5.523	17.535	34200.423	966.729	966.729	963.872	1597.412	BD	3.330	0.032
	WM 116x	31.8	2.858	1.266	34632.180	279.359	279.359	370.563	3297.013	BD	1.850	0.035
	WM117x	79.58	5.139	2.197	11195.974	148.264	148.264	159.425	1537.677	BD	2.187	<0.17
	WM 129Q	79.52	6.252	0.784	3251.486	120.299	120.299	386.476	352.625	BD	2.303	<0.02
	WM 129-S	79.45	8.570	0.891	5989.551	180.015	180.015	381.518	466.745	BD	3.381	<0.02
	WM 129-Z	79.37	2.965	2.375	14164.024	156.734	156.734	303.263	1358.601	BD	4.722	<0.02
	X3-Q		32.264	6.292	94486.043	4504.707	4504.707	13012.896	22184.683	BD	5.115	<0.19
	X10B-u	36.9	2.644	3.388	72564.327	1253.084	1253.084	2208.467	8995.741	BD	3.566	<0.16
	X10B-w	36.9	7.658	6.178	82445.987	1770.773	1770.773	3056.403	14192.687	BD	3.587	<0.15
	X23A-R	57.12	5.115	3.347	49479.597	666.856	666.856	1240.473	9168.909	BD	2.829	<0.16
	X24-v	59.95	2.961	4.375	51633.552	917.984	917.984	1583.128	11302.051	BD	3.674	<0.15
Stratiform Stromat-olite	**WM55y**	0.1	14.827	5.995	36230.157	3687.189	3687.189	4883.220	11872.970	BD	5.396	<0.17
	WM 57	0.2	2.231	2.750	18875.259	233.244	233.244	219.102	1415.520	BD	3.264	0.020
	WM60	2.53	38.349	2.860	16905.112	6435.715	6435.715	13803.482	7056.212	BD	4.589	<0.17
	X3-R		4.571	2.705	31132.330	431.848	431.848	447.144	7277.520	BD	3.583	<0.17

Carbonate Grainstone (Partial Dissolution - ICP MS: MAJORS)												
Sublitho-tope	**Sample #**	**Depth (m)**	**Al (ppm)**	**Ba (ppm)**	**Ca (ppm)**	**Fe (ppm)**	**K (ppm)**	**Mg (ppm)**	**Mn (ppm)**	**Na (ppm)**	**P (ppm)**	**Ti (ppm)**
Massive	**A-35B**	78.39	2.059	4.057	82285.735	1122.172	1122.172	2607.447	6789.189	BD	3.621	<0.02
	A-36	78.44	3.642	4.502	82833.379	1162.838	1162.838	2744.170	6772.190	BD	3.510	0.020
	A-38A	78.55	6.275	6.472	112780.932	1585.613	1585.613	4130.292	10422.498	BD	3.361	0.031
	A-39	78.59	6.430	4.162	85229.699	1004.076	1004.076	2366.670	6897.134	BD	5.240	0.034
	A-41B	78.66	8.329	5.636	103335.614	1573.728	1573.728	3092.878	8555.223	BD	4.131	0.035
	A-52B	79.15	8.947	5.148	84073.074	883.563	883.563	2586.573	6740.293	BD	4.458	0.028
	WM 63	4.5	3.383	1.663	57546.528	1792.777	1792.777	1468.450	5663.822	BD	3.516	0.021
	WM64	7.25	9.813	2.352	41624.600	2794.273	2794.273	2473.472	8717.968	BD	3.037	<0.16
	WM 73	22.5	2.637	3.142	73630.773	1125.375	1125.375	1700.418	4296.788	BD	3.668	0.033

Carbonate Grainstone Continued (Partial Dissolution - ICP MS: MAJORS)												
Sublitho-tope	**Sample #**	**Depth (m)**	**Al (ppm)**	**Ba (ppm)**	**Ca (ppm)**	**Fe (ppm)**	**K (ppm)**	**Mg (ppm)**	**Mn (ppm)**	**Na (ppm)**	**P (ppm)**	**Ti (ppm)**
Massive Continued	**WM125**		11.534	2.691	21733.166	3877.464	3877.464	8117.516	3265.127	BD	3.459	0.067
	X6-Q		26.311	7.787	95849.022	2823.965	2823.965	3299.994	28577.341	BD	8.309	<0.18
	X6-R		75.728	4.543	69195.843	1554.136	1554.136	1699.569	22838.788	BD	7.325	0.317
	X6-S		36.170	3.584	62714.290	1387.756	1387.756	1590.028	21325.229	BD	6.470	0.176
	X8-x	30.5	3.777	7.577	104848.942	2607.572	2607.572	4713.467	15992.517	BD	5.573	<0.16
	X8-y	30.5	7.923	1.509	22736.897	631.089	631.089	561.963	3964.445	BD	2.662	<0.18
Laminated	**WM 69**	14.75	2.475	22.546	<15.89	225.911	225.911	25.662	5.285	BD	21.295	2.079
	WM 71A	17	14.156	0.771	18927.221	82.664	82.664	157.322	932.176	BD	2.850	0.065
	WM 74	26.75	1.590	2.737	58961.015	1050.008	1050.008	959.946	4217.980	BD	4.635	0.025
	WM117y	79.56	4.331	11.596	71033.279	1275.076	1275.076	2579.456	12018.845	BD	3.946	<0.16
Zig Zags	**X12**	39.6	11.882	5.944	84760.194	1242.561	1242.561	888.991	14711.446	BD	6.545	<0.18
	B-1	**~39**	2.038	5.488	51393.594	1811.703	1811.703	2031.003	7610.491	BD	2.140	<0.15
	B-5	**~39**	2.081	8.049	70281.839	3339.415	3339.415	2745.276	11812.124	BD	5.025	<0.17
	B-7	**~39**	6.904	5.683	49732.330	2596.250	2596.250	2395.930	7819.021	BD	3.729	<0.16

Carbonate Microbialite (Partial Dissolution - ICP MS: MAJORS)												
Sublitho-tope	**Sample #**	**Depth (m)**	**Al (ppm)**	**Ba (ppm)**	**Ca (ppm)**	**Fe (ppm)**	**K (ppm)**	**Mg (ppm)**	**Mn (ppm)**	**Na (ppm)**	**P (ppm)**	**Ti (ppm)**
Low Domal Stromatolite	**WM 65**	12.45	8.666	2.849	59669.559	1211.604	1211.604	1039.690	4941.436	BD	2.023	0.047
	WM 67	12.3	18.576	3.466	15107.825	3488.319	3488.319	11909.915	3272.603	BD	4.244	0.127
Stratiform Stromatolite	**WM55x**	0.1	27.367	10.597	63761.653	3942.118	3942.118	3425.752	17606.065	BD	6.609	0.621
	WM58x	0.3	2.626	5.730	50939.470	5603.632	5603.632	1877.830	5224.843	BD	4.072	<0.17
	WM58y	0.3	4.161	6.514	55160.461	2121.409	2121.409	1685.837	9675.965	BD	6.498	<0.18
	WM 115	31	189.692	6.449	62726.771	1409.066	1409.066	2641.211	5788.865	BD	6.068	16.215
	WM 116y	31.8	2.794	7.421	90229.978	2451.191	2451.191	2640.729	5687.500	BD	3.415	0.020
	X31	82.2	4.436	6.446	63124.889	2658.657	2658.657	3371.827	12846.387	BD	4.029	<0.16

Carbonate Microbialite Continued (Partial Dissolution - ICP MS: MAJORS)												
Sublitho-tope	**Sample #**	**Depth (m)**	**Al (ppm)**	**Ba (ppm)**	**Ca (ppm)**	**Fe (ppm)**	**K (ppm)**	**Mg (ppm)**	**Mn (ppm)**	**Na (ppm)**	**P (ppm)**	**Ti (ppm)**
Banded Carbonate	**WM 104**	72.6	4.150	3.719	66373.375	1308.062	1308.062	1865.958	5204.673	BD	2.645	0.039
	WM 107x	56.6	4.240	2.787	68342.718	661.061	661.061	1187.008	5328.362	BD	4.290	<0.02
	WM 107y	56.6	1.764	2.413	55806.018	588.887	588.887	1063.989	4788.299	BD	2.385	0.025
	X10B-R	36.9	2.229	3.819	68827.646	1482.273	1482.273	2369.680	10336.823	BD	3.582	<0.15
	X10B-v	36.9	3.132	6.458	90019.930	2563.240	2563.240	4652.315	15819.967	BD	4.805	<0.15
	X20-y	67.1	4.471	6.285	94457.606	2794.143	2794.143	4375.482	17972.970	BD	8.222	<0.17
	X23D-y	57.27	4.031	7.461	88789.573	1658.427	1658.427	3558.784	20339.514	BD	8.299	<0.18
	X23E-w	57.33	1.772	4.815	57354.372	1168.509	1168.509	1966.563	12564.987	BD	3.644	<0.15
Banded Carbonate	**X23E-x**	57.34	1.352	4.765	58323.703	1157.230	1157.230	2157.420	13276.468	BD	4.337	<0.17
	X23E-z	57.36	1.409	4.647	61145.959	1186.050	1186.050	2353.838	12565.055	BD	4.941	<0.16
	X24-Q	59.9	2.807	4.582	57192.763	1061.733	1061.733	1374.522	11559.065	BD	6.556	<0.14
	X24-R	59.91	3.122	7.697	100352.337	1930.442	1930.442	3351.952	19938.922	BD	9.967	<0.18
	X24-t	59.93	4.801	6.323	89738.861	1687.726	1687.726	3153.830	18279.332	BD	5.539	<0.18
	X24-u	59.94	5.433	4.409	66103.947	1282.480	1282.480	2509.102	12573.957	BD	5.054	<0.19
Fenestrated Stromatolite	**WM 105x**	58.1	12.789	2.046	89135.197	1015.791	1015.791	2303.222	6720.749	BD	3.478	<0.02
	WM 114y	49	1.633	1.791	52098.323	761.476	761.476	1050.542	3507.609	BD	3.415	<0.02
	WM 124		6.189	2.233	66194.869	2137.668	2137.668	2115.315	4397.216	BD	4.231	0.024
	WM 130	~55	2.187	5.216	84513.675	1272.230	1272.230	2073.068	6099.088	BD	4.098	0.033
	X10A-x	37.15	2.401	2.009	69423.075	1556.845	1556.845	3979.249	7902.309	BD	3.116	<0.17
	X10B-t	36.9	2.611	2.618	84015.549	1530.500	1530.500	4172.266	9263.378	BD	4.094	<0.15
	X14-x	43.15	5.665	2.408	71354.598	1306.808	1306.808	4538.845	10249.756	BD	6.838	<0.19
	X16-Q	44.1	5.387	3.559	69165.083	1147.943	1147.943	3595.581	13591.166	BD	1.996	<0.15
	X19-x	60.25	2.354	8.191	108558.420	2054.807	2054.807	4381.734	19124.687	BD	7.291	<0.18
	X21-y	71.3	3.282	5.114	70431.541	1169.128	1169.128	3272.353	14260.945	BD	7.405	<0.15
	B-10B	~39.6	2.132	5.529	52116.582	1989.133	1989.133	2406.875	7651.727	BD	3.472	<0.16
Fenestrae	**WM 105y**	58.1	8.558	2.077	74072.025	625.221	625.221	1713.363	4131.086	BD	3.340	0.028
	X10A-y	37.15	3.919	4.203	71053.208	1376.405	1376.405	4085.165	8120.192	BD	2.799	<0.14
	X10B-Q	36.9	9.068	5.236	77136.427	1902.428	1902.428	2954.521	11865.982	BD	5.014	<0.17

Carbonate Microbialite Continued (Partial Dissolution - ICP MS: MAJORS)												
Sublitho-tope	**Sample #**	**Depth (m)**	**Al (ppm)**	**Ba (ppm)**	**Ca (ppm)**	**Fe (ppm)**	**K (ppm)**	**Mg (ppm)**	**Mn (ppm)**	**Na (ppm)**	**P (ppm)**	**Ti (ppm)**
Fenestrae continued	**X19-M**	60.25	10.375	5.034	127960.571	1365.604	1365.604	3078.141	10718.140	BD	4.069	0.062
	X-20-N	67.1	12.276	3.342	101633.628	1622.156	1622.156	2845.314	8943.828	BD	8.385	0.064
	X-21-M	71.3	15.168	3.720	84843.989	735.403	735.403	1903.935	8027.498	BD	4.424	0.082
	X23D-x	57.26	6.050	7.830	77270.278	1721.736	1721.736	2630.693	15736.788	BD	5.861	<0.18
	X23E-y	57.35	1.691	6.368	71519.814	1406.440	1406.440	2436.756	15189.623	BD	4.360	<0.15
	X-23A-M	57.1	4.317	8.464	147883.368	1420.364	1420.364	3629.040	15226.243	BD	3.831	0.025
	X24-S	59.92	7.987	9.541	85753.752	1788.989	1788.989	3257.332	18119.540	BD	6.906	<0.17
Organic Rich Mud	**X-20-M**	67.1	676.960	24.548	248552.753	3812.306	3812.306	10450.549	19515.214	BD	15.510	0.788
	X-21-N	71.3	39.342	3.369	86211.041	774.380	774.380	2572.475	8883.747	BD	4.110	0.055
	X23A-t	57.15	5.644	6.543	79462.482	1807.121	1807.121	3914.274	16928.953	BD	4.922	<0.18
Fenestrated Microbialite	**A-2**	74.2	1.334	5.852	46282.778	666.050	666.050	1438.124	6618.151	BD	2.358	<0.14
	A-3	74.25	42.239	6.012	170231.911	1309.705	1309.705	5132.792	14620.052	BD	4.730	0.443
	A-9	74.88	4.119	1.375	94296.797	993.156	993.156	4090.164	5141.484	BD	2.440	0.080
	A-12	75.12	11.668	2.430	76421.106	1082.770	1082.770	2878.384	6718.371	BD	2.994	0.114
	A-16	76.1	5.786	2.021	88953.655	1009.822	1009.822	4728.670	5712.859	BD	3.487	0.050
	A-17	76.2	12.643	1.531	80087.729	754.424	754.424	2635.876	5678.812	BD	3.326	0.120
	A-18B	76.3	19.662	3.481	72301.628	257.916	257.916	599.086	5556.841	BD	3.961	0.090
	A-18D	76.38	5.488	2.706	64095.502	242.333	242.333	499.722	5864.842	BD	2.926	0.029
	A-20B	76.56	5.504	4.074	80760.822	898.442	898.442	2827.991	7592.527	BD	4.723	0.030
	A-22	76.85	3.136	3.056	70152.126	464.618	464.618	2001.869	6291.191	BD	3.716	0.026
	A-23B	76.94	3.335	2.004	82332.586	651.689	651.689	2464.984	6288.632	BD	3.286	0.039
	A-28	77.58	11.583	3.019	76762.801	449.846	449.846	2030.264	6031.680	BD	3.016	0.111
	A-48A	78.91	2.040	4.060	82937.046	755.353	755.353	2385.820	6202.090	BD	3.132	<0.02
	WM 108	58	6.283	1.094	70420.033	552.499	552.499	1295.436	3665.208	BD	1.808	0.040
	WM 109	52.15	12.821	2.156	65124.197	485.685	485.685	1321.139	4900.754	BD	4.319	<0.02
	A-32	78.12	5.415	4.188	119046.801	1589.231	1589.231	2540.379	10496.621	BD	2.756	0.026
	A-43	78.75	7.832	2.793	58225.836	449.139	449.139	694.601	4599.917	BD	2.825	0.035
	WM 110	53.4	15.851	1.920	80623.598	839.580	839.580	1470.061	5031.416	BD	2.159	0.026
	WM 111	53.7	6.649	1.856	57109.903	673.926	673.926	1186.750	4142.251	BD	3.029	<0.02

Carbonate Microbialite Continued (Partial Dissolution - ICP MS: MAJORS)												
Sublitho-tope	**Sample #**	**Depth (m)**	**Al (ppm)**	**Ba (ppm)**	**Ca (ppm)**	**Fe (ppm)**	**K (ppm)**	**Mg (ppm)**	**Mn (ppm)**	**Na (ppm)**	**P (ppm)**	**Ti (ppm)**
Fenestrated Microbialite Continued	**WM 112**	54	4.893	1.796	64708.433	674.825	674.825	1361.454	4586.736	BD	3.614	0.021
	WM 113	48.2	4.499	1.469	53925.693	736.349	736.349	1016.496	2762.804	BD	4.099	0.021
	WM 114x	49	4.858	2.910	88583.719	1216.969	1216.969	1950.058	6366.685	BD	4.449	0.066
	WM 129-R	79.49	5.163	4.953	75607.696	1948.736	1948.736	1653.461	4978.666	BD	2.385	0.060
	WM 129-T2	79.41	2.191	7.045	73889.376	2141.272	2141.272	2066.526	5489.960	BD	2.156	0.042
	WM 129-T	79.4	0.888	3.971	49735.606	1243.052	1243.052	1191.326	3464.955	BD	1.148	<0.02
	WM 129 X	79.3	2.067	1.269	37683.383	512.492	512.492	619.882	3210.780	BD	2.165	0.023
	WM 129-Y	79.33	1.091	5.083	56150.803	1317.779	1317.779	1719.184	3751.663	BD	2.437	<0.02
	X2		6.586	7.034	90046.868	2768.494	2768.494	4898.527	15753.573	BD	5.722	<0.16
	X10B-S	36.9	4.114	4.432	71437.476	1763.650	1763.650	2708.793	11380.519	BD	4.370	<0.14
	X14-y	43.15	7.727	2.936	97932.936	1531.692	1531.692	4686.002	13624.253	BD	4.520	<0.16
	X16-R	44.1	14.172	5.006	96409.478	1710.944	1710.944	4741.311	19520.872	BD	5.760	<0.16
	X18	58.4	3.442	4.502	80257.774	1734.915	1734.915	5072.986	9857.942	BD	4.188	<0.18
	X19-y	60.25	5.858	8.768	137052.284	2527.134	2527.134	5535.762	21835.627	BD	9.600	<0.14
	X20-x	67.1	4.943	3.927	78318.870	2138.626	2138.626	3578.191	13966.830	BD	7.094	<0.15
	X21-z	71.3	5.576	4.746	96291.986	1525.576	1525.576	3422.781	15527.868	BD	7.614	<0.18
	X23B	57.16	5.205	23.481	70251.783	1408.526	1408.526	3285.913	14203.777	BD	4.219	<0.15
	X23C	57.19	9.511	3.839	70816.064	1570.262	1570.262	4450.681	14975.293	BD	5.564	<0.15
	X23A-S	57.14	3.173	5.483	74352.107	1442.407	1442.407	3030.610	15504.089	BD	5.800	<0.17
	X23A-Q	59.9	10.548	4.724	69970.611	1091.040	1091.040	2538.386	9762.180	BD	3.312	<0.15
	X24-x	59.97	4.507	2.860	46588.805	857.100	857.100	2927.700	4254.186	BD	2.778	<0.14
	X24-W	59.96	2.529	3.510	61820.252	1055.468	1055.468	2557.389	9612.084	BD	3.460	<0.17
	X29	81	25.869	5.257	14060.224	6275.296	6275.296	19298.522	6274.911	BD	2.540	<0.15
	X30	82	5.668	3.832	50237.343	2306.525	2306.525	5023.821	9733.504	BD	4.965	<0.18
	X32	84.7	7.107	6.013	58440.620	2844.990	2844.990	4188.558	14370.886	BD	4.671	<0.18
	X33	84.3	21.955	9.735	77089.141	3243.918	3243.918	5332.974	18171.747	BD	4.799	<0.18
	X34	88.5	1.840	6.076	52490.747	1823.447	1823.447	2898.367	7175.304	BD	2.307	<0.15
	B-8		1.637	6.150	52344.159	2464.230	2464.230	2103.178	8289.497	BD	3.416	<0.15
	B-10A		1.650	2.701	53002.524	1317.014	1317.014	1658.560	5807.781	BD	2.724	<0.17

Standards (Partial Dissolution - ICP MS: MAJORS)										
Standard	**Al**	**Ba**	**Ca**	**Fe**	**K**	**Mg**	**Mn**	**Na**	**P**	**Ti**
CAL-S	<0.01	<0.11	0.383	2352.051	2.331	<0.01	1.541	BD	0.024	13.554
CAL-S	<0.01	<0.12	0.313	1703.403	2.507	<0.01	1.121	BD	0.017	9.968
CAL-S	<0.01	<0.12	0.367	1918.002	2.573	<0.01	1.222	BD	0.024	10.464
CAL-S	0.005	<0.12	0.318	1157.808	2.703	<0.01	0.767	BD	0.019	8.602
CAL-S	<0.01	<0.12	0.442	1230.468	2.534	<0.01	0.952	BD	0.024	9.770
CAL-S	<0.01	<0.29	0.428	2549.851	2.785	<0.01	1.928	BD	0.027	18.560
CAL-S	<0.01	<0.26	0.497	1765.280	2.541	<0.01	1.421	BD	0.031	12.454
CAL-S	0.001	<0.25	0.726	1744.123	2.452	<0.01	1.574	BD	0.036	13.213

Silicified Microbialite (Partial Dissolution - ICP MS: MINORS)																										
Sample #	**Ba**	**Cr**	**Cu**	**Li**	**Sr**	**V**	**Y**	**Zr**	**Zn**	**As**	**Co**	**Mo**	**Nb**	**Ni**	**Sb**	**Sc**	**Sn**	**Cd**	**Cs**	**Pb**	**Hf**	**Rb**	**Ta**	**Th**	**U**	**W**
A-1	1.182	0.041	0.282	<0.22	7.873	0.318	0.719	<0.02	0.034	<4.57	4.107	<0.41	<0.26	0.066	<0.01	0.025	0.009	0.023	<0.01	0.295	<0.02	0.044	<0.03	0.012	0.055	<4.56
A-5	0.793	0.082	2.875	0.134	4.736	4.092	1.061	<0.23	2.692	<0.06	3.099	<0.13	<0.12	0.255	<0.01	0.178	0.008	1.896	0.028	0.037	<0.28	0.990	<0.02	0.015	0.108	<1.09
A-10	1.560	0.045	0.147	<0.1	25.397	0.381	1.578	<0.23	1.137	<0.06	2.015	<0.12	<0.11	0.038	<0.01	0.119	0.009	0.039	0.008	0.376	<0.27	0.214	<0.02	0.006	0.047	<1.06
A-14	1.643	0.027	0.099	<0.09	25.838	0.052	1.764	<0.21	1.213	<0.05	2.242	<0.11	<0.1	0.041	<0.01	0.072	0.008	0.022	0.019	0.194	<0.25	0.475	<0.02	0.005	0.019	<0.97
A-18A	3.044	0.074	0.113	0.083	49.022	0.114	2.201	<0.19	2.215	<0.05	0.287	<0.1	<0.09	0.035	0.005	0.114	0.011	<0.02	0.011	0.113	<0.22	0.248	<0.02	0.013	0.008	<0.88
A-18C	3.748	0.076	0.086	0.097	42.885	0.144	1.200	<0.2	0.427	<0.05	0.232	<0.11	<0.1	<0.03	0.006	0.088	0.022	<0.02	<0.01	0.083	<0.24	0.025	<0.02	0.006	0.024	<0.93
A-20A	3.537	0.086	0.093	0.092	32.008	0.171	4.633	<0.2	0.948	0.082	2.057	<0.11	<0.1	0.079	0.023	0.736	0.009	0.363	0.014	0.092	<0.24	0.211	<0.02	0.015	0.125	<0.95
A-23A	3.367	0.026	0.066	<0.1	38.539	0.112	1.845	<0.22	1.550	<0.06	1.176	<0.12	<0.11	0.100	<0.01	0.069	0.013	0.020	<0.01	0.074	<0.27	0.066	<0.02	0.004	0.022	<1.06
A-27	0.822	0.064	0.172	<0.09	12.399	1.717	1.188	<0.21	0.856	<0.05	2.441	<0.11	<0.1	0.083	<0.01	0.112	<0.01	0.024	<0.01	0.029	<0.25	0.016	<0.02	0.008	0.071	<0.97
A-31	1.953	0.054	0.031	<0.09	36.083	0.087	1.993	<0.21	1.217	<0.05	0.294	<0.12	<0.1	0.033	<0.01	0.091	0.012	<0.02	0.005	0.077	<0.25	0.037	<0.02	0.009	0.007	<0.98
A-35A	2.743	0.028	0.104	0.111	55.666	0.101	3.909	<0.2	1.443	<0.05	0.417	<0.11	<0.1	0.067	0.006	0.152	<0.01	0.020	0.029	0.050	<0.24	0.096	<0.02	0.009	0.023	<0.94
A-37	5.843	0.116	0.119	0.120	67.968	0.297	4.992	<0.24	0.533	<0.06	0.368	<0.13	<0.12	0.046	<0.01	0.207	0.020	<0.02	<0.01	0.317	<0.29	0.033	<0.02	0.011	0.012	<1.15
A-41A	1.820	0.037	0.132	<0.1	31.246	0.062	2.093	<0.21	0.616	<0.05	1.582	<0.12	<0.11	0.040	<0.01	0.108	0.001	0.021	0.024	0.469	<0.25	0.421	<0.02	0.008	0.039	<1.0

Silicified Microbialite (Partial Dissolution - ICP MS: MINORS)																										
Sample #	**Ba**	**Cr**	**Cu**	**Li**	**Sr**	**V**	**Y**	**Zr**	**Zn**	**As**	**Co**	**Mo**	**Nb**	**Ni**	**Sb**	**Sc**	**Sn**	**Cd**	**Cs**	**Pb**	**Hf**	**Rb**	**Ta**	**Th**	**U**	**W**
A-38B	3.614	0.086	0.019	0.086	45.929	0.136	1.350	<0.2	0.304	<0.05	0.217	<0.11	<0.1	<0.103	0.006	0.066	0.013	<0.02	0.004	0.185	<0.24	0.026	<0.02	0.010	0.009	<0.94
A-48B	3.829	0.039	0.103	0.116	45.791	0.201	3.246	<0.21	0.572	<0.05	0.772	<0.12	<0.11	<0.103	<0.01	0.072	0.010	0.019	0.005	0.682	<0.25	0.088	<0.02	0.006	0.026	<0.99
A-52A	1.666	0.040	0.365	<0.1	26.037	0.198	1.824	<0.21	2.223	<0.05	2.130	<0.12	<0.11	0.151	<0.01	0.056	0.012	0.020	0.005	0.486	<0.26	0.047	<0.02	0.008	0.034	<1.0
A-56	1.680	0.032	0.247	<0.1	24.002	0.070	1.915	<0.22	1.061	<0.06	2.570	<0.12	<0.11	0.048	<0.01	0.036	0.010	<0.02	<0.01	0.321	<0.27	0.033	<0.02	0.007	0.011	<1.04
WM 61	0.509	0.020	0.753	<0.08	3.106	0.010	0.138	<0.19	0.301	0.052	9.366	<0.1	<0.09	0.061	<0.01	<0.01	0.009	0.018	0.008	0.066	<0.23	0.182	<0.02	0.005	0.002	<0.89
WM 66	17.535	0.029	0.339	<0.11	101.670	0.038	0.902	<0.25	0.715	0.065	3.349	<0.14	<0.12	0.096	<0.01	0.052	0.011	0.037	0.040	0.435	<0.3	0.526	<0.02	0.017	0.005	<1.16
WM 116x	1.266	0.012	0.025	<0.1	40.274	0.014	3.841	<0.22	0.128	0.063	1.710	<0.12	<0.11	0.073	0.006	0.059	<0.01	0.019	0.005	0.293	<0.26	0.063	<0.02	0.020	0.006	<1.02
WM117x	2.197	0.039	0.277	<0.22	20.543	0.056	1.738	<0.02	0.284	<4.71	1.582	<0.42	<0.27	0.071	0.007	0.036	<0.01	0.019	<0.01	0.018	<0.02	0.044	<0.04	0.014	0.019	<4.7
WM 129Q	0.784	0.053	0.099	0.282	1.925	2.208	0.496	<0.19	0.176	<0.05	2.438	<0.1	<0.09	0.089	<0.01	0.009	0.008	0.002	<0.01	0.019	0.022	0.048	<0.02	0.003	0.041	<0.87
WM 129-S	0.891	0.057	0.101	0.353	4.022	1.222	0.725	<0.25	0.246	<0.06	2.818	<0.14	<0.12	0.083	0.009	0.009	0.010	0.022	<0.01	0.041	<0.3	0.032	<0.02	0.004	0.027	<1.16
WM 129-Z	2.375	0.039	0.161	0.269	8.941	0.663	1.376	<0.23	0.076	<0.06	1.501	<0.13	<0.12	0.080	<0.01	0.022	<0.01	<0.02	<0.01	0.163	<0.28	0.060	<0.02	0.009	0.022	<1.1
X3-Q	6.292	0.051	0.214	0.681	187.125	0.051	7.476	0.037	0.170	7.324	0.870	<0.47	<0.3	0.077	<0.01	0.822	0.018	0.073	0.055	1.534	<0.34	0.855	<0.04	0.118	0.038	<5.22
X10B-u	3.388	0.128	0.294	<0.21	86.666	0.141	5.305	0.015	0.098	<4.33	3.510	<0.39	<0.25	0.130	0.006	0.310	0.012	0.024	0.008	0.422	<0.02	0.341	<0.03	0.022	0.120	<4.32
X10B-w	6.178	0.148	0.220	<0.2	121.878	0.153	8.507	0.019	0.124	<4.28	1.991	<0.38	<0.24	0.184	0.010	0.539	0.012	0.030	<0.01	0.432	<0.02	0.392	<0.03	0.041	0.222	<4.27

Silicified Microbialite (Partial Dissolution - ICP MS: MINORS)																									
Sample #	**Ba**	**Cr**	**Cu**	**Li**	**Sr**	**V**	**Y**	**Zr**	**Zn**	**As**	**Co**	**Mo**	**Nb**	**Ni**	**Sb**	**Sc**	**Sn**	**Cd**	**Cs**	**Pb**	**Hf**	**Rb**	**Ta**	**Th**	**U**	**W**
X23A-R	3.347	0.073	1.361	<0.2	79.888	0.074	3.582	<0.02	0.485	<4.29	2.646	<0.38	<0.25	0.114	<0.01	0.209	0.022	0.042	0.008	0.854	<0.02	0.464	<0.03	0.034	0.024	<4.28
X24-v	4.375	0.083	0.313	<0.2	67.368	0.096	7.971	0.014	0.948	<4.1	0.694	<0.37	<0.23	0.054	<0.01	0.255	0.016	0.049	<0.01	1.144	<0.02	0.402	<0.03	0.039	0.103	<4.09
WM55y	5.995	0.072	0.257	<0.22	260.730	0.073	10.435	<0.02	0.088	<4.66	0.373	<0.42	<0.27	0.168	0.009	0.354	0.021	0.020	0.037	2.033	0.014	3.421	<0.04	0.153	0.042	<4.65
WM57	2.750	0.014	0.302	<0.1	21.069	0.010	0.699	<0.21	0.499	<0.05	3.434	<0.12	<0.11	0.037	<0.01	0.027	0.007	0.038	0.007	0.295	0.026	0.179	<0.02	0.005	0.001	<1.01
WM60	2.860	0.078	0.149	0.788	62.447	0.092	3.148	<0.02	0.650	<4.63	0.585	<0.41	<0.26	0.452	<0.01	0.308	0.015	0.045	0.030	0.511	0.002	0.674	<0.04	0.196	0.050	<4.62
X3-R	2.705	0.021	0.305	<0.23	89.649	0.076	3.950	<0.02	0.082	<4.82	1.318	<0.43	<0.28	0.050	0.006	0.094	0.017	0.095	0.001	1.557	<0.02	0.061	<0.04	0.052	0.022	<4.81

Carbonate Grainstones (Partial Dissolution – ICP MS: MINORS)																									
Sample #	**Ba**	**Cr**	**Cu**	**Li**	**Sr**	**V**	**Y**	**Zr**	**Zn**	**As**	**Co**	**Mo**	**Nb**	**Ni**	**Sb**	**Sc**	**Sn**	**Cd**	**Cs**	**Pb**	**Hf**	**Rb**	**Ta**	**Th**	**U**	**W**
A-35B	4.057	0.108	0.061	<0.1	57.982	0.200	1.961	<0.22	0.359	<0.06	0.263	<0.12	<0.11	0.028	<0.01	0.098	0.009	0.002	0.008	0.160	0.027	0.082	0.002	0.012	0.006	<1.05
A-36	4.502	0.113	0.094	<0.11	57.719	0.283	3.142	<0.24	0.396	<0.06	0.225	<0.13	<0.12	<0.04	<0.01	0.096	0.013	0.002	<0.01	0.133	0.028	0.009	0.002	0.010	0.006	<1.11
A-38A	6.472	0.158	0.041	0.141	75.577	0.324	5.929	<0.24	0.781	<0.06	0.645	<0.13	<0.12	0.052	0.006	0.133	0.013	0.021	<0.01	0.236	0.029	0.016	0.002	0.015	0.013	<1.13
A-39	4.162	0.090	0.045	0.103	56.401	0.233	2.423	<0.25	0.717	<0.06	0.295	<0.13	<0.12	0.052	<0.01	0.097	<0.01	0.002	0.008	0.165	0.029	0.027	0.002	0.017	0.017	<1.15
A-41B	5.636	0.162	0.102	0.109	74.419	0.463	3.877	<0.21	0.848	<0.05	0.372	<0.11	<0.1	0.038	0.011	0.099	0.016	0.002	0.005	0.245	0.025	0.037	0.002	0.011	0.023	<0.98
A-52B	5.148	0.119	0.090	0.108	60.410	0.340	2.418	<0.24	0.982	<0.06	0.501	<0.13	<0.12	0.041	<0.01	0.095	0.009	0.002	0.007	0.188	0.028	0.037	0.002	0.013	0.017	<1.11

Carbonate Grainstones (Partial Dissolution – ICP MS: MINORS)																										
Sample #	**Ba**	**Cr**	**Cu**	**Li**	**Sr**	**V**	**Y**	**Zr**	**Zn**	**As**	**Co**	**Mo**	**Nb**	**Ni**	**Sb**	**Sc**	**Sn**	**Cd**	**Cs**	**Pb**	**Hf**	**Rb**	**Ta**	**Th**	**U**	**W**
WM63	1.663	0.027	0.035	<0.1	50.602	0.030	2.500	<0.22	0.283	<0.05	0.475	<0.12	<0.11	0.039	<0.01	0.073	<0.01	0.024	0.032	0.502	<0.26	0.860	<0.02	0.024	0.008	<1.02
WM64	2.352	0.055	0.125	0.220	70.493	0.054	5.056	<0.02	0.504	<4.38	0.251	<0.39	<0.25	0.058	0.009	0.197	0.011	0.016	0.021	0.476	<0.02	0.546	<0.03	0.063	0.021	<4.37
WM73	3.142	0.061	0.100	<0.1	51.639	0.081	1.887	<0.23	0.300	<0.06	0.221	<0.12	<0.11	0.032	<0.01	0.305	0.015	<0.02	0.009	0.133	<0.27	0.175	<0.02	0.033	0.013	<1.07
WM125	2.691	0.092	0.006	0.177	15.588	0.131	3.607	<0.21	0.407	0.061	0.197	<0.11	<0.1	0.063	0.005	0.102	0.009	<0.02	0.006	0.515	<0.25	0.392	<0.02	0.052	0.011	<0.98
X6-Q	7.787	0.184	0.327	<0.24	248.275	0.434	20.159	0.110	0.179	8.073	1.204	<0.45	<0.28	0.103	0.008	0.783	0.025	0.045	0.008	2.146	<0.02	0.699	<0.04	0.106	0.041	<4.96
X6-R	4.543	0.143	0.185	0.305	250.637	0.698	10.309	0.211	0.120	5.311	1.078	<0.35	<0.23	0.428	0.008	3.416	0.016	0.041	<0.01	2.279	<0.02	0.580	<0.03	0.478	0.099	<3.95
X6-S	3.584	0.123	1.123	<0.22	208.450	0.188	11.225	0.098	0.128	<4.68	0.826	<0.42	<0.27	0.165	<0.01	1.510	0.019	0.046	<0.01	3.707	<0.02	0.871	<0.04	0.246	0.040	<4.68
X8-x	7.577	0.206	0.317	<0.21	130.136	0.499	5.021	0.038	0.159	4.791	0.627	<0.39	<0.25	0.090	0.007	0.225	0.052	0.027	<0.01	0.515	<0.02	0.022	<0.03	0.015	0.069	<4.34
X8-y	1.509	0.048	0.370	<0.24	31.702	0.072	1.477	<0.02	0.100	<5.08	2.187	<0.45	<0.29	0.064	<0.01	0.214	<0.01	0.024	0.018	0.363	<0.02	0.862	<0.04	0.010	0.052	<5.07
WM69	22.546	0.650	0.473	3.459	550.815	0.511	0.022	<0.2	10.958	9.602	1.115	8.899	<0.1	1.578	2.546	0.397	0.710	2.295	1.729	0.558	<0.25	5.096	0.402	0.033	0.007	<0.96
WM71A	0.771	0.012	0.025	<0.1	14.607	0.121	1.065	<0.21	0.789	<0.05	0.813	<0.12	<0.11	0.033	<0.01	0.071	<0.01	0.019	<0.01	1.615	<0.26	0.061	<0.02	0.017	0.033	<1.0
WM74	2.737	0.024	0.076	<0.1	27.598	0.081	6.483	<0.23	0.193	0.074	0.397	<0.13	<0.12	0.049	<0.01	0.084	0.009	<0.02	<0.01	0.028	<0.28	0.022	<0.02	0.003	0.042	<1.09
WM117y	11.596	0.163	0.541	<0.22	103.294	0.424	4.889	0.021	0.453	<4.55	0.520	<0.41	<0.26	0.099	0.013	0.196	0.019	0.019	<0.01	0.352	<0.02	0.037	<0.03	0.031	0.020	<4.54
X12	5.944	0.065	0.441	<0.24	151.690	0.085	5.417	0.097	0.809	<4.97	0.376	<0.44	<0.28	0.089	<0.01	0.210	0.019	0.054	<0.01	1.145	<0.02	0.115	<0.04	0.025	0.006	<4.96

B-1	5.488	0.224	0.358	<0.2	92.974	0.576	3.503	0.024	0.134	<4.13	0.632	<0.37	<0.24	2.172	0.012	0.171	0.047	0.663	<0.01	0.279	<0.02	0.013	<0.03	0.021	0.032	<4.12
Carbonate Grainstones (Partial Dissolution – ICP MS: MINORS)																										
Sam-ple #	**Ba**	**Cr**	**Cu**	**Li**	**Sr**	**V**	**Y**	**Zr**	**Zn**	**As**	**Co**	**Mo**	**Nb**	**Ni**	**Sb**	**Sc**	**Sn**	**Cd**	**Cs**	**Pb**	**Hf**	**Rb**	**Ta**	**Th**	**U**	**W**
B-5	8.049	0.259	0.028	<0.22	153.814	0.905	6.073	0.044	0.087	<4.71	0.816	<0.42	<0.27	2.661	0.017	0.318	0.017	0.020	<0.01	0.332	<0.02	<0.02	<0.04	0.030	0.045	<4.7
B-7	5.683	0.213	0.026	0.279	111.698	0.420	5.632	0.101	0.045	<4.33	0.632	<0.39	<0.25	0.079	0.024	0.722	<0.01	0.025	<0.01	0.261	<0.02	0.033	<0.03	0.040	0.038	<4.32

Carbonate Microbialite (Partial Dissolution – ICP MS: MINORS)																										
Sam ple #	**Ba**	**Cr**	**Cu**	**Li**	**Sr**	**V**	**Y**	**Zr**	**Zn**	**As**	**Co**	**Mo**	**Nb**	**Ni**	**Sb**	**Sc**	**Sn**	**Cd**	**Cs**	**Pb**	**Hf**	**Rb**	**Ta**	**Th**	**U**	**W**
WM 65	2.849	0.009	0.139	<0.1	65.001	0.044	2.364	<0.23	0.284	0.079	0.432	<0.13	<0.11	0.097	<0.01	0.069	0.013	0.065	0.033	1.022	<0.27	1.117	<0.02	0.026	0.026	<1.08
WM 67	3.466	0.043	0.032	1.079	21.784	0.190	5.186	<0.23	1.036	0.165	0.231	<0.13	<0.12	0.166	0.014	1.144	0.008	0.020	0.029	0.145	<0.28	1.123	<0.02	0.018	0.019	<1.09
WM 55x	10.597	0.081	0.703	0.207	342.281	0.087	13.659	0.043	0.088	<4.26	0.706	<0.38	<0.24	0.173	0.010	0.321	0.045	0.020	0.077	5.008	0.017	5.116	<0.03	0.247	0.057	<4.25
WM 58x	5.730	0.059	0.319	0.336	89.804	0.093	0.735	<0.02	0.117	<4.79	0.685	<0.43	<0.27	0.234	<0.01	0.140	0.042	0.054	0.011	0.286	<0.02	0.038	<0.04	0.015	0.017	<4.78
WM 58y	6.514	0.053	0.272	<0.24	130.628	0.033	2.718	<0.02	0.063	<5.07	1.690	<0.45	<0.29	0.215	<0.01	0.155	0.030	0.047	0.048	0.202	0.002	0.436	<0.04	0.028	0.004	<5.06
WM 115	6.449	0.659	0.090	1.779	64.096	0.724	3.891	0.561	0.402	<0.05	0.139	<0.1	<0.09	0.110	0.013	0.298	0.025	<0.02	0.052	0.401	<0.22	0.904	<0.02	0.161	0.090	3.539
WM 116y	7.421	0.133	0.021	0.102	66.434	0.306	3.791	<0.23	0.248	<0.06	0.158	<0.13	<0.12	0.052	<0.01	0.136	0.009	0.044	<0.01	0.191	<0.28	0.018	<0.02	0.017	0.015	<1.09
X31	6.446	0.143	0.085	<0.21	78.047	0.222	4.859	0.020	0.041	<4.31	0.783	<0.39	<0.25	0.052	0.011	0.165	0.015	<0.02	<0.01	0.272	<0.02	0.081	<0.03	0.039	0.090	<4.3
WM 104	3.719	0.127	0.669	0.101	41.918	0.349	2.775	<0.24	0.551	<0.06	0.180	<0.13	<0.12	0.065	0.006	0.195	0.036	0.026	<0.01	0.149	<0.29	0.111	<0.02	0.006	0.009	<1.12

Carbonate Microbialite (Partial Dissolution – ICP MS: MINORS)																										
Sample #	**Ba**	**Cr**	**Cu**	**Li**	**Sr**	**V**	**Y**	**Zr**	**Zn**	**As**	**Co**	**Mo**	**Nb**	**Ni**	**Sb**	**Sc**	**Sn**	**Cd**	**Cs**	**Pb**	**Hf**	**Rb**	**Ta**	**Th**	**U**	**W**
WM 107x	2.787	0.050	0.249	<0.11	34.748	0.101	3.518	<0.25	0.419	<0.06	0.090	<0.14	<0.12	0.041	0.011	0.080	0.044	0.021	<0.01	0.153	<0.3	<0.01	<0.02	0.004	0.006	<1.17
WM 107y	2.413	0.066	0.340	<0.1	30.090	0.125	3.010	<0.22	0.253	<0.06	0.120	<0.12	<0.11	0.051	0.010	0.085	0.044	<0.02	0.012	0.124	0.026	0.005	<0.02	0.007	0.009	<1.04
X10 B-R	3.819	0.178	0.521	<0.2	78.095	0.348	2.988	0.026	0.111	<4.12	0.611	<0.37	<0.24	0.067	0.006	0.156	0.048	0.016	<0.01	0.137	<0.02	0.015	<0.03	0.009	0.019	<4.11
X10 B-v	6.458	0.347	0.248	0.197	139.877	0.381	8.096	0.030	0.139	<4.15	1.511	<0.37	<0.24	0.084	0.008	0.328	0.024	0.023	<0.01	0.163	<0.02	0.045	<0.03	0.051	0.191	<4.14
X20-y	6.285	0.444	0.285	<0.23	96.480	0.668	9.926	0.053	0.173	<4.74	1.168	<0.42	<0.27	0.330	0.008	0.219	0.090	0.037	<0.01	0.197	<0.02	0.016	<0.04	0.028	0.057	<4.73
X23 D-y	7.461	0.302	0.474	<0.23	98.196	0.438	8.267	0.024	0.113	<4.93	1.950	<0.44	<0.28	0.124	<0.01	0.233	0.050	0.030	<0.01	0.132	<0.02	0.019	<0.04	0.024	0.012	<4.92
X23 E-w	4.815	0.138	0.283	<0.2	58.787	0.247	5.628	0.015	0.072	<4.17	0.759	<0.37	<0.24	0.082	0.005	0.140	0.045	0.024	<0.01	0.155	<0.02	<0.02	<0.03	0.010	0.014	<4.16
X23 E-x	4.765	0.129	0.324	<0.22	63.063	0.324	6.235	<0.02	0.061	<4.67	0.905	<0.42	<0.27	0.068	<0.01	0.137	0.063	0.016	<0.01	0.119	<0.02	<0.02	<0.04	0.013	0.015	<4.66
X23 E-z	4.647	0.308	0.141	<0.21	64.706	0.452	7.651	<0.02	0.052	<4.42	0.779	<0.4	<0.25	0.046	<0.01	0.149	0.040	0.023	<0.01	0.203	<0.02	<0.02	<0.03	0.019	0.017	<4.41
X24-Q	4.582	0.064	0.434	<0.19	65.574	0.103	7.302	<0.02	0.067	<4.0	1.856	<0.36	<0.23	0.047	<0.01	0.142	0.029	0.057	0.009	1.266	<0.02	0.027	<0.03	0.009	0.035	<3.99
X24-R	7.697	0.241	0.390	<0.24	99.398	0.462	10.851	0.032	0.091	<5.01	0.725	<0.45	<0.29	4.944	<0.01	0.248	0.084	0.020	<0.01	0.417	<0.02	0.051	<0.04	0.023	0.042	<5.0
X24-t	6.323	0.306	0.425	<0.24	94.515	0.427	9.699	0.033	0.074	<4.99	0.806	<0.45	<0.29	5.660	<0.01	0.236	0.039	0.024	<0.01	0.369	<0.02	0.056	<0.04	0.037	0.054	<4.98
X24-u	4.409	0.267	0.502	<0.25	71.431	0.333	7.930	0.022	0.079	<5.19	1.115	<0.46	<0.3	0.071	0.006	0.180	0.054	0.036	<0.01	0.407	<0.02	0.040	<0.04	0.025	0.037	<5.18
WM 105x	2.046	0.278	0.344	0.117	48.204	0.239	4.384	<0.23	0.301	<0.06	0.167	<0.12	<0.11	0.115	0.006	0.150	0.009	0.002	<0.01	0.158	<0.27	0.014	<0.02	0.033	0.063	<1.06

Carbonate Microbialite (Partial Dissolution – ICP MS: MINORS)																										
Sample #	**Ba**	**Cr**	**Cu**	**Li**	**Sr**	**V**	**Y**	**Zr**	**Zn**	**As**	**Co**	**Mo**	**Nb**	**Ni**	**Sb**	**Sc**	**Sn**	**Cd**	**Cs**	**Pb**	**Hf**	**Rb**	**Ta**	**Th**	**U**	**W**
WM 114y	1.791	0.089	0.135	<0.09	25.506	0.241	1.662	<0.19	0.231	0.050	0.162	<0.1	<0.09	0.047	<0.01	0.130	0.007	0.023	<0.01	0.149	<0.23	0.014	<0.02	0.005	0.015	<0.89
WM 124	2.233	0.069	0.043	<0.11	47.736	0.080	5.266	<0.24	0.222	<0.06	0.199	<0.13	<0.12	0.059	0.007	0.122	<0.01	<0.02	0.013	0.162	<0.29	0.279	<0.02	0.051	0.046	<1.14
WM 130	5.216	0.078	0.063	<0.11	49.729	0.153	1.541	<0.24	0.279	<0.06	0.537	<0.13	<0.12	0.061	0.008	0.144	0.009	0.036	<0.01	0.116	<0.29	0.028	<0.02	0.008	0.006	<1.13
X10A-x	2.009	0.128	0.565	<0.22	64.252	0.128	2.596	0.036	0.154	<4.67	1.441	<0.42	<0.27	0.133	0.007	0.144	0.026	0.013	<0.01	0.093	<0.02	0.050	<0.04	0.012	0.011	<4.66
X10B-t	2.618	0.213	0.320	<0.2	88.671	0.208	6.857	0.048	0.101	<4.16	0.508	<0.37	<0.24	0.204	0.005	0.227	0.017	0.016	0.009	0.145	<0.02	0.198	<0.03	0.032	0.051	<4.15
X14-x	2.408	0.360	0.459	<0.24	80.068	0.381	4.507	0.032	3.392	7.114	0.948	<0.46	<0.29	0.104	<0.01	0.155	0.060	<0.02	<0.01	0.213	<0.02	<0.02	<0.04	0.032	0.025	<5.12
X16-Q	3.559	0.239	0.265	<0.19	77.821	0.412	3.424	0.036	0.116	<4.04	0.564	<0.36	<0.23	0.112	0.008	0.151	0.026	0.021	<0.01	0.380	<0.02	0.035	<0.03	0.044	0.007	<4.03
X19-x	8.191	0.317	0.528	<0.23	117.677	0.806	7.940	0.052	1.838	6.881	1.327	<0.44	<0.28	0.191	0.007	0.267	0.042	0.023	0.001	0.323	<0.02	0.113	<0.04	0.022	0.080	<4.9
X21-y	5.114	0.277	0.323	<0.2	81.572	0.600	3.161	0.021	0.169	<4.18	0.921	<0.37	<0.24	0.112	<0.01	0.155	0.039	0.013	<0.01	0.304	<0.02	0.117	<0.03	0.027	0.011	<4.17
B-10B	5.529	0.293	0.043	<0.21	94.933	0.350	6.620	0.032	0.044	<4.32	0.394	<0.39	<0.25	0.063	0.017	0.209	0.008	0.021	<0.01	0.263	<0.02	0.115	<0.03	0.037	0.041	<4.31
WM 105y	2.077	0.160	0.413	0.137	44.695	0.114	5.348	<0.22	0.269	<0.06	0.209	<0.12	<0.11	0.113	0.006	0.196	0.008	0.029	<0.01	0.080	<0.27	0.197	<0.02	0.047	0.066	<1.05
X10A-y	4.203	0.074	0.607	0.212	64.918	0.093	3.031	0.042	0.272	<3.94	0.979	<0.35	<0.23	0.194	0.007	0.169	0.018	0.011	0.012	0.097	<0.02	0.263	<0.03	0.018	0.018	<3.93
X10B-Q	5.236	0.202	0.472	<0.23	90.690	0.355	3.813	1.885	0.254	<4.79	0.960	<0.43	<0.27	0.127	<0.01	0.181	0.066	0.021	<0.01	0.209	0.045	0.032	<0.04	0.007	0.014	<4.78
X19-M	5.034	0.163	0.771	0.105	63.019	0.370	3.305	<0.21	1.987	<0.05	0.038	<0.11	<0.1	29.025	0.001	0.146	0.156	0.037	<0.01	0.188	0.025	0.015	<0.02	0.007	0.028	<0.97

Carbonate Microbialite Continued (Partial Dissolution – MINORS)																										
Sample #	**Ba**	**Cr**	**Cu**	**Li**	**Sr**	**V**	**Y**	**Zr**	**Zn**	**As**	**Co**	**Mo**	**Nb**	**Ni**	**Sb**	**Sc**	**Sn**	**Cd**	**Cs**	**Pb**	**Hf**	**Rb**	**Ta**	**Th**	**U**	**W**
X-20-N	3.342	0.278	1.550	<0.17	47.240	0.355	4.217	<0.37	3.255	<0.09	0.250	<0.2	<0.19	1.147	<0.02	0.118	0.242	<0.04	<0.02	0.255	<0.45	0.026	<0.04	0.014	0.039	<1.75
X-21-M	3.720	0.171	0.940	0.134	42.802	0.397	3.719	<0.2	2.114	<0.05	0.078	<0.11	<0.1	8.383	<0.01	0.095	0.068	<0.02	<0.01	0.301	<0.24	0.024	<0.02	0.008	0.007	<0.95
X23D-x	7.830	0.276	0.972	<0.23	94.257	0.533	5.703	0.025	0.230	<4.92	1.531	<0.44	<0.28	0.175	<0.01	0.176	0.060	0.069	<0.01	0.720	<0.02	0.028	<0.04	0.024	0.012	<4.91
X23E-y	6.368	0.206	0.443	<0.2	76.348	0.423	9.223	0.022	0.069	<4.17	0.933	<0.37	<0.24	0.085	<0.01	0.177	0.078	0.024	<0.01	0.263	<0.02	<0.02	<0.03	0.020	0.026	<4.16
X-23A-M	8.464	0.249	1.034	0.260	101.811	0.360	2.665	<0.18	1.312	<0.05	0.129	<0.1	<0.09	85.513	0.005	0.176	0.049	0.019	<0.01	0.256	<0.22	0.018	<0.02	0.018	0.006	<0.86
X24-S	9.541	0.522	1.264	0.334	100.674	0.412	11.392	0.051	0.197	<4.81	0.939	<0.43	<0.27	0.125	0.012	0.242	0.133	0.072	0.013	0.724	<0.02	0.028	<0.04	0.030	0.028	<4.8
X-20-M	24.548	1.967	5.835	2.578	135.480	1.833	18.011	<0.94	5.158	0.595	2.407	<0.51	<0.47	7.161	0.028	1.069	0.079	<0.09	<0.05	0.578	<1.12	2.741	<0.09	0.168	0.159	<4.4
X-21-N	3.369	0.204	2.004	0.203	49.497	0.190	3.880	<0.25	2.153	<0.06	0.192	<0.14	<0.12	3.634	0.008	0.158	0.019	0.021	<0.01	0.401	<0.29	0.130	<0.02	0.022	0.011	<1.16
X23A-t	6.543	0.587	0.290	0.239	189.698	0.733	4.743	0.029	1.494	<4.91	0.462	<0.44	<0.28	0.132	0.007	0.205	0.028	0.036	<0.01	0.367	<0.02	0.024	<0.04	0.049	0.030	<4.9
A-2	5.852	0.063	0.117	<0.19	60.369	0.112	1.652	<0.01	0.312	<3.91	0.297	<0.35	<0.22	3.406	0.008	0.144	0.017	0.020	0.010	0.412	<0.01	0.178	<0.03	0.010	0.048	<3.9
A-3	6.012	0.200	0.236	0.151	78.204	0.309	1.842	<0.24	8.244	<0.06	0.434	0.238	<0.12	0.085	0.014	0.195	0.051	<0.02	<0.01	0.160	<0.29	0.040	0.025	0.008	0.016	<1.15
A-9	1.375	0.044	0.059	0.112	31.448	0.059	1.616	<0.21	0.673	<0.05	0.406	<0.11	<0.1	0.043	0.016	0.111	0.012	<0.02	0.007	0.048	<0.25	0.047	<0.02	0.007	0.005	<0.96
A-12	2.430	0.095	0.114	0.113	37.754	0.136	1.556	<0.23	2.416	<0.06	0.320	<0.13	<0.12	0.030	<0.01	0.092	0.013	<0.02	<0.01	0.058	<0.28	0.043	<0.02	0.009	0.010	<1.09
A-16	2.021	0.050	0.067	0.118	34.468	0.092	1.829	<0.24	1.197	<0.06	0.312	<0.13	<0.12	0.041	<0.01	0.101	0.013	<0.02	0.010	0.059	<0.29	0.280	<0.02	0.011	0.004	<1.14

Carbonate Microbialite Continued (Partial Dissolution – MINORS)																										
Sample #	**Ba**	**Cr**	**Cu**	**Li**	**Sr**	**V**	**Y**	**Zr**	**Zn**	**As**	**Co**	**Mo**	**Nb**	**Ni**	**Sb**	**Sc**	**Sn**	**Cd**	**Cs**	**Pb**	**Hf**	**Rb**	**Ta**	**Th**	**U**	**W**
A-17	1.531	0.046	0.052	<0.1	30.557	0.085	1.854	<0.21	2.720	<0.05	0.384	<0.12	<0.11	<0.03	0.006	0.089	0.010	<0.02	0.007	0.056	<0.26	0.161	<0.02	0.010	0.004	<1.0
A-18B	3.481	0.036	0.145	<0.09	41.931	0.076	2.078	<0.2	4.105	<0.05	0.386	<0.11	<0.1	0.026	0.006	0.083	0.008	0.029	<0.01	0.651	<0.24	0.039	<0.02	0.004	0.026	<0.96
A-18D	2.706	0.022	0.348	<0.09	37.628	0.022	1.597	<0.2	0.476	<0.05	0.475	<0.11	<0.1	0.097	<0.01	0.074	0.020	<0.02	<0.01	0.165	<0.25	0.014	<0.02	0.003	0.015	<0.96
A-20B	4.074	0.116	0.029	0.114	44.668	0.282	4.126	<0.22	0.463	<0.05	0.539	<0.12	<0.11	0.038	0.012	0.319	0.008	<0.02	0.006	0.072	<0.26	0.167	<0.02	0.008	0.148	<1.02
A-22	3.056	0.112	0.036	0.135	39.995	0.197	1.014	<0.2	0.443	<0.05	0.217	<0.11	<0.1	0.029	<0.01	0.080	0.015	<0.02	<0.01	0.052	<0.24	0.005	<0.02	0.005	0.030	<0.95
A-23B	2.004	0.121	0.051	0.087	35.836	0.165	2.882	<0.19	0.607	0.046	0.599	<0.1	<0.09	0.034	0.010	0.095	0.011	0.002	0.005	0.059	0.023	0.150	0.002	0.013	0.007	<0.89
A-28	3.019	0.090	0.088	<0.11	41.566	0.202	1.866	<0.24	2.331	<0.06	0.222	<0.13	<0.12	<0.04	<0.01	0.093	0.013	0.002	<0.01	0.093	0.029	0.053	0.002	0.005	0.012	<1.15
A-32	4.188	0.030	0.048	0.103	72.933	0.118	4.051	<0.21	1.479	<0.05	0.217	<0.12	<0.11	<0.03	<0.01	0.219	<0.01	0.035	0.015	0.836	0.025	0.196	0.002	0.009	0.012	<0.99
A-43	2.793	0.021	0.083	<0.1	38.118	0.313	2.941	<0.23	0.675	<0.06	1.411	<0.12	<0.11	0.071	<0.01	0.074	0.008	0.036	0.017	0.647	0.027	0.366	0.002	0.011	0.049	<1.06
A-48A	4.060	0.118	0.137	<0.1	50.586	0.253	2.323	<0.22	0.347	<0.05	0.323	<0.12	<0.11	0.031	0.007	0.095	0.011	0.002	<0.01	0.175	0.026	0.042	0.002	0.011	0.019	<1.02
WM108	1.094	0.187	0.211	<0.11	43.923	0.132	3.848	<0.23	0.139	0.055	0.385	<0.13	<0.12	0.039	<0.01	0.106	0.001	0.002	<0.01	0.068	0.028	0.011	0.002	0.024	0.020	<1.1
WM109	2.156	0.126	0.250	0.132	36.061	0.259	3.310	<0.23	0.210	0.059	0.392	<0.13	<0.11	0.120	<0.01	0.149	0.001	0.020	<0.01	0.139	0.027	0.056	0.002	0.077	0.015	<1.08
WM110	1.920	0.152	0.085	0.169	42.645	0.283	4.249	<0.22	0.204	0.055	0.340	<0.12	<0.11	0.092	0.006	0.169	0.001	0.002	<0.01	0.181	0.026	0.066	0.002	0.057	0.025	<1.02
WM111	1.856	0.065	0.033	0.095	32.533	0.213	2.223	<0.2	0.126	<0.05	0.117	<0.11	<0.1	0.070	<0.01	0.084	0.013	0.020	<0.01	0.056	0.024	0.024	0.002	0.020	0.010	<0.94

WM 112	1.796	0.104	0.121	<0.11	39.218	0.220	3.397	<0.25	0.205	<0.06	0.279	<0.14	<0.12	0.071	0.011	0.113	0.009	<0.02	<0.01	0.155	<0.3	0.040	<0.02	0.013	0.014	<1.17
WM 113	1.469	0.112	0.063	<0.1	23.948	0.224	2.462	<0.22	0.124	<0.06	0.332	<0.12	<0.11	0.066	<0.01	0.292	<0.01	<0.02	<0.01	0.109	<0.27	0.037	<0.02	0.005	0.008	<1.04
Carbonate Microbialite Continued (Partial Dissolution – MINORS)																										
Sample #	**Ba**	**Cr**	**Cu**	**Li**	**Sr**	**V**	**Y**	**Zr**	**Zn**	**As**	**Co**	**Mo**	**Nb**	**Ni**	**Sb**	**Sc**	**Sn**	**Cd**	**Cs**	**Pb**	**Hf**	**Rb**	**Ta**	**Th**	**U**	**W**
WM 114x	2.910	0.219	0.178	<0.11	54.717	0.294	5.368	<0.24	0.267	<0.06	0.276	<0.13	<0.12	0.408	0.007	0.695	<0.01	0.020	0.005	0.199	<0.28	0.089	0.023	0.012	0.015	<1.11
WM 129-R	4.953	0.093	0.024	0.097	51.071	0.309	3.981	<0.21	0.266	<0.05	0.402	<0.12	<0.11	0.043	<0.01	0.111	0.014	0.031	0.012	0.704	<0.26	0.166	<0.02	0.012	0.028	<1.01
WM 129-T2	7.045	0.131	0.042	0.116	58.437	0.320	3.314	<0.24	0.239	<0.06	0.288	<0.13	<0.12	0.081	<0.01	0.136	0.016	0.044	0.008	0.212	<0.28	0.052	0.024	0.016	0.012	<1.11
WM 129-T	3.971	0.076	0.029	0.073	37.712	0.199	2.355	<0.18	0.122	<0.04	0.196	<0.1	<0.09	0.035	<0.01	0.079	0.013	0.024	0.004	0.355	<0.21	0.061	<0.02	0.009	0.012	<0.84
WM 129 X	1.269	0.019	0.069	0.082	28.515	0.032	1.950	<0.2	0.194	<0.05	0.198	<0.11	<0.1	0.033	<0.01	0.064	0.007	0.040	0.019	0.701	<0.24	0.237	<0.02	0.007	0.007	<0.94
WM 129-Y	5.083	0.096	0.050	0.088	43.044	0.187	2.777	<0.22	0.223	<0.05	0.136	<0.12	<0.11	0.030	<0.01	0.083	<0.01	<0.02	0.013	0.223	<0.26	0.206	<0.02	0.014	0.011	<1.03
X2	7.034	0.302	0.269	<0.21	106.869	0.429	5.812	0.071	2.240	8.659	0.803	0.431	<0.25	0.090	0.010	0.280	0.023	0.024	<0.01	0.520	0.024	0.063	<0.03	0.028	0.041	<4.37
X10 B-S	4.432	0.240	0.382	<0.19	93.355	0.449	4.172	0.029	0.112	<3.89	0.694	<0.35	<0.22	0.222	0.007	0.164	0.027	0.014	<0.01	0.172	<0.01	<0.01	<0.03	0.013	0.063	<3.88
X14-y	2.936	0.513	0.402	<0.21	118.199	0.398	8.214	0.049	0.159	4.504	1.288	<0.39	<0.25	0.192	0.006	0.384	0.034	0.029	<0.01	0.287	<0.02	0.026	<0.03	0.075	0.057	<4.4
X16-R	5.006	0.448	0.533	<0.21	117.860	0.419	9.538	0.093	0.155	<4.47	0.865	<0.4	<0.26	0.273	0.020	0.697	0.045	0.032	<0.01	0.592	<0.02	0.093	<0.03	0.139	0.029	<4.46

Carbonate Microbialite Continued (Partial Dissolution – MINORS)																										
Sample #	**Ba**	**Cr**	**Cu**	**Li**	**Sr**	**V**	**Y**	**Zr**	**Zn**	**As**	**Co**	**Mo**	**Nb**	**Ni**	**Sb**	**Sc**	**Sn**	**Cd**	**Cs**	**Pb**	**Hf**	**Rb**	**Ta**	**Th**	**U**	**W**
X18	4.502	0.083	0.625	<0.24	79.266	0.187	5.789	0.031	0.114	<5.07	0.442	<0.45	<0.29	0.146	0.008	0.198	0.038	<0.02	0.013	0.162	<0.02	0.423	<0.04	0.026	0.017	<5.06
X19-y	8.768	0.564	0.971	<0.19	142.308	0.800	13.132	0.063	0.977	6.373	1.626	<0.36	<0.23	0.276	0.008	0.473	0.078	0.031	0.007	0.476	<0.02	0.185	<0.03	0.054	0.188	<3.97
X20-x	3.927	0.463	0.309	<0.2	75.142	0.553	8.215	0.043	0.126	<4.22	0.676	<0.38	<0.24	0.244	0.006	0.222	0.026	0.025	<0.01	0.101	0.002	0.223	<0.03	0.036	0.052	<4.21
X21-z	4.746	0.330	0.888	<0.24	108.094	0.362	10.780	0.039	0.213	<5.04	1.523	<0.45	<0.29	0.161	0.009	0.380	0.042	0.028	<0.01	0.221	<0.02	0.167	<0.04	0.051	0.017	<5.03
X23B	23.481	0.363	0.460	<0.2	94.962	0.475	3.267	0.032	1.330	4.433	0.365	<0.38	<0.24	0.083	0.007	0.153	0.066	0.015	<0.01	0.249	<0.02	0.034	<0.03	0.033	0.016	<4.27
X23C	3.839	0.284	0.607	<0.19	114.739	0.242	9.562	0.044	0.463	<4.04	1.673	<0.36	<0.23	0.120	0.005	0.399	0.020	0.026	<0.01	0.322	<0.02	0.063	<0.03	0.260	0.099	<4.04
X23A-S	5.483	0.425	0.244	<0.22	107.788	0.461	3.121	0.024	0.850	<4.62	0.507	<0.41	<0.26	0.101	0.007	0.181	0.025	0.023	<0.01	0.286	<0.02	0.021	<0.04	0.037	0.019	<4.61
X23A-Q	4.724	0.236	0.310	<0.2	98.648	0.259	13.828	0.025	0.144	<4.15	0.498	<0.37	<0.24	0.069	0.007	0.458	0.010	0.002	0.010	0.187	<0.02	0.677	<0.03	0.025	0.076	<4.15
X24-x	2.860	0.107	2.560	<0.19	57.239	0.059	8.224	0.018	0.570	<3.99	0.513	<0.36	<0.23	0.076	0.008	0.281	0.022	0.002	0.008	0.239	<0.02	0.426	<0.03	0.076	0.077	<3.98
X24-W	3.510	0.270	0.207	<0.22	87.764	0.238	2.808	0.023	0.063	<4.68	0.369	<0.42	<0.27	0.077	<0.01	0.162	0.041	0.021	<0.01	0.171	<0.02	0.023	<0.04	0.030	0.015	<4.67
X29	5.257	0.202	0.204	0.244	18.013	0.261	3.876	0.181	0.269	<4.14	0.378	<0.37	<0.24	0.323	0.015	0.381	0.013	0.039	0.027	0.177	0.259	0.920	<0.03	0.215	0.056	<4.14
X30	3.832	0.118	0.136	0.365	68.750	0.163	4.795	0.019	0.052	<4.99	0.517	<0.45	<0.29	0.091	0.008	0.192	0.031	0.021	0.011	0.217	<0.02	0.051	<0.04	0.048	0.080	<4.98
X32	6.013	0.149	0.070	<0.24	109.996	0.168	8.071	<0.02	0.069	<4.97	0.400	<0.45	<0.28	0.087	0.009	0.274	0.013	0.028	0.009	0.476	<0.02	0.044	<0.04	0.070	0.056	<4.96
X33	9.735	0.167	0.039	0.329	128.286	0.306	8.636	0.054	0.063	<4.85	0.544	<0.43	<0.28	0.086	0.025	0.438	0.017	0.034	<0.01	0.811	<0.02	0.110	<0.04	0.123	0.100	<4.84

Carbonate Microbialite Continued (Partial Dissolution – MINORS)																									
Sample #	**Ba**	**Cr**	**Cu**	**Li**	**Sr**	**V**	**Y**	**Zr**	**Zn**	**As**	**Co**	**Mo**	**Nb**	**Ni**	**Sb**	**Sc**	**Sn**	**Cd**	**Cs**	**Pb**	**Hf**	**Rb**	**Ta**	**Th**	**U**	**W**
X34	6.076	0.106	0.094	<0.2	77.160	0.219	3.388	<0.02	0.073	<4.12	0.262	<0.37	<0.24	0.060	0.006	0.141	0.009	0.027	0.008	0.302	<0.02	0.071	<0.03	0.020	0.009	<4.11
B-8	6.150	0.210	0.041	<0.2	117.998	0.661	4.514	0.031	0.066	<4.28	0.551	<0.38	<0.24	0.060	0.009	0.244	0.060	<0.02	<0.01	0.264	<0.02	<0.02	<0.03	0.022	0.032	<4.27
B-10A	2.701	0.249	0.092	<0.22	82.431	0.307	5.209	0.023	0.045	<4.68	0.569	<0.42	<0.27	4.178	0.007	0.224	0.023	<0.02	<0.01	0.141	<0.02	<0.02	<0.04	0.036	0.111	<4.67

Standards (Partial Dissolution - ICP MS: MAJORS)																									
Standard	**Ba**	**Cr**	**Cu**	**Li**	**Sr**	**V**	**Y**	**Zr**	**Zn**	**As**	**Co**	**Mo**	**Nb**	**Ni**	**Sb**	**Sc**	**Sn**	**Cd**	**Cs**	**Pb**	**Hf**	**Rb**	**Ta**	**Th**	**U**	**W**
CAL-S	<0.11	0.357	0.023	BD	<0.01	0.168	BD	0.445	0.254	64.514	2.819	0.068	2.406	11.983	0.385	1.003	<0.12	0.014	2.336	<0.01	0.082	5.236	0.014	<1.01	<0.1	<0.26
CAL-S	<0.12	0.265	0.015	BD	<0.01	0.124	BD	0.317	0.197	45.523	2.064	0.065	1.652	8.965	0.314	0.768	<0.13	0.014	2.511	<0.01	0.060	4.046	0.010	<1.08	<0.1	<0.28
CAL-S	<0.12	0.274	0.021	BD	<0.01	0.126	BD	0.375	0.235	52.187	2.281	0.052	2.084	9.663	0.369	1.084	<0.13	0.017	2.578	<0.01	0.081	4.699	0.014	<1.11	<0.11	<0.28

Appendix B: $^{87}Sr/^{86}Sr$, $\delta^{13}C$ VPDB ‰ and $\delta^{18}O$ VPDB‰ Isotopes

$^{87}Sr/^{86}Sr$ and Depth - Silicified Microbialite				
Sublithotope	**Sample Name**	**Sample Depth (m)**	**87Sr/86Sr**	**Precision (1std dev)**
Low Domal Stromatolites	A-1	74.1	0.703158	0.000335
	WM117x	79.58	0.701933	0.000249
	X3-Q		0.706625	8.35E-05
	X10B-u	36.9	0.704609	4.77E-05
	X10B-w	36.9	0.704248	0.000103
	X23A-R	57.12	0.704302	0.000103
	X24-v	59.95	0.703642	0.000148
Stratiform Stromatolites	WM55y	0.1	0.70995	1.65E-05
	WM60	2.53	0.708967	0.000111
	X3-R		0.704502	9.18E-05

$^{87}Sr/^{86}Sr$ and Depth - Carbonate Grainstones				
Sublithotope	**Sample Name**	**Sample Depth (m)**	**87Sr/86Sr**	**Precision (1std dev)**
Massive	WM 63	4.5	0.710259	0.000108
	WM64	7.25	0.708485	3.5E-05
	X6-Q		0.702925	1.5E-05
	X6-R		0.70365	1.09E-05
	X6-S		0.703883	1.77E-05
	X8-x	30.5	0.703261	0.000107
	X8-y	30.5	0.70622	7.78E-05
Laminated	WM117y	79.56	0.701915	0.000164
Zig Zags	X12	39.6	0.704368	6.25E-05
	B-1		0.7036	0.000204
	B-5		0.703738	0.000242
	B-7		0.704392	0.000232

$^{87}Sr/^{86}Sr$ and Depth - Carbonate Microbialite				
Sublithotope	**Sample Name**	**Sample Depth (m)**	**87Sr/86Sr**	**Precision (1std dev)**
Stratiform Stromatolites	WM55x	0.1	0.709198	5.57E-05
	WM58x	0.3	0.701329	0.000273
	WM58y	0.3	0.706056	0.000113
	X31	82.2	0.702422	8.66E-05
Banded Carbonate	X10B-R	36.9	0.703468	1.81E-05
	X10B-v	36.9	0.704052	3.95E-06
	X20-y	67.1	0.701856	0.000136
	X23D-y	57.27	0.701047	5.57E-06
	X23E-w	57.33	0.701356	2.68E-05
Banded Carbonate Continued	X23E-x	57.34	0.700346	0.00013
	X23E-z	57.36	0.702725	2.22E-05
	X24-Q	59.9	0.701538	1.97E-05
	X24-R	59.91	0.700618	6.08E-05
	X24-t	59.93	0.702274	0.000103
	X24-u	59.94	0.702931	0.000125
Fenestrated Stromatolite	X10A-x	37.15	0.70561	0.000107
	X10B-t	36.9	0.705625	0.000196
	X14-x	43.15	0.704606	4.45E-05
	X16-Q	44.1	0.702807	5.36E-05
	X19-x	60.25	0.701189	1.31E-05
	X21-y	71.3	0.702149	3.08E-05
	B-10B	~39	0.70361	0.000302
Fenestrae	X10A-y	37.15	0.705935	0.000208
	X10B-Q	36.9	0.70329	0.000122
Organic Rich Mud	X23A-t	57.15	0.705002	4.68E-05
Fenestrated Microbialite	A-2	74.2	0.701171	0.000605
	X2		0.703797	8.65E-05
	X10B-S	36.9	0.703628	1.3E-05

Fenestrated Microbialite Continued	X14-y	43.15	0.704869	3.6E-05
	X16-R	44.1	0.703434	2.73E-05
	X18	58.4	0.705623	3.31E-05
	X19-y	60.25	0.701987	5.28E-05
	X20-x	67.1	0.702981	3.36E-05
	X21-z	71.3	0.702927	3.29E-05
	X23B	57.16	0.703045	4.79E-05
	X23C	57.19	0.703767	5.19E-07
	X23A-S	57.14	0.702925	8.93E-05
	X23A-Q	59.9	0.706806	5.5E-05
	X24-W	59.96	0.703716	9.15E-07
	X29	81	0.711313	0.000107
	X30	82	0.70422	7.54E-05
	X32	84.7	0.703497	0.000151
	X33	84.3	0.702962	0.000192
	X34	88.5	0.703546	4.94E-05
	B-8	~39	0.703984	0.000209
	B-10A	~39	0.705097	0.00025

$\delta^{13}C$ VPDB ‰ and $\delta^{18}O$ VPDB ‰ - Silicified Microbialite

Sublithotope	Sample #	Sample Depth	$\delta^{13}C$ VPDB ‰	$\delta^{18}O$ VPDB ‰
Low Domal Stromatolite	WM 66	13.1	1.165293	-15.7342
	WM 116x	31.8	0.210669	-12.1586
	WM 129-Z	79.37	-1.1974	-13.2445
Stratiform Stromatolite	WM 57	0.2	-0.69225	-17.9601

$\delta^{13}C$ VPDB ‰ and $\delta^{18}O$ VPDB ‰ - Carbonate Grainstones

Sublithotope	Sample #	Sample Depth	$\delta^{13}C$ VPDB ‰	$\delta^{18}O$ VPDB ‰
Massive	WM 73	22.5	1.132478	-10.9168
	WM125		0.7556	-10.4145
Laminated	WM 69	14.75	-1.08603	-17.7502
	WM 71A	17	-3.82958	-17.6504
	WM 74	26.75	1.301526	-9.90011

$\delta^{13}C$ VPDB ‰ and $\delta^{18}O$ VPDB ‰ - Carbonate Microbialite				
Sublithotope	**Sample #**	**Sample Depth**	**$\delta^{13}C$ VPDB ‰**	**$\delta^{18}O$ VPDB ‰**
Stratiform Stromatoltie	WM 115	31	1.051931	-9.9541
	WM 116y	31.8	1.109606	-11.8336
Banded Carbonate	WM 104	72.6	1.209046	-11.0268
	WM 107x	56.6	0.972379	-10.4971
	WM 107y	56.6	1.058892	-9.64238
Fenestrated Stromatolite	WM 114y	49	1.221974	-8.89669
	WM 124		0.630306	-10.9809
	WM 130		1.233906	-10.6621
	WM 105x	58.1	0.788415	-10.2872
$\delta^{13}C$ VPDB ‰ and $\delta^{18}O$ VPDB ‰ - Carbonate Microbialite				
Sublithotope	**Sample #**	**Sample Depth**	**$\delta^{13}C$ VPDB ‰**	**$\delta^{18}O$ VPDB ‰**
Low Domal Stromatolites	WM 65	12.45	-0.91002	-15.7851
Fenestrae	WM 105y	58.1	0.673065	-9.53236
Fenestrated Microbialite	WM 109	52.15	0.96343	-9.4478
	WM 110	53.4	1.032043	-9.19618
	WM 111	53.7	1.082758	-9.54865
	WM 112	54	1.072814	-9.27666
	WM 113	48.2	1.027071	-8.81723
	WM 114x	49	0.061509	-9.41215
	WM 129-R	79.49	0.775488	-14.5708
	WM 129-T2	79.41	1.097674	-12.561
	WM 129-T	79.4	0.952491	-12.9857
	WM 129 X	79.3	-0.381	-13.8109
	WM 129-Y	79.33	1.014144	-13.7151

Appendix C: LA-ICP-MS

Sub-lithotope	Sample or Standard – Shot # (2nd run on sample). FIN2	La (µg/g)	Ce (µg/g)	Pr (µg/g)	Nd (µg/g)	Sm (µg/g)	Eu (µg/g)	Tb (µg/g)	Gd (µg/g)	Dy (µg/g)	Ho (µg/g)	Er (µg/g)	Yb (µg/g)	Lu (µg/g)
Standards	BIR-1.FIN2	0.617	1.807	0.367	2.701	1.217	0.552	0.342	2.043	2.705	0.546	1.861	1.689	0.293
	BIR-2.FIN2	0.549	1.910	0.361	2.547	1.224	0.628	0.320	1.826	2.200	0.479	1.701	1.529	0.224
	NIST612-1.FIN2	35.807	40.436	39.350	37.046	34.593	33.878	36.627	36.715	36.560	37.458	39.934	35.410	35.667
	NIST612-2.FIN2	32.163	37.630	35.520	36.806	35.349	32.118	34.717	34.155	35.778	37.195	36.980	37.505	34.411
Organic Rich Mud	X10B-1(2).FIN2	1.637	1.361	0.195	0.818	0.166	0.054	0.041	0.270	0.347	0.070	0.333	0.215	0.046
	X10B-2(2).FIN2	1.557	1.208	0.159	0.854	<0.2036	<0.054038	0.038	0.283	0.337	0.097	0.297	0.254	0.046
	X10B-3(2).FIN2	1.437	1.185	0.183	0.843	<0.17784	0.049	0.040	0.299	0.329	0.085	0.299	0.240	0.047
	X10B-4(2).FIN2	1.671	1.268	0.178	0.844	<0.20649	<0.053518	0.051	0.299	0.331	0.092	0.284	0.233	0.046
	X10B-5(2).FIN2	2.013	1.501	0.199	0.690	<0.24566	<0.059147	<0.050546	0.301	0.371	0.105	0.352	0.305	0.044
	X10B-6(2).FIN2	1.574	1.295	0.168	0.688	<0.19364	0.062	0.037	0.381	0.288	0.080	0.274	0.219	0.046
	X10B-7(2).FIN2	1.328	1.063	0.162	0.676	<0.14156	0.051	0.035	0.205	0.282	0.084	0.323	0.238	0.038
	X10B-8(2).FIN2	1.453	1.272	0.166	0.783	<0.27292	<0.059207	<0.054272	0.249	0.305	0.068	0.278	0.000	0.034
	X10B-9(2).FIN2	1.437	1.159	0.152	0.811	<0.20183	0.053	0.038	0.220	0.277	0.073	0.265	0.175	0.045
Fenestrae	X10B-1.FIN2	1.341	0.992	0.144	0.607	<0.29222	0.075	<0.045623	0.149	0.253	0.049	0.172	0.169	<0.036473
Fenestrated Stromatolite	X10B-2.FIN2	0.836	0.625	0.087	0.499	<0.29959	<0.062126	<0.05351	0.292	0.457	0.091	0.311	0.282	0.065
Fenestrae	X10B-3.FIN2	0.763	0.620	0.110	0.523	<0.20415	<0.060413	<0.043158	0.165	<0.13958	0.054	0.151	0.183	<0.032524

	X10B-4.FIN2	1.291	0.919	0.146	0.595	<0.35317	0.065	<0.048164	<0.17237	0.253	0.053	0.183	<0.19343	<0.040874
Sub-lithotope	**Sample or Standard – Shot # (2nd run on sample) . FIN2**	**La (µg/g)**	**Ce (µg/g)**	**Pr (µg/g)**	**Nd (µg/g)**	**Sm (µg/g)**	**Eu (µg/g)**	**Tb (µg/g)**	**Gd (µg/g)**	**Dy (µg/g)**	**Ho (µg/g)**	**Er (µg/g)**	**Yb (µg/g)**	**Lu (µg/g)**
Fenestrae	X10B-5.FIN2	0.848	0.623	0.104	0.431	<0.23374	<0.056591	<0.039975	0.174	0.217	0.058	0.169	0.147	<0.043151
Fenestrated Stromatolite	X10B-6.FIN2	1.413	1.176	0.168	0.743	0.184	0.064	0.051	0.308	0.357	0.104	0.372	0.312	0.056
	X10B-7.FIN2	1.159	0.864	0.131	0.640	<0.22871	<0.04449	0.050	0.277	0.287	0.073	0.314	0.204	0.042
Fenestrae	X10B-8.FIN2	1.350	1.136	0.164	0.766	<0.1334	0.052	0.035	0.232	0.248	0.068	0.241	0.148	0.033
	X10B-9.FIN2	0.679	0.522	0.091	0.349	<0.12635	0.043	0.062	0.298	0.467	0.141	0.536	0.565	0.094
	X10B-10.FIN2	1.218	0.821	0.125	0.518	<0.13498	0.050	<0.025779	0.202	0.268	0.079	0.243	0.248	0.040
	X10B-11.FIN2	0.609	0.625	0.101	0.544	<0.11943	0.053	0.036	0.277	0.234	0.083	0.291	0.229	0.049
	X10B-12.FIN2	0.590	0.463	0.071	0.355	<0.12264	0.047	0.040	0.232	0.281	0.081	0.274	0.212	0.044
	X10B-13.FIN2	0.826	0.634	0.094	0.457	0.121	0.046	0.036	0.206	0.239	0.077	0.274	0.175	0.048
	X10B-14.FIN2	1.089	0.658	0.100	0.350	<0.11477	0.030	<0.022279	0.087	0.117	0.034	0.113	<0.10597	<0.017838
	X10B-15.FIN2	0.683	0.522	0.071	0.405	<0.15228	0.041	0.023	0.208	0.240	0.065	0.223	0.183	0.031
Standard	BCR-1.FIN2	25.354	49.904	6.491	27.045	6.912	2.019	1.021	6.845	6.467	1.282	3.673	3.554	0.507
	BCR-2.FIN2	26.496	49.874	6.653	27.778	6.709	1.912	1.054	7.103	7.097	1.348	3.746	3.528	0.554
	BIR-1.FIN2	0.617	1.807	0.367	2.701	1.217	0.552	0.342	2.043	2.705	0.546	1.861	1.689	0.293
	BIR-2.FIN2	0.549	1.910	0.361	2.547	1.224	0.628	0.320	1.826	2.200	0.479	1.701	1.529	0.224
	NIST612-1.FIN2	35.807	40.436	39.350	37.046	34.593	33.878	36.627	36.715	36.560	37.458	39.934	35.410	35.667

	NIST612-2.FIN2	32.163	37.630	35.520	36.806	35.349	32.118	34.717	34.155	35.778	37.195	36.980	37.505	34.411
Sub-lithotope	**Sample or Standard – Shot # (2nd run on sample) . FIN2**	**La (µg/g)**	**Ce (µg/g)**	**Pr (µg/g)**	**Nd (µg/g)**	**Sm (µg/g)**	**Eu (µg/g)**	**Tb (µg/g)**	**Gd (µg/g)**	**Dy (µg/g)**	**Ho (µg/g)**	**Er (µg/g)**	**Yb (µg/g)**	**Lu (µg/g)**
Organic Rich Mud	X10B-1(2).FIN2	1.637	1.361	0.195	0.818	0.166	0.054	0.041	0.270	0.347	0.070	0.333	0.215	0.046
	X10B-2(2).FIN2	1.557	1.208	0.159	0.854	<0.2036	<0.054038	0.038	0.283	0.337	0.097	0.297	0.254	0.046
	X10B-3(2).FIN2	1.437	1.185	0.183	0.843	<0.17784	0.049	0.040	0.299	0.329	0.085	0.299	0.240	0.047
	X10B-4(2).FIN2	1.671	1.268	0.178	0.844	<0.20649	<0.053518	0.051	0.299	0.331	0.092	0.284	0.233	0.046
Organic Rich Mud	X10B-5(2).FIN2	2.013	1.501	0.199	0.690	<0.24566	<0.059147	<0.050546	0.301	0.371	0.105	0.352	0.305	0.044
	X10B-6(2).FIN2	1.574	1.295	0.168	0.688	<0.19364	0.062	0.037	0.381	0.288	0.080	0.274	0.219	0.046
Organic Rich Mud	X10B-7(2).FIN2	1.328	1.063	0.162	0.676	<0.14156	0.051	0.035	0.205	0.282	0.084	0.323	0.238	0.038
	X10B-8(2).FIN2	1.453	1.272	0.166	0.783	<0.27292	<0.059207	<0.054272	0.249	0.305	0.068	0.278	0.000	0.034
	X10B-9(2).FIN2	1.437	1.159	0.152	0.811	<0.20183	0.053	0.038	0.220	0.277	0.073	0.265	0.175	0.045
Standards	BIR-1.FIN2	0.589	1.913	0.393	2.497	1.202	0.543	0.366	1.959	2.597	0.563	1.861	1.673	0.242
	BIR-2.FIN2	0.610	1.959	0.363	2.505	1.091	0.552	0.344	2.050	2.553	0.574	1.800	1.631	0.266
Fenestrated Stromatolite	X19-1.FIN2	0.700	0.669	0.090	0.444	0.089	0.060	0.026	0.163	0.214	0.048	0.175	0.154	0.028
	X19-2.FIN2	0.921	0.784	0.118	0.478	0.093	0.060	0.020	0.150	0.181	0.051	0.172	0.172	0.023
Fenestrae	X19-3.FIN2	1.284	0.701	0.090	0.333	0.040	0.047	0.009	0.078	0.052	0.017	0.066	0.047	0.008
	X19-4.FIN2	1.174	0.893	0.126	0.478	0.063	0.069	0.010	0.091	0.079	0.023	0.076	0.048	0.009
	X19-5.FIN2	0.765	0.394	0.055	0.243	0.042	0.020	0.005	0.067	0.050	0.013	0.037	<0.028823	<0.0058822
	X19-6.FIN2	0.394	0.340	0.053	0.248	0.061	0.052	0.019	0.132	0.135	0.044	0.153	0.160	0.027
	X19-7.FIN2	0.817	0.509	0.082	0.357	0.051	0.046	0.016	0.106	0.106	0.031	0.100	0.070	0.016
	X19-8.FIN2	0.716	0.367	0.058	0.213	<0.038936	0.019	0.008	0.076	0.085	0.024	0.091	0.071	0.010

	X19-9.FIN2	1.227	0.665	0.103	0.398	0.057	0.035	0.015	0.119	0.086	0.024	0.098	0.078	0.014
Sub-lithotope	**Sample or Standard – Shot # (2nd run on sample) . FIN2**	**La (µg/g)**	**Ce (µg/g)**	**Pr (µg/g)**	**Nd (µg/g)**	**Sm (µg/g)**	**Eu (µg/g)**	**Tb (µg/g)**	**Gd (µg/g)**	**Dy (µg/g)**	**Ho (µg/g)**	**Er (µg/g)**	**Yb (µg/g)**	**Lu (µg/g)**
Fenestrated Stromatolite	X19-10.FIN2	1.008	0.613	0.078	0.276	0.050	0.051	0.013	0.097	0.101	0.028	0.112	0.096	0.018
	X19-11.FIN2	1.000	0.591	0.084	0.287	0.049	0.060	0.013	0.079	0.075	0.023	0.087	<0.079618	0.012
Fenestrae	X19-12.FIN2	0.949	0.498	0.063	0.247	0.032	0.067	0.008	0.069	0.057	0.025	0.084	0.062	0.011
Fenestrated Stromatolite	X19-13.FIN2	0.464	0.316	0.043	0.183	0.032	0.050	0.013	0.087	0.100	0.031	0.120	0.104	0.026
Fenestrae	X19-14.FIN2	0.594	0.263	0.046	0.180	<0.041801	0.018	0.010	0.080	0.071	0.025	0.090	<0.075687	<0.011359
Standard	BIR-1.FIN2	0.610	1.879	0.363	2.415	1.159	0.558	0.338	1.986	2.726	0.590	1.795	1.743	0.239
Standard	BIR-2.FIN2	0.605	1.922	0.387	2.313	1.162	0.525	0.348	1.864	2.559	0.553	1.688	1.785	0.231
Fenestrated Stromatolite	X20-1.FIN2	1.007	1.159	0.161	0.670	0.122	0.088	0.038	0.253	0.305	0.084	0.309	0.306	0.051
Fenestrae	X20-2.FIN2	1.535	1.727	0.226	0.966	0.179	0.099	0.045	0.348	0.364	0.098	0.318	0.290	0.047
Fenestrated Stromatolite	X20-3.FIN2	1.554	1.779	0.244	1.105	0.236	0.115	0.056	0.376	0.455	0.125	0.394	0.352	0.063
	X20-4.FIN2	1.292	1.620	0.228	1.097	0.232	0.113	0.070	0.459	0.534	0.148	0.472	0.417	0.070
Fenestrae	X20-5.FIN2	1.610	1.997	0.285	1.280	0.261	0.130	0.056	0.380	0.406	0.103	0.323	0.294	0.049
	X20-6.FIN2	2.381	2.286	0.248	0.882	0.143	0.157	0.035	0.222	0.306	0.076	0.268	0.260	0.044
	X20-7.FIN2	2.394	2.593	0.322	1.107	0.155	0.114	0.024	0.183	0.197	0.056	0.218	0.195	0.041
	X20-8.FIN2	2.692	3.193	0.435	1.703	0.262	0.229	0.041	0.312	0.313	0.078	0.268	0.209	0.039
Organic Rich Mud	X20-9.FIN2	1.184	1.563	0.226	1.079	0.257	0.085	0.080	0.485	0.601	0.171	0.584	0.613	0.102
	X20-10.FIN2	1.103	1.566	0.229	1.027	0.241	0.112	0.094	0.528	0.639	0.178	0.586	0.558	0.101
	X20-11.FIN2	1.232	1.659	0.235	1.166	0.300	0.099	0.091	0.530	0.784	0.227	0.772	0.818	0.134
	X20-12.FIN2	1.078	1.549	0.221	1.056	0.249	0.101	0.076	0.482	0.590	0.170	0.545	0.600	0.083

	X20-13.FIN2	1.387	1.821	0.271	1.146	0.302	0.112	0.086	0.553	0.707	0.181	0.600	0.602	0.098
Sub-lithotope	**Sample or Standard – Shot # (2nd run on sample) . FIN2**	**La (µg/g)**	**Ce (µg/g)**	**Pr (µg/g)**	**Nd (µg/g)**	**Sm (µg/g)**	**Eu (µg/g)**	**Tb (µg/g)**	**Gd (µg/g)**	**Dy (µg/g)**	**Ho (µg/g)**	**Er (µg/g)**	**Yb (µg/g)**	**Lu (µg/g)**
Standards	BIR-1.FIN2	0.630	1.949	0.380	2.477	1.123	0.507	0.372	2.066	2.645	0.586	1.770	1.828	0.259
	BIR-2.FIN2	0.590	1.959	0.365	2.498	1.102	0.509	0.348	1.939	2.600	0.572	1.691	1.629	0.247
	NIST612-1.FIN2	36.119	40.467	38.589	35.433	33.156	30.970	34.735	39.328	38.416	40.695	39.836	39.148	35.633
	NIST612-2.FIN2	33.927	42.060	40.615	36.648	37.953	35.797	34.963	37.821	34.612	37.579	39.348	40.050	36.864
Fenestrated Stromatolite	X20(2)-1.FIN2	1.019	1.383	0.204	1.013	0.240	0.110	0.067	0.437	0.536	0.136	0.545	0.521	0.095
	X20(2)-2.FIN2	1.379	1.785	0.260	1.294	0.322	0.127	0.086	0.572	0.703	0.169	0.557	0.528	0.091
	X20(2)-3.FIN2	1.689	2.174	0.332	1.615	0.338	0.155	0.098	0.590	0.630	0.161	0.517	0.466	0.084
	X20(2)-4.FIN2	1.356	1.832	0.264	1.315	0.336	0.137	0.085	0.584	0.665	0.169	0.550	0.520	0.095
	X20(2)-5.FIN2	1.367	1.917	0.284	1.321	0.296	0.114	0.078	0.520	0.569	0.153	0.529	0.493	0.090
	X20(2)-6.FIN2	1.409	1.976	0.298	1.421	0.332	0.133	0.081	0.520	0.609	0.144	0.485	0.443	0.073
Fenestrae	X20(2)-7.FIN2	1.055	1.629	0.252	1.383	0.336	0.166	0.064	0.459	0.499	0.143	0.432	0.434	0.077
	X20(2)-8.FIN2	1.763	2.671	0.389	1.841	0.296	0.135	0.050	0.398	0.420	0.121	0.397	0.431	0.070
	X20(2)-9.FIN2	2.110	3.439	0.499	2.480	0.406	0.184	0.082	0.655	0.700	0.190	0.659	0.584	0.095
	X20(2)-10.FIN2	2.884	4.762	0.691	3.092	0.554	0.273	0.067	0.463	0.443	0.112	0.352	0.364	0.064
Fenestrated Stromatolite	X20B-1.FIN2	1.186	1.553	0.218	1.076	0.245	0.086	0.069	0.411	0.586	0.162	0.463	0.493	0.080
	X20B-2.FIN2	1.301	1.801	0.266	1.237	0.296	0.133	0.061	0.419	0.494	0.127	0.373	0.410	0.065
Fenestrae	X20B-3.FIN2	1.554	2.150	0.316	1.275	0.211	0.157	0.045	0.332	0.374	0.096	0.337	0.302	0.058
	X20B-4.FIN2	1.818	2.386	0.337	1.390	0.233	0.168	0.050	0.337	0.415	0.108	0.359	0.364	0.055
	X20B-5.FIN2	1.088	1.556	0.252	1.141	0.315	0.191	0.068	0.419	0.516	0.134	0.410	0.371	0.066
	X20B-6.FIN2	1.356	1.973	0.309	1.316	0.244	0.120	0.047	0.357	0.378	0.097	0.289	0.300	0.045
	X20B-7.FIN2	1.956	2.657	0.401	1.799	0.384	0.182	0.103	0.619	0.786	0.193	0.541	0.489	0.075
Organic Rich Mud	X20B-8.FIN2	1.503	1.970	0.300	1.356	0.361	0.139	0.084	0.488	0.612	0.156	0.550	0.477	0.091
Fenestrae	X20B-9.FIN2	2.018	2.676	0.379	1.590	0.309	0.190	0.099	0.628	0.814	0.230	0.763	0.892	0.167

	X20B-10.FIN2	2.326	3.755	0.583	2.516	0.452	0.223	0.070	0.507	0.521	0.117	0.334	0.243	0.035
Sub-lithotope	**Sample or Standard – Shot # (2nd run on sample) . FIN2**	**La (µg/g)**	**Ce (µg/g)**	**Pr (µg/g)**	**Nd (µg/g)**	**Sm (µg/g)**	**Eu (µg/g)**	**Tb (µg/g)**	**Gd (µg/g)**	**Dy (µg/g)**	**Ho (µg/g)**	**Er (µg/g)**	**Yb (µg/g)**	**Lu (µg/g)**
Organic Rich Mud	X20B-11.FIN2	1.220	1.636	0.246	1.097	0.306	0.124	0.093	0.519	0.687	0.210	0.726	0.744	0.135
Fenestrated Stromatolite	X20B-12.FIN2	1.654	2.158	0.314	1.487	0.366	0.155	0.067	0.486	0.549	0.134	0.448	0.446	0.070
Fenestrae	X20B-13.FIN2	1.787	2.473	0.353	1.710	0.417	0.165	0.088	0.559	0.629	0.167	0.547	0.515	0.081
Organic Rich Mud	X20B-1(2).FIN2	1.530	2.170	0.327	1.477	0.387	0.100	0.093	0.557	0.585	0.178	0.562	0.568	0.087
Fenestrated Stromatolite	X20B-2(2).FIN2	1.541	2.143	0.319	1.526	0.354	0.132	0.067	0.443	0.520	0.146	0.465	0.493	0.085
Fenestrae	X20B-3(2).FIN2	1.841	2.507	0.377	1.829	0.383	0.156	0.083	0.499	0.601	0.166	0.528	0.481	0.078
	X20B-4(2).FIN2	2.457	2.920	0.366	1.409	0.259	0.144	0.049	0.311	0.306	0.077	0.220	0.142	0.023
	X20B-5(2).FIN2	1.272	1.978	0.322	1.735	0.399	0.263	0.066	0.452	0.471	0.114	0.334	0.298	0.050
Fenestrated Stromatolite	X20B-6(2).FIN2	1.217	1.614	0.226	1.070	0.315	0.152	0.081	0.599	0.708	0.188	0.550	0.564	0.114
Fenestrae	X20B-7(2).FIN2	1.320	1.998	0.308	1.579	0.340	0.184	0.103	0.558	0.708	0.214	0.641	0.701	0.106
	X20B-8(2).FIN2	2.747	4.184	0.603	2.783	0.649	0.229	0.120	0.747	0.745	0.167	0.533	0.551	0.095
Fenestrated Stromatolite	X20B-9(2).FIN2	1.423	2.025	0.326	1.547	0.333	0.108	0.098	0.542	0.740	0.223	0.678	0.607	0.117
Organic Rich Mud	X20B-10(2).FIN2	1.091	1.594	0.210	1.073	0.279	0.102	0.081	0.502	0.684	0.174	0.589	0.694	0.105
Standards	BIR-1.FIN2	0.595	1.960	0.356	2.386	1.092	0.543	0.327	1.860	2.580	0.560	1.690	1.665	0.229
	BIR-2.FIN2	0.596	1.977	0.372	2.397	1.046	0.513	0.335	1.863	2.519	0.541	1.715	1.606	0.241
	NIST612-1.FIN2	35.087	38.848	38.620	36.504	38.165	36.516	37.095	37.639	37.844	39.693	38.846	40.073	37.027

	NIST612-2.FIN2	37.201	38.998	38.556	36.593	37.537	36.725	40.691	41.058	39.818	42.042	44.428	40.118	42.472
Sub-lithotope	**Sample or Standard – Shot # (2nd run on sample) . FIN2**	**La (µg/g)**	**Ce (µg/g)**	**Pr (µg/g)**	**Nd (µg/g)**	**Sm (µg/g)**	**Eu (µg/g)**	**Tb (µg/g)**	**Gd (µg/g)**	**Dy (µg/g)**	**Ho (µg/g)**	**Er (µg/g)**	**Yb (µg/g)**	**Lu (µg/g)**
Fenestrated Stromatolite	X21-1.FIN2	0.852	0.567	0.117	0.527	0.096	0.042	0.021	0.147	0.144	0.046	0.154	0.146	0.025
	X21-2.FIN2	0.445	0.273	0.058	0.263	<0.05236	0.035	0.022	0.145	0.191	0.053	0.180	0.141	0.026
	X21-3.FIN2	0.717	0.392	0.092	0.419	0.076	0.042	0.021	0.152	0.164	0.049	0.146	0.103	0.019
	X21-4.FIN2	1.490	1.270	0.195	0.818	0.150	0.045	0.024	0.157	0.155	0.041	0.124	0.084	0.015
	X21-5.FIN2	0.569	0.271	0.055	0.254	0.041	0.031	0.013	0.101	0.127	0.038	0.154	0.095	0.020
	X21-6.FIN2	0.628	0.494	0.089	0.359	0.080	0.031	0.021	0.170	0.181	0.049	0.178	0.162	0.031
Organic Rich Mud	X21-7.FIN2	0.963	0.691	0.103	0.414	0.065	0.024	0.015	0.117	0.124	0.033	0.148	0.121	0.021
	X21-8.FIN2	0.877	0.670	0.099	0.410	0.077	0.029	0.017	0.118	0.151	0.042	0.170	0.146	0.030
	X21-9.FIN2	1.160	0.805	0.129	0.495	0.071	0.023	0.012	0.111	0.116	0.033	0.136	0.117	0.020
Fenestrae	X21-10.FIN2	1.327	0.859	0.148	0.601	0.095	0.030	0.014	0.127	0.123	0.031	0.108	0.087	0.017
	X21-11.FIN2	0.650	0.370	0.077	0.363	0.068	0.030	0.028	0.199	0.239	0.071	0.302	0.275	0.052
	X21-12.FIN2	0.874	0.566	0.103	0.479	0.085	0.026	0.023	0.169	0.194	0.055	0.196	0.166	0.029
	X21-13.FIN2	0.374	0.254	0.060	0.409	0.087	0.038	0.031	0.202	0.270	0.078	0.291	0.232	0.049
	X21-14.FIN2	0.444	0.246	0.059	0.312	0.088	0.029	0.025	0.207	0.246	0.078	0.292	0.233	0.046
Standards	BIR-1.FIN2	0.593	1.987	0.361	2.502	1.096	0.544	0.321	1.883	2.547	0.509	1.641	1.684	0.209
	BIR-2.FIN2	0.569	1.984	0.366	2.356	1.113	0.522	0.323	1.983	2.471	0.518	1.618	1.750	0.238
Fenestrae	X21-1 (2).FIN2	1.266	0.788	0.158	0.673	0.111	0.034	0.016	0.133	0.139	0.035	0.121	0.061	0.009
	X21-2 (2).FIN2	0.921	0.555	0.121	0.515	0.103	0.025	0.020	0.138	0.136	0.042	0.157	0.130	0.026
	X21-3 (2).FIN2	0.314	0.208	0.055	0.308	0.075	0.033	0.037	0.287	0.310	0.111	0.410	0.346	0.065
	X21-4 (2).FIN2	0.671	0.399	0.084	0.435	0.110	0.044	0.028	0.195	0.192	0.073	0.239	0.172	0.038
	X21-5 (2).FIN2	0.729	0.496	0.101	0.472	0.071	0.026	0.020	0.166	0.189	0.051	0.184	0.155	0.024
	X21-6 (2).FIN2	0.810	0.464	0.104	0.418	0.064	0.029	0.018	0.143	0.132	0.040	0.141	0.153	0.027
	X21-7 (2).FIN2	0.374	0.239	0.066	0.343	0.092	0.040	0.026	0.172	0.194	0.064	0.200	0.148	0.027
Organic Rich Mud	X21-8 (2).FIN2	1.174	0.818	0.122	0.523	0.105	0.032	0.021	0.151	0.137	0.046	0.162	0.116	0.023

Fenestrae	X21-9 (2).FIN2	0.482	0.313	0.061	0.292	<0.05565	0.028	0.030	0.198	0.237	0.081	0.265	0.240	0.047
	X21-10 (2).FIN2	0.643	0.370	0.071	0.317	0.065	0.027	0.018	0.146	0.171	0.051	0.191	0.163	0.033
Sub-lithotope	**Sample or Standard – Shot # (2nd run on sample) . FIN2**	**La (µg/g)**	**Ce (µg/g)**	**Pr (µg/g)**	**Nd (µg/g)**	**Sm (µg/g)**	**Eu (µg/g)**	**Tb (µg/g)**	**Gd (µg/g)**	**Dy (µg/g)**	**Ho (µg/g)**	**Er (µg/g)**	**Yb (µg/g)**	**Lu (µg/g)**
Standards	BIR-1.FIN2	0.596	1.995	0.367	2.347	1.085	0.512	0.315	1.711	2.365	0.505	1.471	1.514	0.225
	BIR-2.FIN2	0.550	1.921	0.371	2.313	1.054	0.567	0.331	1.758	2.374	0.510	1.639	1.640	0.221
Fenestrae	X24A-1.FIN2	0.816	0.268	0.070	0.303	0.058	0.031	0.021	0.129	0.204	0.067	0.228	0.189	0.039
Fenestrated Stromatolite	X24A-2.FIN2	0.759	0.403	0.070	0.321	0.066	0.029	0.019	0.140	0.155	0.049	0.182	0.151	0.033
Organic Rich Mud	X24A-3.FIN2	1.131	0.826	0.123	0.545	0.110	0.046	0.022	0.182	0.208	0.061	0.201	0.161	0.025
	X24A-4.FIN2	1.130	0.984	0.135	0.569	0.105	0.043	0.025	0.202	0.213	0.054	0.210	0.151	0.031
Fenestrated Stromatolite	X24A-5.FIN2	1.452	1.152	0.154	0.596	0.097	0.042	0.024	0.194	0.211	0.060	0.188	0.176	0.035
Fenestrae	X24A-6.FIN2	1.589	0.867	0.149	0.631	0.088	0.040	0.021	0.187	0.188	0.069	0.262	0.210	0.047
	X24A-7.FIN2	0.575	0.237	0.062	0.339	0.091	0.050	0.030	0.203	0.253	0.086	0.291	0.261	0.048
Fenestrated Stromatolite	X24A-8.FIN2	1.090	0.752	0.125	0.475	0.085	0.033	0.020	0.179	0.173	0.053	0.210	0.173	0.034
Fenestrae	X24A-9.FIN2	0.970	0.632	0.093	0.417	0.061	0.043	0.025	0.134	0.162	0.050	0.175	0.145	0.033
	X24A-10.FIN2	0.677	0.343	0.066	0.270	0.048	0.029	0.019	0.120	0.156	0.052	0.213	0.176	0.037
Fenestrated Stromatolite	X24A-11.FIN2	1.352	0.809	0.146	0.605	0.107	0.045	0.019	0.168	0.161	0.055	0.198	0.139	0.032
Fenestrae	X24A-12.FIN2	1.122	0.929	0.139	0.592	0.094	0.051	0.024	0.166	0.204	0.056	0.197	0.184	0.037
	X24A-13.FIN2	0.453	0.263	0.068	0.385	0.118	0.071	0.040	0.305	0.330	0.092	0.342	0.273	0.050
Fenestrated Stromatolite	X24A-14.FIN2	1.472	1.226	0.179	0.820	0.146	0.060	0.031	0.224	0.231	0.070	0.240	0.227	0.040

Standards	BIR-1.FIN2	0.575	2.036	0.388	2.248	1.024	0.529	0.334	1.830	2.177	0.525	1.527	1.433	0.228
	BIR-2.FIN2	0.565	2.087	0.376	2.230	1.160	0.510	0.331	1.678	2.309	0.522	1.477	1.309	0.219
Sub-lithotope	**Sample or Standard – Shot # (2nd run on sample) . FIN2**	**La (µg/g)**	**Ce (µg/g)**	**Pr (µg/g)**	**Nd (µg/g)**	**Sm (µg/g)**	**Eu (µg/g)**	**Tb (µg/g)**	**Gd (µg/g)**	**Dy (µg/g)**	**Ho (µg/g)**	**Er (µg/g)**	**Yb (µg/g)**	**Lu (µg/g)**
Fenestrae	X24AII-1.FIN2	0.700	0.397	0.072	0.287	0.074	0.020	0.011	0.099	0.102	0.027	0.083	0.060	0.015
	X24AII-2.FIN2	0.597	0.342	0.074	0.285	0.046	0.016	0.015	0.112	0.090	0.030	0.082	0.071	0.009
	X24AII-3.FIN2	0.913	0.407	0.065	0.235	<0.04171	0.019	0.011	0.085	0.087	0.026	0.092	0.093	0.015
	X24AII-4.FIN2	0.548	0.275	0.055	0.245	0.051	0.017	0.009	0.079	0.089	0.029	0.105	0.082	0.018
	X24AII-5.FIN2	0.245	0.104	0.019	0.079	<0.039902	<0.012086	<0.0097492	<0.02656	<0.029911	<0.0061728	0.033	<0.035793	<0.0082179
	X24AII-6.FIN2	0.360	0.213	0.046	0.217	0.044	<0.020074	0.012	0.079	0.081	0.025	0.079	0.056	0.010
Fenestrae	X24AII-7.FIN2	0.539	0.235	0.042	0.170	0.038	0.020	0.012	0.073	0.066	0.023	0.070	<0.062074	0.011
	X24AII-8.FIN2	0.564	0.253	0.044	0.163	0.029	0.015	0.009	0.057	0.053	0.020	0.058	0.044	0.008
	X24AII-9.FIN2	0.670	0.291	0.049	0.177	0.033	0.018	0.007	0.050	0.053	0.015	0.054	0.041	<0.0084311
	X24AII-10.FIN2	0.232	0.138	0.032	0.170	0.048	0.022	<0.010637	0.076	0.075	0.020	0.079	<0.062515	0.012
Fenestrated Stromatolite	X24AII-11.FIN2	0.629	0.313	0.050	0.219	<0.056925	0.016	<0.014477	0.052	0.057	0.020	0.063	0.056	<0.012195
	X24AII-12.FIN2	0.479	0.217	0.041	0.168	<0.041244	0.017	<0.0074063	0.037	0.054	0.018	0.060	0.056	0.010
	X24AII-13.FIN2	0.477	0.238	0.042	0.185	0.038	0.021	0.011	0.064	0.055	0.017	0.075	<0.055483	0.008
Standards	BIR-1.FIN2	0.601	1.903	0.380	2.443	1.069	0.554	0.338	1.861	2.639	0.522	1.645	1.610	0.225
	BIR-2.FIN2	0.608	2.033	0.374	2.444	1.234	0.537	0.356	2.004	2.528	0.582	1.592	1.609	0.246

	NIST612-1.FIN2	35.184	41.875	38.445	37.230	37.877	36.430	37.858	36.709	37.355	37.502	42.113	36.961	37.990
	NIST612-2.FIN2	36.108	42.002	38.600	34.651	37.954	33.896	38.277	40.773	36.652	40.023	38.087	39.061	39.272
Sub-lithotope	**Sample or Standard – Shot # (2nd run on sample) . FIN2**	**La (µg/g)**	**Ce (µg/g)**	**Pr (µg/g)**	**Nd (µg/g)**	**Sm (µg/g)**	**Eu (µg/g)**	**Tb (µg/g)**	**Gd (µg/g)**	**Dy (µg/g)**	**Ho (µg/g)**	**Er (µg/g)**	**Yb (µg/g)**	**Lu (µg/g)**
Fenestrated Stromatolite	X24B-1.FIN2	2.453	2.127	0.291	1.293	0.272	0.082	0.055	0.463	0.439	0.113	0.372	0.302	0.062
	X24B-2.FIN2	1.982	1.313	0.218	0.863	0.133	0.072	0.031	0.265	0.254	0.070	0.213	0.167	0.035
	X24B-3.FIN2	1.280	0.901	0.157	0.702	0.170	0.059	0.030	0.235	0.249	0.063	0.226	0.187	0.040
	X24B-4.FIN2	2.436	1.734	0.279	1.175	0.192	0.080	0.043	0.285	0.306	0.076	0.241	0.190	0.043
Organic Rich Mud	X24B-5.FIN2	3.465	3.292	0.397	1.666	0.331	0.092	0.066	0.446	0.426	0.104	0.352	0.291	0.059
Fenestrae	X24B-6.FIN2	3.592	3.205	0.361	1.478	0.285	0.079	0.062	0.503	0.514	0.125	0.381	0.301	0.052
	X24B-7.FIN2	2.808	2.042	0.247	1.155	0.219	0.077	0.052	0.451	0.427	0.122	0.431	0.303	0.060
Organic Rich Mud	X24B-8.FIN2	3.526	2.465	0.352	1.423	0.255	0.077	0.065	0.446	0.511	0.150	0.460	0.478	0.089
Fenestrae	X24B-9.FIN2	2.613	1.860	0.271	1.175	0.260	0.072	0.062	0.428	0.477	0.143	0.417	0.307	0.070
	X24B-10.FIN2	3.420	2.380	0.324	1.383	0.271	0.075	0.057	0.442	0.497	0.146	0.455	0.335	0.074
	X24B Fenes Avg	3.108	2.372	0.301	1.298	0.259	0.076	0.058	0.456	0.479	0.134	0.421	0.311	0.064
Organic Rich Mud	X24 Org. rich Avg	3.495	2.878	0.375	1.545	0.293	0.085	0.065	0.446	0.468	0.127	0.406	0.385	0.074
28	X24 "cement" avg	2.038	1.519	0.236	1.008	0.192	0.073	0.040	0.312	0.312	0.081	0.263	0.211	0.045
Standards	BIR-1.FIN2	0.616	2.025	0.379	2.461	1.126	0.538	0.339	1.930	2.665	0.539	1.670	1.667	0.244
	BIR-2.FIN2	0.593	1.970	0.371	2.371	1.076	0.529	0.319	1.815	2.501	0.516	1.569	1.575	0.235
	NIST612-1.FIN2	36.196	40.696	39.596	36.336	38.655	35.747	36.416	37.554	36.628	37.819	39.452	35.913	37.206
	NIST612-2.FIN2	33.205	40.148	36.860	33.786	35.994	35.209	35.424	36.487	35.153	36.915	36.691	36.402	35.654
Fenestrae	X24c-1.FIN2	1.858	1.488	0.214	0.927	0.193	0.062	0.058	0.359	0.420	0.113	0.370	0.284	0.051
	X24c-2.FIN2	1.487	1.229	<0.65545	<3.3926	<5.2814	<1.4719	<1.0497	<3.1152	<3.1045	<0.79888	<2.7209	<4.8958	<0.71598
	X24c-4.FIN2	1.081	0.972	0.149	0.721	0.171	0.059	0.048	0.310	0.346	0.099	0.287	0.193	0.038

	X24c-5.FIN2	0.500	0.406	0.120	0.614	<0.42477	<0.14776	<0.093119	0.321	<0.38216	<0.069951	<0.31376	<0.39409	<0.067511
	X24c-6.FIN2	0.698	0.546	0.121	0.677	0.138	0.063	0.048	0.331	0.390	0.110	0.318	0.280	0.048
	X24c-7.FIN2	1.370	0.972	0.187	0.862	0.145	0.073	0.041	0.287	0.288	0.067	0.226	0.209	0.032
Sub-lithotope	**Sample or Standard – Shot # (2nd run on sample) . FIN2**	**La (µg/g)**	**Ce (µg/g)**	**Pr (µg/g)**	**Nd (µg/g)**	**Sm (µg/g)**	**Eu (µg/g)**	**Tb (µg/g)**	**Gd (µg/g)**	**Dy (µg/g)**	**Ho (µg/g)**	**Er (µg/g)**	**Yb (µg/g)**	**Lu (µg/g)**
Organic Rich Mud	X24c-8.FIN2	2.065	1.917	0.265	1.153	0.201	0.063	0.048	0.361	0.407	0.109	0.352	0.321	0.062
	X24c-9.FIN2	1.954	1.799	0.245	1.069	0.222	0.060	0.044	0.343	0.347	0.104	0.331	0.304	0.054
Fenestrae	X24c-10.FIN2	0.968	0.601	0.114	0.523	0.115	0.048	0.046	0.326	0.409	0.146	0.576	0.479	0.088
	X24c-11.FIN2	0.932	0.536	0.115	0.542	0.113	0.108	0.024	0.160	0.157	0.048	0.151	0.112	0.022
	X24c-12.FIN2	1.326	0.953	0.144	0.731	0.158	0.050	0.045	0.317	0.397	0.128	0.454	0.431	0.080
	X24c-13.FIN2	1.477	1.056	0.165	0.726	0.156	0.075	0.045	0.314	0.368	0.127	0.447	0.407	0.077
	X24c-14.FIN2	1.794	1.284	0.210	0.996	0.215	0.104	0.060	0.407	0.478	0.139	0.506	0.422	0.078
	X24C Fenes Avg	1.163	0.856	0.132	0.639	0.121	0.058	0.036	0.277	0.283	0.086	0.296	0.253	0.046
Organic Rich Mud	X24C org rich avg.	2.009	1.858	0.255	1.111	0.212	0.061	0.046	0.352	0.377	0.107	0.341	0.313	0.058

Appendix D: FE-SEM-EDS

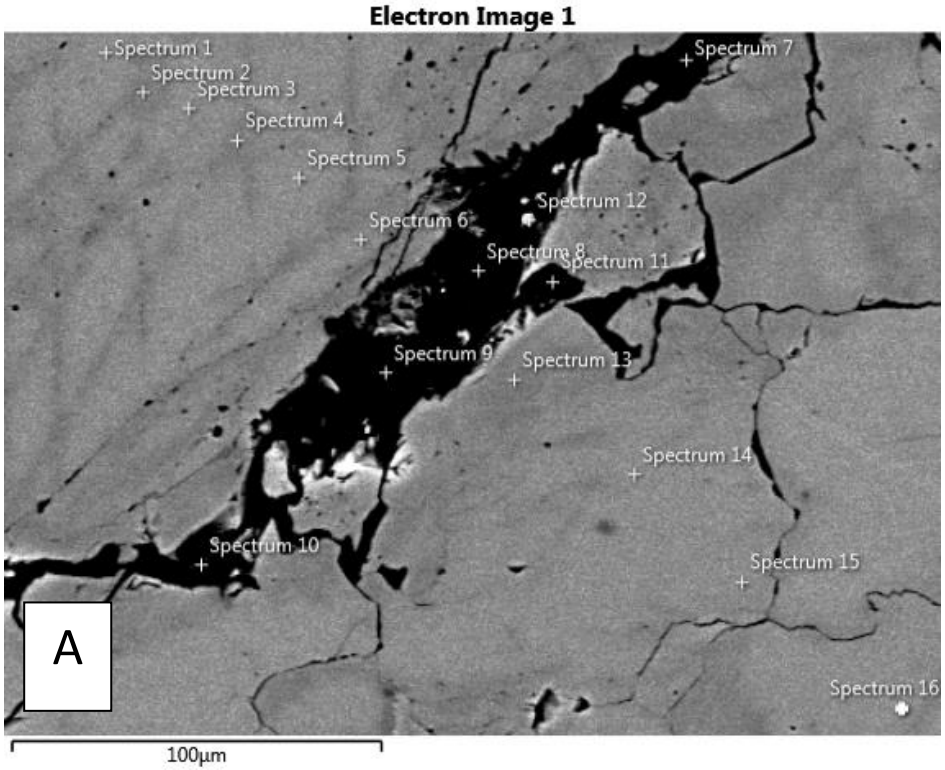

A) FE-SEM-EDS back scatter imaging of black organic rich micritic sized carbonate outlining white blockly fenestral cement (left).
B) Photograph of thick section sample, analyzed on FE-SEM-EDS

Spectrum 1	**Oxide**	**Oxide %**	**Oxide % Sigma**	**Number of Ions**	**Atomic %**	**Wt%**	**Wt% Sigma**
O				6	50.04	15.01	
Mg	MgO	0.55	0.06	0.09	0.73	0.33	0.04
Ca	CaO	50.35	0.18	5.74	47.87	35.98	0.13
Mn	MnO	1.44	0.08	0.13	1.08	1.11	0.06
Fe	FeO	0.18	0.06	0.02	0.13	0.14	0.05
Y	Y2O3	0.31	0.1	0.02	0.14	0.24	0.08
Total		52.82		5.99 (Cation sum)	100	52.82	
Spectrum 2	**Oxide**	**Oxide %**	**Oxide % Sigma**	**Number of Ions**	**Atomic %**	**Wt%**	**Wt% Sigma**
O				6	50	14.87	
Mg	MgO	0.41	0.06	0.07	0.55	0.25	0.03
Ca	CaO	50.37	0.18	5.8	48.34	36	0.13
Mn	MnO	1.31	0.07	0.12	1	1.02	0.06
Fe	FeO	0.16	0.06	0.01	0.12	0.12	0.05
Total		52.26		6.00 (Cation sum)	100	52.26	
Spectrum 3	**Oxide**	**Oxide %**	**Oxide % Sigma**	**Number of Ions**	**Atomic %**	**Wt%**	**Wt% Sigma**
O				6	50	15.08	
Mg	MgO	0.31	0.06	0.05	0.41	0.19	0.03

Ca	CaO	51.31	0.19	5.82	48.52	36.67	0.13
Mn	MnO	1.25	0.07	0.11	0.94	0.97	0.06
Fe	FeO	0.17	0.06	0.02	0.13	0.13	0.05
Total		53.05		6.00 (Cation sum)	100	53.05	
Spectrum 4	**Oxide**	**Oxide %**	**Oxide % Sigma**	**Number of Ions**	**Atomic %**	**Wt%**	**Wt% Sigma**
O				6	50	15.37	
Mg	MgO	0.56	0.06	0.09	0.73	0.34	0.04
Ca	CaO	51.84	0.19	5.77	48.12	37.05	0.13
Mn	MnO	1.36	0.08	0.12	1	1.05	0.06
Fe	FeO	0.22	0.06	0.02	0.16	0.17	0.05
Total		53.98		6.00 (Cation sum)	100	53.98	
Spectrum 5	**Oxide**	**Oxide %**	**Oxide % Sigma**	**Number of Ions**	**Atomic %**	**Wt%**	**Wt% Sigma**
O				5.89	57	6.09	
Mg	MgO	0.38	0.03	0.15	1.4	0.23	0.02
Si	SiO2	5.49	0.08	1.41	13.68	2.57	0.04
S	SO3	0.47	0.04	0.09	0.87	0.19	0.02
Cl		0	0.02	0.11	1.03	0.24	0.02
K	K2O	0.25	0.02	0.08	0.79	0.21	0.02

Ca	CaO	8.54	0.08	2.36	22.78	6.1	0.06
Mn	MnO	0.16	0.04	0.03	0.34	0.12	0.03
Fe	FeO	1.01	0.06	0.22	2.11	0.79	0.05
Total		16.29		4.34 (Cation sum)	100	16.54	
Spectrum 6	**Oxide**	**Oxide %**	**Oxide % Sigma**	**Number of Ions**	**Atomic %**	**Wt%**	**Wt% Sigma**
O				5.95	61.27	6.27	
Mg	MgO	0.19	0.04	0.07	0.73	0.11	0.03
Al	Al2O3	1.26	0.05	0.37	3.86	0.67	0.03
Si	SiO2	4.62	0.08	1.17	12.01	2.16	0.04
S	SO3	2.36	0.07	0.45	4.62	0.95	0.03
Cl		0	0.02	0.05	0.5	0.11	0.02
K	K2O	0.07	0.02	0.02	0.24	0.06	0.02
Ca	CaO	4.84	0.07	1.31	13.49	3.46	0.05
Mn	MnO	0.28	0.04	0.06	0.62	0.22	0.03
Fe	FeO	1.22	0.06	0.26	2.64	0.94	0.05
Total		14.84		3.71 (Cation sum)	100	14.95	
Spectrum 7	**Oxide**	**Oxide %**	**Oxide % Sigma**	**Number of Ions**	**Atomic %**	**Wt%**	**Wt% Sigma**
O				6	57.16	25.44	
Si	SiO2	1.91	0.08	0.12	1.14	0.89	0.04

S	SO3	14.68	0.16	0.69	6.59	5.88	0.06
Ca	CaO	0.92	0.05	0.06	0.59	0.66	0.04
Fe	FeO	68.96	0.31	3.62	34.51	53.61	0.24
Total		86.47		4.50 (Cation sum)	100	86.47	
Spectrum 8	**Oxide**	**Oxide %**	**Oxide % Sigma**	**Number of Ions**	**Atomic %**	**Wt%**	**Wt% Sigma**
O				6	60.53	29.19	
Mg	MgO	14.07	0.12	1.15	11.58	8.49	0.07
Al	Al2O3	13.61	0.13	0.88	8.86	7.2	0.07
Si	SiO2	30.19	0.2	1.65	16.67	14.11	0.09
K	K2O	0.11	0.03	0.01	0.08	0.09	0.02
Ca	CaO	0.76	0.04	0.04	0.45	0.54	0.03
Fe	FeO	3.98	0.09	0.18	1.84	3.09	0.07
Total		62.72		3.91 (Cation sum)	100	62.72	
Spectrum 9	**Oxide**	**Oxide %**	**Oxide % Sigma**	**Number of Ions**	**Atomic %**	**Wt%**	**Wt% Sigma**
O				6	50.03	15.1	
Mg	MgO	0.59	0.06	0.09	0.77	0.35	0.04
Si	SiO2	0.02	0.05	0	0.01	0.01	0.02
Ca	CaO	50.6	0.19	5.74	47.83	36.16	0.13
Mn	MnO	1.53	0.08	0.14	1.14	1.19	0.06

Fe	FeO	0.14	0.06	0.01	0.1	0.11	0.05
Y	Y2O3	0.22	0.1	0.01	0.1	0.17	0.07
Total		53.09		5.99 (Cation sum)	100	53.09	
Spectrum 10	**Oxide**	**Oxide %**	**Oxide % Sigma**	**Number of Ions**	**Atomic %**	**Wt%**	**Wt% Sigma**
O				6	50	14.88	
Mg	MgO	0.25	0.05	0.04	0.34	0.15	0.03
Ca	CaO	51.12	0.19	5.88	48.99	36.54	0.13
Mn	MnO	0.79	0.07	0.07	0.6	0.61	0.05
Fe	FeO	0.09	0.06	0.01	0.07	0.07	0.05
Total		52.26		6.00 (Cation sum)	100	52.26	
Spectrum 11	**Oxide**	**Oxide %**	**Oxide % Sigma**	**Number of Ions**	**Atomic %**	**Wt%**	**Wt% Sigma**
O				6	50	14.56	
Mg	MgO	0.63	0.06	0.1	0.86	0.38	0.04
Ca	CaO	48.86	0.18	5.75	47.88	34.92	0.13
Mn	MnO	1.53	0.08	0.14	1.18	1.18	0.06
Fe	FeO	0.1	0.06	0.01	0.08	0.08	0.05
Total		51.12		6.00 (Cation sum)	100	51.12	

Spectrum 12	Oxide	Oxide %	Oxide % Sigma	Number of Ions	Atomic %	Wt%	Wt% Sigma
O				6	50	13.5	
Mg	MgO	0.45	0.05	0.08	0.66	0.27	0.03
Ca	CaO	45.74	0.18	5.8	48.34	32.69	0.13
Mn	MnO	1.03	0.07	0.1	0.86	0.8	0.05
Fe	FeO	0.17	0.06	0.02	0.14	0.13	0.05
Total		47.39		6.00 (Cation sum)	100	47.39	